

Development of a Novel Motion-Capture Methodology to Assess
Medial Meniscus Displacement during Cadaveric Gait Simulation

Genevieve Pounds

Submitted in accordance with the requirements for the degree of
Doctor of Philosophy

The University of Leeds

School of Mechanical Engineering

April 2023

The candidate confirms that the work submitted is their own and that appropriate credit has been given where reference has been made to the work of others.

This copy has been supplied on the understanding that it is copyright material and that no quotation from the thesis may be published without proper acknowledgement.

Acknowledgements

I would like to thank my supervisors Professor Louise Jennings, Dr Alison Jones and Dr Aiqin Liu for the invaluable support and guidance they have given me over the course of this project. I am very grateful they gave me the opportunity to undertake this research project at the Institute of Medial & Biological Engineering at the University of Leeds. I would also like to thank the EPSRC for providing the funding for this project.

I would like to thank the donors and their families for donating the tissue specimens for the cadaveric knee simulation studies.

I would like to extend a large thankyou to all the iMBE technical staff and researchers for helping me undertake my laboratory experiments. A special mention to Andrew Stockdale who helped me with my manufacturing work requests and to Dr Raelene Cowie who helped me troubleshoot issues with the knee simulator. Thankyou to Dr Nagitha Wijayathunga for MRI scanning the human knee samples and to Dr Blake McCall for performing the meniscus allograft transplantation procedure on the human samples used in the MAT study. Thankyou also to all the participants who took part in the inter-observer and intra-observer variability study.

A special thanks, to all my fellow PhD students in the office, offering great laughs, lunch breaks and support over the years.

Thankyou to all my friends and family for helping me complete this journey. Thank you to my housemates over the years: Rupert Lloyd and Dr Isabel Slark for being amazing during the COVID-19 lockdown and offering timeless friendship and support. Thankyou to Sophie Hutchinson and Dr Bethany Lowe for all the cups of tea, TV evenings and moral support.

Finally, a huge thankyou to my partner who has been through a similar journey and carried me through the ups and downs with plenty of laughs. Thankyou most of all to my Mum and Dad who have given the kindest love, encouragement and support over the years.

Abstract

Pathological meniscal extrusion is commonly associated with knee osteoarthritis. This condition occurs when the meniscus adopts an abnormal position, displacing radially outward from the joint space. This positioning accelerates articular cartilage degeneration by altering the load distribution across the knee joint and is therefore an important measure of meniscus function and a potential metric to assess the biomechanical performance of meniscus interventions. However, *in-vitro* meniscus displacements have rarely been measured under dynamic physiological knee loads and motions. The aim of this thesis was to develop a novel methodology which was sufficient to measure changes in medial meniscus displacement in a tibiofemoral joint model performing physiological gait simulation (displacement-controlled) and additionally to investigate the influence of the knee capsule, medial meniscus posterior root tears and a meniscus allograft transplantation (MAT) on dynamic meniscus displacement during simulated gait.

This aim was achieved through developing a 2D video marker-tracking methodology using an object detection code written on MatLab to estimate the continuous displacement of moving markers throughout the duration of one simulated gait cycle. Reliability assessments estimated minimum error to be within ± 0.1 mm of known simulator translations. Factors such as inter-user variability, lens distortion and the 2D image measurement of 3D tibial displacement were also evaluated. The finalised experimental model incorporated a miniature camera system capturing the anterior-posterior displacement (anterior and posterior regions) and the medial-lateral displacement (medial region) of markers adhered to the medial meniscus and the tibial plateau. The relative displacement described the displacement of the meniscus marker relative to the tibial marker captured in the video frame. The feasibility was assessed on porcine knee joint samples ($n = 4$) and dynamic relative displacement of the medial meniscus was successfully measured throughout a simulated gait cycle in all marker regions. Varying severities of soft tissue constraint and root tears were also able to be measured showing a significant increase in medial-lateral relative displacement when the root was most severely torn, and extrusion was detected throughout the study duration.

The experimental model was applied to human cadaveric knee joints using a similar root tear model ($n = 4$) and an additional MAT model ($n = 3$). High variation in relative displacement occurred between all human samples and the assessed conditions influenced the displacement of both the meniscus and the tibia. The effect of the MAT intervention also varied between samples, however, in some cases corrected the direction of relative displacement to follow a similar pattern to the intact condition. The novel methodology developed herein demonstrates the ability to measure meniscus displacement under simulated gait cycles and could provide a low-cost preclinical tool to assess the mechanical performance of meniscus interventions.

Table of Contents

Acknowledgements	ii
Abstract	iii
Table of Contents	iv
Table of Tables	x
Table of Figures	xii
Abbreviations.....	xx
Chapter 1	1
Introduction and Literature Review.....	1
1.1 Introduction	1
1.2 Anatomy and Biomechanics of the Knee Joint	2
1.2.1 Structure of the Knee Joint	2
1.2.2 Kinematics of the Tibiofemoral Joint	4
1.2.3 Kinetics of the Tibiofemoral Joint during Gait	6
1.3 The Meniscus	7
1.3.1 Gross Anatomy	7
1.3.2 Composition and Microstructure	8
1.3.3 Cellularity and Vascularisation	11
1.4 Meniscus Biomechanics and Structure-Function Relationship	11
1.4.1 Fundamental Tissue Mechanics	11
1.4.2 Functional Biomechanics	15
1.5 Meniscus Injury: Meniscal Extrusion	19
1.5.1 Types of Meniscus Extrusion.....	19
1.5.2 Diagnosis.....	20
1.5.3 Causes and Associations	21
1.5.4 Current Repair and Replacement Techniques	27
1.6 <i>In-Vitro</i> Biomechanical Assessment of Meniscal Injury and Interventions relating to Meniscal Extrusion	33
1.6.1 Problems Associated with Clinical Studies and Animal Models of Meniscus Injury and Intervention	33
1.6.2 Biomechanical Whole-Joint Experimental Models	36
1.6.3 Knee Capsule Constraint in Whole-Joint Models	50
1.7 Conclusions	51
1.8 Project Rationale	52
1.8.1 Aims and Objectives	52

Chapter 2	53
Experimental Materials and Methods	53
2.1 Materials	53
2.1.1 Phosphate Buffered Saline (PBS).....	53
2.1.2 PMMA Bone Cement.....	53
2.1.3 Dissection Tools.....	54
2.1.4 Cementing Fixtures	54
2.2 Methods.....	54
2.2.1 Porcine Tissue	54
2.2.2 Human Tissue	58
2.3 Knee Simulation.....	63
2.3.1 Single Station Knee Simulator	63
2.3.2 Simulated Gait Profile	68
Chapter 3	71
Development of a Measurement Technique to Quantify Dynamic Medial Meniscal Displacement <i>In-Vitro</i>	71
3.1 Introduction.....	71
3.1.1 Aim and Objectives	72
3.2 Measurement Methodology Specification	72
3.3 Frontal Plane Method Development.....	74
3.3.1 Rationale	74
3.3.2 Experimental Set Up.....	74
3.3.3 Results.....	78
3.3.4 Discussion	82
3.4 Sagittal Plane Method Development.....	83
3.4.1 Rationale	83
3.4.2 Experimental Set Up.....	84
3.4.3 Results.....	86
3.4.4 Discussion	88
3.5 Developing Partial Automation of the Measurement Technique	89
3.5.1 Problems with the Current (ImageJ) Measurement Technique	90
3.5.2 Computational Object Tracking	90
3.6 Measuring Dynamic Meniscal Position under Capsule Constraint Conditions: A Comparison of the ImageJ and MatLab methods.....	94
3.6.1 Rationale	94
3.6.2 Sample Preparation, Loading Protocol and Video Capture	94
3.6.3 Results.....	97

3.6.4 Discussion	101
3.7 Video Capture and Mounting Development	103
3.7.1 Design Specification for Improved Method Apparatus.....	103
3.7.2 Camera Hardware and Markers.....	105
3.7.3 Camera Holder Design	105
3.8 Discussion.....	107
Chapter 4	108
Reliability Investigations of the Marker Tracking Method	108
4.1 Introduction.....	108
4.1.1 Aims and Objectives	108
4.2 Dummy Investigation: Understanding the Accuracy and Precision in Response to Sinewave Inputs	109
4.2.1 Rationale	109
4.2.2 Method	110
4.2.3 Results.....	112
4.2.4 Discussion	114
4.3 Image Calibration Error	117
4.3.1 Rationale	117
4.3.2 Method	118
4.3.3 Results.....	118
4.3.4 Discussion	120
4.4 Lens Distortion Error	121
4.4.1 Rationale	121
4.4.2 Method	121
4.4.3 Results.....	122
4.4.4 Discussion	124
4.5 Relative Meniscus Displacement Measurement	124
4.5.1 Rationale	124
4.5.2 Theory	124
4.5.3 Method	125
4.5.4 Results.....	125
4.5.5 Discussion	126
4.6 Investigating the Relative Meniscus Displacement in the Anterior, Posterior and Medial regions of a Porcine Knee	127
4.6.1 Rationale	127
4.6.2 Method	127
4.6.3 Results.....	129

4.6.4 Discussion	133
4.7 Complex Gait Profile	135
4.7.1 Effect of Tibial Rotation on the Measured Anterior-Posterior Displacement in the Video Frame Using Gait Profile Parameters	136
4.7.2 Preliminary Investigation Measuring the Relative Meniscus Displacement using a Displacement Controlled Gait Profile in a Porcine Sample ..	140
4.7.3 Discussion	141
4.8 Discussion.....	144
Chapter 5.....	146
Feasibility Study Assessing Dynamic Medial Meniscus Displacement using the Developed Motion Capture Method in Porcine Tibiofemoral Joints	146
5.1 Introduction.....	146
5.1.1 Aims and Objectives	146
5.2 Porcine Study Methodology	147
5.2.1 Sample Preparation.....	147
5.2.2 Gait Profile and Camera Set Up	147
5.2.3 Capsular Constraint and Root Tear Conditions.....	148
5.2.4 Data Processing and Analysis.....	149
5.3 Results.....	151
5.3.1 Effect of Capsular Constraint and Posterior Root Tear Severity on Relative Displacement.....	151
5.3.2 Meniscus and Tibia Marker Tracking.....	155
5.3.3 Simulator Adduction – Abduction Position	157
5.3.4 Effect of Cyclic Test Duration on Relative Displacement.....	158
5.4 Discussion.....	159
5.4.1 Main Findings.....	160
5.4.2 Evaluation of the Motion Capture Method to Assess Biomechanical Changes with Root Tear Injury	160
5.4.3 Limitations	163
5.4.4 Summary	163
Chapter 6.....	165
Application of the Motion Capture Method to Assess Dynamic Medial Meniscus Displacement in Human Knee Specimens.....	165
6.1 Introduction.....	165
6.1.1 Aim and Objectives	165
6.2 Method Adaptations for Human Specimens.....	166
6.2.1 Camera Rig Adaptations.....	166
6.2.2 Camera Triggering in Python	167

6.2.3 Marker Pin Development	168
6.3 Human Study Methodology.....	168
6.3.1 Sample Preparation.....	168
6.3.2 Developments to the Capsular Constraint and Root Tear Conditions ...	169
6.3.3 Gait Profile and Camera Set Up	172
6.3.4 Data Collection Procedure.....	173
6.3.5 Data Processing and Analysis.....	173
6.3.6 Study Design Summary	175
6.4 Tear Study Results	177
6.4.1 Relative Displacement Individual Sample Detail	177
6.4.2 Relative Displacement Summary.....	182
6.4.3 Tibia and Meniscus Marker Displacements.....	183
6.5 Tear Study Discussion	186
6.5.1 Main Findings.....	186
6.5.2 Limitations	186
6.5.3 Sample Variation.....	187
6.5.4 Intact / Healthy Medial Meniscus Displacement	188
6.5.5 Knee Capsule Constraint.....	189
6.5.6 Root Tear Injury and Meniscal Extrusion.....	191
6.6 Meniscus Allograft Transplantation (MAT) Study.....	194
6.6.1 MAT Methodology.....	194
6.7 MAT Study Results	196
6.7.1 Relative Displacement Summary.....	196
6.7.2 Relative Displacement Directional Analysis.....	200
6.8 MAT Study Discussion.....	203
6.8.1 Main Findings.....	203
6.8.2 Limitations	203
6.8.3 Effect of the MAT Intervention.....	204
Chapter 7	206
Overall Discussion.....	206
7.1 Research Rationale.....	206
7.1.1 Aims 207	
7.2 Main Findings	207
7.2.1 Development of the Marker Tracking Methodology.....	207
7.2.2 Feasibility Assessment of the Experimental Model on Porcine Samples	208

7.2.3 Assessment of the Experimental Model on Human Knee Joint Specimens	208
7.3 The Technical Challenge of the Motion Capture Method	209
7.4 Evaluation of the Experimental Model as a Preclinical Assessment	211
7.5 Limitations.....	213
7.5.1 Limitations of the Motion Capture Method	213
7.5.2 Limitations of the Experimental Procedure.....	214
7.6 Recommendations for Future Motion Capture Method Developments – 3D Estimations	215
7.7 Conclusion	217
References	218
Appendix A – Literature Table	232
Appendix B – Ethical Approval.....	237
Appendix C – Standard Operating Procedure: MATLAB Object Tracking Script.....	241
Appendix D - Standard Operating Procedure: Camera Programming for Meniscus Tracking	256
Appendix E – Porcine Study: Meniscus and Tibial Marker Results	271
Appendix F – Human Study: Meniscus and Tibial Marker Results	275
Appendix G – Figure Permissions	282

Table of Tables

Table 1.1. Material properties of human medial meniscus tissue specimens.	14
Table 1.2. Surgical repair and replacement techniques for meniscus extrusion.	28
Table 1.3. Defining load and motion conditions in biomechanical models of meniscus experimental research.	37
Table 2.1. Summary of the key mechanical motion axes' sensor control information and limits.	65
Table 2.2. Maximum and minimum values for each gait profile axis of the porcine and human profiles.	69
Table 2.3. Polarity differences of the tibial rotation (TR) and the adduction-abduction (AA) axes during left and right human knee simulation.	70
Table 3.1. Meniscus displacement measurement method specification and comparisons.	73
Table 3.2. Mean (+/- SD) relative displacement in the medial direction of the intact and torn medial meniscus, relative to the tibia as the load increased from 800 to 900 N.	81
Table 3.3. Individual sample results showing the mean displacement of the anterior and posterior regions of the medial meniscus, relative to the tibia during increasing load. Values taken at the 1000 N force interval.	88
Table 3.4. Comparison table of the two measurement techniques.	97
Table 3.5. MatLab measurement method validation displacement results.	98
Table 3.6. ImageJ measurement method validation displacement results.	98
Table 3.7. Specifications for designing and sourcing the cameras, markers and camera holder for the improved method set up illustrated in Figure 3.12.	104
Table 4.1. Study 1 known and measured displacements for each driven anterior- posterior (AP) sinewave case (all measurements in mm) including statistical results of mean percentage error (MPE) and coefficient of variance (CV).	113
Table 4.2. Study 2 marker tracking measured displacements and calculated coefficients of variation (CV) from three repeat trials of each driven AP translation sinewave case with associated driven tibial rotation sinewave cases (500N constant axial load applied).	114
Table 4.3. Measured pixel diameters of the marker in the calibration image (Study 1) across 8 healthy subjects to assess intra and inter observer variability (All measurements in pixels).	120
Table 4.4. Total displacements and percentage errors of the calibrated and uncalibrated results (all measurements in mm).	123
Table 5.1 Mean relative displacements (\pm 95% CI) taken from specific gait time-points (TP) and the range (maximum-minimum) across cycle 3. All units in mm. * = significant difference from one group $p < 0.05$	154
Table 6.1. Details of tested human samples and assessed initial and revised conditions.	171

Table 6.2. Description of the opposing measurement polarity in the video frame for left and right human knees in relation to the medial-lateral and anterior-posterior motion directions.....	175
Table 6.3. Mean relative displacements (\pm 95% CI) taken from specific gait time-points (TP) and the range (maximum-minimum) for cycle 10. All units in millimetres (all cases $p > 0.05$).....	182
Table 6.4. Comparison of dynamic intact (healthy) human medial meniscus displacement (mean \pm SD) from previously published <i>in-vivo</i> and <i>in-vitro</i> radiographical studies with the tear study results of this thesis (bottom row). The arrows illustrate the measurement locations and the direction of displacement of the medial meniscus during the various experiments.	190

Table of Figures

Figure 1.1. Annotated frontal view of the knee joint (Reproduced with permission from: Hamill et al., 2015).....	2
Figure 1.2. Annotated sagittal cross section view of the knee joint (Reproduced with permission: Hamill et al., 2015).....	3
Figure 1.3. Three anatomical planes and six degrees of freedom of the knee joint.	5
Figure 1.4. Schematic showing the key parts to the human gait cycle and how the knee joint changes during each period.	6
Figure 1.5. Transverse plane section of the tibial plateau showing the medial and lateral menisci and tibial root attachments (Adapted from: Kean et al., 2017).	8
Figure 1.6. Cross-section illustrating the meniscus collagen organisation and differing levels of vascularisation.	9
Figure 1.7. Central cross-section of a bovine meniscus showing the varying density of collagen (stained fast-green) and proteoglycans (stained safranin-orange) between the inner and outer zones. (Reproduced with permission: Andrews et al., 2017, p. 274).....	10
Figure 1.8. Meniscus tissue mechanics stress – strain curve under tensile forces.	12
Figure 1.9. Meniscus tissue mechanics under compressive forces showing (A) creep characteristics when subject to a constant load and (B) stress relaxation characteristics when held at a constant deformation.	13
Figure 1.10. Simple geometric model of meniscus function reducing the contact pressure through increasing the contact area on the flat surface. The ball represents the femoral condyles, the plate represents the tibial plateau and the shallow cup represents the meniscus. An axial load of 1800 N approximately represents 2.5 times BW of a 70kg man during the stance phase of gait.	16
Figure 1.11. Load bearing mechanism of the meniscus showing radial expansion of the meniscus caused by the horizontal pressure of the femoral axial force converted to the radial vector which is distributed through the circumferential force of the collagen network.	17
Figure 1.12. Schematic representation of the meniscal movement from 0° extension to 90° flexion during weight bearing (A) and non-weight bearing (B) conditions. Measurements are in millimetres (Reproduced with permission: Vedi et al., 1999, p. 39).	18
Figure 1.13. Loading differences across the knee between a healthy meniscus and an extruded meniscus.	20
Figure 1.14. Morphological classification of meniscal root tears. The tear most associated with meniscus extrusion is number 2; the complete radial root tear.	22
Figure 1.15. Frontal plane (central slice) of the medial side of the knee joint showing the knee capsule and supporting structures; the superficial knee capsule line (arrowheads), the superficial line of the MCL (curved arrows) and the menisiofemoral (mf) and meniscotibial (mt) ligament extensions located in the deep portion of the MCL. (Reproduced with permission: De Maeseneer et al., 2002. p.243).....	24

Figure 1.16. Changes in the position and shape of the lateral meniscus (green) and medial meniscus (red) in (a) healthy patients, (b) loading effects on the medial meniscus in patients with medial compartment OA and (c) loading effects on the lateral meniscus in patients with medial compartment OA (Reproduced with permission: Wenger et al., 2013, p. 1808).....	25
Figure 1.17. Anatomical differences between the human and porcine knee and menisci (measurements in mm) (Takroni et al., 2016, p.6).	35
Figure 1.18. ISO 14243-3: 2014 force-controlled simulated gait cycle inputs. (A) axial force (red line) and flexion-extension (blue dashed line) inputs. (B) anterior-posterior (AP) force (solid red line) and tibial rotation (TR) torque (blue dashed line) inputs (Reproduced with permission from: Abdelgaied et al., 2022, pp. 3 - 4).	38
Figure 1.19. Average peak contact pressures over an ISO simulated gait cycle at 33% load for the intact (black), lateral meniscus posterior root tear (blue) and tibial tunnel root repair (red) conditions (n = 8). (Reproduced with permission from: Schillhammer et al., 2012).....	40
Figure 1.20. (A) Tekscan K-scan 4011 contact pressure sensors for biomechanical knee joints. (B) Image of the Tekscan sensors being used for cadaveric assessment.	42
Figure 1.21. Meniscus displacement measurement techniques. (A) Radiographical X-ray methods such as roentgen stereo-grammatic analysis (RSA) (Reproduced with permission from: Tienen et al., 2005, p. 289). (B) Ultrasound methods. (C) Probe methods such as using linear variable displacement transformers (LVDTs) (Reproduced with permission from: Hein et al., 2011, p. 190). (D) Motion capture using optical cameras and retro-reflective markers.....	46
Figure 2.1. A-F. Porcine knee joint with capsule retained dissection process.....	55
Figure 2.2. Porcine knee joint centre of rotation (COR) positioning for the medial and lateral condyles (indicated by the red arrows in the images).....	56
Figure 2.3. Porcine femoral side alignment and cementing procedure.....	57
Figure 2.4. Example MRI images to obtain distance measurements and scanning reports on the bone, meniscus and cartilage condition prior to testing.....	59
Figure 2.5. A-C. Human knee specimen dissection procedure.....	60
Figure 2.6. Human knee joint centre of rotation (COR) approximation from the (A) medial and (B) lateral epicondyles. (C) Lining up the COR holes with the simulator centre of rotation axes in the transverse and frontal plane.....	61
Figure 2.7. Human knee specimen femoral side alignment and cementing procedure.....	62
Figure 2.8. (A) Porcine knee sample set up in the Leeds single station knee simulator. (B) Sagittal plane and (C) frontal plane schematics of the rotation (blue arrows) and translation (red arrows) movement axes for a right knee sample in the knee simulator. The axial force is applied vertically to the femoral components of the knee sample. The force is applied perpendicular to the axis of centre of rotation of the flexion – extension arm whilst other parts of the machine drive tibial rotations (internal-external) and tibial translations (anterior-posterior). The abduction-adduction rotation axis was left unconstrained (free), and the medial-lateral translation axis was fixed at zero.....	64

Figure 2.9. Schematic showing the mechanical parts of the simulator facilitating movement of the rotation and translation movement axes during knee gait simulation.	65
Figure 2.10. Simulator calibration images showing the set up of the (A) centring jig to zero all positional axes and (B) the axial force load calibration set up.	67
Figure 2.11. The Leeds high kinematics gait profile driven inputs for porcine and human knee simulation (driven at 0.5 Hz). (A) Modified two-peak axial force profile, (B) flexion extension, (C) anterior-posterior tibia translation and (D) tibial rotation. .	69
Figure 2.12. Inversion of the tibial rotation input axes for right and left human knee simulation.	70
Figure 3.1. Experimental set up: (A) marker placement on the porcine medial meniscus and the tibia. (B) Diagram of the digital camera positioning in the simulator (SSKS). (C) Schematic of the step-ramp loading profile used for biomechanical investigation.....	75
Figure 3.2. Complete radial root tear creation of the porcine medial meniscus posterior root. (A) Measurement of 6 mm from the root insertion. (B) Scalpel cut in the inferior direction at 6 mm from the insertion.....	77
Figure 3.3. Validation method for the ImageJ measurement technique. (A) Method set up showing a marker adhered to a solid piece of plastic, cemented into one of the knee pots and screwed into the tibial base of the simulator. (B) Video camera view of the validation marker annotated with the known medial-lateral axis translation.....	78
Figure 3.4. Difference in the relative medial meniscus displacement with increasing axial force for (A) Knee A, (B) Knee B and (C) Knee C, between the intact and torn conditions at 0° and 10° flexion. As shown in the schematic, positive results equate to medial marker displacement (n= 3, error bars = SD of 3 repeat measurements, porcine).....	79
Figure 3.5. Screenshots of the 0° flexion angle test, showing maximum displacement of the intact conditions (left) and the torn conditions (right) for (A) Knee A, (B) Knee B and (C) Knee C (porcine).	80
Figure 3.6. (A) Anterior (ANT) and posterior (POST) marker placement on the porcine medial meniscus, in relation to the anterior and posterior meniscal root insertions. (B) Smartphone camera position and screenshot of analysis carried out on ImageJ.	85
Figure 3.7. Relative displacement of the anterior (ANT) and posterior (POST) meniscal markers with respect to the tibia for (A) Knee SagA, (B) Knee SagB and (C) Knee SagC, at 0° and 10° static flexion angles. As illustrated in the schematic, positive values indicate an anterior direction of movement for the ANT region. Positive values indicate a posterior direction of movement for the POST region (n = 1, porcine).....	87
Figure 3.8. (A) Test video screenshot. (B) Image binarisation of the coloured marker in the test video. (C) Bounding box (blob) identifying the marker to track in the video.	91
Figure 3.9. Spatial change (x-axis and y-axis pixel position) of the marker in the test video over the image resolution.	92

Figure 3.10. Temporal change of the x-axis and y-axis position of the test video marker over the video duration. Calibrated to the known size of the marker.	93
Figure 3.11. (A) Positioning of the anterior (A), posterior (P) and medial (M) meniscal markers using distances Pd and Ad , in relation to the position of the MCL and PCL. (B) Loading profile for the experiment. All tibial axes (AP, AA, TR, ML) were fixed, only the FE axis was driven (porcine).	95
Figure 3.12. Comparison of the meniscal displacement between porcine knee sample dissection conditions, capsule intact (CAP, capsule removed (NOCAP) and ligaments removed (NOLIG), of the posterior marker (A, B), anterior marker (C, D) and the medial marker (E, F) results using two different measurement methods ($n = 1$). Shaded error bars equate to the highest measured absolute value from the validation study. ImageJ method ± 0.29 mm; MatLab method ± 0.10 mm.	100
Figure 3.13. Schematic of the tissue-level test set up for the medial meniscus of a right knee in the simulator, showing the medial, anterior, and posterior camera views and the polarity of measured medial-lateral and anterior-posterior movement directions in the video frames. A tibial reference marker will also be introduced so two markers will be tracked with the MatLab script in the same video to find the meniscus displacement, relative to the tibia.	103
Figure 3.14. (A) Annotated exploded SolidWorks assembly and (B) complete SolidWorks assembly of the camera holder design. (C) Manufactured camera holder adhered to the simulator and (D) with the Raspberry Pi cameras mounted.	106
Figure 4.1.(A) Dummy study set up in the simulator. (B) Tibial base top view showing the marker position (attached to the tibial base) in relation to the camera position and the directions of the simulators driven sinewave anterior-posterior translation and internal-external rotation of the tibial base. (C) Camera frame video of the marker attached to the tibial base with labelled simulator translation and rotation axes.	111
Figure 4.2. Sinewave input profiles used for the anterior-posterior (AP) translation and the internal and external tibial rotation (TR).	112
Figure 4.3. Study 1 results from repeat trial 1 showing the agreement of the marker-tracking method (blue lines) in measuring known anterior-posterior sinewave translations driven by the simulator (grey/black lines).	113
Figure 4.4. Study 2 results from repeat trial 1 showing the effect of applying tibial rotation on the anterior-posterior measurement of the marker in the video for the (A) ± 0 mm (black/grey) AP sinewave condition and (B) the ± 2 mm (blue) and the ± 6 mm (red) AP conditions (500N constant load applied).	115
Figure 4.5. Sensitivity analysis of the marker pixel diameter calibration on the measured ± 6 mm anterior-posterior translation sinewave result from the dummy investigation (Study 1).	119
Figure 4.6. Types of lens distortion: (A) no lens distortion, (B) barrel distortion and (C) pincushion distortion.	121
Figure 4.7. (A) An example checkerboard image and (B) the reprojection errors.	122

- Figure 4.8. Calibrated (red) and uncalibrated (blue) anterior-posterior displacement results. Calibrated image (right) shows a narrow border (coloured red) around the edge of the frame to undistort the image using the intrinsic camera calibration method. 123
- Figure 4.9. Schematics of the meniscus (M) and tibial (T) markers viewed in the video frame to understand the resultant relative displacement (R) (red arrow) of the meniscus marker relative to the tibial marker. 125
- Figure 4.10. Finding the relative displacement of the meniscus marker to the tibial marker on the dummy with the simulator driving a +/- 6.0 mm anterior-posterior translation sinewave profile at 0.5 Hz. 126
- Figure 4.11. (A) Positioning of posterior (POST) meniscus and tibia markers using the equation $d = TW \times 0.4$, measuring from the lateral edge of the PCL identified through the bony prominence. (B) Positioning of the medial (MED) markers on the posterior edge of the MCL and using this to measure to the position of the anterior (ANT) markers with the distance d . (C) The anterior-posterior (AP) translation (black solid) (+/- 0 mm, +/- 2 mm and +/- 6 mm) and tibial rotation (TR) (grey dashed) (+/- 0°, +/- 1°, +/- 2° and +/- 4°) simulator profiles used. 128
- Figure 4.12. (A) POST, (B) ANT and (C) MED displacements of the meniscus marker, tibia marker and calculated relative displacement for the +/- 6 mm AP sinewave condition with applied TR sinewave magnitudes of +/- 0° (black), +/- 1° (blue), +/- 2° (red) and +/- 4° (grey). Schematics indicate the marker position and the video frame polarity ($n = 1$). 131
- Figure 4.13. Results for the posterior (POST) meniscus region showing the measured (A) tibia marker displacements, (B) meniscus marker displacements and (C) the relative displacements (R) calculated from the equation $D_R = D_M - D_T$ for all AP (+/- 0 mm (red), +/- 2 mm (blue) and +/- 6 mm (black)) and TR (+/- 0° (circle), +/- 1° (triangle), +/- 2° (diamond) and +/- 4° (square)) sinewave conditions ($n = 1$). 132
- Figure 4.14. Schematic of the tibia deforming during the study and the capsule pulling in the opposite direction to resist the movement of the anterior-posterior carriage 134
- Figure 4.15. Measured displacement of four markers in four different positions along the tibia whilst simulating the +/- 6.0 AP sinewave profile ($n = 1$). 135
- Figure 4.16. Mathematical model of the relationship between the applied AP and measured AP (blue line) with applied TR (red line) to find the total measured AP displacement in the video frame. Assumes a linear relationship between the applied and measured AP and that the tibia is circular with a radius of 30 mm. 136
- Figure 4.17. Mathematical model applied to the (A) TR and AP porcine simulator gait inputs. (B) The relationship between measured AP and applied AP (using the equation in Figure 4.16) of the AP only (blue), AP + TR 1.6° (red narrow-dashed) and AP + TR 5° (red wide-dashed). (C) Represents these variables across a gait cycle to show the predicted measured AP in the 2D video frame when TR is applied (the variables start at zero to mark the beginning of the gait cycle in the video frame). 138

Figure 4.18. Experimental data showing the measured AP displacement of the marker in the video frame whilst increasing the magnitude of the applied TR input as the AP input was driven. In this case the AP translation input was moved to begin at zero to better compare the marker tracking measurements with the profile and assess the sensitivity of increasing the TR on the measurement (n = 1, porcine).	139
Figure 4.19. Relative (red - square), Meniscus (black – triangle) and Tibia (black – circle) displacement results across one 0.5 Hz cycle (cycle 3) for the (A) POST, (B) ANT and (C) MED meniscal regions. Knee sample tested with the capsule retained (n = 1).	142
Figure 4.20. New direct LED lighting set up and video frame images showing the original lighting (before) compared with the colour contrast achieved when the new lighting set up was implemented (after)	143
Figure 5.1 Test set up showing a porcine sample in the simulator with the medial, anterior, and posterior camera viewing the meniscus and tibia markers for each corresponding region of the medial meniscus. Screenshots of the video frame show the marker tracking bounding box and the direction of measured movement in a right knee: anterior (A) – posterior (P) and medial (M) - lateral (L)	148
Figure 5.2. Porcine experimental conditions: (A) CAP, knee capsule intact; (B) NOCAP, knee capsule removed but ligaments retained; (C) NOLIG, collateral and cruciate ligaments removed. Medial meniscus posterior root tear conditions: (D) TORN1, 15% width tear; (E) TORN2, 46% width tear and (F) TORN3 92% width tear.	149
Figure 5.3 Time points from the (A) axial force (AF) and (B) flexion-extension (FE) porcine gait inputs where values were taken to generate relative displacement means for statistical analysis. Frontal plane (medial region) data uses the axial load time-points and sagittal plane (anterior region and posterior region) uses the flexion-extension time points.	150
Figure 5.4 A-F. Cycle 3 relative displacement results for the medial, anterior, and posterior regions of Samples A and B (porcine).	152
Figure 5.5 A-F. Cycle 3 relative displacement results for the medial, anterior, and posterior regions of Samples C and D (porcine).	153
Figure 5.6. Sample A representative example of the meniscus marker, tibia marker and calculated relative displacement results for the (A) medial, (B) posterior and (C) anterior region of the CAP and TORN3 conditions for across cycle 3 (porcine).	156
Figure 5.7. Comparative example of varying adduction-abduction angle between samples showing the simulator output and tibia marker displacement results during cycle 3 for (A) Sample B and (B) Sample C (porcine).	157
Figure 5.8. Sample C anterior and posterior region relative displacement results for cycle 3, 10, 25 and 50 for the CAP, NOLIG and TORN3 conditions (porcine).	158
Figure 5.9. Medial region TORN3 relative displacement results for cycle 3 and cycle 50 for all tested porcine knee samples A-D (corresponding graphs to each sample).	159
Figure 5.10. Porcine sample A TORN3 condition screenshots for cycle 3 and cycle 50 showing the extrusion measured between the centroid of the meniscus (2) and tibia (1) markers.	161

Figure 6.1. Camera rig adaptations to enable compatibility with human specimens. (A) SolidWorks models of newly manufactured parts for left knee specimens. (B) Image of manufactured parts allowing attachment of the abduction-adduction arm during left knee testing. (C) SolidWorks assembly of human anterior and posterior camera attachment. (D) Manufactured human component and comparison with the porcine component.	167
Figure 6.2. Revised human study dissection/torn conditions: (A) Intact, knee capsule fully intact. (B) Capsule removed, knee capsule and ligaments excised. (C) Partial root tear, medial posterior root tear at the insertion spanning 50% of the root width. (D) Complete root tear, 100% of root width.	170
Figure 6.3. Human study test set up showing the differences in anterior-posterior (AP) and medial-lateral (ML) image measurement polarity with a (A) right and (B) left knee.	172
Figure 6.4. Data collection procedure repeated for all three meniscus regions (anterior, posterior and medial) during each of the four dissection/root tear condition (a total of 12 repeats for each sample).	173
Figure 6.5. Human study design flow chart showing the fragmenting of the scanned human knee samples into three different studies (Development Study, Tear Study and MAT study) and the analysis of the outcome tracking data.	176
Figure 6.6. Measured cycle 10 relative displacement for the medial, anterior and posterior regions of (A-C) LTKN1017 and (D-F) LTKN0812 (human).	180
Figure 6.7. Measured cycle 10 relative displacement for the medial, anterior and posterior regions of (A-C) RTKN1064 and (D-F) LTKN2083 (human).	181
Figure 6.8. Representative example of the comparison between the simulator abduction-adduction output and measured medial region tibial marker displacement for (A, B) LTKN1017 and (C, D) RTKN1064 (human).	184
Figure 6.9. Human sample LTKN0812 representative example of the (A) anterior region and (B) posterior region tibial marker displacement in relation to the anterior-posterior (AP) translation and tibial rotation (TR) gait profile inputs. The left-knee tibial marker polarity was inverted to match the polarity of the anterior-posterior (AP) simulator input.	185
Figure 6.10. MAT intervention procedure in steps 1-6.	195
Figure 6.11. Complete MAT procedure on two human samples.	196
Figure 6.12. Human sample LTKN1409 relative displacement results for the (A) medial, (B) anterior and (C) posterior regions across one simulated gait cycle.	198
Figure 6.13. Relative displacements for the medial, anterior and posterior regions of (A-C) LTKN1017 and (D-F) RTKN1952 (human).	199
Figure 6.14. Medial meniscus directional analysis for human sample LTKN1409, showing the driven axes of the simulated gait cycle and schematics of the estimated direction of regional relative displacement for each 0.5 second gait cycle period. See key at the top.	201
Figure 6.15. Medial meniscus directional analysis for human sample (A) LTKN1017 and (B) RTKN1952, showing the schematics of the estimated direction of regional relative displacement for each 0.5 second gait cycle period. See key on previous page.	202

Figure 7.1. Future developments of the motion capture methodology to estimate 3D changes in meniscus movement with internal/external (I/E) tibia rotation. (A) Camera triangulation. (B) Estimation of changing distance of the marker away from the camera lens using the width of the marker in pixels (p).216

Abbreviations

2D	Two Dimensional
3D	Three Dimensional
AA	Abduction - Adduction
ACL	Anterior Cruciate Ligament
ADC	Analog to Digital Converter
AF	Axial Force
ANT	Anterior Region
AP	Anterior-Posterior
CAP	Capsule retained (intact) condition
CI	Confidence Interval
COR	Centre of Rotation
CV	Coefficient of Variance
DIC	Digital Image Correlation
DNA	Deoxyribonucleic acid
ECM	Extracellular Matrix
FE	Flexion-Extension
fps	Frames per second
GAG	Glycosaminoglycan
HD	High Definition
Hz	Hertz
IE	Internal-External
ISO	International Standards Organisation
KL	Kellgren Lawrence (grade)
LCL	Lateral Collateral Ligament
LED	Light Emitting Diode
LVDT	Linear Variable Differential Transformer
MAT	Meniscus Allograft Transplantation
MCL	Medial Collateral Ligament

MED	Medial Region
ML	Medial-Lateral
mm	Millimetre
MPa	Mega Pascal
MPE	Mean Percentage Error
MRI	Magnetic Resonance Imaging
N	Newton
NOCAP	Capsule removed condition (ligaments retained)
NOLIG	No ligaments condition
OA	Osteoarthritis
PBS	Phosphate Buffered Saline
PCB	Printed Circuit Board
PCL	Posterior Cruciate Ligament
PMMA	Polymethyl methacrylate
POST	Posterior Region
RSA	Radio-stereometric analysis
SD	Standard Deviation
TKR	Total Knee Replacement
TR	Tibial Rotation
USB	Universal serial bus

Chapter 1

Introduction and Literature Review

1.1 Introduction

It is estimated that osteoarthritis (OA) affects 10% of the world's population over 60 years old (Buckwalter et al., 2004). The knee joint is the most common site for OA to develop. This is due to the translational, rotational, and planar motions the knee joint must facilitate under high loads and torques from weight bearing. Total knee replacement (TKR) is the end-stage therapy for knee OA and are generally more successful in older sedentary patients. In younger, more active patients (< 60 years old) these devices have a higher failure and revision rate. One in three patients between the ages of 50 - 55 years would require a TKR revision surgery in their lifetime; compared to between 1% and 6% of patients > 70 years old (Bayliss et al., 2017). The need for alternative early-stage knee interventions is required to delay the need for a TKR and reduce the cost to healthcare services.

The menisci function to protect the articular cartilage and stabilise the knee joint. The menisci are one of the most commonly injured soft tissues in the knee joint and have a strong clinical relationship with OA (Roemer et al., 2009; Englund, Guermazi, Roemer, et al., 2009; Englund, Guermazi and Lohmander, 2009; Siemieniuk et al., 2018). Meniscal extrusion is a pathological state that has been linked as a single predictor of OA (Costa et al., 2004). This occurs when the body of the meniscus moves radially outside the edge of the tibial plateau, reducing the joint congruency and inhibiting the meniscus to carry out its load distributing function. Meniscal extrusion can be a good indication of other underlying knee pathologies, but the majority of previous research is retrospective, failing to identify the cause-effect relationship. Developing methods to improve *in-vitro* biomechanical assessment in meniscal research is an important way to reduce the amount of costly animal studies and improve clinical translation of meniscal interventions.

This chapter provides a comprehensive review of the structure and function of the knee joint and the meniscus, as well as the current clinical research field surrounding meniscal extrusion and the *in-vitro* biomechanical assessment of meniscal injury and interventions related to meniscal extrusion. Finally, the aims and objectives of this thesis will be formulated from the key research themes discussed in this opening chapter.

1.2 Anatomy and Biomechanics of the Knee Joint

The anatomy and biomechanics of the human knee joint dictate the forces transmitted to the articulating surfaces such as the menisci.

1.2.1 Structure of the Knee Joint

The knee joint is a complex joint located between the two longest lever arms in the body, the femur and the tibia. The knee joint therefore experiences mechanical forces and moments in the regions of 200% – 400% of an individual's body weight (BW) during activities of daily living (Nordin and Frankel, 2001). The knee joint is adapted predominantly through soft tissue alignment and congruency to allow large amounts of movement as well as stabilisation during load bearing. However, the increased reliance on soft tissue support, rather than bony stabilisation, means the knee joint is more susceptible to injury than other joints in the body (Hamill et al., 2015). The whole knee joint can be split into three sub-joints; the tibiofemoral joint, the patellofemoral joint and the fibula-femoral joint. The primary focus of this review will be on the tibiofemoral joint. The major structures are illustrated in Figure 1.1 and Figure 1.2.

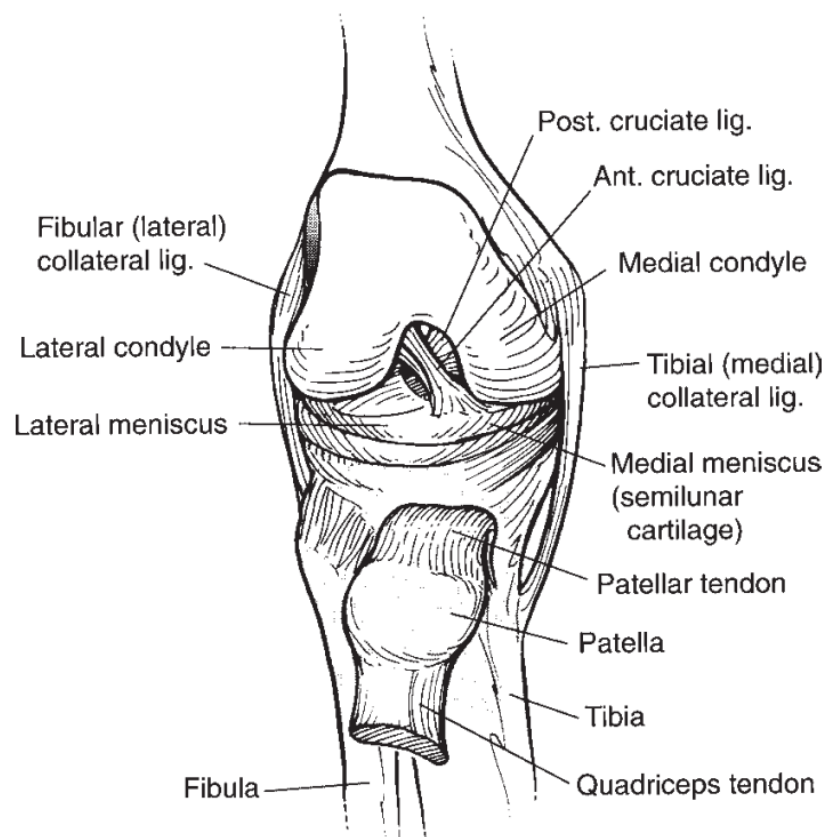


Figure 1.1. Annotated frontal view of the knee joint (Reproduced with permission from: Hamill et al., 2015).

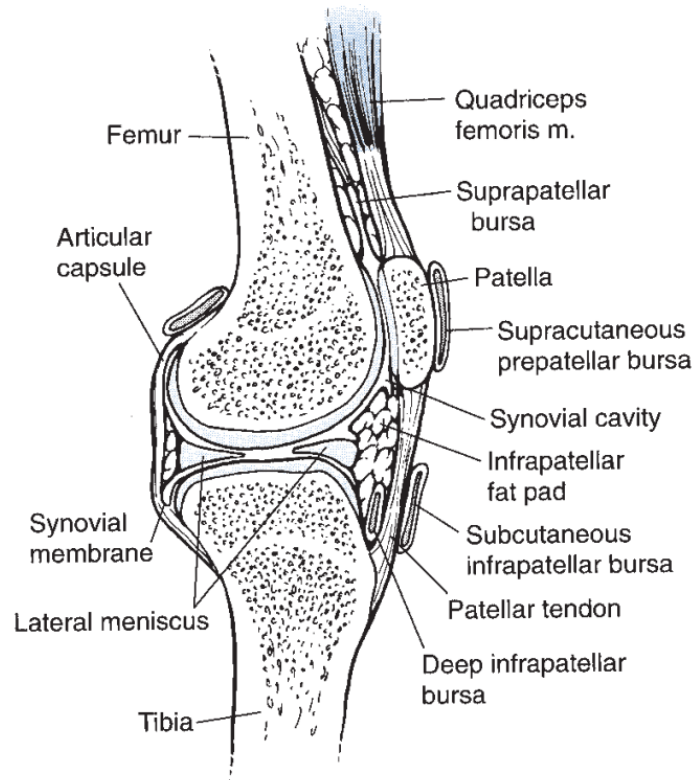


Figure 1.2. Annotated sagittal cross section view of the knee joint (Reproduced with permission: Hamill et al., 2015).

1.2.1.1 Ligaments

There are four main ligaments in the knee joint: the anterior cruciate ligament (ACL) which connects the femur to the tibia and limits anterior tibial translation. The posterior cruciate ligament (PCL) which also attaches to the femur to the tibia to prevent excessive posterior tibial translation during movement. The medial collateral ligament (MCL) attaches the medial epicondyle of the femur to the tibia and limits valgus forces as well as internal and external rotations. The lateral collateral ligament (LCL) attaches the lateral epicondyle of the femur to the head of the fibula and resists varus forces (Hamill et al., 2015).

1.2.1.2 Tendons

The major tendons of the knee are the quadriceps, patella and hamstrings tendons. These structures attach muscles to bone to facilitate movement.

1.2.1.3 Bursae

Several bursae surround the joint capsule (Figure 1.2). These synovial fluid-filled structures provide cushioning and reduce the friction between mobile tendons and bones.

1.2.1.4 Articular Cartilage

Articular cartilage has an incredibly low coefficient of friction to protect the underlying bone and provide smooth articulation of surfaces. Articular cartilage is located on parts of the joint where the most movement occurs such as on the femoral condyles and the articulating surface of the patella and the tibial plateau. Areas of the articular cartilage on the femoral condyles and the tibial plateau interact with the menisci to facilitate fluid sliding surfaces and enhanced chondroprotection (see section 1.4.2.3). Traumatic or degenerative changes to surrounding knee structures and wear overtime can alter the biomechanical equilibrium and damage the articular cartilage as this tissue has a very limited healing capacity (Nordin and Frankel, 2001).

1.2.2 Kinematics of the Tibiofemoral Joint

The tibiofemoral joint is described as hinge-like in nature, because the largest range of motion is along the sagittal plane in flexion-extension (160° to -5°). However, the structural asymmetry also allows rollback, sliding and pivoting motions, causing a range of movements about six degrees of freedom. These include three rotational motions: flexion-extension (FE), abduction-adduction (AA) and internal-external (IE) rotation, and three translational motions: anterior-posterior (AP), medial-lateral (ML) and axial compression-distraction (Shenoy et al., 2013). These six degrees of freedom in terms of the anatomic (frontal, sagittal, transverse) planes of the human body are shown in Figure 1.3.

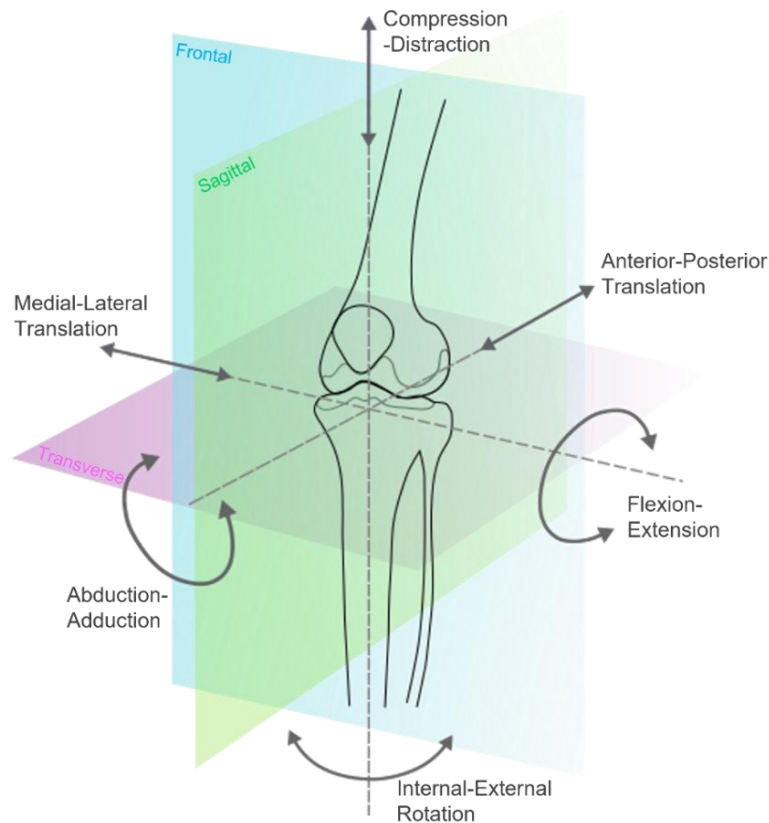


Figure 1.3. Three anatomical planes and six degrees of freedom of the knee joint.

1.2.2.1 Posterior Rollback and Screw Home Mechanism

The tibiofemoral joint facilitates greater degrees of flexion under high loads due to rolling as well as sliding motions performed on the articular surfaces. As the knee flexes, a posterior rollback occurs which causes posterior translation of the contact area and the instantaneous centre of rotation, which is guided by the cruciate ligaments. This increases the lever arm of the quadriceps muscle meaning less effort is required for motion. As flexion increases further, a sliding motion then follows which translates more posteriorly in the lateral compartment due to the asymmetric geometry; this causes the tibia to internally rotate relative to the femur. There can be up to 30° of rotational motion through the tibiofemoral joints full range of motion. As the knee extends, the opposite occurs, and a motion called the screw-home mechanism is facilitated by the condylar geometry as well as the tension in the popliteus muscle. This is when the tibia anteriorly translates and then externally rotates within the last 20° extension. This motion locks the knee into a position of maximum rotational stability, conserving muscular energy at full extension (Stewart and Hall, 2006; Shenoy et al., 2013; Lamb and Guy, 2016).

1.2.3 Kinetics of the Tibiofemoral Joint during Gait

There have been numerous studies quantifying knee motion during the human gait cycle (Figure 1.4). These include cadaveric models, gait-analysis and in-vivo fluoroscopic analysis (Shenoy et al., 2013).

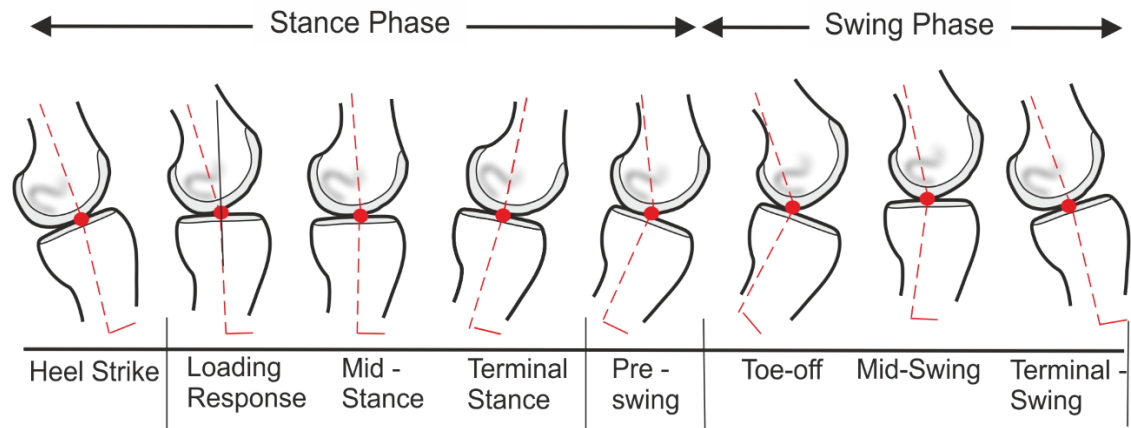


Figure 1.4. Schematic showing the key parts to the human gait cycle and how the knee joint changes during each period.

In the sagittal plane, knee extension peaks at ~ 0 to $\sim 5^\circ$ around mid-stance and knee flexion peaks initially at 20% of the gait cycle during stance phase at $\sim 20^\circ$ to 30° . Later during swing phase at 70% of the gait cycle, flexion peaks again to $\sim 50^\circ$ to $\sim 80^\circ$ just after toe-off. The anterior-posterior tibial translation also follows a similar pattern to the peaks in flexion-extension, with posterior translation of the tibia peaking at 20% and 70% of the gait cycle at values ranging from ~ 2 mm to ~ 6 mm and ~ 11 mm to ~ 18 mm, respectively. The anterior translation of the tibia also peaked at ~ 1 mm to ~ 2 mm past neutral position at the same point in mid-stance when knee extension peaks (Lafortune et al., 1992; Rowe et al., 2000; Baudet et al., 2014).

In the frontal plane, abduction-adduction rotations are minimal during stance phase support, however, after toe-off where flexion peaks at 70%, an increase of either adduction or abduction to $\sim 6^\circ$ to $\sim 8^\circ$ has been observed (depending on subject-specific alignment). Medial-lateral tibial translations of approximately ± 5 mm from the neutral position generally follow a similar pattern to the peaks in flexion-extension during gait, with medial translation of the tibia during flexion and lateral translation of the tibia during extension (Lafortune et al., 1992).

In the transverse plane, throughout the stance phase initiating at heel strike the tibia externally rotates $\sim 3^\circ$ to 5° and then fluctuates around neutral 0° position just before toe-off. As swing phase occurs the tibia internally rotates to a peak of $\sim 9^\circ$ at around 90% of the gait cycle, before heel strike occurs again (Lafortune et al., 1992). Although, more

recent gait analyses in healthy groups have reported peak values of around $\sim 2^\circ$ to $\sim 5^\circ$ (Baudet et al., 2014; Bytyqi et al., 2014).

External forces and moments acting upon the knee include the ground reaction force, gravitational force and inertial forces from the upper leg and foot. These forces and moments are counterbalanced by the surrounding soft tissues and muscles (Kutzner et al., 2010). Such loads have been estimated previously using instrumented prosthesis and inverse dynamics, where the forces and torques are computed from limb motions and the approximate mass of bodily segments (Hamill et al., 2015). Although there are large variations in the literature, it has been generally reported that 200 – 400% of an individual's BW is exerted on the knee joint during the stance phase of gait and the largest contact forces of 3 times BW occur just before toe-off (B Morrison, 1970; Taylor et al., 2004; D Lima et al., 2005; Heinlein et al., 2009; Kutzner et al., 2010).

1.3 The Meniscus

The menisci are highly specialised load transfer devices, functioning under shear, tensile and compressive forces to protect the opposing articular cartilage. The specialised shape and regional cellularisation, vascularisation and microstructural organisation, as well as the interplay between fluid and solid components, allow the menisci to perform a variety of functions critical to knee joint health (Allen et al., 1995; McDermott et al., 2008; Makris et al., 2011).

1.3.1 Gross Anatomy

The medial meniscus and lateral meniscus are semilunar fibro-cartilaginous structures located between the femoral condyles and the tibial plateau (Figure 1.5). The lateral meniscus tends to be more circular in shape and is generally more mobile than the medial meniscus. The medial meniscus is wider posteriorly than anteriorly and has a larger radius of curvature than the lateral meniscus. The medial meniscus is also more tightly connected to the joint capsule. These differences in shape are caused by the asymmetry of the tibial compartments and the differences in loading. Typically, the lateral tibial compartment is convex and the medial tibial compartment is concave, to facilitate internal rotation with flexion (Allen et al., 1995; Fox et al., 2012).

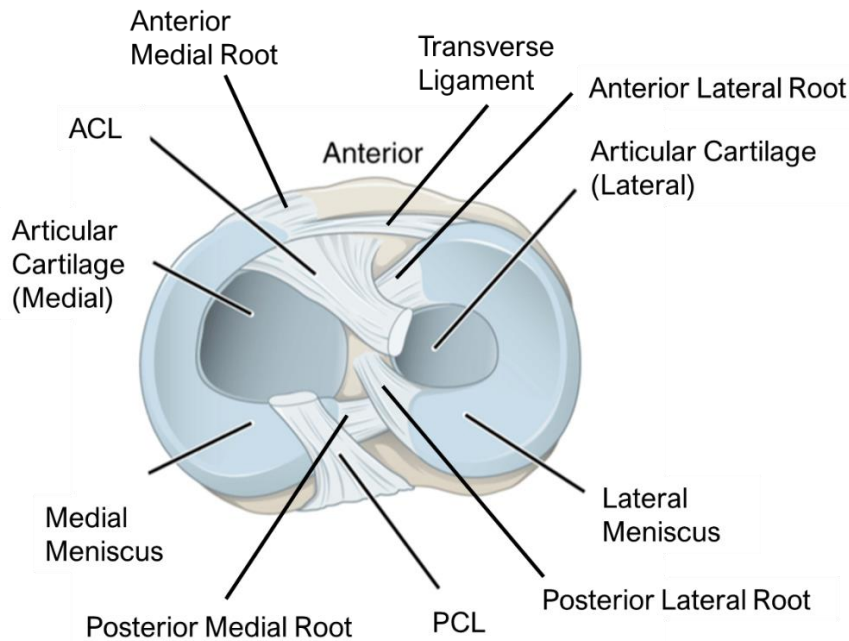


Figure 1.5. Transverse plane section of the tibial plateau showing the medial and lateral menisci and tibial root attachments (Adapted from: Kean et al., 2017).

The menisci are stabilised by strong anterior and posterior roots which connect to intercondylar areas on the tibial plateau (Figure 1.5). The ligament of Humphrey and Wrisberg are auxiliary meniscofemoral ligaments which originate from the posterior root of the lateral meniscus and insert into the posterior medial condyle. It has been estimated that both these ligaments are present in at least 50% of the population and 93% have one of these ligaments (Allen et al., 1995; Athanasiou and Sanchez-Adams, 2009).

1.3.2 Composition and Microstructure

1.3.2.1 Fluid Phase and Solid Phase

The meniscus has been described as a biphasic tissue, meaning it adopts a fluid component and a solid component, which interplay to allow the meniscus to exhibit time-dependent energy absorbing material behaviour under load (Mow et al., 1980; Mow and Lai, 1980; Favnesi et al., 1983; Fithian et al., 1990). The mechanics relating to this material behaviour are explained in section 1.4.1. The meniscus is highly hydrated and made up of around 70% water, which is the most abundant component (Peters and Smillie, 1972). The movement of fluid flow in and out of the meniscus during loading plays a large role in the material properties (Fithian et al., 1990). The remaining 30% consists of the organic (solid) component, of which collagen makes up ~75%. Proteoglycans (~17%), adhesion glycoproteins (<1%), cellular DNA (~2%) and elastin (<1%) make up the remaining composition of the meniscus (Peters and Smillie, 1972; Makris et al., 2011).

The solid component is also termed the extracellular matrix (ECM), mostly consisting of collagen and proteoglycans which have specialised interactions to provide structural integrity and allow the movement of fluid in and out of the meniscus, facilitating its mechanical function (Sanchez-Adams et al., 2011).

1.3.2.2 Collagen

Collagen is a highly abundant fibrillar protein in connective tissues. Collagen types I, II, III, IV, V, VI and XVIII have been found to be present in the meniscus. However, the most abundant type is Type I (~90% of the collagen) (Hasan et al., 2014). Bullough et al. (1970) were the first to report the microscopic ultrastructure and organisation of collagen in the meniscus which was later supported by Petersen and Tillmann (1998) through advances in scanning electron microscopy. The findings of Peterson and colleagues presented distinct layers in collagen structural organisation throughout the meniscus tissue. The meniscal collagen network was found to be arranged into three layers: the superficial, lamellar and the deep (central) layer, these layers are displayed in Figure 1.6.

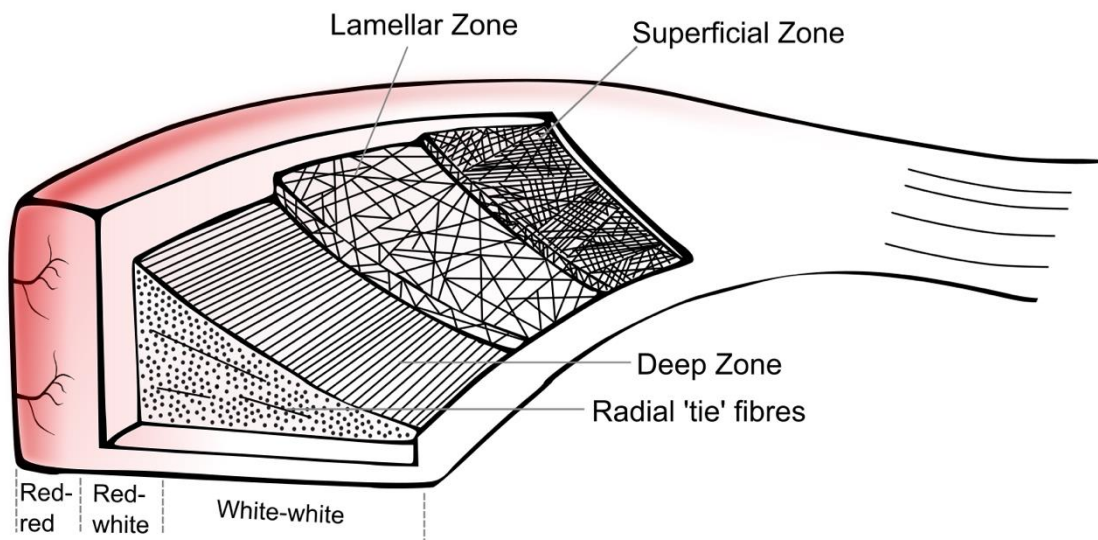


Figure 1.6. Cross-section illustrating the meniscus collagen organisation and differing levels of vascularisation.

Collagen fibres are randomly orientated in the superficial layer and in the lamellar layer, however, in the lamellar layer there is more radial organisation in the anterior and posterior meniscal horns. This random orientation strengthens the surface in all axes to counteract the shear forces from rolling and sliding femoral contact (Abraham et al., 2011). The fibres in the deep region are oriented in a circumferential alignment with radial 'tie' fibres extending from the peripheral regions to the centre of the meniscus. Collagen

fibrils are orientated in the direction of greatest tensile stress, because when axial load is applied, the amount of movement radially outward is limited because the meniscus is anchored to the tibial plateau via the anterior and posterior horns. The orientation of the collagen fibrils in the deep zone reflect the transmission of this load circumferentially into longitudinal hoop stresses to dissipate the load (Petersen and Tillmann, 1998; Hasan et al., 2014). Collagen Type II and Type III fibres are predominantly found in the inner-deep region as well as a higher proportion of proteoglycans; this region has been found to adopt a similar composition to articular cartilage and contributes largely to the compressive properties of the meniscus (Athanasίου and Sanchez-Adams, 2009).

1.3.2.3 Proteoglycans

Proteoglycan molecules constitute a key component of the meniscus ECM and are composed of a core protein with glycosaminoglycan's (GAGs) attached onto it. These GAGs are negatively charged sulphate groups and therefore attract water into the tissue to produce a hydrostatic swelling pressure which resists the compressive forces experienced during loading. The spatial organisation of GAGs agrees with the area of the tissue where the highest compressive load is experienced in the inner-deep zone (Figure 1.7) (Athanasίου and Sanchez-Adams, 2009).

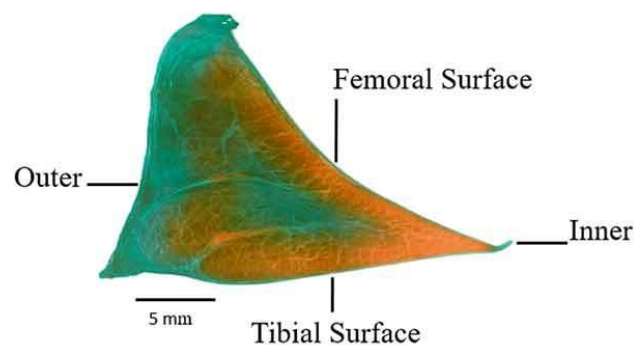


Figure 1.7. Central cross-section of a bovine meniscus showing the varying density of collagen (stained fast-green) and proteoglycans (stained safranin-orange) between the inner and outer zones. (Reproduced with permission: Andrews et al., 2017, p. 274).

1.3.2.4 Elastin

Elastin is another fibrillar protein found in the meniscus and constitutes only a small amount of the total composition (< 1%) (Peters and Smillie, 1972). Elastin's role in meniscal function is largely unknown, however, in other tissues such as blood vessels, elastin provides the recoil resiliency (Athanasίου and Sanchez-Adams, 2009). Therefore, it

is thought that small amounts of elastin fibres bridge with the collagen fibres to allow the meniscal shape to recover after deformation (Höpker et al., 1986).

1.3.3 Cellularity and Vascularisation

Meniscal cells are termed fibrochondrocytes as they have characteristics of both fibroblasts and chondrocytes. Chondrocytes are found in articular cartilage and synthesise Type II collagen, whereas fibroblasts are found in connective tissues and predominantly synthesise Type I collagen. Regional and morphological variations of fibrochondrocytes exist throughout the meniscus and correlate with tensile and compressive function. The cells in the outer region adopt a more fibroblast-like appearance, whilst in the inner region of the meniscus the cells adopt more of chondrocyte appearance, similar to that of articular cartilage (McDevitt and Webber, 1990; Makris et al., 2011).

As well as cellularity, the meniscus is specialised to have differing regions of vascularity. As presented previously in Figure 1.6, these regions are labelled: the red-red zone (outer region, vascularised by the peri-meniscal capillary plexus (PCP) attached to the joint capsule), the red-white zone (transition zone, semi-vascularised) and the white-white zone (inner region, avascular). The zone of vascularisation relates to the healing capacity of the meniscus and therefore surgical decision. Damage to the avascular white-white zone, constituting about two-thirds of the meniscus is usually permanent and may require surgical intervention (Petersen and Tillmann, 1995).

1.4 Meniscus Biomechanics and Structure-Function Relationship

In the early-mid 1900's the meniscus was thought to be a functionless piece of detached muscle and pain occurring after removal of the meniscus (meniscectomy) was thought to be due to residual pieces of the meniscus remaining in the knee (McMurray, 1942; McDermott and Amis, 2006). Since then, numerous studies have shown the meniscus plays a vital mechanical role in knee joint chondroprotection, stabilisation and lubrication through various structural mechanisms.

1.4.1 Fundamental Tissue Mechanics

Prior to reviewing the functional biomechanics of the meniscus in whole knee joint models, it is important to understand the fundamental tissue mechanics and the research endeavouring to define the material properties of the meniscus.

1.4.1.1 Tension

A stretching force applied to a fibrous biological tissue, such as the meniscus, will cause a resultant deformation. The tensile properties are defined as the tissue behaviour in response to a stretching force. Two things occur in this situation: (1) the tissue will elongate and (2) a force will develop and increase within the tissue, up until the point of fracture/breakage of the specimen. The curve shown in Figure 1.8 can be related to the action of the collagen fibrils within the tissue. The toe region shows relaxed collagen fibrils as only a small amount of force is required to elongate the specimen initially. During the linear region, the collagen fibrils stretch and a linear relationship occurs prior to early signs of individual collagen fibre failure; shown through small load decreases. The yield point describes the point where major breakages of collagen fibres bundles occur and therefore irreversible (plastic) deformation. The maximum force measured is the ultimate tensile load of the specimen and the stiffness is a structural property which describes the linear relationship between load and elongation (McDermott et al., 2008). This relationship can be represented as a stress-strain curve to describe the material properties of the specimen so comparisons can be made between other tissues, independent of the specimen dimensions. The stress and strain calculations adjust for the specimen cross-sectional area and specimen length, respectively, to give the Young's Modulus of the material (Nordin and Frankel, 2001; McDermott et al., 2008).

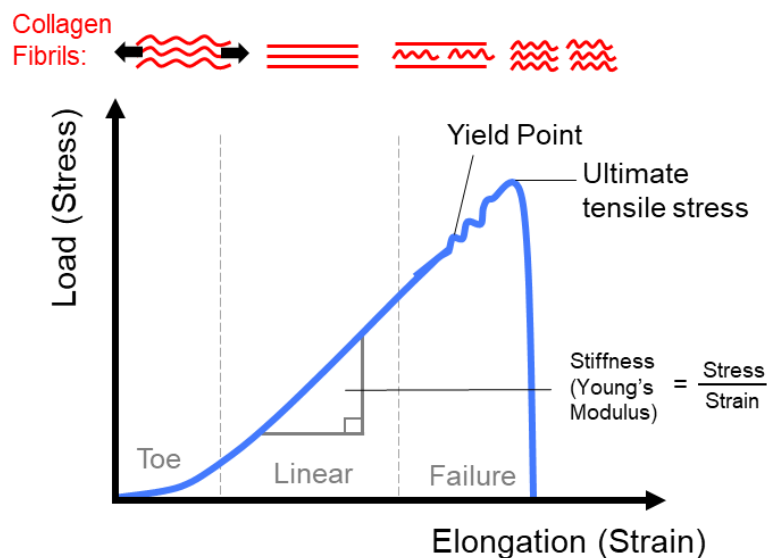


Figure 1.8. Meniscus tissue mechanics stress – strain curve under tensile forces.

1.4.1.2 Compression

The compressive properties of the meniscus are described as the tissue behaviour in response to a pushing force. The compressive resilience of the meniscus as a material

follows the biphasic theory firstly proposed by Mow et al. (1980) for articular cartilage and later supported for the meniscus by Favenesi et al. (1983) examining bovine menisci. Research suggests the mixture and interplay between the solid and fluid components of the meniscus are crucial for it functioning under high compressive loads.

The meniscus is described as a time-dependent material under compression because the properties, and therefore the functionality, change with the duration of the applied load. This behaviour can also be described as viscoelasticity, which refers to the interplay between elastic (reversible) behaviour of the collagen fibres of the solid phase and the simultaneous interstitial pressure and extrusion of the fluid phase, which is dependent on fluid viscosity and tissue permeability (McDermott et al., 2008). Viscoelastic materials adopt two main sub-behaviours: creep and stress-relaxation.

As illustrated in Figure 1.9, creep response is the behaviour which occurs when a constant compressive force is applied to meniscus tissue, a resultant near-linear deformation occurs initially, which is mostly due to the elastic response behaviour of the collagen network. Concurrently, the proteoglycan GAGs which attract water into the tissue ensue a high osmotic pressure of the fluid component. As the duration of load-application increases the rate of deformation decreases to a plateau, where the fluid-phase dominates as there is gradual extrusion of the fluid from the tissue. On the other hand, stress relaxation describes the time-dependent reduction in the applied load required to maintain a defined deformation (Figure 1.9). This occurs in a similar way because the water is slowly exuded from the meniscus tissue. The low relative permeability of the meniscus tissue compared with cartilage tissue allows effective maintenance of volume underload, giving an immense chondroprotective effect (Nordin and Frankel, 2001; McDermott et al., 2008).

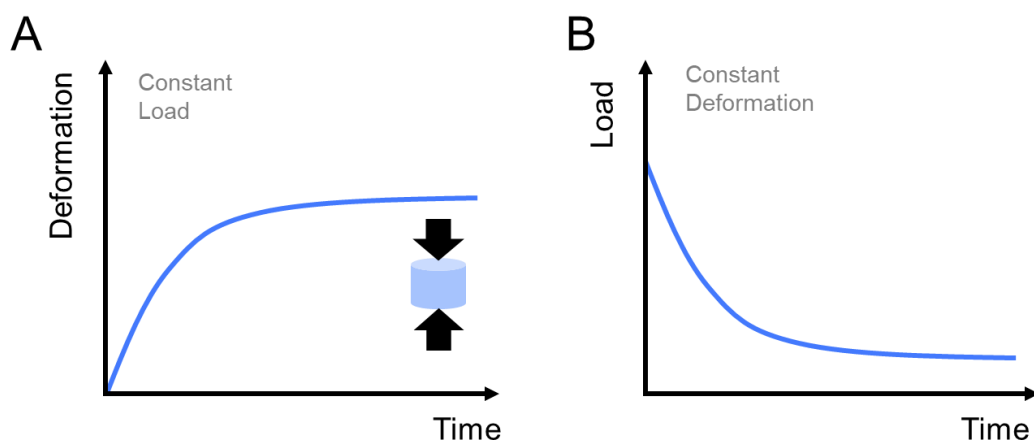


Figure 1.9. Meniscus tissue mechanics under compressive forces showing (A) creep characteristics when subject to a constant load and (B) stress relaxation characteristics when held at a constant deformation.

1.4.1.3 Material Properties

A summary of the tensile and compressive material properties of human menisci studies is shown in Table 1.1 on the next page. These properties vary depending on meniscus body location (anterior, posterior, middle), structural / zonal depth (inferior, superior) and section orientation (Setton et al., 1999; Makris et al., 2011).

Table 1.1. Material properties of human medial meniscus tissue specimens.

<i>Properties</i>	<i>Study</i>	<i>Direction</i>	<i>Location</i>	<i>Stiffness (MPa ± SD)</i>
Tensile	Tissakht et al.	Circumferential	Anterior	106.21 ± 77.95
			Central	77.95 ± 25.09
			Posterior	82.36 ± 22.23
		Radial	Anterior	48.31 ± 24.35
			Central	46.20 ± 27.56
			Posterior	32.55 ± 11.27
<i>Properties</i>	<i>Study</i>	<i>Zone/Depth</i>	<i>Location</i>	<i>Aggregate Modulus (MPa ± SD)</i>
Compressive	Sweigart et al.	Superior	Anterior	0.15 ± 0.03
			Central	0.10 ± 0.03
			Posterior	0.11 ± 0.02
		Inferior	Anterior	0.16 ± 0.05
			Central	0.11 ± 0.04
			Posterior	0.09 ± 0.03

Tensile properties of the human meniscus and other mammalian species have been previously reported (Whipple et al., 1985; Fithian et al., 1990; Tissakht and Ahmed, 1995; Goertzen et al., 1997). Tensile assessment has been achieved through extracting a dumbbell shaped section of the meniscus. This geometry is useful in defining the cross-sectional area for stress calculation whilst ensuring the ends of the specimen can be clamped by the force apparatus. The meniscus tissue is described as an anisotropic material because it has a higher tensile stiffness in the circumferential direction compared with the radial direction, which is largely due to the circumferentially aligned collagen network in the deep zone (Whipple et al., 1985; Fithian et al., 1990). Whipple et al. (1985) were the first to show the anisotropy of the bovine meniscus tissue in tension by assessing circumferential and radial orientated dumbbell sections. This was then later found for human meniscus sections (Fithian et al., 1990; Tissakht and Ahmed, 1995). In addition, Lechner et al. (2000) investigated the tensile circumferential modulus of 30 human medial meniscus samples and found that the cross-sectional area of the sample had a significant inverse effect on the tensile stiffness. However, the researchers also reported a high amount of sample failure within the smallest slice-thickness group. The researchers

suggested this could be due to some specimens being composed of solely matrix (taken from the gaps in between the collagen bundles) and other sections including the collagen bundles; causing stiff and weak samples in the same group.

Compressive meniscus properties are usually assessed through extracting cylindrical plugs from meniscal regions. As shown in Table 1.1, the compressive properties of meniscus tissue are usually measured as the aggregate modulus and the permeability. The aggregate modulus takes into account both the measured Young's modulus and the Poisson Ratio, which is a measure of the material stiffness when fluid flow has ceased. A higher aggregate modulus denotes higher resistance to deformation under load. Previous literature has found that the compressive properties vary with respect to meniscus region (anterior, middle, posterior) and zonal depth (superficial vs deep) (Favenesi et al., 1983; Proctor et al., 1989; Sweigart et al., 2004).

These factors demonstrate the difficulty in defining comparable meniscus material properties due to the complex heterogeneity of the meniscus structure. Designing and developing a new intervention to be biomechanically similar to the natural meniscus should not solely rely on uniaxial assessment of tissue sections, because in the natural knee joint, the meniscus is subject to highly specific shear, compressive and tensile forces concurrently.

1.4.2 Functional Biomechanics

The menisci are frequently described as having separate biomechanical functions to ultimately protect the articular cartilage. However, all these functions described in the following sub-sections are not mutually exclusive from one another; if one function is impeded, the other functions will be hindered. The meniscus can be seen as having simultaneous functionality.

1.4.2.1 Load Transmission

The specialised geometry and microstructure allow the meniscus to achieve the goal of protecting the articular cartilage by transmitting 45% – 75% of the axial load between the femoral condyles and the tibia (Fairbank, 1948; Seedhom, 1979; Ahmed and Burke, 1991). In numerous experimental studies, removal of the meniscus (meniscectomy) has been shown to increase joint contact pressure through the reduction of contact area (Walker and Erkman, 1975; Krause et al., 1976; Kurosawa et al., 1980; Baratz et al., 1986).

Fairbank (1948) were the first to radiologically investigate changes to the knee joint before and after meniscectomy. Joint space narrowing and flattening of the femoral

condyles were observed from the radiographs. In later years, the load bearing function was further established in biomechanical studies using pressure-sensitive films (Kurosawa et al., 1980; Baratz et al., 1986). Kurosawa et al. (1980) found that the average stress increased by 2-3 fold with meniscectomy. Similarly, Baratz et al. (1986) measured a 2-fold increase in contact pressure with meniscectomy and found the amount of meniscus removed positively correlated with increased contact pressure.

The fundamentals of this mechanism can be explained through the simple contact force, contact pressure, and contact area equation using rigid bodies shown as a ball (femoral condyle) and a shallow cup (meniscus) on a flat surface (tibial plateau) (Figure 1.10).

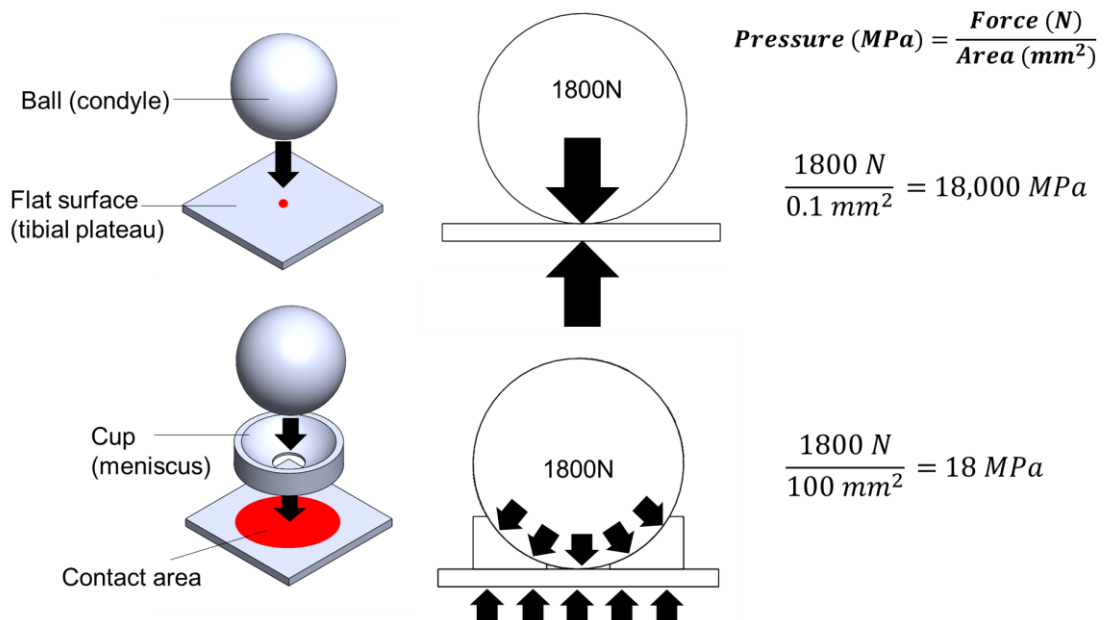


Figure 1.10. Simple geometric model of meniscus function reducing the contact pressure through increasing the contact area on the flat surface. The ball represents the femoral condyles, the plate represents the tibial plateau and the shallow cup represents the meniscus. An axial load of 1800 N approximately represents 2.5 times BW of a 70kg man during the stance phase of gait.

The simple model above can be further applied to the deformable meniscus macro and microstructure bearing load between the femoral and tibial contact (Shrive et al., 1978; McDermott et al., 2008; Fox et al., 2012). As shown in Figure 1.11, when axial load is applied initially, the shape of the meniscus allows the pressure from the curved femur to be applied as a horizontal and vertical pressure (F_{Femur}). Because the tibia is relatively flat, this applies an opposing vertical pressure (F_{Tibia}). The vertical pressures cancel out, leaving the femurs horizontal pressure to act as a radial vector on the tissue. The hydrostatic pressure of the tissue and the circumferential alignment of collagen in the deep zone converts the radial vector into hoops stresses causing a resultant circumferential

force (F_{cir}) which causes the tissue to radially deform and dissipate the load (Shrive et al., 1978). This deformation keeps the loaded knee in a stable position by widening the contact base and maintaining congruent contact with the femur.

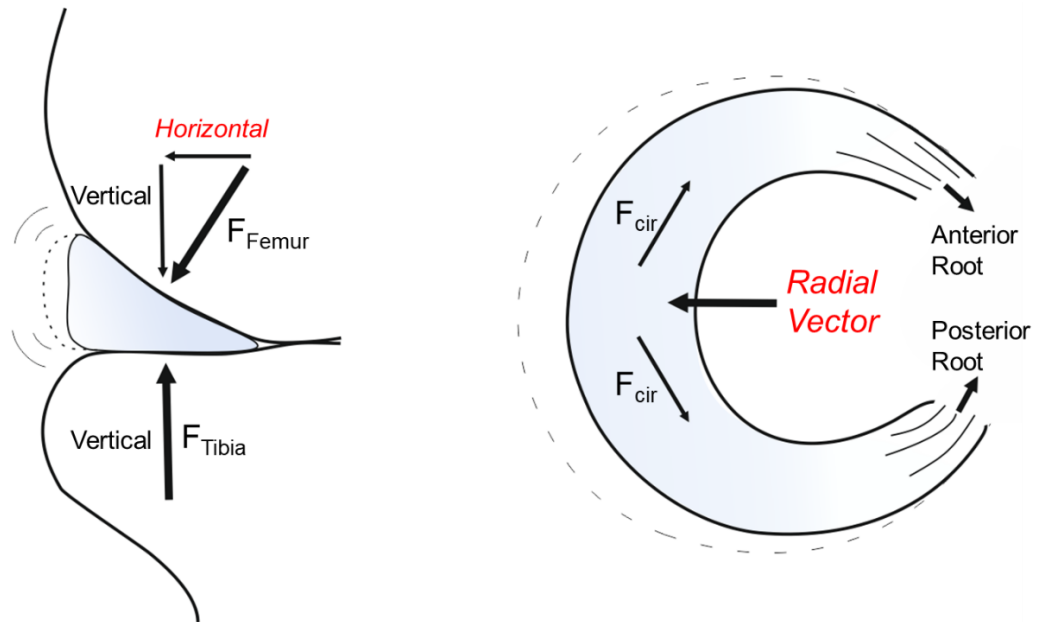


Figure 1.11. Load bearing mechanism of the meniscus showing radial expansion of the meniscus caused by the horizontal pressure of the femoral axial force converted to the radial vector which is distributed through the circumferential force of the collagen network.

1.4.2.2 Meniscal Motion and Joint Stabilisation

The menisci play a crucial role in keeping the articulation within the knee's kinematic constraints. Meniscal movement is facilitated by the structure and the root attachments which stabilise the changing position and curvature of the incongruent femoral and tibial surfaces during the translational and rotational kinematics during gait (Fukubayashi et al., 1982; Shoemaker and Markolf, 1986; Thompson et al., 1991). As the knee flexes the instantaneous centre of rotation shifts posteriorly (see section 1.2.2), and the menisci also move posteriorly and deform in order to stabilise the knee and keep the articulation within the greatest area of contact (Thompson et al., 1991; Vedi et al., 1999; Kim et al., 2015). This movement means the contact area is continuously satisfying the load transmitting behaviour of the meniscus microstructure.

This movement was firstly presented by Walker and Erkman. (1975) using a qualitative casting technique in cadaveric knee joints and an Instron. Cement (methylmethacrylate) castings were made of the tibial plateau at 0°, 30°, 60° and 90° flexion angles, whilst applying 0N, 500N, 1000N and 1500N loads at each flexion angle.

The results showed the contact area moved posteriorly and spread toward the lateral edges of the tibial plateau with increasing flexion and load.

In later years, further advances in imaging technology such as magnetic resonance imaging (MRI) allow this effect to be measured quantitatively during in-vitro cadaveric studies (Thompson et al., 1991) and in-vivo participant studies (Vedi et al., 1999; Yao et al., 2008). Potentially the most notable study on meniscus translation was Vedi et al. (1999) who quantified in-vivo movement of the menisci using MRI and infrared trackers on 16 young healthy males. A novel seating set up was used so participants could squat, stand and sit whilst being scanned. In the transverse plane, the medial and lateral menisci deformed towards the posterior direction from 0° extension to 90° flexion in weight bearing and non-weight bearing conditions. On average the lateral menisci moved more than the medial menisci and the anterior more than the posterior (Figure 1.12).

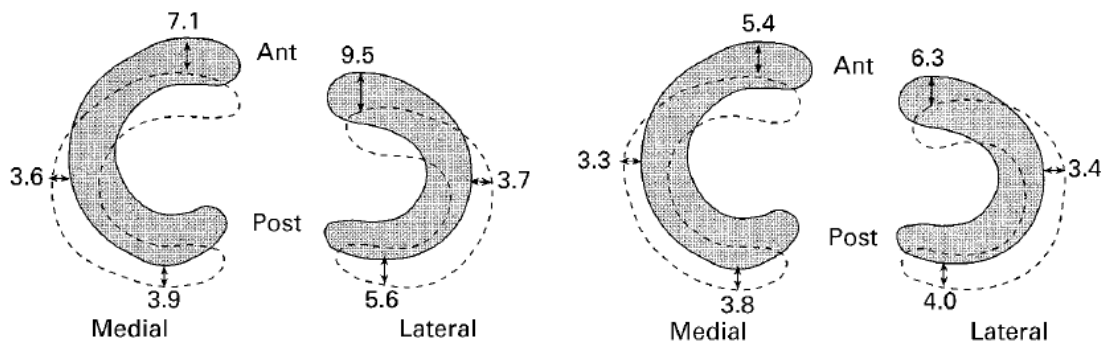


Figure 1.12. Schematic representation of the meniscal movement from 0° extension to 90° flexion during weight bearing (A) and non-weight bearing (B) conditions. Measurements are in millimetres (Reproduced with permission: Vedi et al., 1999, p. 39).

Moreover, the mechanics under compression, the specialised wedge shape and the meniscus mobility are believed to contribute to joint stabilisation, similar to a secondary ligament (McDermott et al., 2008; Fox et al., 2012). The stability of the joint can be described as the resistance to large rotations or translations when subject to external forces (Reynolds et al., 2017). There have been a handful of studies reporting the stabilising effect of the meniscus under load and in the absence of key stabilising ligaments, such as the ACL (Hsieh and Walker, 1976; Shoemaker and Markolf, 1986).

1.4.2.3 Biotribology and Joint Lubrication

The term biotribology describes the study of two contacting biological surfaces in relative motion and includes the principles: friction, wear and lubrication (Zhou and Jin, 2015). Experimental simulation studies have shown the effect of the bovine meniscus

reducing the amount of friction and wear on opposing articular cartilage (McCann et al., 2008; McCann et al., 2009). However, despite both the femoral and tibial surfaces of the meniscus being in direct sliding contact with the articular cartilage of the knee joint, only a small amount of research has been carried out examining the specific tribological mechanisms which occur between these surfaces.

The meniscus is proposed to control excessive friction and wear on the cartilage surfaces through specific lubrication regimes. The meniscus has been found to be a biphasic tissue like cartilage and it is postulated a low-friction area of contact is formed between the two surfaces through a similar biphasic lubrication process (Mow et al., 1980; Forster and Fisher, 1996). Biphasic lubrication theory states that friction is modulated initially by the hydrostatic pressure of the fluid, taking on approximately 90% of the contact load. As the fluid is slowly exuded, the solid matrix starts to take on more of the contact load. This reduces the friction and wear between the solid phases of the tissues, until the majority of the fluid is exuded and the solid phases start to solely bear the contact load (Nordin and Frankel, 2001; Ateshian, 2009).

Further research includes findings to suggest the autologous nature of the meniscus and cartilage surfaces (Andrews et al., 2017). Schumacher et al. (2005) found that meniscus fibrochondrocyte cells secrete a protein called proteoglycan 4 or lubricin, and that this protein was present in a thin layer on the meniscus surface, which had also been found in a thin layer on the cartilage surface. The researchers proposed that lubricin may aid a boundary lubrication regime with articular cartilage. Boundary lubrication describes the reduction of friction through molecules rolling over each other at the contact surfaces.

1.5 Meniscus Injury: Meniscal Extrusion

The meniscus is one of the most commonly injured tissues in the knee joint, affecting 60 - 70 per 100 000 people in the UK (Ahmed et al., 2020). There are many forms of meniscus pathology, however, this review will focus on the relatively overlooked clinical condition of meniscus extrusion, due to its high clinical association with osteoarthritis (Gajjar et al., 2021).

1.5.1 Types of Meniscus Extrusion

Meniscal extrusion is described as the displacement of the meniscus, protruding past the tibial plateau margin (Costa et al., 2004). Meniscal extrusion can manifest in two forms: physiological and pathological (Gajjar et al., 2021).

1.5.1.1 Physiological

A certain degree of meniscal movement is required for the meniscus to dissipate load and stabilise the knee joint due to the natural action of the collagen fibres responding to tensile strain. However, there is little research on quantifying this movement in response to natural loading as imaging studies usually only have sample sizes of around 20 subjects. For example, it has been previously estimated using frontal plane MRI scans that the medial meniscus moves on average 2mm (range: 1.2 mm – 2.6 mm) outside the medial border of the tibial plateau during natural weight bearing in healthy subjects (Boxheimer et al., 2004). However, a more recent study of 75 healthy subjects found that this measurement is dependent on age, BMI and the loading condition the medial image was taken from (Achtnich et al., 2018).

1.5.1.2 Pathological

On the other hand, meniscal extrusion is a pathological condition where the meniscal body is displaced outside of the joint space in an abnormal manor. This is typically described in clinic as a displacement > 3 mm (Costa et al., 2004; Lee et al., 2011). Pathological extrusion can be divided into two forms: traumatic and degenerative, described later in section 1.5.3. Both forms result in a disruption to the circumferential collagen fibre structure causing a loss of hoop strain resistance (Muzaffar et al., 2015). This results in load being applied to a reduced contact area and therefore increases the contact pressures upon the articulating cartilage leading to accelerated chondral degeneration (Figure 1.13). Meniscal extrusion has been associated with joint space-narrowing, knee deformities, osteonecrosis and OA (Gajjar et al., 2021).

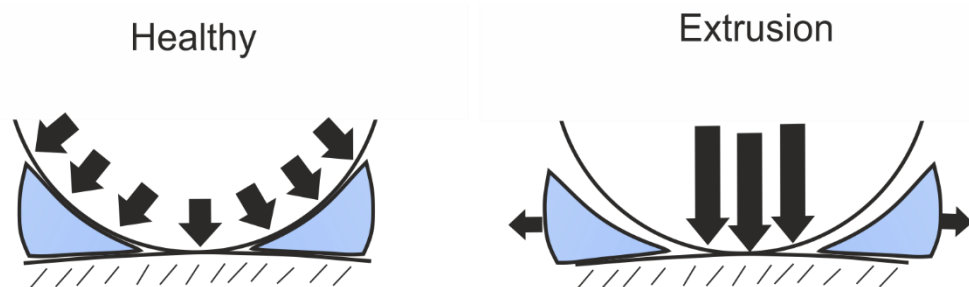


Figure 1.13. Loading differences across the knee between a healthy meniscus and an extruded meniscus.

1.5.2 Diagnosis

The 'gold standard' to diagnose meniscal extrusion is a non-weight bearing mid-frontal plane MRI scan, where the chosen measurement slice is the one with the largest

area of medial tibial spine. If the meniscus is extruded > 3 mm past the line of the tibial plateau, at the posterior border of the MCL, this is classed as severe meniscal extrusion (Costa et al., 2004; Lee et al., 2011; Nogueira-Barbosa et al., 2015).

Efforts could be made to improve the gold standard to diagnose meniscus extrusion. This method is relatively robust, however, abnormal meniscus position in other areas, changes during weight bearing and changes during movement are disregarded. Extending the method to view a slice in the sagittal plane or at different flexion angles may be beneficial (Kim et al., 2015; Masuda et al., 2018). The complexity of meniscal kinematics makes it very difficult to quantify thresholds for pathological extrusion.

One of the research challenges is quantifying the degree of extrusion that is classed as healthy and what is classed as a biomechanical risk. However, the clinical foundation from which the > 3 mm threshold manifested is unclear and the severity is likely underestimated as the radiographs are usually taken in the unloaded supine position. Costa et al. (2004) firstly used this measure on 105 knees with damaged menisci, to determine whether the severity of meniscal extrusion, defined as minor (< 3 mm) and major (> 3 mm), related to degeneration and type of meniscal damage. Findings suggested that major meniscal extrusion highly correlated with degeneration, tears of the root and large radial tears to the body of the meniscus. However, this study failed to separate age groups and had a large age range of 34-83 years. It is likely that the older patients have underlying chondral damage which presents confounding factors when measuring meniscal extrusion.

Other previous studies have used different methods to measure extrusion, such as calculating the distance from the tibial margin as a percentage of the meniscus body, using different planes/flexion angles (Crema et al., 2012; Kim et al., 2015; Masuda et al., 2018; Paletta et al., 2020). There have also been some developments in quantifying the position of the meniscus body using quantitative MRI scans and 3D modelling software (Wenger et al., 2013). However, the majority keep to the mid-frontal plane body measurement due to the ease and reproducibility (Swamy et al., 2018).

1.5.3 Causes and Associations

1.5.3.1 Traumatic Meniscal Extrusion

Meniscal tears are the most common injury reported by orthopaedic clinicians with an annual incidence of ~ 61 per 100,000 people (McDermott and Amis, 2006). Tears are caused by degenerative changes in older patients (> 50 years old) and traumatic injury, most commonly ACL injury, in younger patients (< 50 years old). Tears can occur anywhere in the meniscal body and are classified in terms of their morphology observed on MRI scans and through arthroscopy (Hasan et al., 2014). Although, any meniscal

trauma can result in meniscal extrusion, the most common type of tears causing medial meniscal extrusion are located in the posterior root of the medial meniscus (Costa et al., 2004; Kim et al., 2020). Currently, there is no official standardised classification system for meniscal root tears, however, a previous study grouped 71 torn menisci into five groups using morphological arthroscopic examination. This study found the most common type and location of medial meniscus root tear is a complete radial tear within 3 to 9 mm of the root insertion (Type 2, Figure 1.14) (LaPrade et al., 2015).

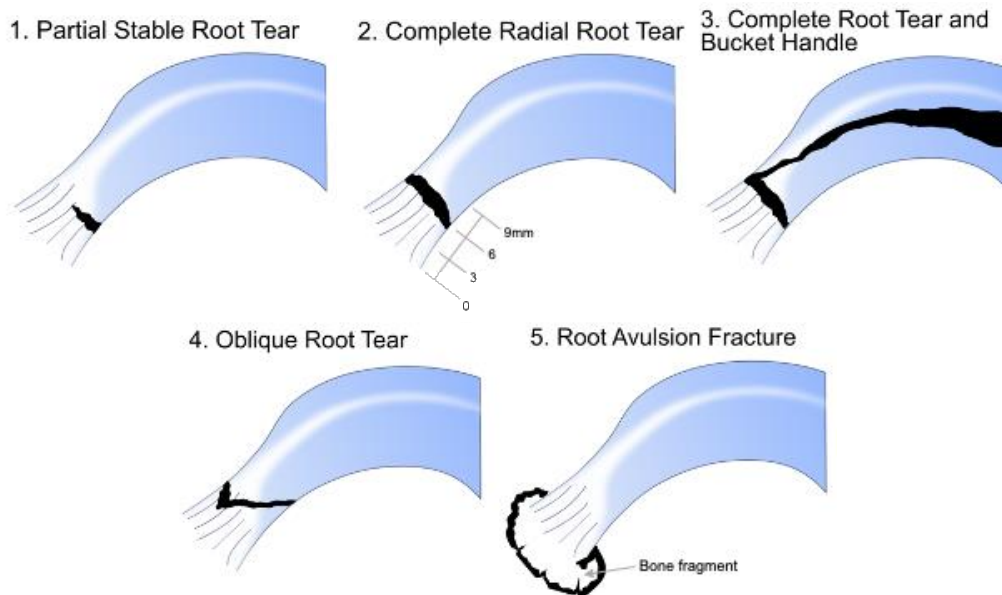


Figure 1.14. Morphological classification of meniscal root tears. The tear most associated with meniscus extrusion is number 2; the complete radial root tear.

Root tears cause severe disruption to the load dissipating properties (hoop tension) of the meniscus structure as they propagate perpendicularly to the circumferential collagen alignment (Petersen et al., 2014). The medial posterior region has a higher stiffness and reduced mobility in order to bear more load during deep knee flexion, however, this makes this region more susceptible to injury (Costa et al., 2004; Crema et al., 2012). Biomechanical cadaveric studies have previously reported that the presence of these tears increase tibial contact pressures similar to that of meniscectomy conditions (Allaire et al., 2008; Marzo and Gurske-DePerio, 2009; Kim et al., 2013).

A recent study by Krych et al. (2020) reporting variations in clinical decisions and outcomes between lateral and medial meniscus root tears found that of the 109 patients with medial meniscus root tears, 79 had meniscus extrusion > 3mm (72.5%). Only 6 of the 30 patients with lateral meniscus root tears had meniscus extrusion > 3mm (20%). On the other hand, 24 patients with lateral meniscus root tears had concurrent ACL injury. The lateral meniscus root tears more acutely in younger active patients and medial meniscus root tears are usually chronic, occurring in older patients with underlying degeneration.

Minor acute events can trigger a complete medial meniscus root tear with underlying degeneration. To the authors knowledge, there is only one study which comments on the acute aetiology of a medial meniscus posterior root tear. In a sample of 100 patients (age 50 -70 years), 38% were descending stairs, 18% were walking at a normal pace and 13% initiated the tear through high flexion activities such as squatting. Other activities such as standing up from a chair or sports accidents were <10% of cases (Furumatsu et al., 2019). Unfortunately, root tears are less sensitive to MRI scans, meaning it is likely the incidence of meniscal root tears is under-reported due to the difficulty in diagnosis compared to other tear types (LaPrade et al., 2015).

1.5.3.2 Degenerative Meniscal Extrusion

It is possible that over a longer and slower period of time, the microarchitecture of the meniscus loses integrity due to repetitive loading and natural aging. This cause's degenerative meniscus extrusion, however, this form is generally under reported and undetected compared with traumatic meniscus extrusion. Due to the slow nature of this pathology, by the time it is diagnosed, patients would likely have associated OA or other knee pathologies. Clinical OA studies have shown a difference between the numbers of patients with meniscal tears and the number of patients with meniscal extrusion; degenerative extrusion could represent these patients (Roemer et al., 2009). In addition, tears also result from underlying degeneration, therefore it is likely that degenerative and traumatic meniscal extrusion occur together.

1.5.3.3 Meniscocapsular Separation / Meniscotibial Ligament Injury

Meniscocapsular separation describes the detachment of the medial meniscus with the capsule and are usually caused in conjunction with ligament injury. These tears are relatively infrequent but are likely underreported as they heal more readily in the red-red zone. There is some conflicting evidence, but it remains unknown if these tears lead to meniscal extrusion (De Maeseneer et al., 2002). In addition, the meniscotibial and meniscofemoral (coronary) ligaments are located between the medial meniscus and the deep portion of the MCL (Figure 1.15). There are reports of damage to specifically the meniscotibial ligament leading to increased meniscal displacement as the medial meniscus is less restricted by the capsular boundary which may have less stabilising tension from the injury. Meniscus extrusion is rarely an acute isolated disease, with most cases associated with previous trauma or knee pathology, however a study by Krych, Bernard, Leland, et al. (2020) found that 20 / 3244 MRI (0.62%) reports with meniscal extrusion had no reported knee pathology. However, all these patients with > 3mm meniscal extrusion (n = 9) had associated meniscotibial ligament abnormality. In general,

there is a lack of research investigating interactions between the capsule and the medial meniscus.

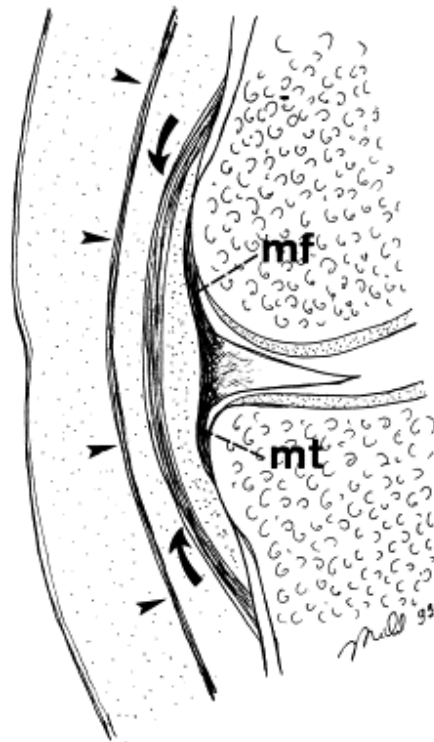


Figure 1.15. Frontal plane (central slice) of the medial side of the knee joint showing the knee capsule and supporting structures; the superficial knee capsule line (arrowheads), the superficial line of the MCL (curved arrows) and the meniscofemoral (mf) and meniscotibial (mt) ligament extensions located in the deep portion of the MCL. (Reproduced with permission: De Maeseneer et al., 2002. p.243).

1.5.3.4 Post-Operative Meniscal Extrusion

There is a handful of research relating to meniscal extrusion which occurs post-operatively after meniscal root repair, allograft replacement and ACL reconstruction procedures (Gajjar et al., 2021). Post-operative meniscal extrusion increases a patient's risk of OA in later life and should be reported to evaluate the efficacy of treatments. Meniscal allograft transplantation (MAT) is rarely performed but post-operative extrusion has been shown to occur frequently at follow-up. A meta-analysis of MAT procedures and follow-up MRI examinations found in 21 MAT studies a pooled mean of 53% showed major extrusion (> 3mm) on MRI within 1 year of surgery (Lee, 2018).

On the other hand, there are studies which support MAT, finding no significant incidence of graft extrusion within 1 year of surgery (Kim et al., 2018). However, extrusion has not been extensively assessed at medium to long term follow up, nor has native extrusion prior to surgery been considered. Post-operative extrusion could occur due to the replacement tissue integrity, loading differences, recovery protocols or non-anatomic

surgical positioning, or potentially a combination of all these factors? It is possible the surgical damage associated with graft insertion might have an effect, as the meniscotibial ligament and popliteomeniscal fascicle are sometimes removed in MAT which both function to provide anchorage for the meniscus (Krych et al., 2018; Paletta et al., 2020). Again, the interactions between the native knee fascia and meniscus function need to be better understood.

1.5.3.5 Meniscal Extrusion and Osteoarthritis

Meniscal extrusion can not only be indicative of meniscus trauma or degeneration but can also highlight other underlying pathologies. OA is usually defined as a disease with a non-linear progression, meaning some patients may deteriorate rapidly and some may deteriorate gradually. It is still unclear whether meniscal extrusion precedes or proceeds OA, however there is a strong relationship between both pathologies (Gajjar et al., 2021). Wenger et al. (2013), used quantitative MRI scans and 3D modelling to define the coverage of meniscal body in patients with medial compartment OA. This group found that the patients with OA had significantly less medial meniscus coverage of the tibial plateau, significantly increased medial meniscus extrusion and a significantly more convex shape to the peripheral medial meniscus border in the frontal plane. In addition, the lateral meniscus in OA patients showed significantly more meniscus extrusion and convex 'bulging' of the peripheral margin, but no significant difference in tibial plateau coverage (Figure 1.16).

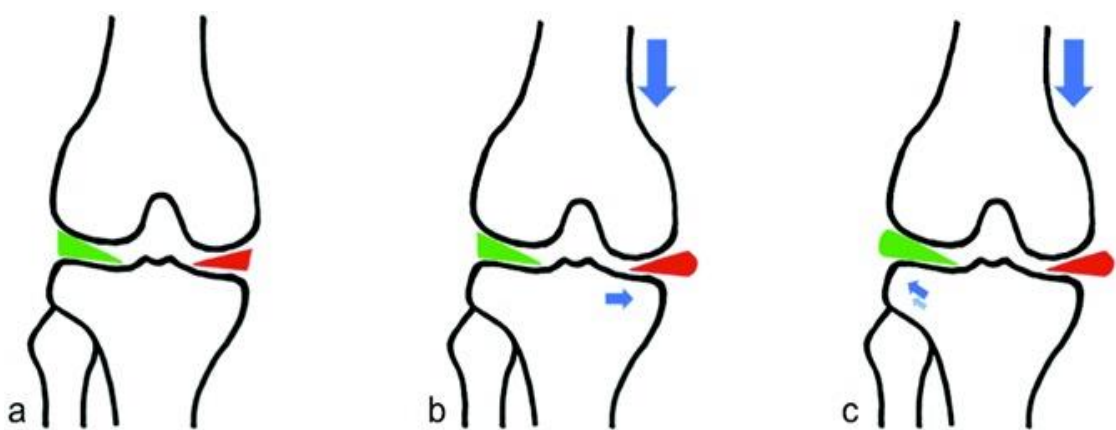


Figure 1.16. Changes in the position and shape of the lateral meniscus (green) and medial meniscus (red) in (a) healthy patients, (b) loading effects on the medial meniscus in patients with medial compartment OA and (c) loading effects on the lateral meniscus in patients with medial compartment OA (Reproduced with permission: Wenger et al., 2013, p. 1808)

The Multicentre Osteoarthritis Study (MOST) prospectively assessed patients at risk of developing OA between the ages 50-79. Roemer et al. (2009) used 347 knees from this study to assess potential predictors of fast and slow articular cartilage loss over a 30-month prospective period using radiographs and MRI. Within this time, 257/347 had no articular cartilage loss, 70/347 exhibited slow articular cartilage loss and 20/347 showed fast articular cartilage loss. Meniscal extrusion was shown to be significantly associated and an independent predictor with fast and slow articular cartilage loss; 12/20 patients with fast articular cartilage loss presented with meniscal extrusion. Later, Crema et al. (2012) examined 1527 subjects (2131 knees) taken from the same MOST study to assess cross-sectional associations with meniscal extrusion. Cartilage damage in both the medial and lateral compartment was found to be independently and significantly associated with medial and lateral meniscal extrusion, respectively. In theory, a reducing cartilage thickness would cause the joint space to narrow, pushing the meniscus outside the joint space, leading to extrusion. Unfortunately, the nature of the grading system and study design makes it difficult to understand the extent, but the association with respect to a large sample size is valuable for the research area.

On the other hand, Lee et al. (2011) assessed 102 knees pre-operative radiographs and MRI scans of patients which underwent partial meniscectomy after medial meniscus damage. This was to better understand the predictors of degenerative meniscal extrusion. Joint space width and varus alignment were measured as well as Kellgren Lawrence (KL) grades which grouped knees depending on chondral changes shown through osteophytes present in the bone. Multiple linear regression analysis showed that KL grades were significantly indicative of meniscal extrusion, however, joint space narrowing, and varus alignment were not significant. The researchers concluded meniscal extrusion is likely to precede OA rather than the inverse because KL grades relate more to osteophytic changes rather than arthritic changes like varus alignment and joint space narrowing. However, using joint space width as a sole measure for arthritic changes has inherent limitations, as it does not solely relate to articular cartilage loss as width reduction can be caused by changes in other areas of the knee joint (Roemer et al., 2009).

Despite extensive study, quantification of OA markers using imaging remains elusive. This is likely because of the retrospective nature of the majority of imaging studies, failing to properly identify the cause-effect relationship. Experimental modelling would aid this investigation, however, there is a considerable underrepresentation of this in relation to meniscal extrusion.

1.5.4 Current Repair and Replacement Techniques

The meniscus has a limited capacity for self-regeneration, meaning there is a great need for effective repair and replacement techniques. In general, factors which determine which treatment line to go down include patient age, injury type (acute/chronic), injury location (vascular/avascular zone), cartilage condition, BMI, knee alignment and the presence/absence of symptoms. Currently, there is a limited understanding of the effect of meniscal extrusion on treatment protocols and further research is required to categorise the severity of meniscal extrusion more accurately and whether it could be used as a marker for clinical decisions.

1.5.4.1 Conservative Treatment

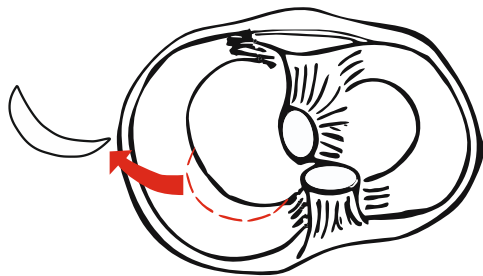
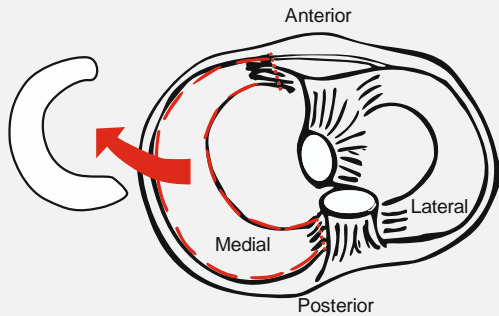
Conservative treatment relates to non-operative management of the injury and in most cases these methods should be exhausted to eliminate the need for unnecessary arthroscopic surgery. Conservative treatment mainly consists of physiotherapy, weight loss and anti-inflammatory drugs. This treatment tends to be administered to older patients (> 50 years) with mostly degenerative meniscal damage as there is a high chance these patients also have chondral degeneration and therefore, it would not be cost effective to repair the degenerative tear when a TKR is likely to be administered to the patient soon. Conservative treatment is rarely used with traumatic tears in younger patients (< 50 years) and surgical repair is likely to be undertaken. However, younger patients who may have tears in the outer red-red zone of the meniscus, such as during meniscocapsular separation, are treated with conservative methods due to the higher healing capacity in that region (Vaquero-Picado and Rodríguez-Merchán, 2018; Krych, Bernard, Kennedy, et al., 2020).

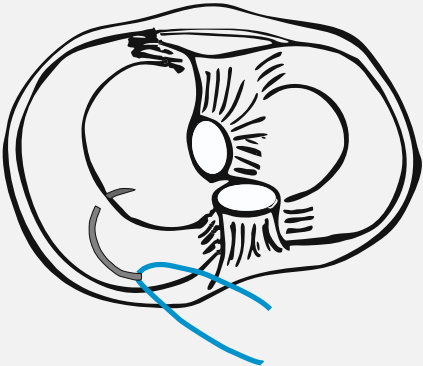
1.5.4.2 Surgical Treatment

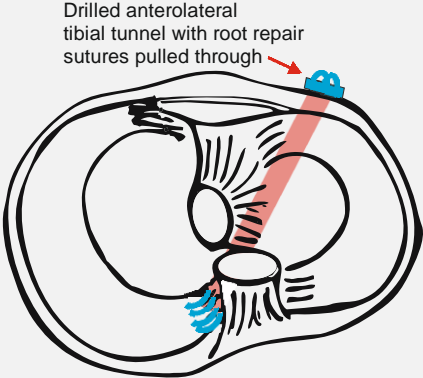
Generally, surgical treatment is required for younger patients (< 50 years old) with meniscal damage and meniscal extrusion. A thorough arthroscopic examination is required to see if the repair is possible and meets specific criteria. These include partial/total meniscectomy, suture repair techniques and total meniscus replacement (MAT / tissue engineered scaffolds). Table 1.2 summarises and evaluates these techniques from the literature.

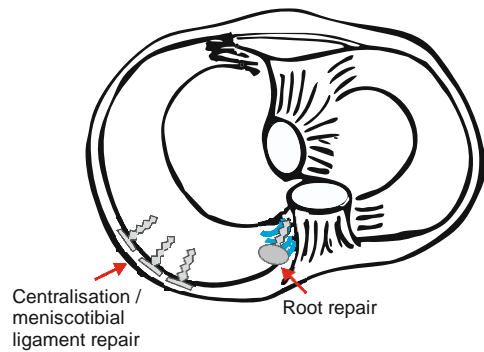
Table 1.2. Surgical repair and replacement techniques for meniscus extrusion.

Intervention	Description	Pros	Cons
Meniscectomy			
Total Meniscectomy	<ul style="list-style-type: none"> • Procedure involves removal of the whole meniscus • May have to be performed in severe cases of meniscal trauma 	<ul style="list-style-type: none"> • Short-term benefits of pain reduction and patients returning to work (Perey, 1962) • Standard approach for most of the 20th century (Jeong et al., 2012), however, the current advice is to repair the meniscus than remove it completely 	<ul style="list-style-type: none"> • Significantly reduces contact area, increasing contact pressure on the opposing articular cartilage, causing accelerated degenerative changes and wear (Krause et al., 1976; Kurosawa et al., 1980; Alhalki et al., 1999; Lee et al., 2006) • A directly proportional relationship between the amount of meniscal tissue removed and the amount cartilage degeneration (Jeong et al., 2012) • A 10-20 fold increased risk of developing OA (Roos et al., 1998)
Partial Meniscectomy	<ul style="list-style-type: none"> • Arthroscopic removal of meniscal tissue around a tear of the meniscal body or horns • Considered the gold standard for meniscal repair 	<ul style="list-style-type: none"> • Effective pain relief and quick to perform operatively • Peripheral rim of the meniscus is preserved; aiding biomechanical function compared to total meniscectomy (Jeong et al., 2012) 	<ul style="list-style-type: none"> • Strongly correlated with increased prevalence of OA from clinical outcomes (Hulet et al., 2015), gait analysis (Sturnieks et al., 2008), cadaveric investigation (Zhang et al., 2015) and computational techniques (Mononen et al., 2013) • No significant improvement in patients' functional outcomes when compared to a sham surgery or non-operative treatment (Sihvonen et al., 2013; Krych et al., 2018)



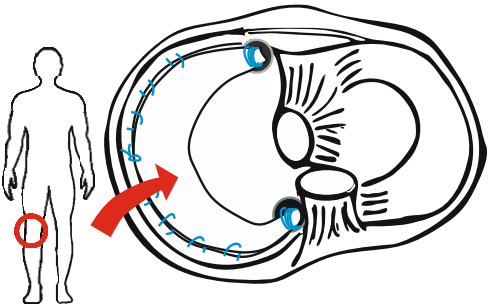
Intervention	Description	Pros	Cons
<p>General meniscus body tear suture repair techniques ('Outside-in', 'inside-out', and 'all-inside' repair)</p> 	<p style="text-align: center;">Suture Repair</p> <ul style="list-style-type: none"> • The 'outside in' describes when the needle is fed from the outside of the joint capsule, through the two parts of the tear and then back through the capsule • The 'inside-out' technique is performed using double armed needles which are fed through needle cannulas. This allows the tear to be sutured from the inside and fastened on the outside of the capsule • The 'all-inside' technique has evolved from the development of second-generation suture fixators which can self-fasten over the tear site (Laible et al., 2013). The 'Centralisation' technique is commonly associated with meniscotibial ligament repairs and meniscus extrusion and is a form of all inside repair, anchoring the peripheral border of the meniscus to the capsule. 	<ul style="list-style-type: none"> • Unlike partial meniscectomy; repair of meniscal tears using suture techniques better preserves the biomechanical loading capabilities through preservation of the tissue and have been reported to have improved long-term outcomes (Paxton et al., 2011; Vaquero-Picado and Rodríguez-Merchán, 2018) • Suture techniques show better outcomes when performed in conjunction with ACL reconstruction (Wasserstein et al., 2013) 	<ul style="list-style-type: none"> • Increased risk of complications when passing sutures through major structures of the knee which can result in higher reoperation rates (Paxton et al., 2011) • Generally, a move toward 'all-inside' suture repair techniques vs 'outside-in' and 'inside-out' (Kwon et al., 2019)

<i>Intervention</i>	<i>Description</i>	<i>Pros</i>	<i>Cons</i>
Transtibial Pull-Out (Root Repair)  <p data-bbox="235 459 481 523">Drilled anterolateral tibial tunnel with root repair sutures pulled through</p>	<ul style="list-style-type: none"> This technique involves drilling a bone tunnel through the anterior aspect of the tibia directly towards the insertion site of the torn root. Using a suture passer, sutures are fed through the tibial tunnel and the root tear is stitched up from the inside and pulled out manually to be fastened by an anchor on the bone (Laible et al., 2013) 	<ul style="list-style-type: none"> Aims to reduce possible meniscal extrusion as well as promote healing of the root tear Bone drilling releases more regenerative cells and growth factors, which is believed to promote faster healing of the meniscus (Kwon et al., 2019) Significant improvement in functional scores and chondral scores at 7- 48 month follow up (Feucht et al., 2015) Biomechanical studies have found that the transtibial pull-out method performed on cadaveric samples restored tibial contact pressures back to intact knee values (Allaire et al., 2008; Marzo and Gurske-DePerio, 2009; Kim et al., 2013) 	<ul style="list-style-type: none"> Mixed clinical results about the meniscus extrusion reduction potential of this procedure Post-operative imaging showed only 56% of patients presented reduced meniscal extrusion values, and failed or reduced healing rates were reported where the boundary of the bone and the meniscal root had not properly formed (Feucht et al., 2015) Potential risk to surrounding structures with procedures which involve drilling bone tunnels
Suture Anchor (Root repair / mensicotibial ligament repair)	<ul style="list-style-type: none"> This technique does not involve drilling bone tunnels but uses specialised bone anchors fed through portals to secure the torn root onto the tibia. A knot pusher is used to push down the knots of the sutures after fixation (Navasartian and DeBerardino, 2018). 	<ul style="list-style-type: none"> The suture anchor technique maybe preferred in conjunction with ACL reconstruction to avoid drilling additional bone tunnels (Navasartian and DeBerardino, 2018) Kim et al. (2011) prospective study of two patient groups concluded similar improvements in functional outcomes of the 	<ul style="list-style-type: none"> Technically difficult to insert the suture anchor into the correct anatomical position (Lee et al., 2018) Fewer biomechanical studies on suture anchor vs transtibial pullout procedure

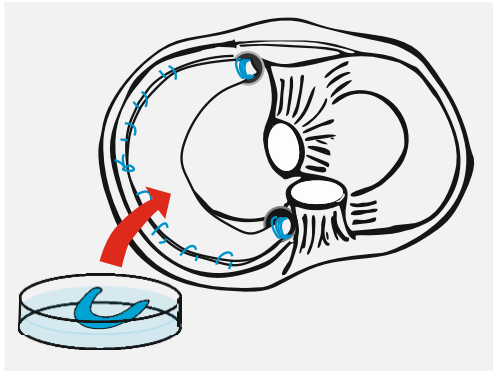


suture anchor vs tibial tunnel
 medial meniscus posterior root
 repair procedure at two years
 follow up

- Optimisation of tension control compared to the transtibial pull-out due to the closer working distance to the torn root

Intervention	Description	Pros	Cons
<p data-bbox="159 871 472 903">Allograft Transplantation</p> 	<p data-bbox="936 826 1301 858" style="text-align: center;">Total Meniscus Replacement</p> <ul data-bbox="719 874 1061 1209" style="list-style-type: none"> • Meniscus Allograft Transplantation (MAT) involves the removal of the damaged meniscus body and root attachments, whilst retaining the peripheral rim • A human donor allograft is then sutured in place of the removed meniscal body 	<ul data-bbox="1128 874 1516 1074" style="list-style-type: none"> • MAT is considered the 'gold standard' total replacement intervention, with studies showing improved long-term chondroprotective benefits (Verdonk et al., 2006) 	<ul data-bbox="1608 874 2074 1311" style="list-style-type: none"> • High expense, inadequate size matching and low allograft availability • Risk of immune rejection • MAT is only carried out on patients < 50 years old with symptomatic meniscal deficiency • At 10 year follow up, 70% of patients presented partial graft extrusion (Verdonk et al., 2006) • Due to ease, cost and short-term relief, surgeons tend to opt for partial meniscectomy or conservative treatment, rather than MAT

Tissue Engineered Substitutes



- A biological or synthetic replacement of the meniscus is surgically implanted, rather than an allograft
- There have been vast amounts of *in-vitro* and *in-vivo* research, using various combinations of synthetic and natural scaffolds, with or without the use of cells to promote differentiation and aid regeneration (Hasan et al., 2014)
- Examples which have been previously FDA approved, or near completion of clinical trials include: the collagen meniscus implant (CMI®, Stryker Corp. USA), ACTifit® (Orteq Sports Medicine, UK), NUsurface® (Active Implants LLC, USA) and the Tramppolin® (ATRO Medical, ND)
- A promising way to solve the problems associated with the limited availability of allografts and the poor chondroprotective benefits of partial meniscectomy
- The Actifit® was originally designed as a total meniscus replacement, however, the results of two different animal studies showed promotion of tissue ingrowth and a reduction in cartilage damage; when it was used as a partial meniscectomy substitute rather than a total meniscectomy substitute (Vrancken et al., 2013). After clinical investigation, the Actifit® showed promising functional improvements and chondroprotective benefits against a partial meniscectomy group (Verdonk et al., 2012)
- In a recent cadaveric study, the NUsurface® implant showed restoration of native contact pressures and contact areas (Shemesh et al., 2020)
- Despite large quantities of research, clinical translation of these substitutes remains low and the efficacy debated
- Generally, *in-vitro* biomechanical outcome measures are underrepresented across the literature
- Most require an intact peripheral rim to be surgically implanted
- The long term follow-up of the CMI®, made from bovine type 1 collagen, was withdrawn by the FDA in 2010 due to poor functional scores, chondro-protective capabilities and graft shrinkage at long-term follow up (Grassi et al., 2014)
- Leroy et al. (2017) reported a high failure rate of ACTifit® in 3/13 cases within 6 years follow-up, meaning the FDA approval of the Actifit® implant remains ongoing
- The Tramppolin® implant has been biomechanically compared to an intact, allograft and meniscectomy condition. The results indicated that the implant was significantly more mobile and produced higher mean contact pressures than the intact meniscus but was not significantly different from the allograft meniscus (Vrancken et al., 2016; Vrancken et al., 2017)

1.6 *In-Vitro* Biomechanical Assessment of Meniscal Injury and Interventions relating to Meniscal Extrusion

Due to the heterogeneity of the meniscus tissue structure and the specialised mechanical environment of the knee joint; this review argues that biomechanical assessment of meniscus function in response to injury or intervention conditions can be aided using *in-vitro* whole-joint models. Cadaveric studies have allowed meniscal function to be better understood incrementally over the last 50 years (Mohamadi et al., 2021). This section discusses the current spectrum of *in-vitro* biomechanical research surrounding the meniscus and meniscal interventions. Specifically, this section focuses on the methodologies and outcome measures used in *in-vitro* studies related to meniscal extrusion, evaluating key themes and gaps within the literature.

1.6.1 Problems Associated with Clinical Studies and Animal Models of Meniscus Injury and Intervention

Expensive, lengthy, and sometimes inconclusive *in-vivo* animal models can be reduced with the use of more effective *in-vitro* biomechanical methods. A key objective of meniscus substitutes is to have biomechanical properties close to those of the native tissue and produce similar loading patterns and kinematics as the healthy knee joint.

1.6.1.1 Clinical Outcomes

Retrospective clinical studies form a large amount of the literature focusing on meniscal interventions. These studies are suitable to describe relationships and differences using large cohorts of patients which meet the inclusion criteria set. Some studies use statistical methods such as multiple regression analyses to assess the importance of factors such as gender, age and BMI on the dependent variables to support their findings. However, factors such as patient activity level before and after injury, or the quality of the meniscal tissue prior to injury are impossible to control. In addition, the concept of pain as an outcome measure is subjective using visual analogue scales, as well as assessing function via questionnaires. Therefore, the cause-effect relationship cannot be determined by such research methods.

1.6.1.2 Animal models

In-vivo animal studies are advantageous as it is possible to assess the regenerative capacity and immune response of meniscal interventions. Animal models which have previously been used include sheep, pigs, rabbits, cows, goats, and dogs. However, no single model has been chosen as the most appropriate for human meniscal research (Deponti et al., 2015). The dog model was predominantly used in meniscal studies of the late 20th century, as dogs could be trained to comply with surgery and post-operative protocols. Understandably, the use of dogs has stopped due to the rise of animal rights groups and ethical considerations (Arnoczky et al., 2010). The sheep and pig model are now more readily used due to their higher economical availability and use in the food industry. It has been found that the adult sheep and pig meniscus has similar levels of vascularisation to the adult human meniscus, which may suggest similar pathways of regeneration (Deponti et al., 2015). However, the cost and ethical concerns of undertaking live animal trials remain high and are continually increasing. In addition, there are significant gait differences between animals and humans, making conclusions elusive in relation to biomechanics and intervention longevity in the knee and the menisci. The focus of present and future research should be on applying more effective *in-vitro* methodology, therefore, reducing the need for *in-vivo* animal research.

Anatomical Differences between the Porcine and Human Knee for in-vitro Research

Porcine tissue is cost effective and readily available from the food industry. Breeding programs also reduce tissue variation, making it a standard animal model to use for *in-vitro* method development (Liu et al., 2015; Bowland et al., 2018; Ozeki et al., 2020; Hirose et al., 2022). However, prior to assessing human specimens, it is important to discuss anatomical and biomechanical differences between these species' knees, to identify limitations and possible difficulties with method transfer.

The human and porcine knees have similar connective tissue organisation. The porcine knee has cruciate ligaments, collateral ligaments, articular cartilage and menisci, making it a suitable species for *in-vitro* assessment. Upon gross examination, the human knee femoral condyles are shaped differently to the porcine condyles (Figure 1.17). The menisci of mammalian species retain the semilunar shape, however, there are some morphological differences. In an anatomical study, the majority of mean porcine menisci measurements were significantly thicker than mean human menisci measurements, however, the weight and volume of the medial menisci were statistically similar. These results are summarised in Figure 1.17. Gross examination indicated the porcine menisci were stiffer than the human menisci and during the dissection process, there was a tighter capsular attachment of the porcine medial meniscus than in the human knee. This

suggests porcine menisci are likely to be less mobile compared to human menisci, however, interspecies anatomical differences in capsular stability have not been extensively studied. Additionally, the porcine meniscal roots insert in different locations to human meniscal roots. Notably, the porcine lateral meniscus posterior root firmly attaches to the lateral-posterior aspect of the medial femoral condyle, whereas in the human knee, this root attaches to the posterior intercondylar fossa (Takroni et al., 2016).

These differences are brought on by several factors, but the overriding factor is the differences in bipedal and quadrupedal gait between the two species causing differences in loading patterns and mechanotransduction on the tissues. Unlike human knees, the knee joints of pigs are in a constant state of flexion, approximately 24° equates to full extension at heel strike (Thorup, 2007). Therefore, biomechanical loading profiles need to be altered to adhere to the porcine limits in motion.

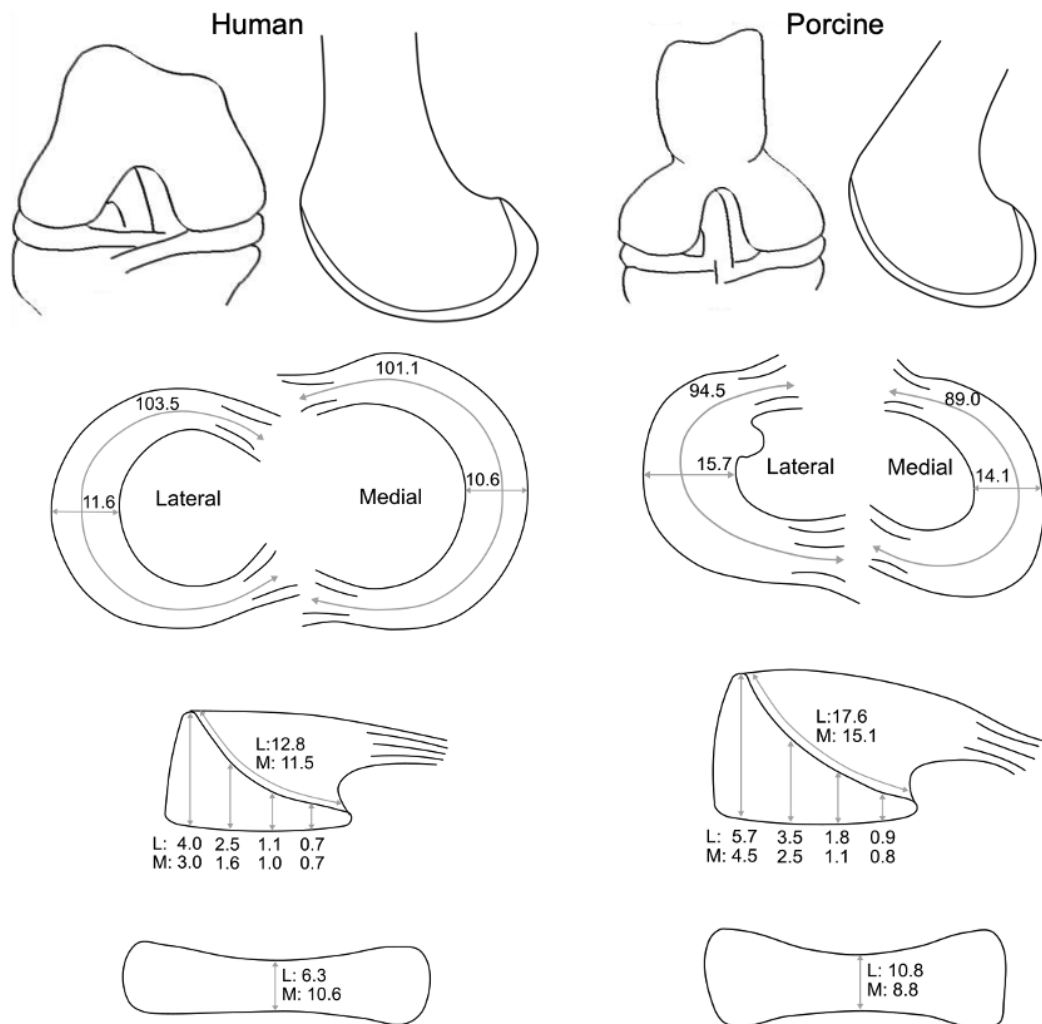


Figure 1.17. Anatomical differences between the human and porcine knee and menisci (measurements in mm) (Takroni et al., 2016, p.6).

1.6.2 Biomechanical Whole-Joint Experimental Models

Whole-joint experimental studies over the last 25 years assessing meniscus injuries (body tears, root tears, meniscotibial injury) and interventions (meniscectomy, MAT, transtibial tunnel root repair, suture anchor repair / centralisation and total meniscus replacement) relating to meniscus extrusion were gathered (see section 1.5). A table summarising these studies can be found in Appendix A. The first aspect to highlight from this table are the low sample sizes ($n = 5 - 11$, mean: 8). Most biomechanical studies have low power and high variability due to the difficulty of sourcing, assessing and storing cadaveric tissue. This aspect alone generates difficulty in drawing reliable conclusions about meniscus biomechanics in general. The following sections evaluate the outcome measures, loading regimes and capsular constraint from these studies.

1.6.2.1 Loading and Motion Regimes

Static and dynamic analyses can be classified according to the force, motion, material, and deformation. The definition of these terms can be confusing throughout the literature, however, to this review's understanding, testing protocol within meniscus biomechanical research can include static load, static motion, quasi-static load, quasi-static motion, dynamic load, and dynamic motion. Table 1.3 summarises these terms in association with the reviewed studies.

Static and Quasi-static Load and/or Motion

As shown in Table 1.3, the majority of biomechanical studies incorporate static or quasi-static loading regimes, typically applying maximum loads of 1000 N or 1800 N for cadaveric specimens. The 1800 N value is used regularly, as this has been described as 2.5 times the BW of a 70 Kg man (Paletta et al., 1997; Marzo and Gurske-DePerio, 2009; Hein et al., 2011; Walczak et al., 2021). Others have used lower loads, most likely to protect the cadaveric knee joints from fracture (Allaire et al., 2008; Kim et al., 2013; Daney et al., 2019; Debieux et al., 2021).

During these experiments, load is usually applied over a given time (eg: 75 N per second) to a set maximum load (eg: 1800 N). The rate of load application, as well as the maximum load and tibial motion conditions vary across the literature. In most cases, biomechanical studies apply this type of loading regime with either fixed or unconstrained axes of tibial motion for a series of static flexion angles. This review defines quasi-static motion as non-driven unconstrained motions which occur during axial knee loading experiments. Experimental testing in this way can be beneficial as loads and motions are isolated and simplified, therefore, a better understanding of tissue effects can be evaluated

in relation to a reduced and controlled number of variables. In addition, contact pressure and meniscal position measurements are usually easier to implement during static tests. However, these experimental models do not apply the correct sliding and rolling actions or shear and rotational forces experienced by the cartilage and the menisci during physiological knee biomechanics.

Table 1.3. Defining load and motion conditions in biomechanical models of meniscus experimental research.

	<i>Load</i>	<i>Motion</i>	<i>Studies</i>	<i>Max load</i>
Static	Ramped increase to a set maximum	Fixed	Marzo and Gurske DePerio, 2009	1800 N
			Ozeki et al. 2019	200 N Porcine
			Debieux et al. 2021	1000 N
			Hirose et al. 2022	300 N Porcine
Quasi-Static	Ramped increase to a set maximum	Uncon - strained / free tibial axes	Paletta et al. 1997	1800 N
			Allaire et al. 2008	1000 N
			Hein et al. 2011	1800 N
			Kim et al. 2013	300 N
			Daney et al. 2019	1000 N
			Walczak et al. 2021	1800 N
Dynamic	Variable load applied over a given time	Driven movement of 1+ degrees of freedom	Brophy et al. 2010	300 N Ovine
			Bedi et al. 2012	2280 N
			Schillhammer et al. 2012	~1000 N
			Vrancken et al. 2014 and 2016	1000 N
			Brial et al. 2019	2280 N

Dynamic Load and Motion

Dynamic load refers to the application of a variable axial force overtime and dynamic motion refers to a continuous application of motion from one or more degrees of freedom during a test. There have been a handful of meniscal studies which have included a continuous range of dynamic motion of one or more degrees of freedom and /or used a dynamic load. As discussed in section 1.4, the meniscus has simultaneous functionality, including dual mechanical functions of load transmission and stability. It is better to assess meniscus function in a mechanical environment which satisfies these characteristics.

Over the last decade, there has been an increasing amount of study assessing the biomechanics of meniscus injury and interventions during dynamic load and motion

regimes using various electro-mechanical (Brophy et al., 2010; Bedi et al., 2012; Liu et al., 2020), servo-hydraulic (Sutton et al., 2010; Schillhammer et al., 2012) or robotic apparatus (Vrancken et al., 2014; Vrancken et al., 2016). Knee simulators are machines which allow the application of gait cycles to whole-knee joints, allowing the meniscus to perform under functional cyclic loading conditions similar to that *in-vivo* (Brophy et al., 2010; Bedi et al., 2012; Schillhammer et al., 2012; Brial et al., 2019).

International Standards Organisation (ISO) gait inputs for total knee replacement assessment (ISO-14243-3, 2014; Abdelgaied et al., 2022) have been applied to a handful of natural knee simulation studies and include driven control of the axial compression, flexion-extension, anterior-posterior and tibial rotation axes (Figure 1.18).

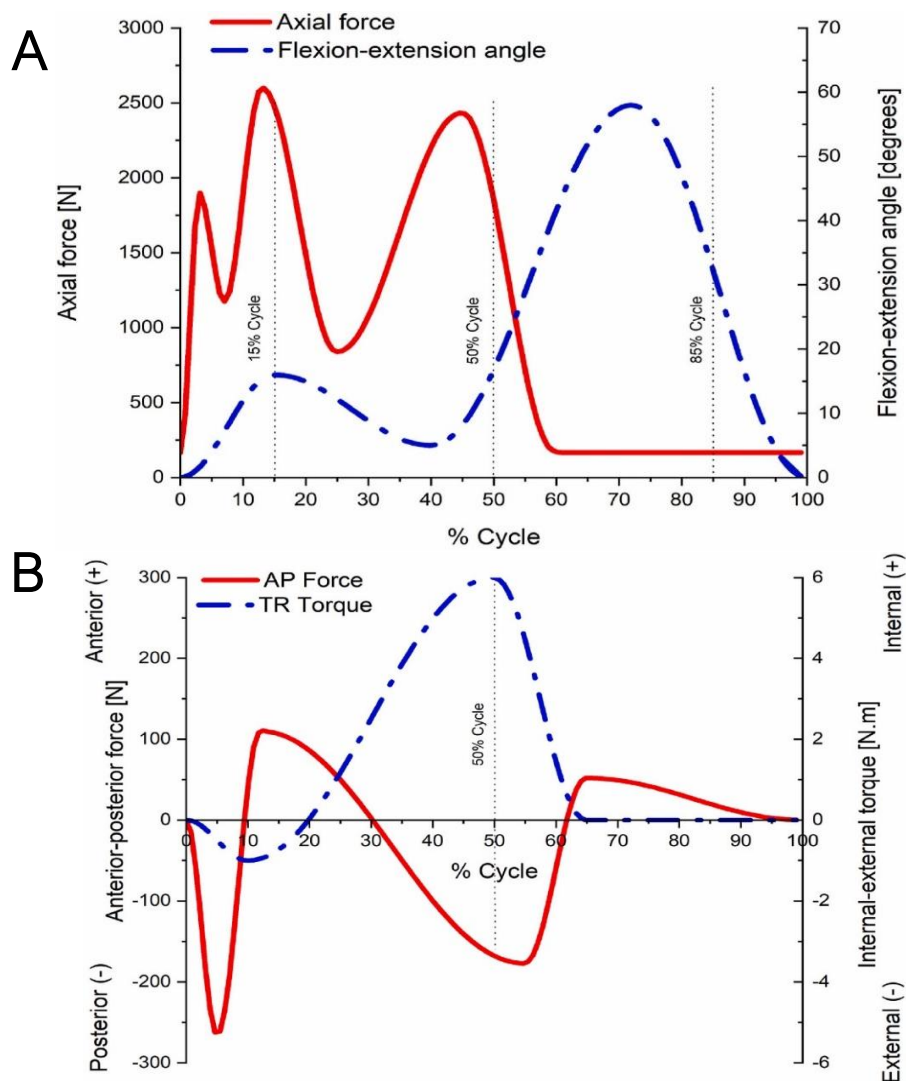


Figure 1.18. ISO 14243-3: 2014 force-controlled simulated gait cycle inputs. (A) axial force (red line) and flexion-extension (blue dashed line) inputs. (B) anterior-posterior (AP) force (solid red line) and tibial rotation (TR) torque (blue dashed line) inputs (Reproduced with permission from: Abdelgaied et al., 2022, pp. 3 - 4).

The ISO standard force inputs were taken from previous quasi-static ground-reaction studies which have been verified through data taken from instrumented knee prosthesis (B Morrison, 1970; D Lima et al., 2005). The displacement inputs were derived from previous in-vivo gait analysis data from patients with a semi-constrained TKR (Johnson et al., 2000).

Brophy et al. (2010) evaluated differences in contact mechanics (see section 1.6.2.2) between the intact knee, a lateral meniscus partial meniscectomy and an ACTifit® polyurethane meniscus scaffold in an ovine knee model using simulated ISO gait inputs, however, scaled down to the estimated walking kinetics of a sheep. Findings showed no significant differences were found between the peak contact pressures of intact (2.2 MPa) and implant (3.0 MPa) conditions. However, the mean contact area of the implant was significantly lower than the intact. The partial meniscectomy condition significantly increased peak contact pressures (3.9 MPa) and reduced mean contact area in the lateral compartment from the intact and implant condition. However, the results only described the mean and peak contact pressures and contact areas experienced in the lateral compartment, averaged over 10 cycles. The implant could have behaved differently at points throughout the simulated gait cycle.

Schillhammer et al. (2012) assessed human cadaveric samples using a force-control knee simulator. However, only 33% of the ISO gait force and torque inputs were used to protect the knee specimens and the contact pressure sensors during the experiment. Contact mechanics and tibial rotation position outputs were evaluated and compared between three conditions (intact, lateral meniscus posterior root tear, tibial tunnel repair) throughout the gait cycle. To illustrate how the lateral compartment contact pressures behaved during a dynamic load, the peak contact pressures were calculated for each time point during the simulated gait profile and averaged across the eight cadaveric knees. The torn (detached) condition significantly increased peak contact pressures during stance phase compared with the intact condition (Figure 1.19). The largest difference occurred at mid stance where peak pressures increased from ~2.8 MPa to ~4.2 MPa (49% increase), from intact to torn, respectively. The repair condition subsequently reduced the peak contact pressures to values not significantly different from the intact condition. No differences in tibial rotation were found, however, the scaled-down loads may have been too small to create measurable differences in the kinematics between the conditions. Anterior-posterior tibial translations were also not measured as an output during this experiment, even though this parameter is a good indicator of function as the menisci are believed to offer stabilising effects in the absence of the cruciate ligaments (Shoemaker and Markolf, 1986). In addition, each knee performed five slow 20-second duration gait cycles, due to the capabilities of the simulator. The speed of the applied loads and motions may affect how the meniscus functions to stabilise and distribute load.

Applying a frequency more accustomed to the average human walking speed, would apply more physiological loading characteristics.

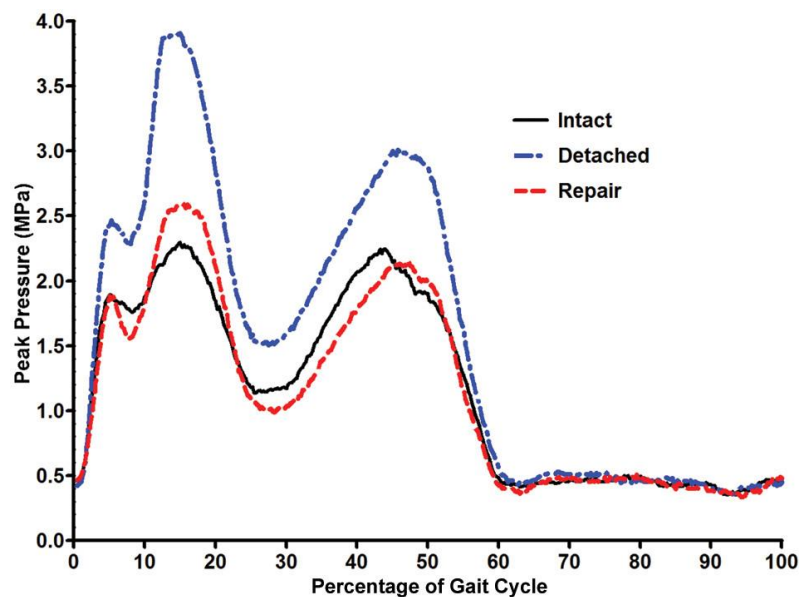


Figure 1.19. Average peak contact pressures over an ISO simulated gait cycle at 33% load for the intact (black), lateral meniscus posterior root tear (blue) and tibial tunnel root repair (red) conditions ($n = 8$). (Reproduced with permission from: Schillhammer et al., 2012).

The same knee simulator used during Brophy et al. (2010) ovine knee study was used to assess meniscus function in response to lateral meniscus injury and intervention in cadaveric knee joint samples at higher axial loads of 2280 N, were based on the inputs from the ISO standard (Figure 1.18 previously) but capped at the 2.3 kN maximum axial load of the specific simulator (Bedi et al., 2012; Brial et al., 2019).

Bedi et al. (2012) assessed the effect of lateral radial tears in order of increasing severity (intact, 30%, 60%, 90% radial cut) followed by a suture repair and a partial meniscectomy procedure. Contact pressures and contact areas were extracted from the two highest axial load peaks during mid stance of the gait cycle (14%: 2280 N, 15° flexion; 45%: 2130 N, 8° flexion). The knees were simulated for 20 gait cycles at 0.5 Hz and contact pressure/area means were calculated from the last 8 cycles. Peak contact pressures were significantly higher for most severe (90%) radial tear compared to intact, 30% tear and 60% tear conditions at 45% of gait the cycle. Results for the suture repair and partial meniscectomy were not significantly different from the 90% tear condition and did not restore meniscal function to intact levels. The researchers also segmented the sensor maps into quadrants to identify the spatial differences in contact pressures. The 90% radial tear in the posterior-peripheral quadrant showed the most significant

increases. However, it is unclear how the researchers controlled the sensor positioning between samples, which could have the distribution analysis. Similarly, Brial et al. (2019) used the same simulator, driven ISO inputs and contact mechanics methodology as Bedi et al. (2012) to assess fixation methods (bone-plug or suture) of a lateral meniscus MAT. The researchers found that both MAT fixation methods reduced peak contact stress at 14% and 45% of the gait cycle closer to that of the intact condition versus a total meniscectomy condition.

Soft-tissue constraint is frequently mimicked using compressive springs during knee simulation. Bedi et al. (2012) and Brial et al. (2019) described above used 14.5 N/mm springs to mimic soft tissue constraint. This spring constraint was defined based on the findings of van Houtem et al. (2006) whom assessed hard (33.8 N/mm) (ACL and PCL intact) and soft (7.24 N/mm) (ACL and PCL cut) springs on the anterior-posterior displacement output in simulated cadaveric knees. These values were taken from TKR wear assessment literature. The conclusion was an intermediate spring constraint maybe more appropriate to simulate intact anterior-posterior soft tissue constraint, hence 14.5 N/mm.

Furthermore, the work of Liu and colleagues has shown that non-linear spring parameters (spring forces and free lengths) applied to the anterior-posterior and tibial rotation axes can influence the kinematic (anterior-posterior displacement, internal-external rotation angle) and tribological (anterior -posterior shear force) outputs in both a porcine natural knee simulation model and more recently a human model using the Leeds single station knee simulator (see section 2.3) (Liu et al., 2015; Liu et al., 2019; Liu et al., 2020). Liu et al. (2020) applied the ISO gait inputs at full load and motion parameters with a modified two-peak axial force. This study showed the large variability which occurs in the output anterior-posterior displacement and tibial rotation angle between each intact human knee sample (with natural soft-tissue ligamentous control). In addition, with the incremental and systematic application of varying spring forces and free lengths (non-linear region) when the soft-tissues were resected, it was found that not one spring constraint for the anterior-posterior displacement and tibial rotation was consistent between human knee specimens and each were unique to each knee specimen.

1.6.2.2 Quantitative Outcome Measures: Contact Mechanics

The outputs measured in experimental meniscal studies are usually mean or peak contact areas and contact pressures; using pressure sensitive films and sensors (Figure 1.20) (Allaire et al., 2008; Brophy et al., 2010; Schillhammer et al., 2012; Kim et al., 2013; Walker et al., 2015; Ozeki et al., 2020). A handful of similar studies arose around 10 -15 years ago, assessing the biomechanical effects of medial meniscus root tears on knee

contact mechanics, however, there has not been much progression since. These conditions included an intact state, a simulated root tear and a root repair method. Some also included a meniscectomy condition as a positive control.

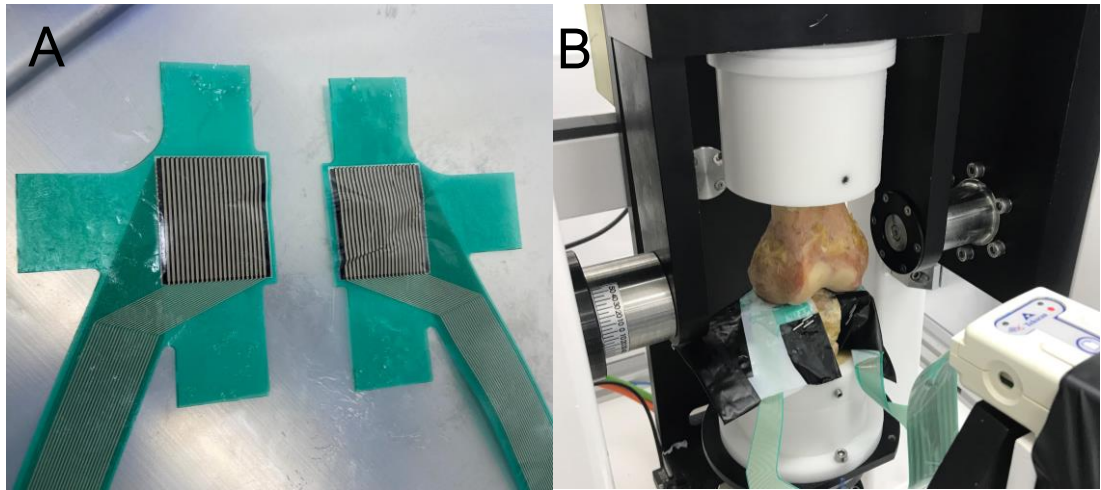


Figure 1.20. (A) Tekscan K-scan 4011 contact pressure sensors for biomechanical knee joints. (B) Image of the Tekscan sensors being used for cadaveric assessment.

Allaire et al. (2008) examined contact pressures and kinematics in 6 cadaveric knees with a scalpel cut tear 5 mm away from the attachment insertion of the medial posterior horn. A static load of 1000 N was applied at 0°, 30°, 60° and 90° flexion and small incisions into the joint capsule allowed the insertion of Fuji Prescale Film sensors (Fujifilm, NY, USA) under the medial meniscus and on top of the tibial cartilage. These sensors imprint the area of contact between two surfaces and estimate pressure using a colour intensity scale. Mean contact pressure significantly increased in the medial compartment by 25.4% across all flexion angles in the presence of a root tear when compared to the intact condition. These figures were not significantly different to mean contact pressures recorded for total meniscectomy (38% increase from intact). Similarly, Marzo and Gurske-DePerio (2009) found a 24.4% increase in mean contact pressure when the knee was loaded in the presence of a medial meniscus root avulsion. However, unlike Allaire et al. (2008), this study applied a higher axial force of 1800N, which roughly equates to 2.5 times BW of a 70kg man and is a commonly used maximum load in quasi-static biomechanical meniscus research. In addition, the knee was kept in full extension and piezo-electric pressure sensitive Tekscan sensors (Figure 1.20) were used to assess the contact mechanics. Interestingly, despite the higher axial load, the results were ~2 MPa lower than the 0° flexion results of Allaire et al. (2008). This could be reflected by the different measuring equipment as Tekscan may underestimate values as the electronically equipped sensors are less conformable over uneven surfaces. The Fuji Prescale films are

more conforming to the condyles and tibial plateau, but pressure maps cannot be viewed in real-time as with Tekscan sensors.

Following on from this, Kim et al. (2013) conducted a similar study with a novel electronic pressure sensor system (Pliance X, Munich, Germany), which was typically used to assess foot plantar pressures for diabetic foot ulcer research. The justification was that this sensors system allowed better conformity of the pressure film over the tibial surface than Tekscan sensors. In addition, an additional MAT condition and MCL release condition were implemented to understand the effects of these procedures compared to the intact, root repair and meniscectomy conditions. The MCL release is a surgical technique sometimes conducted during MAT to improve joint space access, however, the biomechanical effects are not well understood. Due to the conformable sensors, the compressive load had to be limited to 300N in this study. This load was applied to a rig which allowed unconstrained tibial motion and a femoral part which aligned the knees at 0°, 30°, 60° and 90° flexion. Findings showed a root tear significantly increased the mean contact pressures from the intact condition. The root repair and MAT surgery both reduced the contact pressures but not back to the previous intact values. In addition, there was no significant effect of MCL-release reported. However, considerable variation is apparent in the standard deviations reported which could be due to sample variation or the added film conformity causing a more uneven pressure map. In this case, reporting the mean pressures may not have been the most descriptive analysis. In addition, the use of a 300N load is low and not physiological for cadaveric specimens.

It is important to note the levels of soft tissue constraint also differ between all three of these studies. In addition, to measure contact mechanics, several steps must take place to insert and protect the equipment, which potentially reduces the clinical and physiological relevance of the experiment. For example, Marzo and Gurske-DePerio (2009) excised the coronary meniscal ligaments, to aid the conformity of the Tekscan sensors. Kim et al. (2013) and Allaire et al. (2008) retained as much of the capsule as possible when testing the intact condition, but it is unclear whether certain structures were excised or retained in the subsequent surgeries. Furthermore, Kim et al. (2013) tested six serial knee conditions, which arise questions regarding the quality and integrity of the tissues during the subsequent tests. These aspects could have affected how far the medial meniscus displaced, and therefore the contact area (Debieux et al., 2021), however, meniscal displacements in these studies were not quantified despite there being strong clinical associations with root tears and meniscus extrusion (see section 1.5.3).

On the other hand, measuring contact mechanics is important because higher pressure values suggest damage to cartilage and OA risk. In addition, as discussed in the previous section, dynamic contact mechanics have been measured during knee simulation studies applying dynamic load and motion regimes (Brophy et al., 2010; Bedi et

al., 2012; Schillhammer et al., 2012; Brial et al., 2019), however, there is discrepancy as to how durable and repeatable pressure readings are in the presence of shear forces (Wilharm et al., 2013).

Further work could focus on predicting the longevity of meniscal interventions in the knee joint by regionally dividing pressures across the meniscus, rather than reporting means. Thus, gaining a better understanding how the meniscus, or intervention, moves in relation to the loading and how this effects the contact mechanics. Walker et al. (2015) investigated the basic load transmitting and stabilising functions of the medial meniscus by regionally defining the Tekscan sensor area into anterior, posterior and middle sections as well as using a dynamic continuous range of flexion-extension motion. The loading apparatus applied a 500 N load and a mathematical method was used to estimate the effect of 100 N of anterior or posterior shear force whilst the knees were manually moved through -5° to 135° flexion. The load carried by the meniscus remained the same throughout flexion, however, the load distributions differed. After 30° , the posterior region had an increased stabilising effect when posterior shear was applied as over 50% of the load was taken on by this region. The anterior region took on about 35% of this load at lower flexion angles $< 30^{\circ}$, and when anterior shear force applied this was higher during extension (-5° - 0°) but again the posterior region dominated with increasing flexion angle. However, the 10 specimens were of older age (range: 55 - 91 years), which meant that some samples were not able to be tested at the extremes of motion due to tissue integrity, therefore, reducing the sample size for analysis at these flexion angles. The tibial cartilage covered by the meniscus experiences less damage than the uncovered cartilage during the progression of OA; the researchers concluded that this could be mechanically due to the sliding motion this area takes on. This study shows that the sliding as well as the loading component upon cartilage is important to consider in experimental investigation; something which can be modelled with dynamic biomechanical assessment.

1.6.2.3 Quantitative Outcome Measures: Meniscus Displacement / Position

Contact mechanics are usually reported in biomechanical studies, however, the measurement of changes in meniscus displacement or position remains underrepresented in comparison. However, the use of this outcome measure has increased in experimental literature over the last 5 years. This is possibly due to the increasing clinical awareness of meniscus extrusion and its association with OA (see section 1.5).

Meniscus displacement defines a linear change in position of the meniscus in any measured direction (typically anterior-posterior and medial-lateral directions) and usually

with reference to points on the tibial plateau. Meniscus displacement contains both the deformation and the movement of the tissue in response to load facilitated by the microstructure of the meniscal tissue and the action of the root attachments stretching and facilitating sliding with knee joint motion (see section 1.4.2). Recently, Debieux et al. (2021) biomechanically modelled the effect of meniscus displacement in the medial direction on the contact area and pressure of cadaveric samples through pulling the medial meniscus 1 mm, 2 mm, 3 mm, 4 mm and maximum outward (radially) from the medial margin of the tibial plateau. Modelling extrusion was achieved by passing sutures through the peripheral meniscus body and a traction device pulled the meniscus centrifugally. Medial meniscus extrusion was measured using a digital calliper from a fixed point on the tibia. A medial condyle osteotomy was performed to access the medial tibial plateau to measure the extrusion. The coronary ligaments (meniscotibial, meniscofemoral) were released to achieve the maximum extrusion of each sample. A suture repair method was also performed as the final condition, which reattached the meniscus to the stabilising structures. Samples were axial loaded to 1000N at 0°, 30°, 60° and 90° flexion angles to assess each extrusion condition on the contact mechanics; measured using Tekscan pressure sensors. The most significant findings were that contact area significantly reduced with increased medial meniscus extrusion > 4 mm at all flexion angles. Average maximum extrusion (with intact roots) for all specimens was 5.3 mm (range: 4.0 mm – 8.9 mm). However, no significant differences and trends were found between mean or peak contact pressures with increasing meniscus extrusion. Despite fixation plate reattachment of the medial condyle after the osteotomy, which was performed to access the medial tibial plateau, it is possible this procedure may have destabilised the bone geometry and effected the joint load applied to the sensors.

Various methods have been used to measure meniscus displacement in the literature, such as: radiographical (Bylski-Austrow et al., 1994; Vrancken et al., 2014; Paletta et al., 2020), probe methods (Hein et al., 2011; Walczak et al., 2021), coordinate measuring equipment (Daney et al., 2019) and motion capture (Hirose et al., 2022) (Figure 1.21).

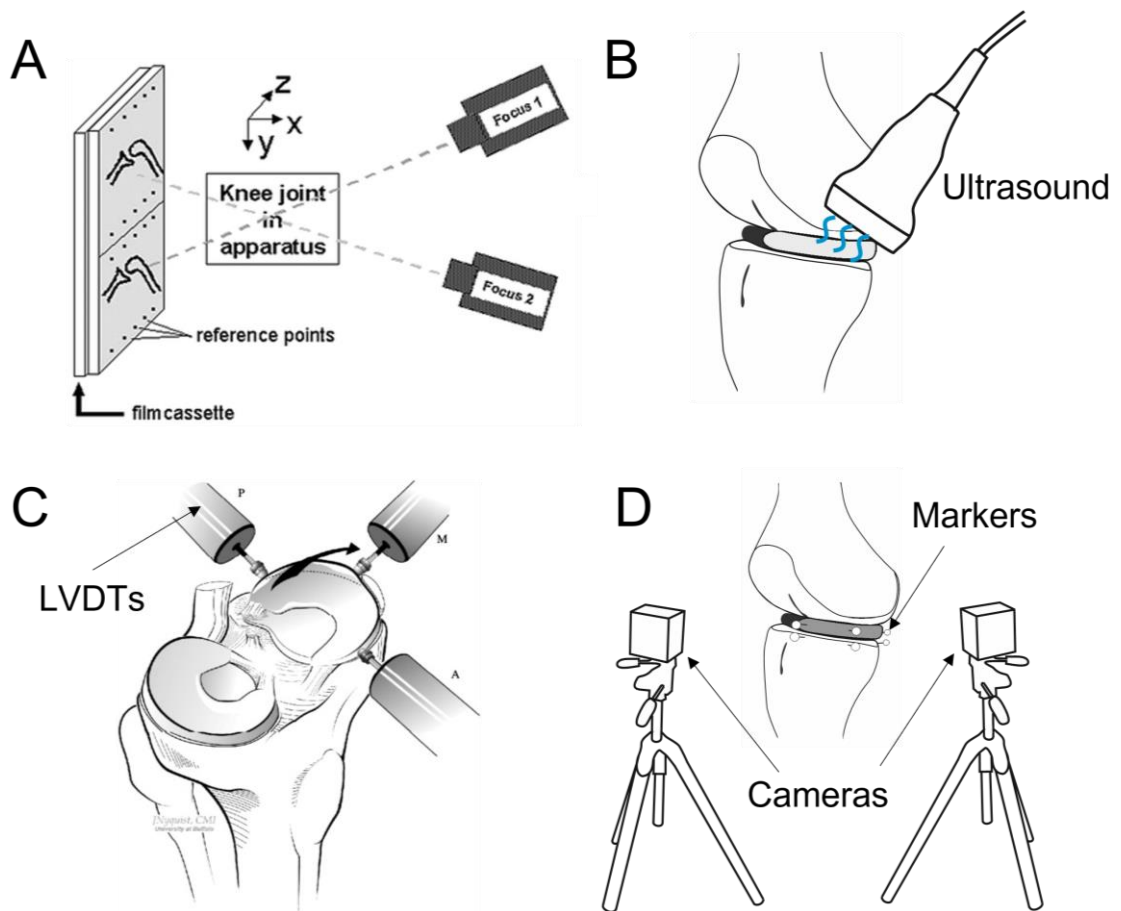


Figure 1.21. Meniscus displacement measurement techniques. (A) Radiographical X-ray methods such as roentgen stereo-grammatic analysis (RSA) (Reproduced with permission from: Tienen et al., 2005, p. 289). (B) Ultrasound methods. (C) Probe methods such as using linear variable displacement transformers (LVDTs) (Reproduced with permission from: Hein et al., 2011, p. 190). (D) Motion capture using optical cameras and retro-reflective markers.

Radiographical methods can be accurate in locating the position of metal markers inserted into or attached onto the menisci of cadaveric samples, however, due to the surrounding equipment, continuous dynamic motion is usually limited. Bylski-Austrow et al. (1994) used this technique to assess the displacements of the medial and lateral menisci in response to tibial rotation and translation under 1000 N axial compression and at 0°, 15° and 30° static flexion angles. Lead markers were adhered to the superior surfaces of the menisci; however, the exact positioning of these markers was not stated, nor whether the positioning was controlled in between samples. X-rays were taken in the transverse plane whilst 11 different loading conditions were performed on each knee. Displacements were measured from the reference load case radiographs, which comprised of 1000 N axial compression and unconstrained tibial axes. Generally, the lateral meniscus moved posteriorly with internal tibial rotation and anteriorly with external tibial rotation; the inverse was reported for medial meniscus. Anterior translation of the tibia generated posterior

movement of the menisci and posterior translation of the tibia generated anterior movement of the menisci. The effect of flexion angles 0°, 15° and 30° did not have a profound effect on meniscal position, nor did the effect of increased axial compression from 250 N to 1000 N. It was likely that most of the radial displacement occurs from 0 – 250 N compressive load, but this was not measured as, all displacements were measured from the reference X-ray and not from a zero position. The researchers concluded that due to the redistribution of water molecules, the stiffness of the tissue increases as axial compression increases; thus, the rate of radial expansion reduces as increasing load is applied. These early analyses highlight the importance of characterising the meniscus as a dual functioning tissue by measuring meniscus tissue displacement in response to load.

Progressing from the work of Bylski-Austrow et al. (1994), roentgen stereogrammetric analysis (RSA) has been used to radiographically measure changes in meniscal displacement in cadaveric samples. RSA has been previously used to measure *in-vivo* implant migration or micro motion in the initial stages of prosthesis clinical trials (Selvik, 1989). This method uses x-ray photographs taken at different angles to measure the positions of tantalum beads inserted into the body of the meniscus in cadaveric knee joints (Figure 1.21 A). Assuming the beads move in response to the meniscus displacement, researchers have verified this method to be highly accurate (Tienen et al., 2005; Vrancken et al., 2014; Vrancken et al., 2016). Tienen et al. (2005) were the first to apply this to the meniscus and found similar results to those reported in an *in-vivo* MRI study assessing unloaded and loaded meniscus kinematics during 90° squatting (Vedi et al., 1999) (see section 1.4.2.2).

More recently, Vrancken et al. (2016) applied RSA to assess the kinematics of a polyurethane total meniscal replacement compared with an intact, MAT and meniscectomy condition during a simulated squat scaled to 1000 N maximum load. Findings indicated a significant increase in posterior translation of the implant and allograft condition when compared with the intact condition. Generally, the implant and allograft conditions were more mobile than the intact condition but not significantly different from one another; therefore, the researchers concluded that the implant could not restore the native meniscal function as increased meniscal mobility alludes to increases in abnormal cartilage loading and knee laxity. These factors were reported in the contact mechanics and knee laxity test results of this study. It should be noted however, that there were differences in the attachment methods between the implant and allograft conditions which could have affected the results. Additional fixation sutures were used to attach the allograft to the capsule; however, this was not performed for the implant, in line with the implants surgical protocol. Nevertheless, the implant tested in this study underwent further product development and is currently in clinical trials; potentially offering an effective alternative solution to MAT. This is an example of how measuring meniscal displacement

can be beneficial in prediction of intervention longevity. Moreover, ultrasound is a cheaper radiographical alternative to RSA or MRI (Figure 1.21 B), and has been used in a recent cadaveric study assessing meniscus extrusion and the repair of the meniscotibial ligament using suture anchors (Paletta et al., 2020). Lesions of the meniscotibial ligament and MCL attachments to the medial meniscus were made arthroscopically and the knee specimens underwent 100 flexion-extension cycles using a novel pulley system in an E10000 Instron before ultrasound images were taken at full extension with a 10 Nm varus load. This study found the meniscotibial ligament lesion significantly increased meniscus extrusion from 1.5 mm (intact) to 3.4 mm (damaged) (55.8%). The repair procedure reduced the meniscus extrusion from the damaged condition by 35.8 %, however, remained significantly different than the baseline means.

In contrast to radiographical methods, flexible tipped probes have been previously used to measure changes in radial meniscal displacement during axial load of natural knee joints (Ikeuchi et al., 1998; Hein et al., 2011; Walczak et al., 2021). Ikeuchi et al. (1998) developed a novel flexible needle device which was able to measure radial displacement of the porcine meniscus within 10 μm of the operating range of ± 3 mm during axial loading. Later, Hein et al. (2011), measured the change in position of the anterior, posterior and middle regions of the medial meniscus whilst simulating a medial meniscus posterior horn complete rupture. An 1800 N maximum load was applied to seven human knees position at full extension. Three linear variable differential transformers (LVDTs) (Figure 1.21 C) were placed around the medial meniscus to measure meniscal displacement. The results showed the medially positioned LVDT showed a significant increase in mean displacement from the intact (1.67 mm) to the avulsed condition (3.28 mm). Displacements recorded by the anterior and posterior LVDTs were lower but not significant between the avulsed and intact state. These results were in agreement with previous MRI studies of healthy patients and those with meniscal extrusion (Boxheimer et al., 2004; Lee et al., 2014).

Probe methods, such as LVDTs, have a high precision, can be calibrated easily, and do not require beads or markers to be inserted into the meniscus. However, the soft deformable meniscus pushing against the probe tip may have underestimated the displacement. A certain amount of force is required to push the probe to record displacements; if the meniscus deforms around the probe, there would be a lag in initial meniscal displacement compared to the displacement the probe records. Although probe methods are precise, the loading regime and applied motions are usually slow and controlled to maintain probe contact with the meniscus body and obtain measurements. Applying dynamic loads and motions at physiological walking frequencies may damage the probe tips.

Studies assessing meniscal displacement in the presence of root tears and meniscal extrusion are relatively limited but have increased in recent years. Ozeki et al. (2020) examined the effect of the lateral meniscus suture anchor centralisation procedure (see section 1.5.4) in a porcine experimental model. This procedure reduces meniscal extrusion after a root tear by attaching the protruding peripheral edge of the meniscus to the tibia, preventing the meniscus displacing radially. The simplistic loading regime incorporated a 200N axial load at a 45° angle, whilst simulating three conditions: intact, extrusion (1 cm radial root cut) and suture anchor repair (centralisation). Extrusion was measured using 3 mm diameter markers placed on the PCL and the peripheral edge of the lateral meniscus. The distance in between these markers was measured for each condition and the means were reported (Intact: 18.1 mm. Extrusion: 21.9 mm. Centralisation: 15.3 mm), contact mechanics using Tekscan sensors were also measured. The researchers confirmed the creation of an extrusion model as there was a significant difference between the intact and the extrusion condition. However, the researchers did not consider the kinematic capabilities of the pig stifle joint, as a 45° flexion angle would be too large (Thorup, 2007). In addition, measuring the distance from the PCL does not relate to the clinical method, which is measured from the line of the tibial plateau, however, this did allow more space for the pressure film to be inserted. Furthermore, the technique used to measure this distance was not described. Arguably, the primary aim of this study was to report the differences contact mechanics between each condition and the measure of extrusion was more supportive to denote the effectiveness of the centralisation procedure. Interestingly, the centralisation seemed to have a tightening effect on the meniscus, this in turn could cause areas of operated tissue to struggle to withstand higher tensile stress than usual (Ozeki et al., 2020).

Other more recent studies include the use of expensive but precise three dimensional (3D) coordinate measurement and motion capture equipment (Daney et al., 2019; Hirose et al., 2022) (Figure 1.21 D). Hirose et al. (2022) assessed changes in the distance between anterior and posterior markers adhered to the peripheral body of the porcine lateral meniscus with varying severities of radial meniscal body tears (Intact, 30%, 60% and 90% width) using a commercial motion capture system (OptiTrack Inc, Oregon, USA) and a robotic arm system (FRS Robotics, Leuven, Belgium). The loading protocol incorporated three pre-conditioning 20° to 90° flexion-extension cycles with a 100 N constant load. The marker distance measurements were taken at 30° and 60° flexion angles with a higher load of 300 N applied. All tibial movement was fixed in this loading regime and at the time of meniscus displacement measurement, the experiment more so resembled a static loading regime. The most severe tear (90% of the lateral meniscus width) caused a significant increase in the measured distance between the meniscus body markers in the anteroposterior direction. This also coincided with a 62 % reduction in the

resultant force transmitted through the tibia measured using a force transducer. The increase in the distance between the markers near the tear site suggest abnormal tissue deformations and displacements due to the loss in continuity of the meniscus body in dissipating load. This study highlights that motion capture is possible at the tissue level and can give important insights into meniscus function. However, a maximum load of 300 N was applied during this study, due to the limitations of the robotic arm system used.

In summary, meniscus displacement has been measured using a variety of techniques, however, static or quasi-static loading regimes are usually applied, which do not consider the cyclic loading experienced by the meniscus *in-vivo*. This is true for all the discussed biomechanical studies measuring meniscus displacement in this section. To the authors knowledge, research involving measurement of meniscal displacement has yet to be performed under a physiological dynamic loading regime *in-vitro*.

1.6.3 Knee Capsule Constraint in Whole-Joint Models

The knee joint capsule, or fascia, is made up of an inner and outer network of fibrous membranous tissue and protective fat deposits surrounding the major structures of the knee, including the ligaments, patella, cartilage, menisci, and bursae (see section 1.2.1). The primary function of the capsule is to provide joint stability and contain the synovial fluid to lubricate the articulating surfaces (Hamill et al., 2015). The knee capsule keeps moving structures in the correct position to aid motion and lubricate the joint. However, the effect of the knee capsule on meniscus biomechanics is not well understood.

Within the literature, varying levels of capsular constraint are used during biomechanical meniscus assessment. The majority retain as much of the capsule as possible during the initial intact knee specimen, but further incisions are made in subsequent surgeries, and it is unclear how much of the capsule is retained by the final test condition. A handful of studies adopt the technique of cutting the insertion of the collateral ligaments and attaching a bolt to the insertion. This is so the LCL/MCL is detached to perform an intervention and then reattached for testing (Brophy et al., 2010; Schillhammer et al., 2012; Vrancken et al., 2016; Ozeki et al., 2020). The problem with this alteration is the uncertainty whether these ligaments are offering enough physiological constraint and whether this is affecting the results.

Dissection of the capsule is frequently performed to access specific structures and perform interventions, however, in the case of meniscal extrusion, it is unclear whether tampering with the capsule in this way alters the meniscal kinematics. For example, Bylski-Austrow et al. (1994) removed the LCL during their radiological study in order to insert

markers to measure meniscal position. Interestingly, the lateral meniscus was more mobile than the medial meniscus in all kinematic cases tested. Although similar findings have been reported previously (Thompson et al., 1991; Vedi et al., 1999). The effect of removing the LCL but retaining the MCL and connective fascia could have affected the results. Unlike the LCL, the MCL is interwoven with the outer edge of the medial meniscus and the capsule. Some research suggests that this could be the reason the medial meniscus is less mobile than the lateral meniscus, causing a higher occurrence of injury (Allen et al., 1995; Fox et al., 2012). Kim et al. (2013) (described previously in section 1.6.2.2), the final condition assessed involved detaching the medial meniscus from the MCL after a MAT. No significant differences in contact mechanics were reported as compared to the MAT (with MCL attachment) condition. Similarly, Vrancken and colleagues used RSA to measure meniscal displacement in response to different capsular conditions. Three conditions were examined, the knee intact, the medial meniscus detached from the capsule and then re-sutured (centralised). Findings suggest that the medial meniscus detachment did not have any significant effects on the mobility of the meniscus (Vrancken et al., 2014). However, considerably older cadaveric specimens were used in this study (n = 6, age 75 to 90 years old) which could have affected the tissue integrity (Tsuji et al., 2017). More recently, biomechanical studies have shown that creating lesions in the meniscotibial ligament, attaching the medial meniscus to the capsule, significantly increases the amount of meniscal extrusion compared to the intact condition (Paletta et al., 2020; Ozeki et al., 2020). However, it is unknown whether analysing meniscal mobility is more sensitive to varying levels of capsular constraint when using a loading regime incorporating dynamic motion, rather than static and quasi-static motion.

1.7 Conclusions

Meniscal extrusion is a condition commonly associated with the onset of OA, this occurs when the meniscus adopts an abnormal position, moving radially outward from the joint space. Pathological meniscal extrusion is usually preceded by traumatic meniscal injury, such as a medial meniscus posterior root tear, or from underlying degeneration of the internal collagen network. This abnormal meniscal position accelerates cartilage degeneration by affecting the load distribution across the knee joint. Therefore, meniscal position or meniscal displacement is an important measure of function, however this metric is underrepresented pre-clinically and particularly in a functional setting, where physiological loads and motions of the whole knee joint are applied. Loads applied to the knee and its articulating tissues are rarely constant, therefore, modelling dynamic knee kinetics allows results to be obtained whilst the meniscus is mechanically responding to forces and motions like those experienced *in-vivo*. This improves pre-clinical studies of

new meniscal interventions in a functional setting, so engineers can better predict intervention longevity, or identify further avenues to redesign or develop. Developing a biomechanical assessment model of meniscus position in whole-knee joints experiencing dynamic physiological loads and motions with would be an effective way of addressing some of these issues. To this review's knowledge, this has not been attempted before, highlighting the importance and novelty of this project.

1.8 Project Rationale

1.8.1 Aims and Objectives

There were two key aims of this project:

1. To develop a novel method to measure dynamic meniscus displacement in a human tibiofemoral joint undergoing a physiologically relevant simulated gait profile in a six degrees of freedom knee simulator.
2. To develop a pre-clinical biomechanical model measuring meniscus displacement to assess the effects of meniscus extrusion and the efficacy of a meniscus intervention in comparison with a healthy and a damaged (root tear) condition.

The overall objectives were:

- To develop a measurement technique to measure dynamic displacement within the sample area of the knee simulator;
- to further understand the reliability of the dynamic meniscus measurement method in response to known simulator inputs, building up to complex gait profiles;
- to assess the feasibility of the experimental model on porcine tibiofemoral joints driven through a simulated gait cycle, whilst incorporating the meniscus displacement measurement system in response to soft tissue constraint levels and root tear severity;
- to apply the experimental model and meniscus displacement measurement technique to human cadaveric tibiofemoral joints in response to soft tissue constraint levels and root tear severity;
- to assess the efficacy of the experimental model in human tibiofemoral joints with an applied meniscus allograft transplant intervention.

Chapter 2

Experimental Materials and Methods

2.1 Materials

In accordance with the Human Tissue Act 2004 and laboratory regulations, all lab equipment was duplicated and split into two groups for use on animal (porcine) tissue or human cadaveric tissue. Materials associated with human tissue studies materials were clearly labelled with a brightly coloured permanent marker and stored in a separate room to materials associated with animal studies.

2.1.1 Phosphate Buffered Saline (PBS)

Phosphate Buffered Saline (PBS) is a pH balanced isotonic solution which was used to maintain tissue hydration throughout all dissections and experiments. This included fridge and freezer storage, as the samples were wrapped in tissue paper and soaked in PBS to maintain tissue hydration as much as possible over the course of the experiment. The PBS solution was prepared by dissolving one tablet into 100ml of distilled water, according to the manufacturer's instructions (MP Biomedicals LLC, UK).

2.1.2 PMMA Bone Cement

Polymethymethacrylate (PMMA) bone cement purchased from WHW Plastics (Hull, UK) was used as a fixing material throughout this project. The femur and the tibia of each knee specimen were aligned and fixed with PMMA to the corresponding tibial and femoral pots, enabling the knee to be screwed into the knee simulator and tested. PMMA consisted of a cold cure polymer powder (methylmethacrylate and 2-ethylhexylacrylate) and a liquid monomer and was prepared according to the manufacturer's instructions. The PMMA bone cement was always mixed and left to set in a fume cupboard.

2.1.3 Dissection Tools

The dissection tools used during this project included: scalpel handles, disposable scalpel blades (Swann-Morton, Sheffield, UK), forceps, chainmail glove, hacksaw, cordless hand drill (Bosch Ltd, Stuttgart, Germany), drill bit (3.5 mm and 4.1 mm) and fixation screws. Human tissue dissection was always carried out in a Class II Biological Safety Cabinet (Monmouth Scientific, UK). After use, all the dissection tools were cleaned with laboratory regulation disinfectant.

2.1.4 Cementing Fixtures

The cementing fixtures and associated equipment were used to align and cement each knee specimen for simulation. These included the tibial pot, femoral pot, lower base component, upper fixture arm, tibial spike, locating pins, fixation screws, grub screws, cap screws and hex keys. After use, all the cementing fixtures were cleaned with laboratory regulation disinfectant.

2.2 Methods

2.2.1 Porcine Tissue

2.2.1.1 Procurement

The right hind legs of skeletally immature (4 to 6 months) female pigs were procured from a local abattoir (John Penny & Company, Leeds, UK) within 24 hours of slaughter. The right hind legs were cut at the pelvis, near the hip joint, and all the skin and muscle on the leg, including the trotter were received intact (Figure 2.1A).

2.2.1.2 Dissection

The dissection process of right porcine hind legs was based on previously documented methods (Liu et al., 2015; Liu et al., 2019). The complete porcine knee joint was harvested from the leg whilst keeping the knee capsule fully intact containing the patella, Hoffas pad, cruciate and collateral ligaments, menisci, synovial fluid and articular cartilage. To ensure the knee joint was kept in the in-situ alignment, a small window was cut deep into the lateral side of the leg and in the location of knee joint. Tissue was carefully cut back until the LCL was visible and tissue could be shaved around the LCL insertions to expose part of the lateral femoral condyle and the proximal tibia. A metal

brace was drilled and screwed onto the exposed areas of the femur and the tibia just anterior to the LCL and fitting to the contours of the joint (Figure 2.1B). This process was then repeated on the medial side of the knee, securing metal brace to the femoral condyle and the tibia just anterior to the MCL. All excess skin and muscle tissue in the thigh and calve region was excised and the femoral head was lifted out of the acetabular cup (Figure 2.1C). The bones were shaved of excess muscle and fat tissue and the knee capsule was left intact. The tibia and fibula were sawed through roughly 10mm above the ankle joint (Figure 2.1D), and the femur was sawed just below the head and greater trochanter (Figure 2.1E). The harvested knee joint is displayed in Figure 2.1F. PBS spray was used frequently to hydrate the tissue.

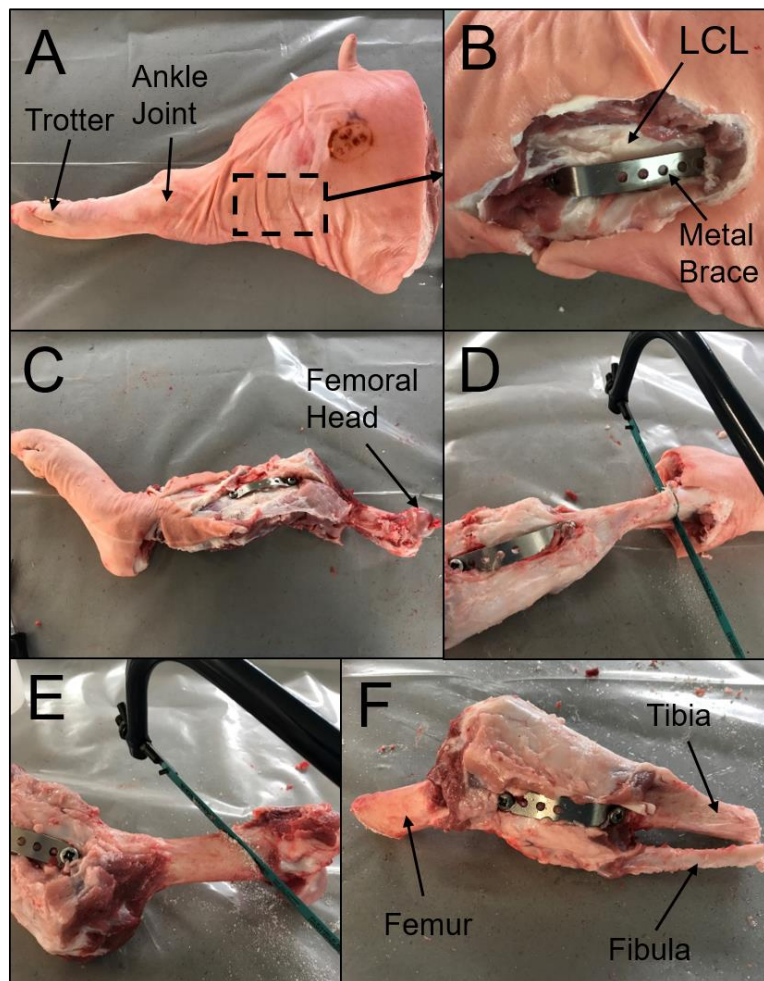


Figure 2.1. A-F. Porcine knee joint with capsule retained dissection process.

2.2.1.3 Alignment and Cementing

Once dissected, the porcine knee joints were prepared for simulation by fixing the femur and the tibia in PMMA bone cement, and aligned in an anatomical position (Liu et

al., 2015; Liu et al., 2019). The centre of rotation (COR) points were determined for the medial and lateral femoral condyle. The COR locations were determined by identifying the anatomical landmarks of the MCL and LCL insertions on the knee sample. The CORs were located just distal to the insertions of the MCL and LCL on the corresponding femoral condyles (Figure 2.2). Map pins were used to mark the location and a small scalpel incision through the capsule to the insertion sites prevented the fascia from pulling and tearing whilst the COR holes were drilled. Once the locations were determined, the COR holes were drilled using a small 3.5 mm drill bit. The COR location method was adapted in this project from previously documented methods which involved using transparent templates to estimate the diameter, circumference and therefore centre point of each condyle (McCann et al., 2008; Liu et al., 2015). The reason for adapting the COR locating method was because the knee capsule was retained and therefore the condyles were not exposed to line up the condylar curvature with the COR templates. Once the CORs had been drilled, the offset of the cementing jig was shifted to ensure a higher percentage of the load travels down the medial compartment of the knee (McCann et al., 2008). ISO standards for TKR simulation recommended the medial offset should be set at 7% of the tibial plateau width (Liu et al., 2015). The tibial plateau width was measured using callipers and the offset was calculated. The dial was adjusted on the upper fixture arm from the zero position to this calculated offset in millimetres. The medial offset value for porcine knees ranged between 4.5 – 5.0 mm.

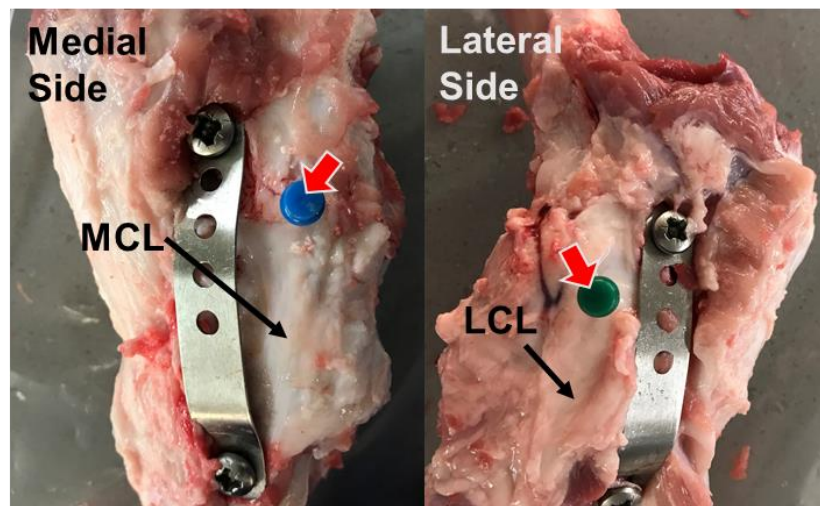


Figure 2.2. Porcine knee joint centre of rotation (COR) positioning for the medial and lateral condyles (indicated by the red arrows in the images).

Two delrin cementing pots were used to fix the femur and tibia in alignment and to allow attachment to the tibial base and flexion-extension arm of the simulator. The tibial and femoral pots were greased, and grub screws were screwed into the tapped holes to

be flush against the outer surface of the pot. The grub screws prevented the cement moving within the pot and allowed removal of the knee joint from the pots for storage and/or disposal after simulation.

As illustrated in Figure 2.3, the fixture rig incorporated an upper fixture arm and a base component which replicated the sample area of the simulator. The tibial spike was attached to the upper fixture arm (with the medial offset applied), the knee sample was inverted, and the tibial bone marrow was pushed into the tibial spike. The femoral pot and all the cementing jig components were screwed together and the COR holes in the knee joint sample were aligned with the COR locating pins. The pig stifle joint falls in a natural state of flexion, therefore a flexion offset of $\sim 24^\circ$ flexion at heel strike was applied to the porcine knee samples. This flexion offset was estimated from a pig gait analysis study (Thorup, 2007). This offset was applied by tilting the upper arm and using the angle dial on the side of the fixture rig. The fixture rig was secured at the offset angle and PMMA bone cement was poured into the femoral pot, fixing the femur in alignment (Figure 2.3).

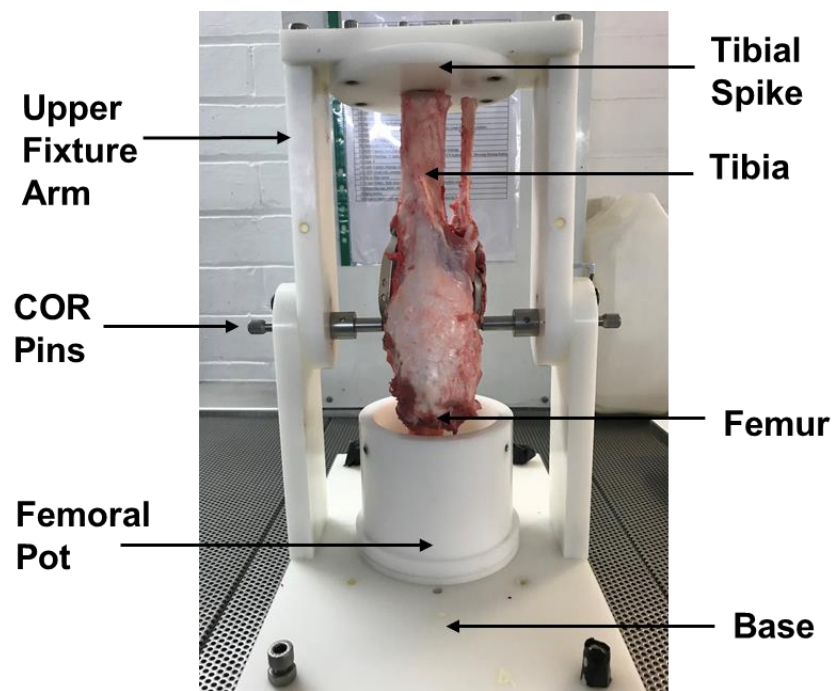


Figure 2.3. Porcine femoral side alignment and cementing procedure.

The tibia was potted relative to the femur; the upper fixture arm and tibial spike were removed, and the medial offset gauge was set back to 0 mm. The cemented femoral pot was unscrewed from the base component and attached to the upper fixture arm in place of the tibial spike. The tibial pot was attached to the lower platform and the fixture rig

was erected and secured again with the COR locating pins at the 0° angle. The PMMA cementing process was repeated for the tibial pot.

2.2.2 Human Tissue

2.2.2.1 Ethical Approval, Procurement and Storage

Ethical approval for use of cadaveric human knee specimens in this research project was granted by the National Health Service (NHS) Health Research Authority Ethics Committee (REC reference: 18/EM/0224. IRAS project ID: 239594) (Appendix B).

The human knee specimens were purchased from MedCure Limited (Oregon, US) as fresh-frozen whole joint specimens, clearly labelled with an anonymous donor identification code and details of gender, age and BMI. The human specimens were stored at -40°C in airtight bags in a securely locked and alarmed human tissue freezer. When required for imaging/testing, human specimens were moved from the freezer and defrosted at 2 °C to 5 °C for 72 hours in a designated human tissue fridge.

2.2.2.2 Human Specimen Recording and Tracking

The donor identification codes, details and storage location of each human knee specimen were uploaded to a secure online tracking system (Achiever Solutions, Interactive Software Limited, Solihull, UK). At all stages of the experiment, the specimen storage location was recorded, including all excised tissue from the experiment. Air-tight fridge and freezer bags containing the human specimen and human specimen excised tissues were labelled with the donor identification code, specimen details (eg: patella), date and principal investigator to allow identification within the storage locations.

2.2.2.3 Magnetic Resonance Imaging (MRI)

All human knee specimens underwent one thaw cycle to allow for Magnetic Resonance Imaging (MRI) (Siemens Magnetom Prisma (3T), Erlangen, Germany), prior to dissection. This was done by a colleague who was trained in radiography. The scans were analysed by the same colleague and the tibial width, epicondylar axis and condylar dimensions were measured to use as a guide during alignment and cementing. An imaging report for each specimen was circulated which detailed the quality of the bone, meniscus and cartilage prior to simulation. The criterion of consistent bone quality (i.e: no spaces indicating bone loss/low bone density) was deemed the most important due to the

high physiological loads (~ 3000 N) the knee would have to experience during knee simulation. An example of the MRI scans are displayed in Figure 2.4.

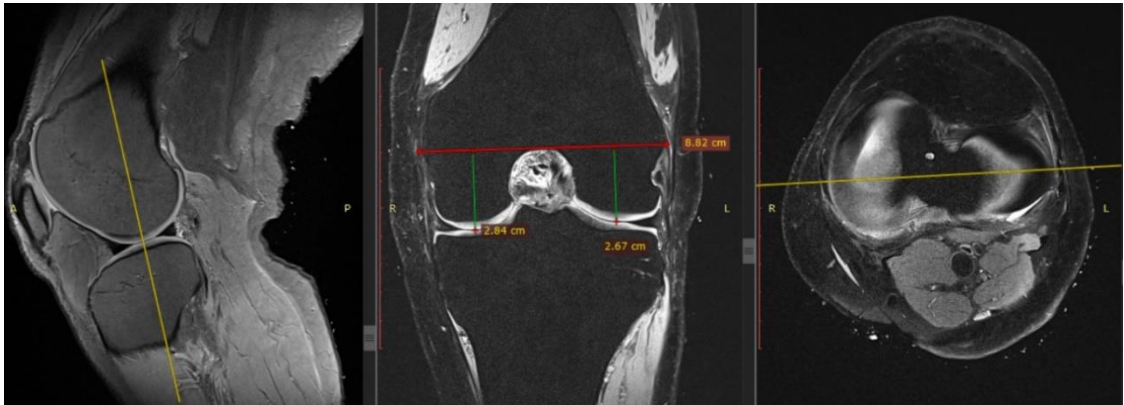


Figure 2.4. Example MRI images to obtain distance measurements and scanning reports on the bone, meniscus and cartilage condition prior to testing.

2.2.2.4 Dissection

The human knee dissection procedure followed a method developed in previously published literature (Liu et al., 2020). All human cadaveric specimen preparation was carried out in a Class II Biological safety Cabinet (Monmouth Scientific, UK), using specific equipment and tools for human tissue use and appropriate personal protection equipment. The human specimens throughout this project were received as whole joints with part of the upper calf and the lower thigh included (Figure 2.5A). The human knee joint was dissected from the leg whilst keeping the knee capsule intact, containing muscular attachments, patella, ligaments, menisci, articular cartilage and synovial fluid.

Avoiding the knee joint articulation area, the skin and fat around the femur and the tibia were removed first, exposing the thigh and calf muscles. The muscle was then removed in these areas to expose the femur, tibia and fibula bones (Figure 2.5B). It was important to retain as much muscle as possible around the knee joint articulation to retain the natural soft tissue constraint prior to the alignment and cementing procedure. The skin, fat and a small amount of muscle was removed from the posterior portion of the knee joint articulation area. Caution was taken around the medial head of the gastrocnemius muscle which was connected to the knee capsule and attached directly to the medial condyle. The lateral and medial condyles sit close to the skin; therefore, caution was taken in these areas to expose the LCL and MCL, without cutting the knee capsule. A thin layer of fibrous connective tissue usually covered the LCL and MCL (Figure 2.5C).

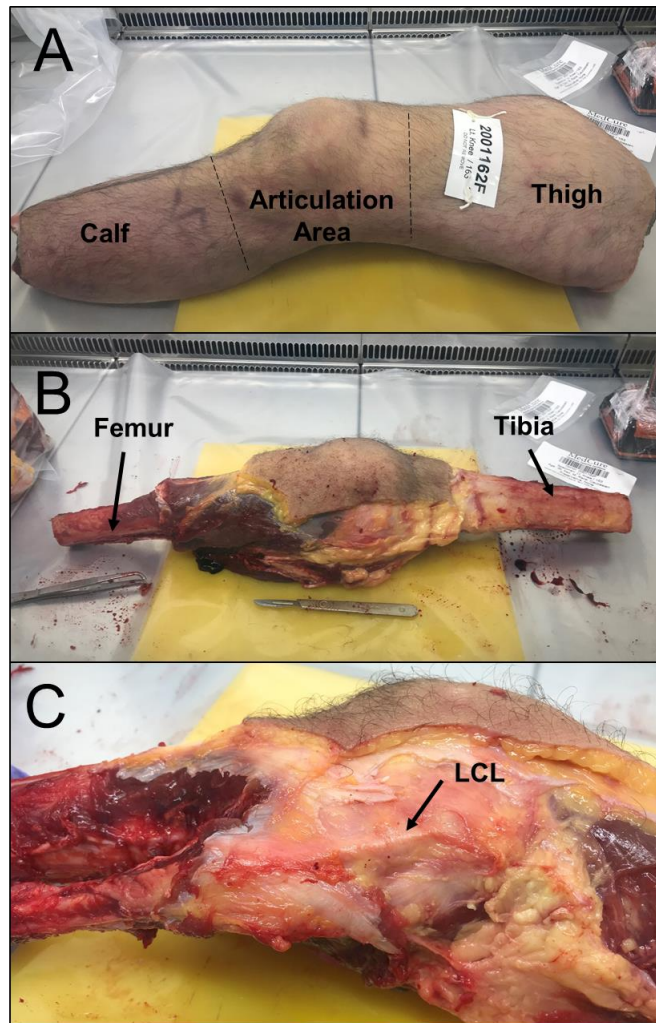


Figure 2.5. A-C. Human knee specimen dissection procedure.

The femur, tibia and fibula were sawed to size, so the specimen was able to fit into the cementing jig. The cementing jig was constructed to estimate the cutting locations on the bones. Anti-rotation screws were drilled into the ends of the cut femur and tibia bones. These screws prevented movement of the bone within the PMMA cement during human knee simulation.

2.2.2.5 Alignment and Cementing

The alignment and cementing procedure for human knee specimens followed a similar process as previously described for porcine (section 2.2.1.3) and in Liu et al. (2020). Firstly, the medial and lateral centre of rotation (COR) positions were located. Previous literature suggests that the transepicondylar axis more closely reflects the true COR of the knee during flexion, and that this axis is usually located between the medial sulcus or furrow and the lateral prominence (Hollister et al., 1993; Churchill et al., 1998;

Yin et al., 2015). In this study, the COR holes for each condyle were located using these landmarks and were positioned just posterior to the bony prominences (epicondyles) of the MCL and LCL insertions (Figure 2.6A and B).

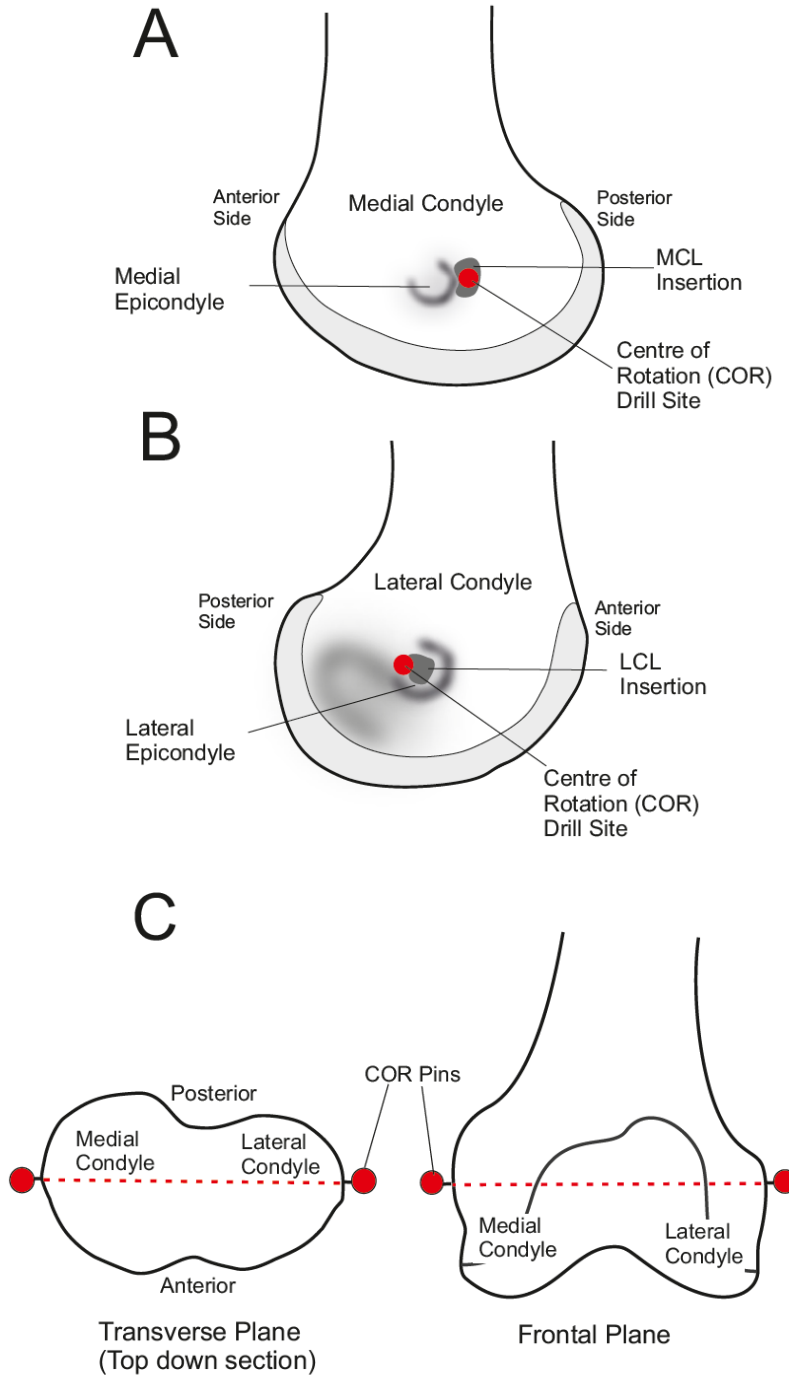


Figure 2.6. Human knee joint centre of rotation (COR) approximation from the (A) medial and (B) lateral epicondyles. (C) Lining up the COR holes with the simulator centre of rotation axes in the transverse and frontal plane.

The epicondyles were palpated, and the femur was rotated to aid the COR location estimation. Due to the heterogeneity of human knee anatomy, in some cases the insertions of the MCL and LCL were difficult to locate through the capsule, or the epicondyle axis was at a large angle. It was important that the lateral and medial COR holes were approximately level in the frontal and transverse planes, to line up with the simulator COR flexion-extension axis (Figure 2.6C). Therefore, if in the case that the COR holes were not visually level, one COR hole may be moved within a 10 mm radius to prevent overly twisting or tilting the knee joint during alignment. Pins were inserted to mark the COR hole location before drilling. The limitations of the alignment and cementing methodology is explained in more detail in the final discussion section of this thesis (see section 7.5.2.5). The medial offset was applied in the same way as the porcine method by calculating 7% of the tibial width (mm) and adjusting the medial offset gauge on the upper fixture arm. Due to the larger human knee size, the medial offset was 5.5 – 6.0 mm. The tibia was pushed through the tibial spike and human cementing fixture was constructed so the COR pins lined up with the drilled COR holes on the specimen. The human knee joint is roughly 0° at full extension, therefore, no angular offset was applied to the upper fixture arm and a spirit level was used to ensure the alignment was at 0° . A clamp was used to pull the excess skin and muscle on the anterior portion of the knee away from the pot. PMMA bone cement was poured into the femoral pot and the femur was fixed in the alignment (Figure 2.7). After the cement had set, the cementing jig was deconstructed and the medial offset gauge on the upper arm was moved back to zero. The tibia was then cemented relative to the femoral alignment.

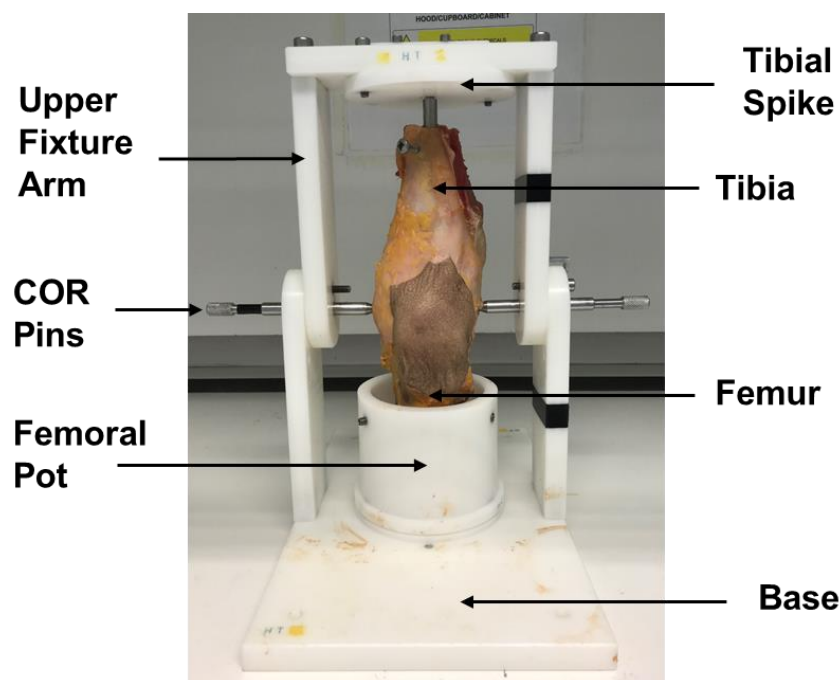


Figure 2.7. Human knee specimen femoral side alignment and cementing procedure.

2.2.2.6 Post Experiment Handling of Human Knee Specimens

As described in section 2.2.2.2 each knee specimen and the associated excised tissue were recorded and stored appropriately throughout the experiment. After the experiment, the distal femur and the tibia plateau (including menisci) of the remaining knee specimen were stored at -40°C in the same freezer compartment as the excised tissue. The airtight freezer bags were clearly labelled with the donor identification code, specimen details (eg: femur), freezing date and the name of the principal investigator (grant holder). All parts of the assessed human specimens were available to use by trained colleagues to maximise the accessibility of human tissue for other research projects in the institute in accordance with the ethical approval obtained.

2.3 Knee Simulation

2.3.1 Single Station Knee Simulator

The Leeds Single Station Knee Simulator (Simulation Solutions, Stockport, UK) was used throughout this research project (Figure 2.8A). Based on total knee replacement wear simulators; this knee simulator had been adapted to simulate natural tissue to facilitate biomechanical and tribological research on early knee interventions (Liu et al., 2015; Bowland et al., 2018; Liu et al., 2019; Liu et al., 2020).

The knee simulator is electromechanically driven and able to cyclically simulate walking gait motion by driving two translation axes: compression-distraction (axial translation), anterior-posterior translation; and driving three rotation axes: flexion-extension rotation, internal-external rotation and abduction-adduction rotation (Figure 2.8 B, C and Figure 2.9). The natural knee joint moves about 6 degrees of freedom, however, the medial-lateral axis of the simulator was not able to be driven and therefore was fixed at zero. The simulator has the capability of driving these axes with displacement inputs (displacement-controlled) or force inputs (force controlled). Table 2.1 describes a breakdown of the motion axes parameters and limits used in this project. The axial force axis was always driven in force control. The flexion-extension and abduction-adduction axes were always driven in displacement control. In line with previous knee simulation work, the abduction-adduction axis was not driven and left to move freely (Liu et al., 2015; Liu et al., 2020). The anterior-posterior translation and tibial rotation axes could either be controlled with force or displacement inputs, depending on the research question. In this research project, both the anterior-posterior translation and tibial rotation were displacement controlled at predefined profile parameters to control more factors affecting meniscus displacement measurements (see section 2.3.2).

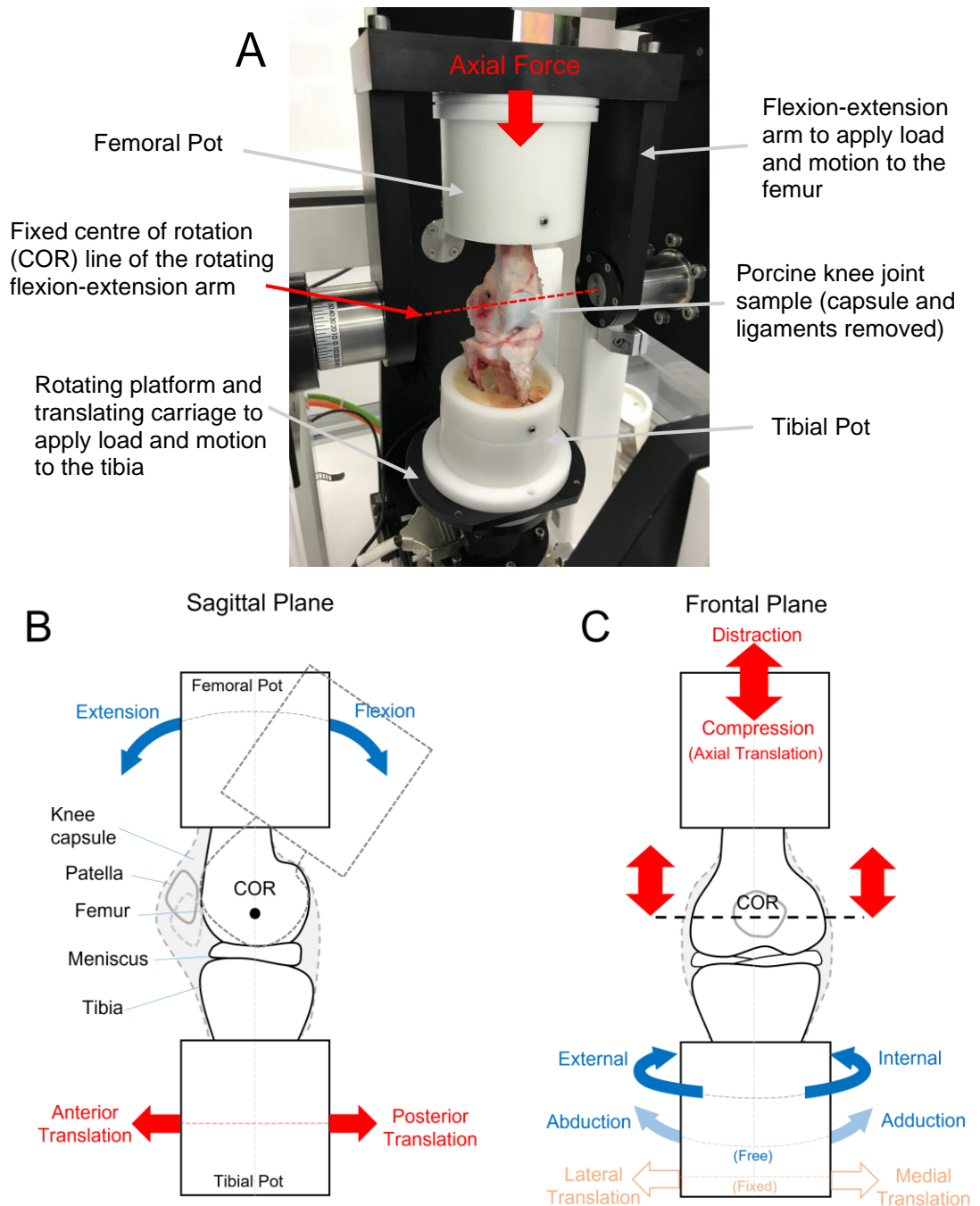


Figure 2.8. (A) Porcine knee sample set up in the Leeds single station knee simulator. (B) Sagittal plane and (C) frontal plane schematics of the rotation (blue arrows) and translation (red arrows) movement axes for a right knee sample in the knee simulator. The axial force is applied vertically to the femoral components of the knee sample. The force is applied perpendicular to the axis of centre of rotation of the flexion – extension arm whilst other parts of the machine drive tibial rotations (internal-external) and tibial translations (anterior-posterior). The abduction-adduction rotation axis was left unconstrained (free), and the medial-lateral translation axis was fixed at zero.

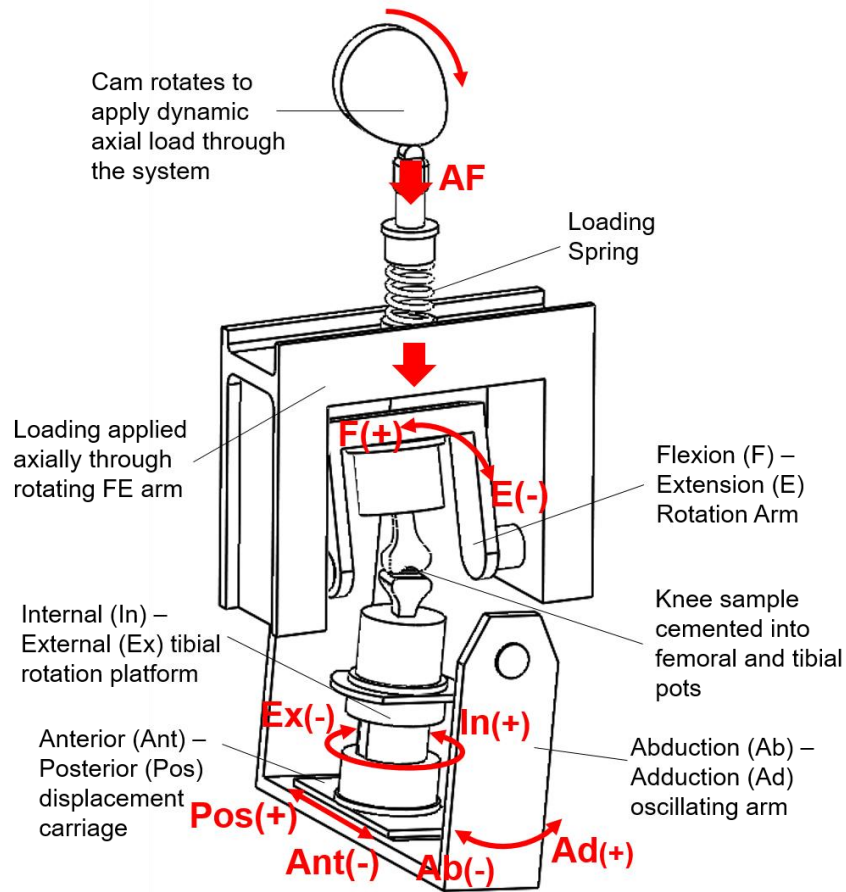


Figure 2.9. Schematic showing the mechanical parts of the simulator facilitating movement of the rotation and translation movement axes during knee gait simulation.

Table 2.1. Summary of the key mechanical motion axes' sensor control information and limits.

<i>Axis of Motion and Polarity</i>	<i>Control Mode</i>	<i>Range</i>	<i>Accuracy</i>
Axial Force	Force	0 – 5kN	± 30N
Flexion (+) / Extension (-) Angle	Displacement	± 90°	± 0.03°
Abduction (-) / Adduction (+) Angle	Displacement	± 10°	± 0.03°
Anterior (-) / Posterior (+) Translation	Force or Displacement	± 30mm	± 0.1mm
Internal (+) / External (-) Rotation	Force or Displacement	± 15°	± 0.09°
Medial (+) / Lateral (-) Translation	Not controlled (Fixed at zero)	± 10mm	N/A

Studies using force-controlled anterior-posterior translation and tibial rotation have the benefit of achieving kinematic output data, providing that suitable spring constraints were applied. The springs limit the motion of the axes produced by the applied force and may be in the form of natural collateral/cruciate ligaments of the tibiofemoral joint sample, programmed virtual springs of the simulator, or physical springs attached to the machinery (Bowland et al., 2018; Liu et al., 2019; Abdelgaied et al., 2022).

The simulator contains a six-axis load cell within the tibial platform which gives the axial load output as well as a force or torque output for each translation or rotation axis, respectively. The simulator also has an additional shear force load cell to determine the AP shear force, which describes the force transmitted between the femoral to tibial components. To summarise, the force outputs were axial force, flexion-extension torque, tibial rotation torque, anterior-posterior force, anterior-posterior friction (shear force) and abduction-adduction torque.

The simulator was operated with a connected computer using the ProSim graphical user interface, which enabled the configuration and execution of cyclic gait profiles, driven at a specific frequency. The ProSim software used the numbers in the gait profile input file (text file) to drive the motors to move the axes of the simulator across 1 cycle. This was the demand and repeats for a defined number of cycles. The simulator's sensors fed-back the output displacement/force data to the computer as analog to digital converter (ADC) values. The ADC values were then converted by the computer using recent axis-specific calibration values to generate the digital output of load/displacement for each axis during operation. The output data was automatically saved as tab delimited text files during simulation.

2.3.1.1 Calibration

The sensors of the simulator can drift overtime due to factors such as mechanical vibrations and temperature changes. Therefore, to maintain measurement accuracy, the simulator was routinely calibrated by a trained Simulation Solutions engineer prior to each individual porcine and human study. To carry out the calibration, all the mechanical axes were enabled and the abduction-adduction component and anterior-posterior carriage were connected to their corresponding motors. An initial check was carried out to verify the zero readings using the centring jig; this jig ensured all the mechanical axes were in the zero position to check the positional readings of the sensors (Figure 2.10A). Calibration procedures were not required for the flexion-extension and tibial rotation positional axes as optical encoder sensors were built within the corresponding motors (Bowland, 2016). Rarely changes in the zero values for these axes would occur, however, if errors became present, the engineer would reprogram the coupling of the sensor with

the motor using code. The anterior-posterior translation and abduction-adduction axes were calibrated and verified using slip gauges and an inclinometer, respectively. The slip gauge calibration process for the anterior-posterior translation axis has been previously described in detail in Bowland. (2016).

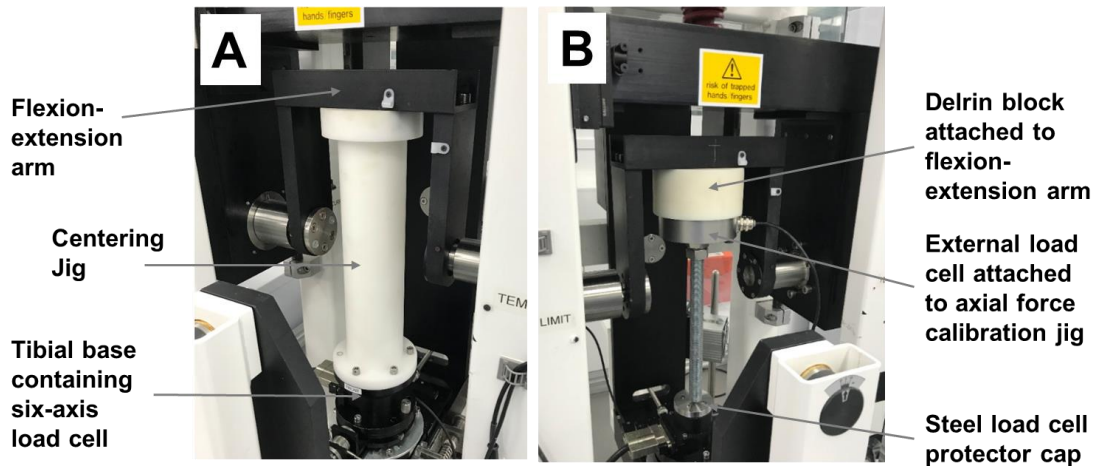


Figure 2.10. Simulator calibration images showing the set up of the (A) centring jig to zero all positional axes and (B) the axial force load calibration set up.

Axial force calibration:

Force axis calibration was achieved using an external calibrated USB load cell (5kN), plugged into the USB port of the connected computer. The axial force axis was the only force-controlled axis used during this project and this was calibrated using the mechanical set-up jig pictured in Figure 2.10B. The tibial base plate of the simulator was removed, and a steel cap was attached to protect the exposed simulator load cell. The simulator predominantly used during this project was equipped with an automatic load calibration procedure built into the software. Using the ProSim software, all the loads were tared, and connection was made with the external load cell. Ensuring the simulator was in calibration mode, the axial force axis was selected in the 'auto load calibration' dialog box, then 'auto-run' was selected to begin the automatic calibration process. The calibration process applied five demand loads of: 100N, 750N, 1500N, 2250N and 3000N and produces two calibration graphs, one graph comparing the demand load vs actual load and another graph comparing the sensor ADC values to real-world newton values with deviations corrected through calibration. The software calculated a set of calibration constants to account for the variation in actual vs demand load for the observer to either accept or re-run the calibration process.

2.3.2 Simulated Gait Profile

The Leeds high kinematics displacement-controlled gait profile with modified two-peak axial force input was used to simulate walking motion throughout this project. This profile was used in previously published natural knee simulation studies (Liu et al., 2015; Liu et al., 2019). The kinematic inputs of the gait profile were based on the results from Lafortune et al. (1992) healthy participant bone-pin gait study. The gait profile was developed from wear simulation studies (Barnett et al., 2001; McEwen et al., 2005; Abdelgaied et al., 2022) and simulates a high magnitude (0-10 mm) of anterior tibial shift to replicate the posterior roll-back of the femur during flexion (Brockett et al., 2016).

In previous literature, a three peak axial force input was used in knee simulation, based on the early findings of Morrison (1970) (Liu et al., 2015; Liu et al., 2019). However, more recent gait analysis and instrumented prosthesis studies show that the axial force profile commonly exhibits two-peaks (D Lima et al., 2005; Heinlein et al., 2009; Kutzner et al., 2010). This was modified in a recent study simulating human knee gait and was used throughout this project (Liu et al., 2020). The driven input axes of the porcine and human Leeds high kinematics gait profile (with the modified two-peak axial force) are presented for a right knee in Figure 2.11 on the next page.

The flexion-extension rotation, anterior-posterior translation, and internal-external rotation were all driven in displacement control. The axial load was driven in force control. The gait profile used for porcine knee joints was scaled down from the human gait profile for each driven axes using parameters based on a 70kg pig (Liu et al., 2015). This scaling factor was approximately one third of the human gait parameters. The frequency of gait simulation using in this project was 0.5 Hz (2 seconds per gait cycle). This was slower than the standard (1 Hz) and average physiological gait (~ 0.8 Hz) (Heinlein et al., 2009; Kutzner et al., 2010; Reinders et al., 2015), however, this speed was important to obtain meaningful displacement data from the videos, as explained later in section 4.2.2.1. The maximum and minimum values for each driven axes of the human and the porcine input profile are described in Table 2.2 on the next page.

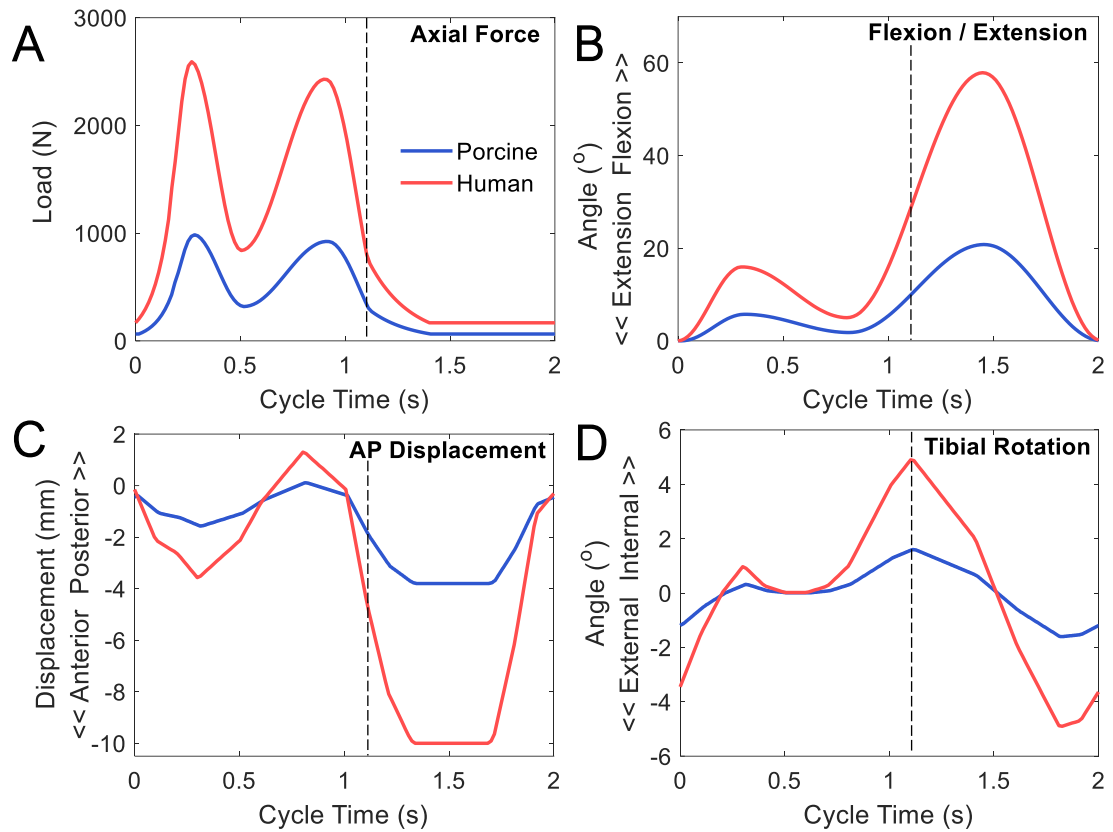


Figure 2.11. The Leeds high kinematics gait profile driven inputs for porcine and human knee simulation (driven at 0.5 Hz). (A) Modified two-peak axial force profile, (B) flexion extension, (C) anterior-posterior tibia translation and (D) tibial rotation.

Table 2.2. Maximum and minimum values for each gait profile axis of the porcine and human profiles.

<i>Gat Profile Axis</i>	<i>Control Mode</i>	<i>Sample</i>	<i>Minimum</i>	<i>Maximum</i>
Axial Force	Force	Porcine	63.5 N	984.7 N
		Human	167.6 N	2592 N
Flexion (+) / Extension (-) Angle	Displacement	Porcine	0.0°	20.8°
		Human	0.0°	57.9°
Anterior (-) / Posterior (+) Translation	Displacement	Porcine	- 3.8 mm	0.1 mm
		Human	- 10 mm	1.4 mm
Internal (+) / External (-) Rotation	Displacement	Porcine	- 1.6°	1.6°
		Human	- 5.0°	5.0°
Adduction (+) / Abduction Angle (-)	Free	Porcine	N/A	N/A
		Human	N/A	N/A

2.3.2.1 Left Knee Joint Simulation

The standard model for natural knee simulation was based on right knees, however, human specimens came as left and right knee joints. As described in Table 2.3, the polarity of the tibial rotation and abduction-adduction axes were inverted when characterising left and right knee movement. Rather than changing the mechanical polarity of the simulator, the polarity of the tibial rotation was inverted on the gait profile to simulate left knee gait in the correct direction of rotation (Figure 2.12). The polarity of the passive abduction-adduction axis for left knee simulation was inverted during the post processing of the results.

Table 2.3. Polarity differences of the tibial rotation (TR) and the adduction-abduction (AA) axes during left and right human knee simulation.

<i>Axis</i>	<i>Direction</i>	<i>Right Knee</i>	<i>Left Knee</i>
TR	Internal	+	-
	External	-	+
AA	Adduction	+	-
	Abduction	-	+

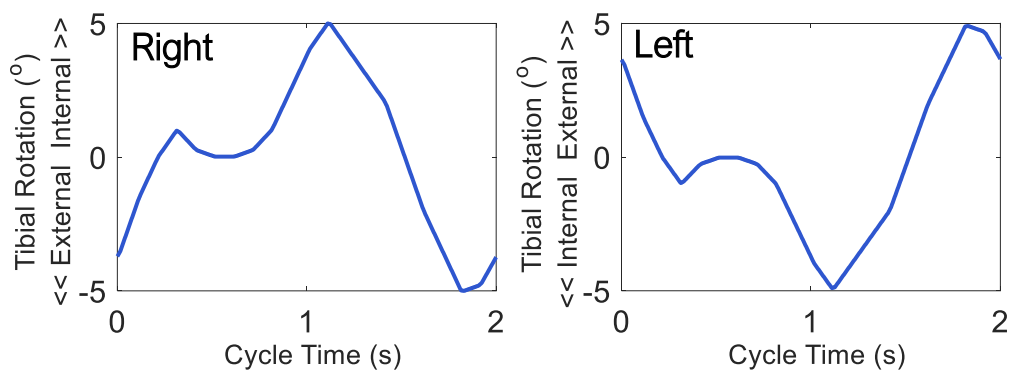


Figure 2.12. Inversion of the tibial rotation input axes for right and left human knee simulation.

Chapter 3

Development of a Measurement Technique to Quantify Dynamic Medial Meniscal Displacement *In-Vitro*

3.1 Introduction

This thesis has discussed that meniscal extrusion manifests in two forms: degenerative extrusion or traumatic extrusion (see section 1.5.3). Degenerative extrusion is caused by a degenerated meniscus, where the internal microstructure loses its integrity over time, meaning that the meniscus adopts an altered position when it is not bearing bodyweight and is permanently deformed. Degenerative extrusion is rarely reported and usually goes undetected until the patient is older and has been diagnosed with OA. Traumatic extrusion occurs due to an injury, most commonly a root tear caused by a mix of high load, flexion and torsion of the knee. The avascular and aneural nature of the meniscal tissue can mean that a root injury might be undetected, or the current repair and replacement methods might not be sufficient to restore healthy meniscal position and kinematics. Traumatic extrusion more commonly occurs in younger active patients and because the focus of this thesis is the prevention/delay of OA using early knee interventions, modelling a traumatic injury to model meniscal extrusion is more appropriate.

However, the same result occurs for both forms of extrusion, which is a change in position of the meniscus and an altered dynamic meniscal kinematics with knee load and motion. These factors create an imbalance in the functionality of the meniscus, which effects the stability of the knee joint and increases the likelihood of cartilage degeneration. Therefore, measuring the change in position or displacement of the meniscus, which includes both deformation and the movement of the tissue, is an effective way to investigate deviations from normal and signify negative biomechanical effects under a variety of conditions. The herein method could be applied to both forms of extrusion, however, the focus is on traumatic extrusion.

This chapter discusses the process of developing a method to measure medial meniscal displacement in the frontal and sagittal plane, whilst the knee is driven through

quasi-static and dynamic profiles in the knee simulator. The method was developed systematically, using a simple video camera, loading profile and image acquisition technique. Further method developments included optimising the loading regime and automating the measurement technique using computational methods.

3.1.1 Aim and Objectives

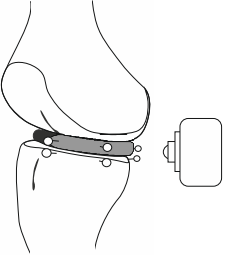
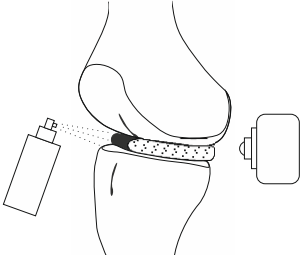
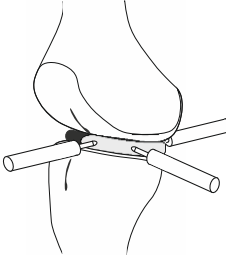
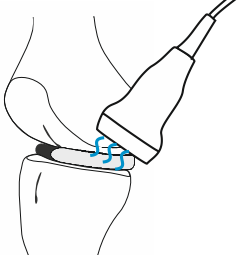
The overall aim was to develop a method to measure medial meniscal displacement in a whole knee joint sample, performing a dynamic gait cycle in the simulator. The medial meniscus was chosen because it is more clinically associated with meniscal extrusion than the lateral (Krych, Bernard, Kennedy, et al., 2020). Due to the anatomical differences of porcine and human knee joints and menisci (see section 1.6.1.2), porcine knee joints will only be used for method development before transferring the method to human samples. To achieve this aim, the following objectives were:

1. to create and validate a motion capture method to measure the medial meniscal displacement in the frontal plane and medial-lateral direction, under a simplified quasi-static loading protocol;
2. to apply and develop this method to measure the sagittal plane anterior-posterior displacement of the medial meniscus simultaneously;
3. to perform this method on a porcine knee performing a simple dynamic flexion-extension profile;
4. to improve the objectivity, repeatability and precision of the measurement technique using computational techniques;
5. to fully pilot the developed method on one porcine knee under different soft tissue constraint conditions.

3.2 Measurement Methodology Specification

As described in Table 3.1, potential meniscus displacement measurement methods were evaluated. The decision was made to use a marker-based tracking method as there was minimal contact with the tissue enabling free knee movement and the application of complex dynamic simulator gait inputs. In addition, capsular constraint could be assessed whilst maintaining marker positioning. The markers can be pinned through the capsule, and the capsule dissected away. The other evaluated methods maybe more effective in measuring strains and slow deformation in static environments under increasing load. The objectives of this method were to measure meniscal displacement undergoing dynamic physiological load and motion.

Table 3.1. Meniscus displacement measurement method specification and comparisons.

<i>Method Type</i>	Marker Tracking / Motion Capture	Digital Image Correlation (DIC)	Linear Variable Differential Transformers (LVDTs)	Ultrasound
				
<i>Description</i>	Markers are pinned to the tissue. Images are taken during loading and a software is used to calculate the change in position of the markers between each image.	A speckle pattern is applied to the tissue. Images are taken during loading and an algorithm calculates the speckle size and distance to estimate displacement and strain.	Operates through electromagnetic coupling principles. Transmitting mechanical linear motion into electrical signals.	A transducer emits and detects soundwaves. The distance between the transducer and the tissue boundary is calculated from the speed and frequency of reflecting soundwaves.
<i>Possible to apply dynamic load and motion regimes?</i>	Yes, allows free dynamic movement at 0.5Hz to 1Hz gait speeds.	Yes, allows free dynamic movement but at slower frequencies < 0.5Hz	No, a slower controlled / static regime would need to be applied to measure accurately	No, a slower controlled / static regime would need to be applied to measure accurately.
<i>Tissue Contact?</i>	Minimal from markers	No	Yes	Yes
<i>Ability to assess knee capsule constraint and meniscus injury?</i>	Yes, marker pins penetrate through the capsule and positions can be controlled.	No, incompatible with capsule intact as the speckle pattern is applied to the capsule surface.	Yes, however LVDT tip locations on the meniscus must be controlled.	Yes, most effective when the capsule is fully intact. Conditions could be applied arthroscopically
<i>Compact size for simulator?</i>	Yes, providing small cameras are used.	Yes, providing small cameras are used.	Yes, providing < 30 mm total lengths are acquired	No. Difficult to position the transducer in the sample area
<i>Estimated Cost</i>	< £500 (2D) - £30,000 (3D)	< £500 (2D) - £100,000 (3D).	~ £200 - £1000 each	~ £3,000 – £15,000
<i>References</i>	(Bilesan et al., 2018; Hirose et al., 2022)	(Palanca et al., 2016)	(Hein et al., 2011; LORD Corp. MircoStrain, 2013)	(Paletta et al., 2020; NiBIB, 2023)

3.3 Frontal Plane Method Development

3.3.1 Rationale

An experimental method was trialled using a video camera and an ImageJ (Schneider et al., 2012) image measurement technique to measure the displacement of the medial meniscus under increasing load, in relation to the tibial plateau. The purpose of this work was to develop and validate a novel method in the simulator and observe trends of the medial meniscus displacement in the frontal plane with increasing load and fixed flexion angles in intact porcine samples. An additional aim was to simulate a complete medial meniscus posterior root tear and compare the torn and intact conditions.

3.3.2 Experimental Set Up

3.3.2.1 Sample preparation

Fresh whole knee joint samples ($n = 3$) were dissected from the right hind legs of 6-month-old female pigs (84.7kg, 100.2kg and 90.7kg). Samples were dissected no greater than 24 hours after slaughter and stored in 4°C wrapped in tissue soaked with PBS before testing. The full dissection process is described in section 2.2.1.2. For this preliminary study, the fascia around the medial collateral ligament (MCL) was carefully removed to expose the ligament, and a line was scored on the tibia and along the posterior aspect of the ligament to mark their position for marker placement. In other work, the posterior aspect of the MCL line was used as the position to measure quasi-static medial-lateral meniscal displacement (Hein et al., 2011). After the line was scored, the MCL the and lateral collateral ligaments (LCL), and the anterior and posterior cruciate ligaments (ACL and PCL) were removed in accordance to previously performed sample preparation protocol (Liu et al., 2015; Bowland et al., 2018). The alignment and cementing process followed methods described in section 2.2.1.3.

Map pins of 5 mm diameter with black and white centroid quadrants were used as markers. A fixed reference marker was pinned and adhered with superglue, to the tibial plateau on the scored MCL line. A moving meniscal marker was placed on the medial meniscus directly above this marker, with the knee aligned at 0° extension (Figure 3.1A). Control markers were also placed on the anterior aspect of the femur and tibia to measure the vertical displacement of the femur relative to the fixed tibia. However, due to narrow space and limited focusing distance of the camera, this data was excluded as the markers were not in clear focus to give an accurate measurement. Markers were also placed on the lateral meniscus and acted as a control for the torn condition.

3.3.2.2 Video Camera Specifications and Positioning

A Panasonic Lumix GF7 (Panasonic, Osaka, Japan) was used for video recording. This camera records at a HD resolution of 1920 x 1080 pixels at 60 frames per second (fps) for a quality image and clarity of motion. The focusing system was set to manual focus and no zoom was used. The camera was positioned in the simulator, viewing the knee in the frontal plane, and held by a universal bracket arm attached to the marked point on the simulator. Care was taken to ensure the camera remained in the same position for all tests and repeats, therefore, as well as the fixed bracket, position measurements were taken with a tape measure from the bottom and back of the camera to the abduction-adduction (AA) arm of the simulator and kept constant (Figure 3.1B).

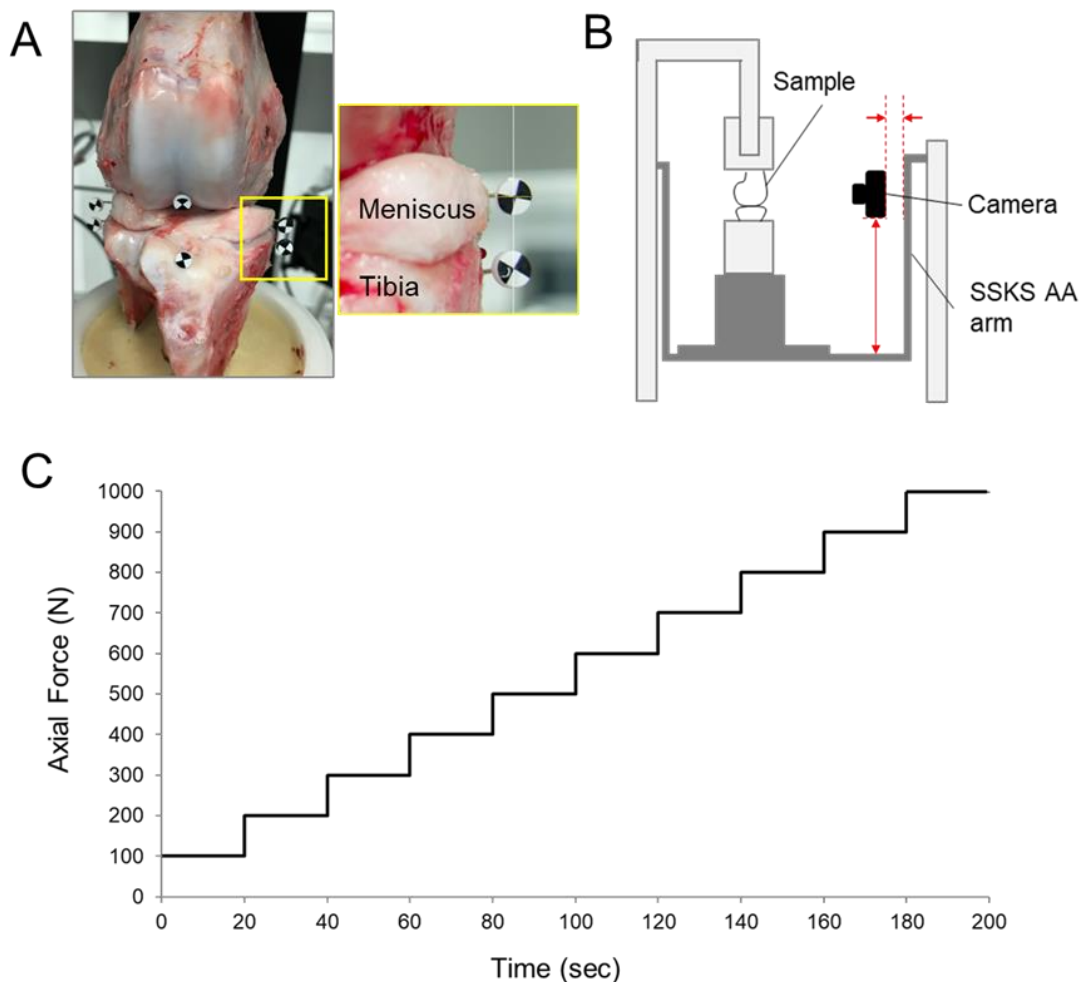


Figure 3.1. Experimental set up: (A) marker placement on the porcine medial meniscus and the tibia. (B) Diagram of the digital camera positioning in the simulator (SSKS). (C) Schematic of the step-ramp loading profile used for biomechanical investigation.

3.3.2.3 Loading Protocol

Details of the simulator and its axes are described previously in section 2.3.1. A simplified 'step - ramp' loading protocol was created for this preliminary investigation (Figure 3.1C). The profile consisted of ten sequential 20 second 100 N sub-profiles, cumulating to reach a maximum of 1000 N axial force. The anterior-posterior translation, tibial rotation, abduction-adduction position, and medial-lateral translation tibial axes were constrained to ensure the tibial bone marker was fixed for reference. The flexion-extension axis was also constrained at either 0° or 10° for each condition. As the pig knee is in a constant state of flexion, 10° flexion equates to ~ 30° human knee flexion. An additional static flexion condition was used as this represented another kinematic point in the gait cycle, other than 0°.

3.3.2.4 Video Data Acquisition and Image Analysis

Videos were imported from the camera and the start of simulator movement in the videos was identified as the audible sound of the axial force cam contacting the load spring. This start point was then calibrated to the start of the 200 second 'step-ramp' test at 1000 milliseconds per cycle (1.0 Hz). A video frame was measured at approximately 17 seconds into each 20 second sub profile, this ensured that the maximum marker movement during that axial force gain was captured, and that the first 10 seconds and the last 3 seconds of the sub-profile were avoided because the simulator can produce load stabilisation signal noise immediately before and after initiating a new sub-profile. Image J software (Schneider et al., 2012), was used to measure the meniscal displacement during each sub-profile.

The known 5 mm diameter of the marker was used to calibrate the pixel scale on the image prior to using the measure function. A vertical line was drawn up through the fixed bone marker centre and the horizontal displacement (mm, medial (+ve) and lateral (-ve)) was measured from this line to the centre of the moving meniscal marker. A short validation study was performed using this measurement technique (see section 3.3.2.6). Three repeats of the experimental loading protocol were performed for each knee, and three repeat measurements were performed at each sub-profile screenshot. After each experimental repeat, the sample was sprayed with PBS and given 10 minutes of unloaded rest, before the next repeat. The data was inputted into MatLab R2020a (The MathWorks Inc, Natick, USA) and the 0 N sub-profile measurements were assumed to equate to a displacement of 0 mm. The difference in displacement was calculated for each sub-profile load from the 0 N measurement. A paired samples t-test was performed to investigate if the method was sensitive enough to detect a difference in meniscus displacement between the intact and torn conditions. The t-test was performed with means taken at two

time/load points during the test, the 300 N and the 900 N point. Ideally the peak load (1000 N) would have been used, however, in most of the torn cases the radial displacement at 1000 N was unmeasurable as the meniscus moved outward and covered the tibial reference marker. Confidence intervals (95% CI) were also calculated to understand the uncertainty of the measurements around the mean.

3.3.2.5 Torn Condition

After assessing in the intact condition, an additional injury condition was simulated, and the experiment was repeated. A scalpel was used to cut a complete radial medial meniscus posterior root tear along the superior - inferior axis, in the inferior direction. This tear was simulated as this was the most common type of root attachment tear previously classified arthroscopically; 68% of cases reported a complete radial tear within 3 mm to 9 mm from the root attachment edge (LaPrade et al., 2015). Therefore, the root was cut at 6 mm from the root attachment edge (LaPrade et al., 2015). Therefore, the root was cut at 6 mm from the root insertion Figure 3.2. Although porcine tissue was used for the method development, the rationale for the tear was based on studies of human knees, as the method will be translated to investigate human knees in later chapters.

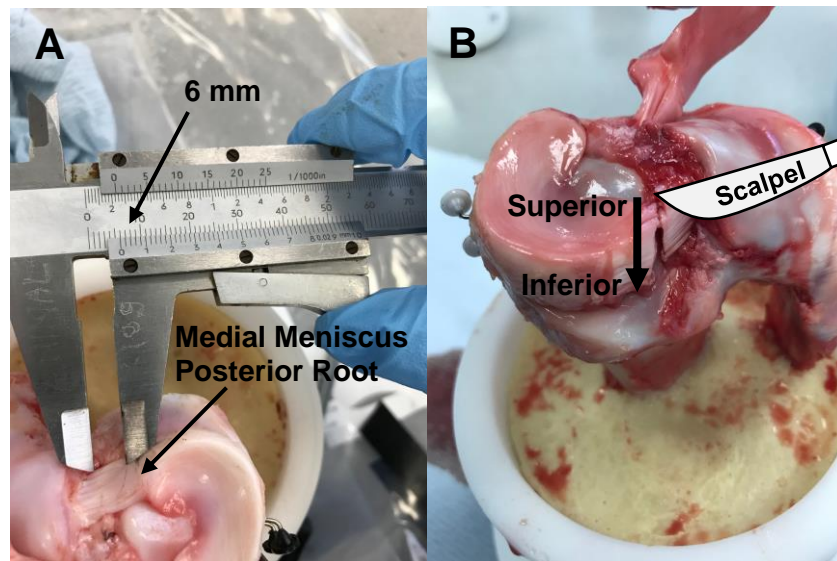


Figure 3.2. Complete radial root tear creation of the porcine medial meniscus posterior root. (A) Measurement of 6 mm from the root insertion. (B) Scalpel cut in the inferior direction at 6 mm from the insertion.

3.3.2.6 Validation Study

The ImageJ measurement technique was validated by using the same camera-marker setup and moving a marker along the medial-lateral axis to a known distance on

the simulator (+/- 1, 2 and 3 mm) (Figure 3.3). The 0 mm start point was marked with an image overlay on the video, so it was clear where to measure from. The 5 mm diameter of the marker stickers were used as the known distance to calibrate the images to the number of pixels in millimetres. The simulator medial-lateral translations (actual values) were compared to the ImageJ medial-lateral displacements (measured values) and the percentage error were calculated (Equation 3.1 and 3.2). The error was also calculated whilst simulating subjective factors, such as being +/- 1 pixel out using the 'measure' function on ImageJ or being +/- 1 pixel out when calibrating the image from the 5 mm marker. This was to understand the observer (user) sensitivity of the method.

$$\text{Equation 3.1. } \textit{Percentage Error} = \left(\frac{(\textit{measured value} - \textit{actual value})}{\textit{actual value}} \right) 100\%$$

$$\text{Equation 3.2. } \textit{Absolute Error} = (\textit{measured value} - \textit{actual value})$$

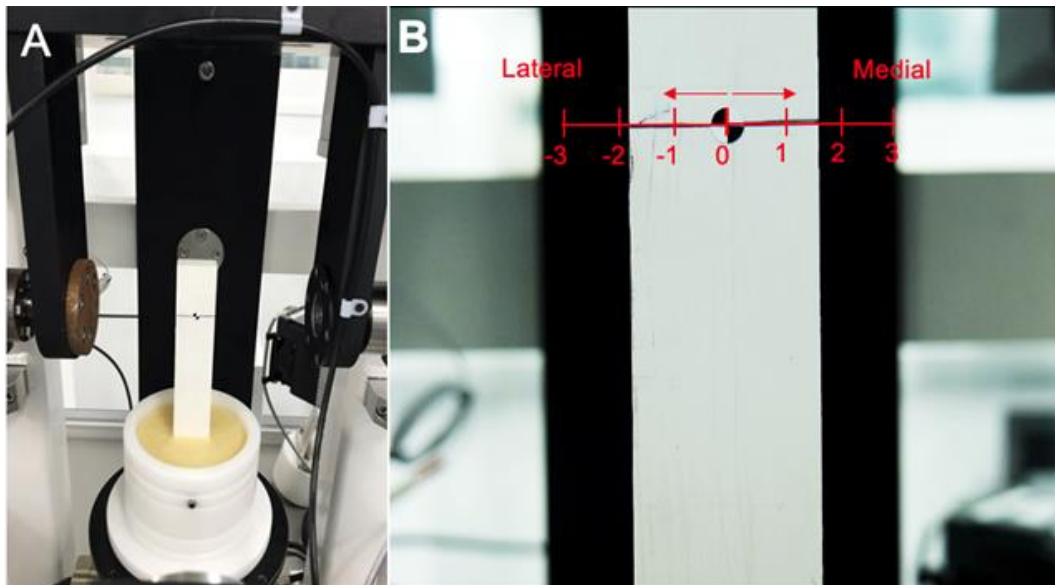


Figure 3.3. Validation method for the ImageJ measurement technique. (A) Method set up showing a marker adhered to a solid piece of plastic, cemented into one of the knee pots and screwed into the tibial base of the simulator. (B) Video camera view of the validation marker annotated with the known medial-lateral axis translation.

3.3.3 Results

3.3.3.1 Intact vs Torn Results

The intact and torn meniscal displacement results for each tested knee are displayed in Table 3.2 and Figure 3.4. Images of the final measurement screenshots for the intact and torn knees are presented in Figure 3.5.

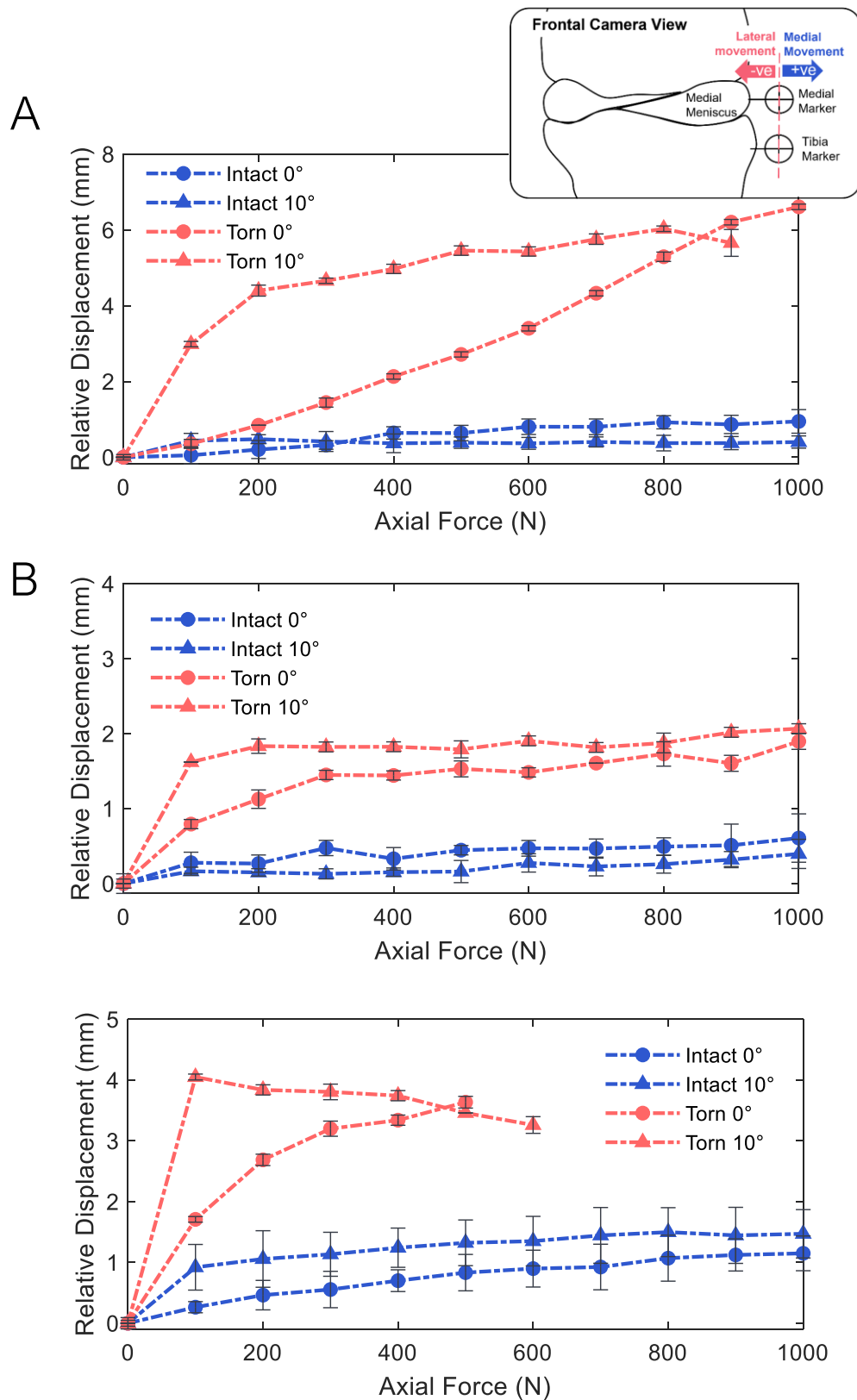


Figure 3.4. Difference in the relative medial meniscus displacement with increasing axial force for (A) Knee A, (B) Knee B and (C) Knee C, between the intact and torn conditions at 0° and 10° flexion. As shown in the schematic, positive results equate to medial marker displacement ($n=3$, error bars = SD of 3 repeat measurements, porcine).

The results show the relative meniscal displacement increased throughout the experiment with the presence of a medial meniscus posterior root tear, when compared to the intact conditions. As presented in Table 3.2, Knee A, Knee B and Knee C presented a significant increase ($p < 0.05$) in meniscal displacement at the 300 N point. Knee A and Knee B further presented a significant increase in displacement at the 900 N point of the torn medial meniscus at both 0° and 10° flexion angles. Flexion angle seemed to have an effect in the torn results but not in the intact results. A 10° flexion angle generated larger displacements in the torn condition results compared to the 0° flexion angle. Knee A and Knee B followed similar trends, however Knee C differed. Knee C's torn condition was only measured to 500 N and 600 N for the 0° and 10° tests respectively. This was because the test had to be stopped prematurely as the medial meniscus fell out of the joint space during the test and the marker was unable to be measured (Figure 3.5C).

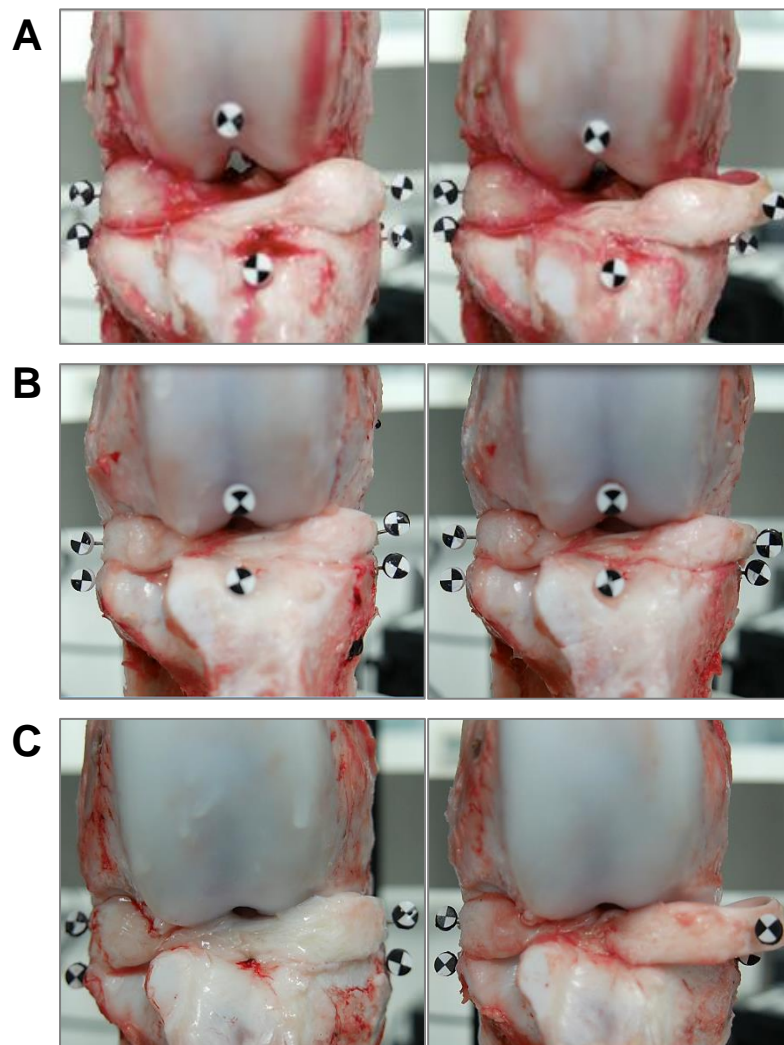


Figure 3.5. Screenshots of the 0° flexion angle test, showing maximum displacement of the intact conditions (left) and the torn conditions (right) for (A) Knee A, (B) Knee B and (C) Knee C (porcine).

In most cases the greatest change in displacement happened between 0 and 100 N, followed by some plateauing for the remainder of the test. Generally, displacements of the meniscus as load increased became more random and variable with a root tear. It was not possible to show the 95% confidence intervals for the torn condition results as Sample C was excluded in the final mean calculation (Table 3.2).

Table 3.2. Mean (+/- SD) relative displacement in the medial direction of the intact and torn medial meniscus, relative to the tibia as the load increased from 800 to 900 N.

^ = 300 N axial force interval value taken as 900 N was unmeasurable.

* = significant at 300N axial force interval $p < 0.05$

** = significant at 300N and 900N axial force interval $p < 0.05$

$n=2$ = sample C excluded

Sample	Intact		Torn	
	0°	10°	0°	10°
A	0.87 (\pm 0.24)	0.37 (\pm 0.17)	6.21 (\pm 0.07) **	5.66 (\pm 0.35) **
B	0.51 (\pm 0.28)	0.32 (\pm 0.11)	2.34 (\pm 0.11) **	3.18 (\pm 0.07) **
C	1.12 (\pm 0.26)	1.45 (\pm 0.46)	3.20 (\pm 0.12) ^*	3.81 (\pm 0.05) ^*
Mean (σ)	0.83 (\pm 0.31)	0.71 (\pm 0.64)	3.90 (\pm 2.30) $n=2$	3.84 (\pm 1.82) $n=2$
SE (σ_M)	0.18	0.37		
95% CI	\pm 0.76	\pm 1.58		

All dimensions in millimetres.

3.3.3.2 Validation Study Results

The percentage error ranged from 1.93 % - 6.97 % (mean = 4.2 %) between the actual and measured medial-lateral displacement values. When the measurement was +/- 1 pixel out, the mean percentage error was higher for the +1 pixel ranging from 4.92 % - 15.93 % (mean = 8.85 %) and the -1 pixel ranged from 0.49 % - 7.90 % (mean: 3.36 %). In terms of the calibration error, -1 pixel generated a larger range of error 0.23 % - 11.10 % (mean: 6.33 %) compared with the +1 pixel; 1.72 % - 8.08 % (mean: 4.73 %). The maximum absolute error recorded for this study was 0.25 mm.

3.3.4 Discussion

3.3.4.1 Overview

The ImageJ method was sensitive enough to detect differences in meniscal displacement between an intact and a torn condition. The cases with the completely torn meniscal root showed increased, random, and variable meniscal displacement, especially at higher loads. It was likely the meniscus became decoupled from the applied axial force to transmit load through the joint effectively.

The ImageJ method was sufficiently sensitive to measure meniscal displacement after the application of 100 N axial force in almost all cases. The results may somewhat reflect the material characteristics of the meniscus as a whole tissue in response to load. There was an initial increase in the displacement with load, followed by a reduction and plateauing in displacement when further load was applied. Biological tissues adopt a creep response, where deformation increases under constant load and the largest amount of deformation occurs at the initial application (see section 1.4.1). Even though the displacement measurement was not able to distinguish between deformation and displacement, it is likely that creep properties were reflected in the results.

3.3.4.2 Evaluation of the Method

Measurement Sensitivity: The ImageJ technique was accessible and easy to use. Actual displacements of the porcine menisci are unknown; therefore, a validation experiment was created to compare the known medial-lateral displacement of the simulator to the measured ImageJ values. A mean % absolute error was found to be 4.2% and the maximum was ~7% for the measured values. However, the validation experiment has a potential observer bias, as the observer was aware of the known simulator measurement.

Observer Sensitivity: The method has a large reliance on the observer; a measurement made by one observer on ImageJ could be more accurate than another. These errors are likely to occur from visual and coordination differences between individuals and potentially reduces the reproducibility of the method. The observer sensitivity could be better understood by conducting a multiple participant sensitivity study. Participants would measure a marker in an image to generate an error value of inter-observer variability. This was performed later in this project after further developments and reliability assessments of the marker-tracking methodology (see section 4.3.2.2).

The validation experiment in this study included parameters relating to observer error. The maximum margin for error increased to ~16% for the +1 pixel 1 mm measurement (mean: 8.85%). With this error margin, it would be possible to distinguish between the intact and torn conditions for the same knee samples but not between individual knee samples, which is important to consider in future method developments. Moreover, a maximum absolute value of 0.25mm was established from the validation study. However, this margin of error kept on or within the standard deviations of the results, meaning that in the individually analysed samples, the measurement error was predominantly due to systematic error and not random occurrences. However, when the error was examined between the knee cases (Table 3.2), large amounts of variation were evident and random error likely occurred, which may be generated by some uncontrollable factors, such as variation between porcine knee anatomy, or controllable factors in future study, such as evaluating the camera position set-up (see section 3.7 and Chapter 4).

3.3.4.3 Limitations

The meniscal displacement relative to the tibia was dictated solely through the location of the markers, however, this position was chosen as it is of the highest interest, as meniscal extrusion is measured and diagnosed in this location on frontal plane radiographs (see section 1.5.2). Moreover, only 2D linear measurements were taken, therefore deformations in other planes were disregarded. However, the aim was to develop a simple and robust method which was able to measure a difference in relative meniscal displacement between an intact and torn condition. In addition, the use of a complete radial tear at this stage in method development was useful to show a clear difference, however, *in vivo* the capsule would provide a barrier against complete subluxation of the meniscus outside the joint space. Therefore, it would not be sensible to test this condition in a cyclic loading study. Finally, the tissue relaxation time was not addressed during this study, which would have affected the results as reduced water retention would limit the deformation of the tissue under load. Further developments will include a calculated time for the tissue to relax between each test.

3.4 Sagittal Plane Method Development

3.4.1 Rationale

The knee joint allows the greatest amount of motion along the sagittal plane during flexion and extension. The meniscus moves along this plane in response to flexion and extension to keep the area of contact continuously satisfying the moving geometry the

femur and tibia (Vedi et al., 1999). Meniscal extrusion is frequently described in the frontal plane; however, little is known for the sagittal plane. When evaluating changes in meniscal kinematics in response to traumatic extrusion, assessing changes in the anterior and posterior meniscal regions are of high interest. Therefore, developing the method described in the previous section to measure sagittal plane meniscal displacement of the anterior and posterior regions of the medial meniscus is important when the dynamic knee axes in the simulator will be incorporated into the profile.

This section describes the application of the same ImageJ method, to measure the displacement of the anterior and posterior meniscal regions under increasing static load in intact porcine samples. A torn condition was not studied for the initial sagittal plane investigations as the aim in this preliminary stage was to investigate if it was possible to translate the frontal plane method to the sagittal plane. Therefore, this section focuses on the application of the method to measure markers on the anterior and posterior regions of the medial meniscus with intact meniscal roots and reports on trends observed across three samples.

3.4.2 Experimental Set Up

3.4.2.1 Sample Preparation and Loading Protocol

Fresh whole knee joint samples ($n = 3$: labelled Sag A, Sag B and Sag C) were dissected from the right hind legs of 6-month-old female pigs (67.2kg, 84.3kg and 84.6kg). The methods for sample preparation, including dissection and cementing are previously described in section 2.2.1. The fascia and the ligaments were removed during dissection, following the same conditions as those carried out for the frontal plane investigations (section 3.3.2.1). The same ramp loading protocol was used, as previously described in section 3.3.2.3. In addition to the loading protocol, a tissue rest period was included between each test. Each sample was left hydrated with PBS and unloaded for 10 minutes, so the compressed tissues recovered.

3.4.2.2 Camera Specifications

Due to the limited space in the simulator, a discrete camera with a small focusing distance was required. The focusing distance, or focal length, is the smallest distance the object can be away from the lens, and still be in focus. A digital camera, such as the one used for the frontal plane method in the previous section, was too large to fit in-between the sample and the simulator. A smartphone (iPhone 7, Apple Inc. CA, USA) had a camera which is capable of filming in 1080 x 1920 resolution and has a relatively small

focusing distance (~ 100 mm), with a thin casing. The distance between the medial meniscus of the sample and the smartphone lens was measured at ~ 50 mm, therefore, the focusing distance of the smartphone camera had to be reduced by around 50%. This was achieved with a clip-on macro lens, attached to the smartphone camera and with the addition of more artificial light to brighten the markers.

3.4.2.3 Anterior and Posterior Meniscal Marker Positioning

To attach the 5 mm diameter markers on the anterior and posterior regions of the medial meniscus, the tibial width was measured with callipers and then multiplied by a factor of 0.4 to give a distance in millimetres, which was used to pin the anterior and posterior markers away from the anterior and posterior horn insertions of the medial meniscus, respectively (Figure 3.6A). Corresponding markers were placed directly below the meniscal markers on the tibia. The sample was kept at 0° extension when attaching the markers. The markers were adhered with superglue as well as pinned.

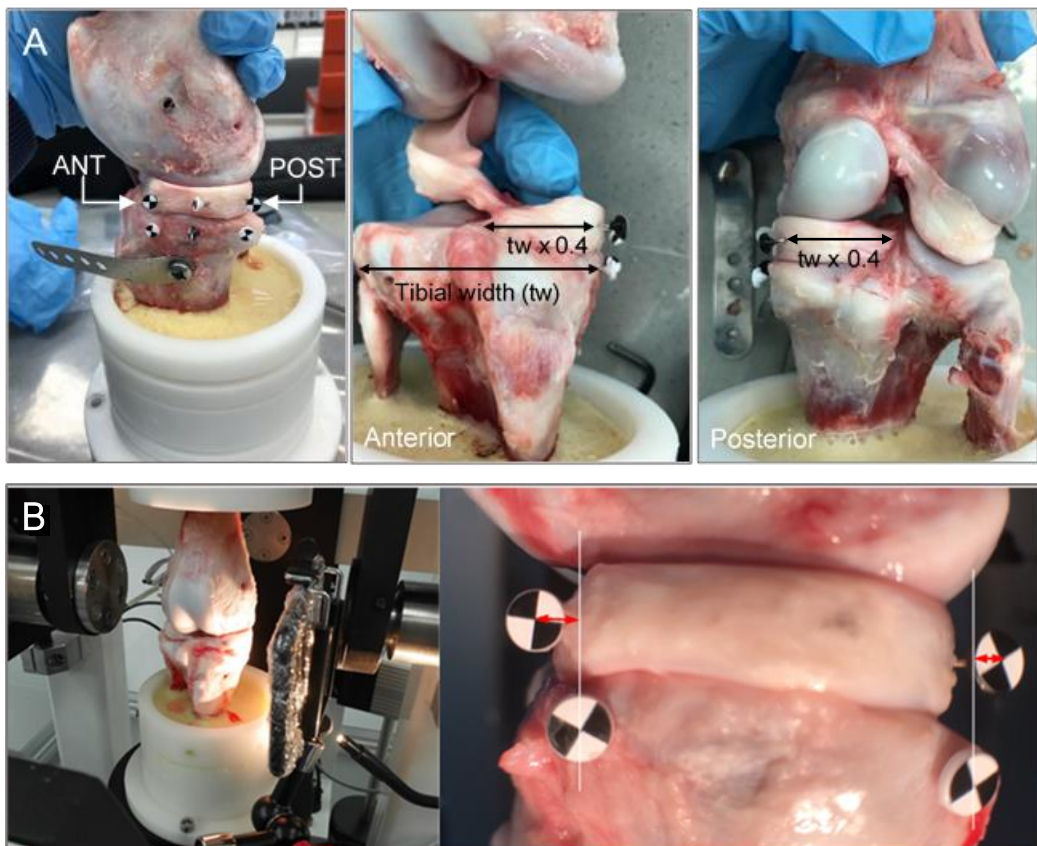


Figure 3.6. (A) Anterior (ANT) and posterior (POST) marker placement on the porcine medial meniscus, in relation to the anterior and posterior meniscal root insertions. (B) Smartphone camera position and screenshot of analysis carried out on ImageJ.

3.4.2.4 Video Data Acquisition and Data Analysis

The same ImageJ image acquisition and data analysis measurement technique was used to calibrate and measure the displacements of the anterior and posterior markers, relative to the fixed tibia marker, for each 100 N axial force increase. This is previously described for the frontal plane protocol in section 3.3.2.4. The only difference for the sagittal plane protocol was that each screenshot had two markers to collect data from, because both the anterior and posterior marker were visible in the same frame (Figure 3.6B). In addition, each extracted frame was calibrated according to the known 5 mm diameter of each marker. This was performed individually on the anterior and posterior markers to account for slight differences in marker depth from the camera lens. One repeat test was carried out for each knee sample in the sagittal plane study, this was because ImageJ measurement consistency from repeated experiments was observed during the preliminary results and validation reported in section 3.3.2.6 and to reduce the effect of unnecessary repeated loading which affects the tissue compression.

3.4.3 Results

The trends in relative meniscal displacement measured from the locations of the anterior and posterior markers for each sample are displayed in Figure 3.7 and Table 3.3.

In most cases, increasing the load increased the amount of anterior and posterior displacement of the medial meniscal markers, except for the anterior marker of SagA and SagB, which displaced minimally and posteriorly during the 10° conditions. The rate of increase of relative posterior marker displacement, was highest in the first 100 N of the 10° flexion results, whereas the 0° flexion conditions did not present a sharp initial increase. The trends shown for samples SagA and SagB were similar, whereas SagC differed compared to the other samples. Mean values are reported in Table 3.3 with standard error and 95% CI, reflecting the variation between the results.

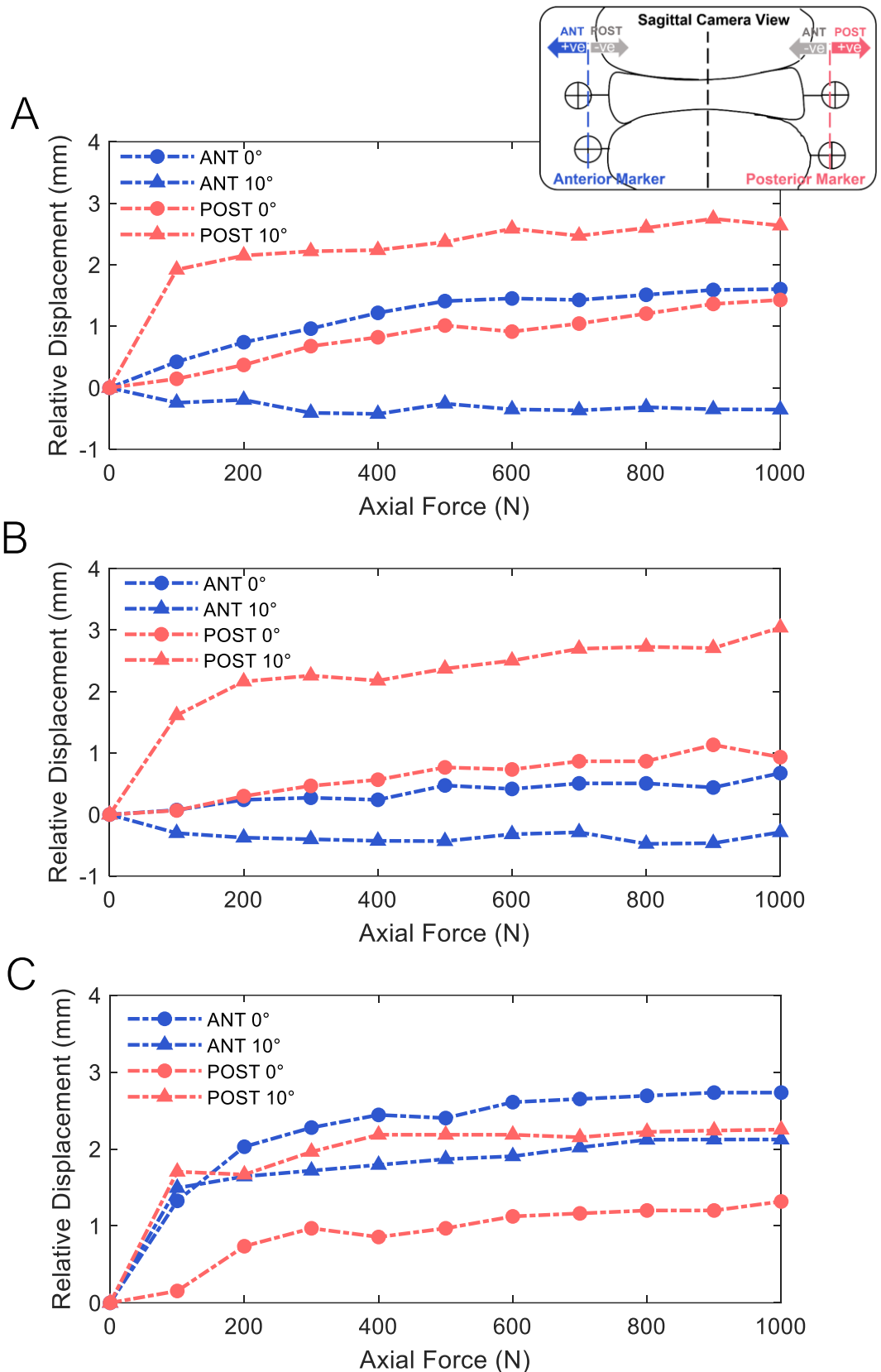


Figure 3.7. Relative displacement of the anterior (ANT) and posterior (POST) meniscal markers with respect to the tibia for (A) Knee SagA, (B) Knee SagB and (C) Knee SagC, at 0° and 10° static flexion angles. As illustrated in the schematic, positive values indicate an anterior direction of movement for the ANT region. Positive values indicate a posterior direction of movement for the POST region (n = 1, porcine).

Table 3.3. Individual sample results showing the mean displacement of the anterior and posterior regions of the medial meniscus, relative to the tibia during increasing load. Values taken at the 1000 N force interval.

<i>Sample</i>	<i>Anterior</i>		<i>Posterior</i>	
	0°	10°	0°	10°
<i>SagA</i>	1.60	- 0.35	1.43	2.64
<i>SagB</i>	0.67	- 0.29	0.93	3.04
<i>SagC</i>	2.73	2.12	1.32	2.25
<i>Mean (σ)</i>	1.67 (\pm 1.03)	0.49 (\pm 1.41)	1.23 (\pm 0.26)	2.64 (\pm 0.39)
<i>SE (σ_M)</i>	0.60	0.82	0.15	0.23
<i>95% CI</i>	\pm 2.56	\pm 3.51	\pm 0.65	\pm 0.98

All dimensions in millimetres.

3.4.4 Discussion

This study showed that it was possible to use the ImageJ method in the sagittal plane as well as the frontal plane, to measure a change and observe trends in meniscal displacement, relative to the tibia, with only 100 N axial force applied. However, from the mean values and 95% CI's little can be deduced about the relationship between the relative displacements of the meniscal regions under increasing load. Herein, trends showing similar behaviour were observed for samples SagA and SagB. The sample SagC could have had a more posteriorly positioned tibia relative to the femur, potentially due to the cementing procedure, or from anatomic sample variations. This may have contributed to an abnormal distribution of load on the anterior portion of the medial meniscus. However, it is difficult to analyse the data presented in this preliminary work with a small sample size and until confounding factors are addressed in further study. The main conclusion to progress with is that the motion capture method can be applied to the sagittal plane despite the limited space in the knee simulator.

3.4.4.1 Limitations and Confounding Factors

Due to the nature of the chosen method, limitations involving the marker positioning and 2D characterisation remain the same (section 3.3.4.3). However, placing

markers in multiple key meniscal regions across multiple motion planes, increases the overall kinematic characterisation of the meniscus. In this study, 10 minutes of tissue rest was given between each condition in the sagittal plane study, to reduce the issues associated with tissue compression reported in the frontal plane study.

As indicated in Figure 3.7, positive values equated to net movement in the anterior or posterior direction for the anterior and posterior marker, respectively. This was presented in this way to illustrate overall expansion of these regions with axial load, however, when applying this method to dynamic profiles with changing flexion, this system would become confusing. Therefore, a logical coordinate system was required and will be discussed in the latter sections of this chapter.

Moreover, aspects of the measurement technique and experimental control need to be addressed. The macro lens produced a small wide-angle distortion on the videos to increase the field of view. Due to this, there was a chance that as the markers moved towards the periphery of the frame during loading, measurements were underestimated. In addition, placing both markers in one sagittal camera frame provided just enough clearance for the porcine knee markers to move out radially in the video. However, the human tibia is wider, meaning both markers would not be visible in the video. In addition, camera positioning needs to be kept consistent between knee samples, a higher amount of control is required in the current set up. Finally, the measurement technique was observer dependent, and a fair amount of concentration and screen time was required to complete measurements from one sample's video screenshots. This increases the risk of fatigue and limits the number of data points collected. In the following section, measurement automation, camera positioning and lens distortion were developed.

3.5 Developing Partial Automation of the Measurement Technique

During the preliminary experiments described in the previous sections of this chapter, a camera marker method was able to obtain 2D position data from markers attached to medial, anterior, and posterior regions of the medial meniscus undergoing a quasi-static loading protocol in the knee simulator. The validation study described previously in section 3.3.2.6 showed that the ImageJ method was able to measure displacement within an estimated mean error of $\pm 4.2\%$. However, when comparing results between multiple samples, there was a large amount of variation, some of which was due to anatomical differences when studying natural tissue and some of which were due to confounding factors of the methodology. Therefore, addressing some of the confounding factors (measurement automation, camera positioning and lens distortion) was important to mitigate error. This section describes how the measurement technique

was developed to become a more automated process, putting less reliance on the observer to measure accurately and more reliance on the computer.

3.5.1 Problems with the Current (ImageJ) Measurement Technique

Video processing and data analysis is laborious for the observer in the current method. Prolonged concentration is required from the observer, which increases the risk of error and limits the number of data points collected. An acquisition bias also occurs after time because one observer who performs this analysis regularly may produce more accurate results than another observer. The reproducibility and the objectivity of the measurement technique was improved using a computational method developed on MatLab R2020a (MatLab, The MathWorks Inc.) to track the moving marker in the video.

3.5.2 Computational Object Tracking

A code was developed on MatLab to detect and track the movement of multiple moving objects in a 1080 x 1920 resolution video (The MathWorks Inc., 2017; Kikawada, 2023). Specific details of how to implement this code can be found in the standard operating procedure in Appendix C.

3.5.2.1 Object Identification

The first stage of the process was the object identification. There are a variety of ways for a computer vision system to detect an object in a video frame or image. Systems such as traffic monitoring use object detection to identify and track specific vehicles. Methods of identifying an object in an image include segmenting the colour, contours, or the geometry from the background of the image. In this case, a MatLab computer vision program called the Colour Thresholder Application (The MathWorks Inc., 2023) was used to filter out the specific colour of the marker from the rest of the colours in the image frame. Firstly, the HSV (hue, saturation, value) colour space was chosen as supposed to the RGB (red, green, blue) as this broadens the spectrum of colours detected by the model. The code was capable of tracking multiple objects of the same colour in the video, which was important when tracking simultaneous tibial and meniscus movement in the following chapters.

To trial the script, a simple test video was created which incorporated a 5 mm red square of card attached to a pin and a 50 mm scale, the pin was manually moved along the scale in the video (Figure 3.8A). The colour thresholding process involved toggling

colour parameters in the MatLab application to highlight the colour of the red marker, whilst other background colours were blacked out. Once complete, the colour thresholding parameters were contained and saved as a '.Mask' function, which overlays a black and white binary image on the first frame of the video (Figure 3.8B). The white pixels of the image are assigned the number '1' and represent the marker. The black pixels of the image represent the background and are assigned the number '0'.

Blob analysis is a form of object detection which applies to images having undergone binarisation (Jia et al., 2008). The function places a bounding box, or a 'blob' around the object. This bounding box gives us quantitative pixel information from the image including the centroid pixel, total area, and the corner pixels (Figure 3.8C).

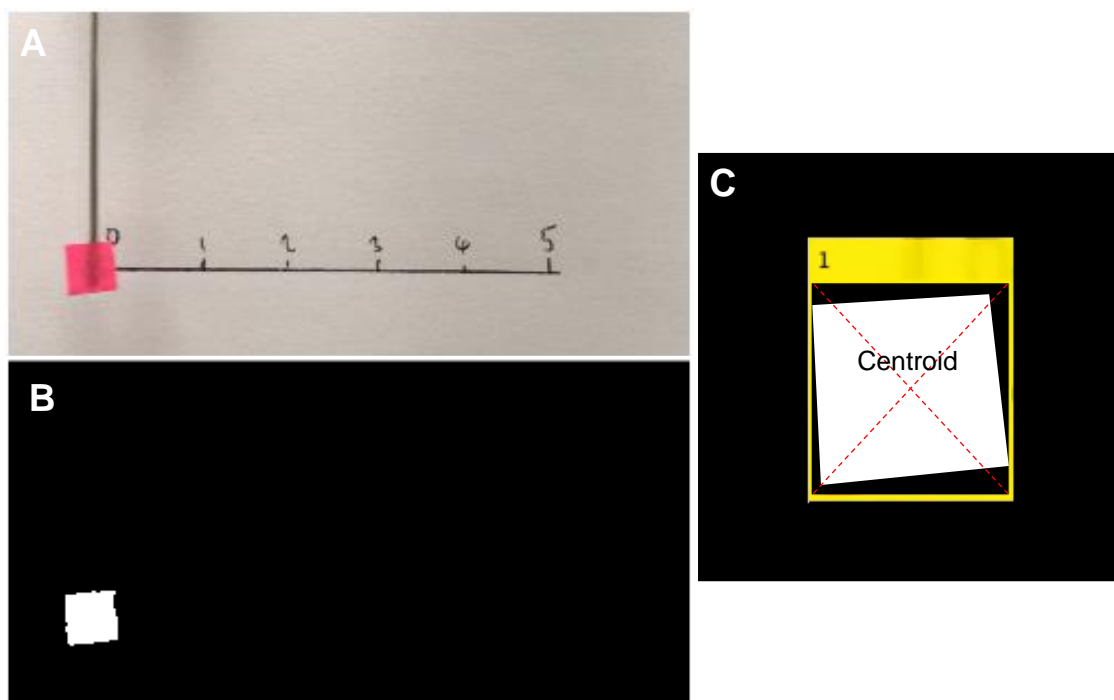


Figure 3.8. (A) Test video screenshot. (B) Image binarisation of the coloured marker in the test video. (C) Bounding box (blob) identifying the marker to track in the video.

3.5.2.2 Object Tracking and Segmentation

The marker-tracking script contains a loop which applies the object detection parameters as a binary image overlay ('.Mask' function) to all the frames in the video. Concurrently, a computer-vision MatLab function called the 'Blob Analyser' tracks the marker across all the frames in the video by locating the area of the frames assigned the binary number '1' (i.e. the colour segmented object). Once all the frames in the video had

been processed in the loop, an additional resultant video was written in the output, showing the bounding box attached to the marker throughout the video.

During the tracking-loop, the centroid of the bounding box (Figure 3.8C) was the point at which the x and y coordinates of the pixel data were collected from each frame in the video and were logged on an empty spreadsheet. The y-axis pixel coordinate data logs in the odd numbered cells and the x-axis pixel coordinate data logs in the even numbered cells of the spreadsheet. This data was then arranged into two column arrays of x-axis and y-axis pixel data to plot against the video time. The resolution of the image (1080 x 1920 pixels) governs the x-axis and y-axis scales which can be logged in pixels. The output produces a plot showing the spatial change of the marker throughout the video (Figure 3.9).

The bounding box around the object flickered as the video played which increased and decreased the pixel area in an oscillating fashion between each frame. This caused oscillations or noise in the centroid position of the bounding box, which was reflected as noise in the tracking results. To reduce this noise, it was important to have a coloured marker which was highly contrasting to the background.

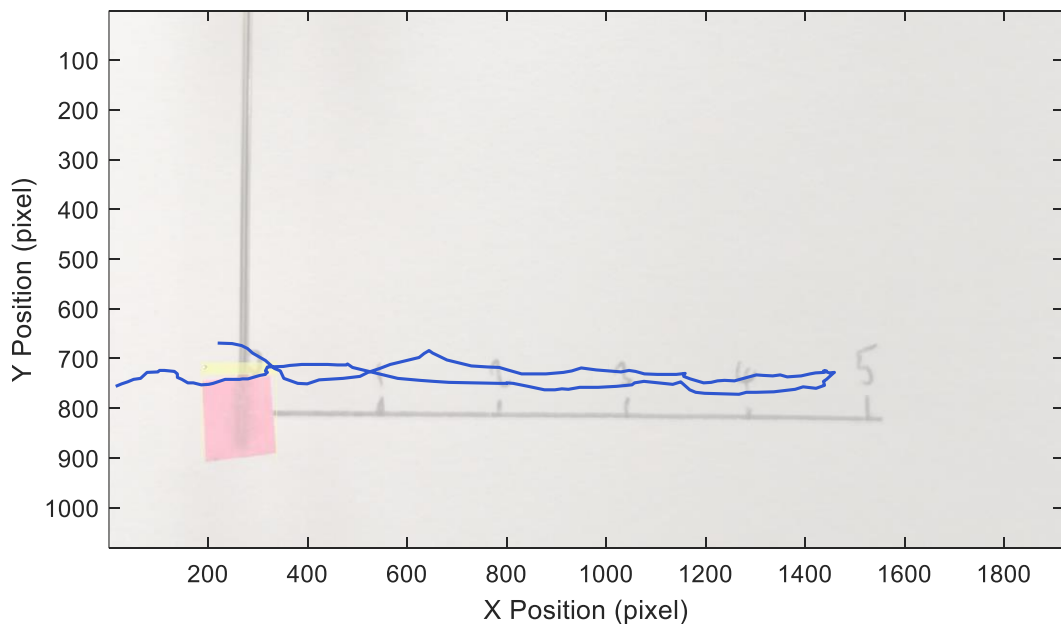


Figure 3.9. Spatial change (x-axis and y-axis pixel position) of the marker in the test video over the image resolution.

3.5.2.3 Image Calibration

To present the tracking results, the first element was zeroed and the difference in pixel distance from this element in the x-axis and y-axis arrays was computed. The y-axis

results were inverted because the y-axes of images are read from top to bottom, whereas in graphical representation the y-axis is read from bottom to top. Inverting the y-axis results meant that downward motion of the marker equated to decreasing or negative displacement, making graphical representation more intuitive. The MatLab image tool was used to measure the size of the marker in the frame in pixels. The pixel calibration factor was found using Equation 3.3; this factor was multiplied with the x-axis and y-axis results to convert the data to millimetres. This factor also equates to the smallest division that can be measured, or the resolution of the measurement. In the test video, the marker was manually moved ~ 50 mm horizontally and back again, as shown in Figure 3.10. The output of the script represents what was happening to the object in the video as a displacement-time graph; this was the primary goal at this stage.

$$\text{Equation 3.3. Pixel Calibration Factor} = \frac{\text{Known Marker Diameter (mm)}}{\text{Pixel Marker Diameter (pixel)}}$$

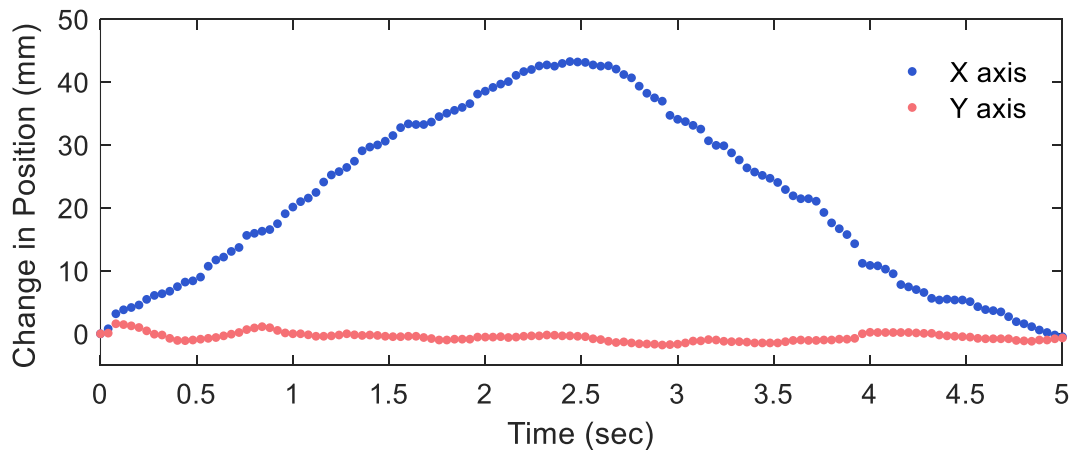


Figure 3.10. Temporal change of the x-axis and y-axis position of the test video marker over the video duration. Calibrated to the known size of the marker.

3.6 Measuring Dynamic Meniscal Position under Capsule Constraint Conditions: A Comparison of the ImageJ and MatLab methods

3.6.1 Rationale

In this section, the ImageJ and the MatLab measurement techniques described in the previous sections were trialled using the same experimental protocol. The experimental protocol was advanced to include dynamic flexion-extension motion as well as axial load, as the primary aim was to be able to develop a method which can measure meniscal position under dynamic simulator loads and motions. Both measurement methods are similar as 2D displacement data is estimated from calibrated frames in a video. However, the MatLab technique is more automated than the ImageJ technique; it requires less concentration from the observer and is likely more applicable when performing complex gait cycles in the simulator. In this study, the experimental set up was also progressed to include dissection conditions of knee fascia/capsule removal, this was to simulate differing levels of soft tissue constraint and is something which would be applied in human studies as the method progresses. Therefore, evaluating the measurements technique with respect to these conditions was important to develop at this stage.

3.6.2 Sample Preparation, Loading Protocol and Video Capture

One fresh whole knee joint was dissected from the right hind leg of a 6 month old female pig weighing 72.3 kg. The dissection protocol is outlined in section 2.2.1, where the capsule was initially retained and then dissected away in stages during the investigation. The dissection conditions tested were labelled as follows: the knee capsule fully intact (CAP), the knee capsule removed (NOCAP), and the ligaments (ACL, PCL, MCL, LCL) removed (NOLIG). Markers were positioned on the medial meniscus as previously described in section 3.4.2.3. However, the marker positioning method for the anterior marker was adapted because with the capsule retained the anterior horn was not visible. The anterior marker was placed relative to the medial and posterior marker. The distance Ad is equal to the distance between the posterior edge of the MCL and the posterior marker (Figure 3.11A).

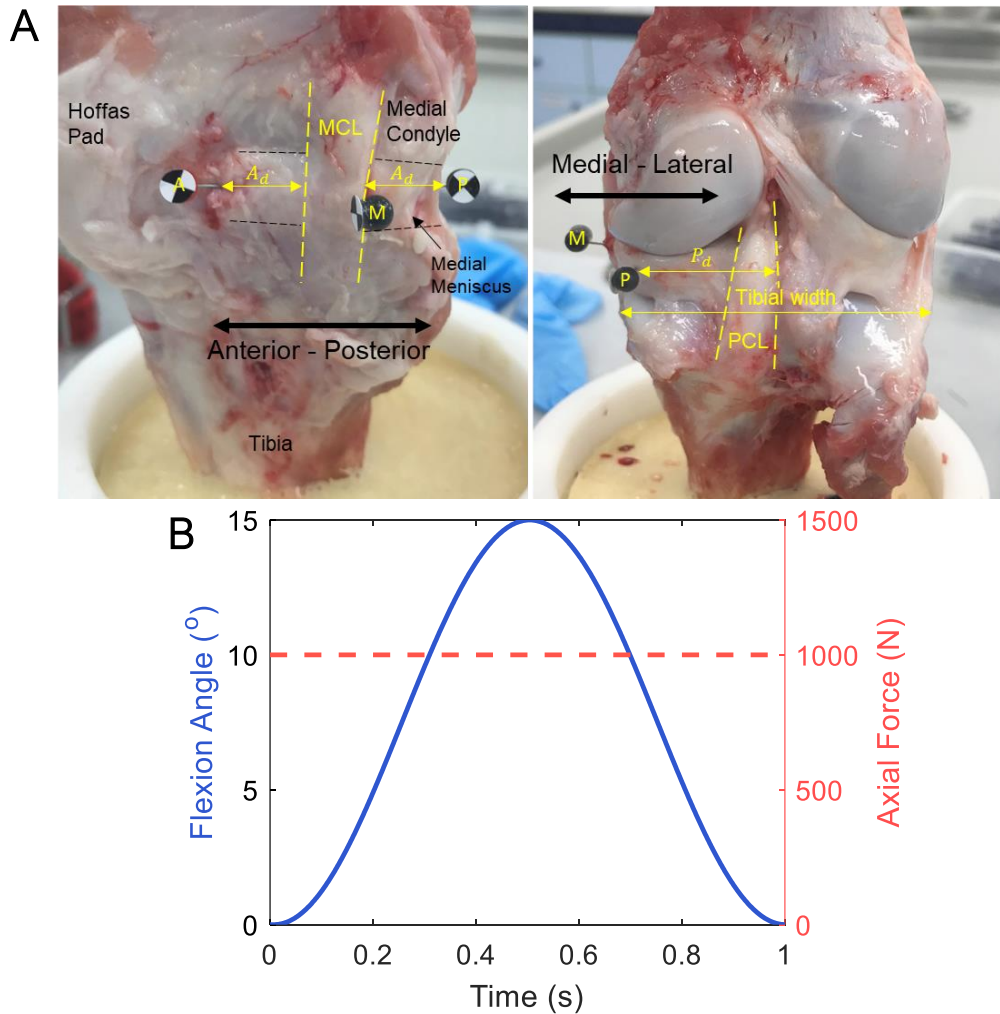


Figure 3.11. (A) Positioning of the anterior (A), posterior (P) and medial (M) meniscal markers using distances P_d and A_d , in relation to the position of the MCL and PCL. (B) Loading profile for the experiment. All tibial axes (AP, AA, TR, ML) were fixed, only the FE axis was driven (porcine).

The simulator was used to perform a simplified loading and motion regime on the specimen. The specimen was subjected to 50 cycles (1 Hz (+/- 0.1) frequency) of a simple dynamic profile, which consisted of an extension/flexion position of 0 - 15° and a 1000 N constant axial force (Figure 3.11B). All other axes were constrained to simplify the input and aid the comparison of the two measurement techniques. Eventually the relative meniscal displacement will be calculated using the moving tibia as a reference, but for the purposes of this preliminary study, the tibia was fixed and just the meniscal displacements were measured in response to load and flexion-extension. After each test, the knee was dissected down to the next condition and kept hydrated with phosphate-buffered saline (PBS). The tissues were also left to relax (unloaded) for 10 minutes prior to the next test.


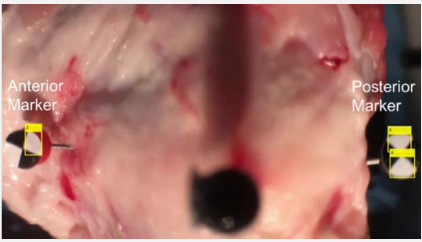
The digital camera and the smartphone camera, described in previous sections 3.3.2.2 and 3.4.2.2, were used to video marker motion in the frontal plane (measuring

medial-lateral displacement) and sagittal plane (measuring anterior-posterior displacement) at 30 frames per second and a resolution of 1080 x 1920 pixels. The cameras were stationary and securely mounted in brackets throughout the experiment and a light box was also used to illuminate the markers during the experiment. The cameras were manually triggered prior to starting the simulator and recorded the full 50 cycle tests. The video files were imported and trimmed to 5 seconds (5 cycles) in duration, at cycles 25 – 29, located by audible signals on the videos. The change in position of the medial, anterior, and posterior marker for the three test conditions were measured using either the ImageJ® or the MatLab method and presented over one cycle (cycle-25). Information on the similarities and differences between the two measurement methods are described in Table 3.4.

3.6.2.1 Validation

The same validation study, which was previously carried out using the ImageJ method, was also performed using the MatLab method. This method was described previously in section 3.3.2.6. The medial-lateral axis of the simulator was manually moved to known translations of +/- 1mm, 2mm and 3mm and three repeats were performed using each measurement method. The known translations were compared to the measured displacements and the mean percentage error (MPE), standard deviation (SD) and coefficient of variance (CV) were calculated. The precision of the method was calculated using the CV ($SD / \text{Mean} \times 100$) and in accordance with general practices a threshold of <10 % data dispersion around the mean was desirable as a guideline. Due to the novelty of this work, determining the threshold for the accuracy was difficult as the true values for porcine meniscal displacement are unknown. As a guideline, having a MPE within a +/- 5% threshold was deemed a good starting point to evaluate method accuracy. However, at this stage, the main goal is to determine a method which was systematically consistent, easy to implement and reproducible.

Table 3.4. Comparison table of the two measurement techniques.

	<i>Measurement Method 1 (ImageJ)</i>	<i>Measurement Method 2 (MatLab)</i>
<i>Description</i>	Photogrammetry method used on screenshots taken from the video, previously described in sections 3.3.2.4 and 3.4.2.4.	Computational object tracking method. Markers were tracked using the code outlined in section 3.5.2. The white areas of the map pins were segmented during object identification and tracking.
<i>Software</i>	ImageJ	MatLab 2020a
<i>Data Collection Cycle</i>	Cycle 25	Cycle 25
<i>Output Number of Data Frames</i>	10	30
<i>Image Calibration</i>	5 mm marker	5 mm marker
<i>Data Set Analysis Duration</i>	8 hours	10 minutes
<i>Reference</i>	Overlaid stationary image signalling the location of the marker at 0° extension on the video	First frame of the video was the reference. A single cycle was filtered out from the troughs in the graph recorded for the 5-cycle duration of the video.
<i>Frontal Plane Measurements</i>	Medial (+ve) - Lateral (-ve) Direction (x-axis)	Medial (+ve) - Lateral (-ve) Direction (x-axis)
<i>Sagittal Plane Measurements</i>	Anterior (-ve) - Posterior (+ve) Direction (x-axis)	Anterior (-ve) - Posterior (+ve) Direction (x-axis)
<i>Screenshot of sagittal plane camera view for the CAP condition</i>		

3.6.3 Results

The displacement results using both measurement techniques are presented in Figure 3.12. The validation study results comparing both methods are displayed in Table 3.5 and Table 3.6.

Table 3.5. MatLab measurement method validation displacement results.

<i>Known (mm)</i>	<i>Measured (mm)</i>			<i>Mean</i>	<i>SD</i>	<i>MPE (%)</i>	<i>Abs Value</i>	<i>CV (%)</i>
	<i>Trial 1</i>	<i>Trial 2</i>	<i>Trial 3</i>					
3.00	3.04	2.96	2.99	2.99	0.04	0.19	0.01	1.35
2.00	1.97	2.00	1.96	1.98	0.02	1.11	0.02	1.17
1.00	0.98	1.07	0.95	1.00	0.06	0.21	0.00	6.05
-1.00	-1.07	-0.96	-1.05	-1.02	0.06	2.39	0.02	5.84
-2.00	-2.10	-1.97	-2.02	-2.03	0.07	1.47	0.03	3.28
-3.00	-3.08	-3.03	-3.05	-3.05	0.02	1.78	0.05	0.70

The MPE ranged from 0.19 % to 2.39 % (mean: 1.19 %) for the MatLab measurement method (Table 3.5) and from 1.93 % to 6.97 % (mean: 4.20 %) for the ImageJ measurement (Table 3.6). The maximum percentage error found for individual measurements were +/- 5 % for the MatLab method and +/- 14.5 % for the ImageJ method. This equated to an absolute value of 0.1 mm for MatLab and 0.29 mm for ImageJ, respectively.

Table 3.6. ImageJ measurement method validation displacement results.

<i>Known (mm)</i>	<i>Measured (mm)</i>			<i>Mean</i>	<i>SD</i>	<i>MPE (%)</i>	<i>Abs Value</i>	<i>CV (%)</i>
	<i>Trial 1</i>	<i>Trial 2</i>	<i>Trial 3</i>					
3.00	3.04	3.09	3.13	3.09	0.05	2.91	0.09	1.48
2.00	1.85	2.28	2.29	2.14	0.25	6.97	0.14	11.79
1.00	0.98	1.09	1.10	1.06	0.07	5.60	0.06	6.44
-1.00	-1.01	-0.92	-1.01	-0.98	0.05	1.93	0.02	5.36
-2.00	-1.96	-1.93	-1.93	-1.94	0.02	3.02	0.06	0.77
-3.00	-3.15	-3.13	-3.15	-3.14	0.01	4.79	0.14	0.38

These error margins were applied to the results in Figure 3.12 to illustrate the largest error threshold, calculated from the validation study, which maybe expected for a single measurement for each measurement method. Both methods showed a good amount of precision as the majority CV's showed low data dispersion (< 10 %) for each

measurement method, with only one value (11.79 %) just exceeding this threshold for the ImageJ method. In addition, the SD for the MatLab method was low and ranged from 0.02 mm to 0.07 mm, whereas more variation was present with the ImageJ method ranging from 0.01 mm to 0.25 mm.

As presented in Figure 3.12, the ImageJ and MatLab measurement techniques were able to track similar shaped profiles of meniscal displacement for the anterior, posterior, and medial markers, however, there were differences in the magnitudes of the results. The posterior marker results followed the motion of the flexion-extension arm on the simulator. For the condition with the capsule fully intact, at 15° flexion a 0.93 mm peak displacement of the medial meniscus was measured with the ImageJ method (Figure 3.12A), and a 0.82 mm peak displacement was measured with the MatLab method (Figure 3.12B). An increase of ~ 72 % in posterior displacement was measured after the knee capsule and collateral and cruciate ligaments were removed using the MatLab measurement technique, whereas an 25 % increase was measured with the ImageJ method. Both methods measured minimal differences in displacement between the capsule removed and ligaments removed conditions.

Unexpectedly, the anterior marker moved minimally during the study and did not follow the motion of the flexion-extension arm. At 15° flexion, the ImageJ and MatLab methods measured minimal medial meniscus displacement at 0.02 mm and 0.03 mm for the capsule intact condition, respectively (Figure 3.12C and D). Each method was also not able to distinguish between the dissection conditions for the anterior marker as all the error boundaries overlapped. However, as both methods measured a similar profile for the anterior results, it is likely that other factors of the methodology, not the measurement technique, were causing this result.

The medial marker displacement results showed the largest displacement in the medial direction at 15° flexion. For the capsule intact condition, a peak displacement of 0.47 mm was measured with the ImageJ method (Figure 3.12E) and 0.65 mm using the MatLab method (Figure 3.12F). No trends were observed between the capsule intact, capsule removed, and ligaments removed conditions for the medial marker results. The MatLab technique produced some 'noise' in the medial marker displacement data. This was due to the MatLab bounding box flickering in response to certain aspects of the test set up, such as lighting conditions and the camera distance.

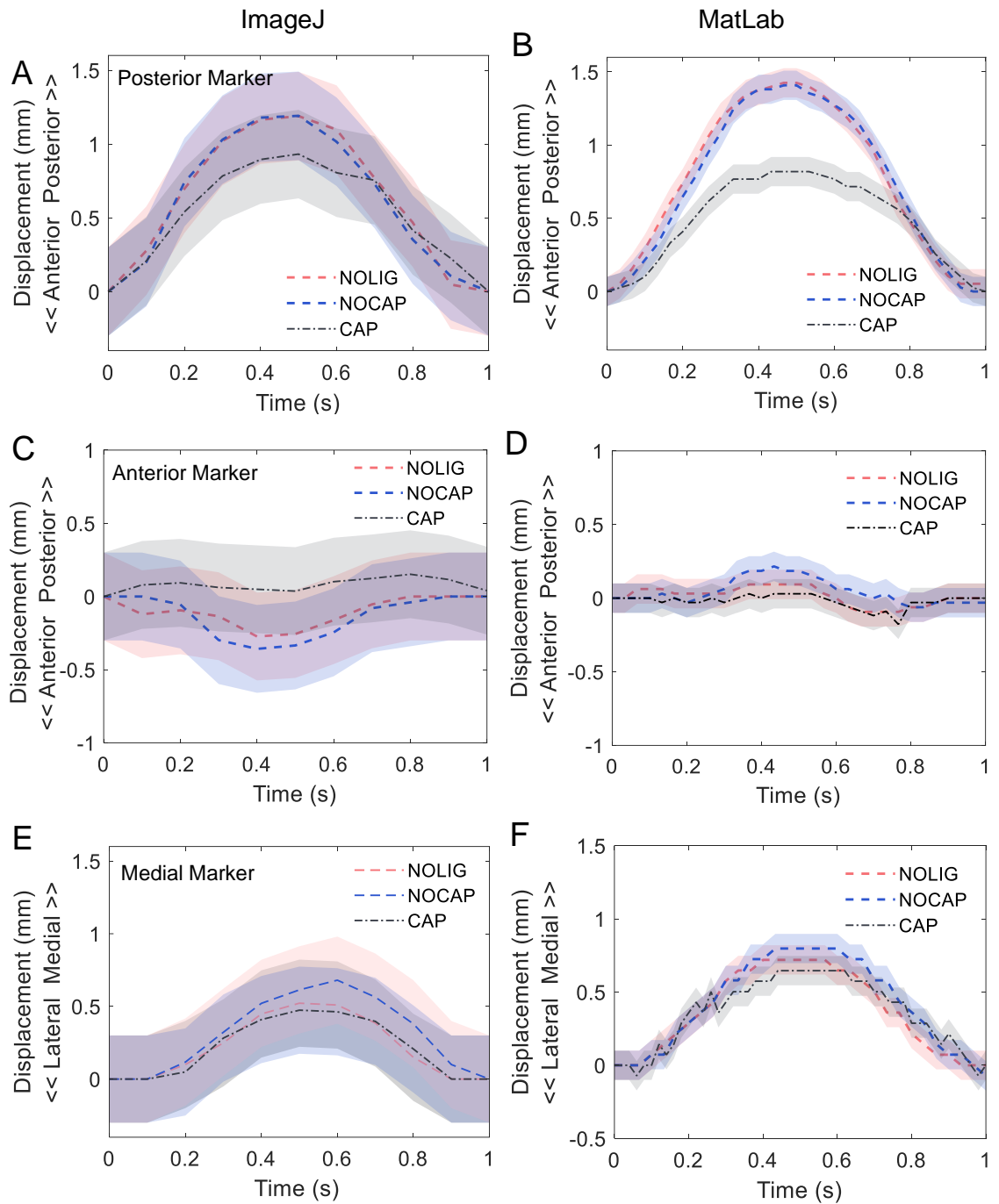


Figure 3.12. Comparison of the meniscal displacement between porcine knee sample dissection conditions, capsule intact (CAP, capsule removed (NOCAP) and ligaments removed (NOLIG), of the posterior marker (A, B), anterior marker (C, D) and the medial marker (E, F) results using two different measurement methods ($n = 1$). Shaded error bars equate to the highest measured absolute value from the validation study. ImageJ method ± 0.29 mm; MatLab method ± 0.10 mm.

3.6.4 Discussion

The aim of this study was to develop a method which can measure meniscus displacement over a single dynamic profile cycle, performing flexion-extension motion with a constant load. In addition, to compare two measurement techniques on the same sample undergoing the same protocol. It is important to note that only a single porcine sample has been evaluated thus far, because at this stage the measurement technique was the focus and progression onto human samples is of upmost importance for clinical relevance.

Radiographical studies in the literature studying human meniscal movement with flexion - extension have shown that the whole meniscus moves posteriorly with flexion (Vedi et al., 1999; Boxheimer et al., 2004; Scholes et al., 2015). Although it is difficult to make direct comparisons between the results of this preliminary study on porcine specimens and those reported in the literature, it was observed during the study that anterior and posterior region of the porcine menisci were moving posteriorly during flexion to stabilise the knee. However, the results show minimal movement of the anterior region of the porcine meniscus; yet the posterior region followed the motion of the simulators flexion arm. Therefore, the sagittal plane video capture was not emulating real motion, which is likely a result of camera lens distortion and camera positioning. To bring the sagittal plane markers into focus, a macro lens was placed on the smartphone camera, however, this created a wide-angle distortion on the outer edges of the frame. It is important for the cameras to emulate what the eye sees, having lens distortion means that the marker motion is being underestimated towards the edges of the frame. This could be why the anterior marker results were minimal compared to the posterior marker results, due to the positioning the markers on the frame. In addition, it was important that the camera was positioned at 90° to the marker to measure the most anterior-posterior movement. Further method developments were applied to control these factors and are described in the next sections.

3.6.4.1 MatLab vs ImageJ Method Evaluation

The ImageJ and the MatLab method represent two forms of video marker tracking measurement techniques, this section discusses each method based on the results.

Repeatability and Ease of Use: One of the main advantages of the MatLab method is that the computational automation has considerably reduced the time taken to analyse results. Observer bias has also been reduced to one instance (the image calibration) which increases the objectivity of the method. The ImageJ method requires the user to measure the distance between each frame manually, generating the likelihood for more

random errors at each instance. In addition, developing this method on a popular and accessible package such as MatLab increases the reproducibility. Due to the limitations of time and observer concentration, the ImageJ method could only produce 10 data points, whereas the MatLab method produced 30 data points throughout a single 1 second duration cycle. This meant that more descriptive displacement information was gathered within the same timeframe using the MatLab method.

Margin for Error and Precision: The MatLab method had a lower margin for error (within 0.1 mm) than the ImageJ method (within 0.29 mm). Due to the novelty of this application, there is little evidence for acceptable error margins in the literature. However, the validation suggests that the MatLab method is more likely to be sensitive to detect differences between test conditions than the ImageJ method. Even though, no definitive conclusions between the dissection conditions can be drawn from this preliminary work, the only case which showed a trend between the capsule intact and capsule sacrificed conditions were the posterior marker results using the MatLab technique.

The MatLab method was also found to have a fair level of precision with the majority of SD's falling within the <10% threshold. This suggests that measurement error could be attributed more toward systematic error and less to random error. Even though both methods require the observer to measure the marker size to calibrate the results from pixels to millimetres, the ImageJ method relies heavily on the observer as the measurement of the distance between the marker and the tibia is taken at each interval. Meaning there is an increased risk of random error and bias with the ImageJ method, creating variation within the results, and reflected in the standard deviations.

3.6.4.2 Conclusion

This preliminary study has shown that it is possible to adhere markers to the medial, anterior, and posterior regions of the medial meniscus and estimate the movement of these regions during dynamic flexion-extension motion. In addition, as explained above, the MatLab method will be chosen to progress with the methodology and further camera and marker developments are required to understand the measurement thoroughly before implementing more complex gait profiles and an injury condition.

3.7 Video Capture and Mounting Development

This section describes developments made to the experimental apparatus, to mitigate the risk of confounding factors such as camera position, lens distortion and low marker-background colour contrast. The goal is illustrated in Figure 3.13, where three separate cameras are held in the simulator, each filming a region of the meniscus in the whole joint sample. The method can now be described in a coordinate system with a consistent set of polarities between the markers, where the polarities match the axes of the simulator.

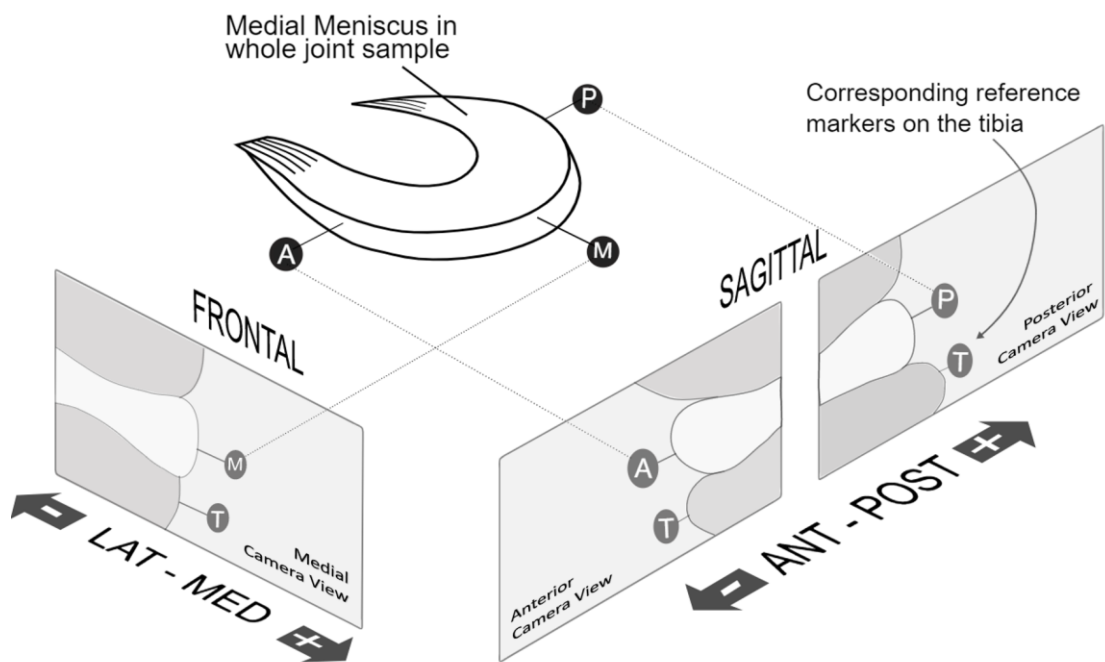


Figure 3.13. Schematic of the tissue-level test set up for the medial meniscus of a right knee in the simulator, showing the medial, anterior, and posterior camera views and the polarity of measured medial-lateral and anterior-posterior movement directions in the video frames. A tibial reference marker will also be introduced so two markers will be tracked with the MatLab script in the same video to find the meniscus displacement, relative to the tibia.

3.7.1 Design Specification for Improved Method Apparatus

Table 3.7 summaries the requirements which were put in place to source the appropriate video cameras and markers, and to design the camera holder which attached to the simulator in order to facilitate data collection.

Table 3.7. Specifications for designing and sourcing the cameras, markers and camera holder for the improved method set up illustrated in Figure 3.12.

Video Camera Requirements	
<i>Quantity</i>	3 x cameras were required to film the meniscus and tibia markers on each individual region (medial, anterior and posterior) of the knee joint
<i>Lens Field of View</i>	To have a narrow and near-natural field of view of 50° – 70° to avoid large lens distortions affecting the tracking estimations.
<i>Size</i>	As small and thin (< 30 (w) x 30 (h) x 10 (d) mm) as possible. The space to fit the anterior and posterior cameras between the knee and the FE arm of the simulator could be as small as 50 mm for porcine knees and 30 mm for human knees.
<i>Focusing Distance</i>	To have a small minimum focusing distance of < 20mm which could be adjusted manually depending on the size of the sample.
<i>Resolution</i>	To have a high-definition resolution of 1080 x 1920 pixels
<i>Frame Rate</i>	To have a minimum frames per second of 30 fps to be able to track the markers moving in the frame.
Marker Requirements	
<i>Size / Diameter</i>	Pins of diameter 2 mm > 4 mm. The meniscus and the tibial marker will be displayed in the same frame and therefore the markers need to be small enough to be measured in the frame.
<i>Colour</i>	To have a solid contrasting colour (green/yellow) to the background. This helps the colour threshold process and reduces the noise generated from the MatLab script.
Camera Holder Rig Requirements:	
<i>Function</i>	To attach to the simulator and be adjustable in the x, y and z directions to allow for varying sized knees. To hold three video cameras in the correct position at the tissue level to enable clear filming of the markers attached in the medial, anterior and posterior meniscal regions.
<i>Durability and Fixation</i>	To be able to maintain secure fixation throughout each full sample experiment and dissipate any simulator vibrations to ensure a stationary video capture. To avoid and camera movement/tilt which would reduce the accuracy of measurements taken from the videos.
<i>Usability</i>	To allow easy removal (clip on, clip off) from the knee simulator. Modular design to be able to change singular parts easily in case of damage or readjustments to material/size/dimensions. Standard camera mount tapped thread used (UNC 1/4" – 20).
<i>Material</i>	To be made from a material which is corrosion resistant, waterproof, and easy to clean. The porcine and human knees will have to be sprayed with PBS to be kept hydrated, therefore the holder needs to be resistant to PBS as well as laboratory regulation disinfectants.
<i>Size and Dimensions</i>	To be able to hold cameras at the tissue level in an estimated sample area/volume of 150 cubic millimetres and avoid contacting moving parts of the simulator. Simulator measurements indicate an adjustable size within an area of: width: 265 mm; height: 200 mm; depth: 270 mm.

3.7.2 Camera Hardware and Markers

Raspberry Pi v2 camera modules (Raspberry Pi, UK) connected to a Raspberry Pi Zero (Raspberry Pi, UK) printed circuit board (PCB) were chosen as video capture hardware. The cameras were capable of filming at 1080 x 1920 resolution at 30 frames per second. Three of these cameras were purchased and programmed on Python (Python Software Foundation, Delaware, USA) to be recognisable by computer as a webcam. The miniature size (Height: 25 mm x Width: 23 mm x Depth: 9 mm) and the adjustable focus was able to show a clear image with an object ~10 mm away. The field of view was also within specification at 62° to reduce the amount of lens distortion.

For the frontal plane, 4 mm diameter map pins with a round yellow head were used. The sagittal plane meniscal markers were made from plastic delrin ball bearings of 2 mm diameter (Simply Bearings, UK). These were then superglued to a 10 mm long piece of metal wire 0.017 mm thick. The glued ball bearings were dipped twice in florescent green petrol resistant paint to make them appropriate for colour segmenting in MatLab. The markers were measured after painting to take into account any increases in diameter.

3.7.3 Camera Holder Design

Details of the simulator camera holder are outlined in Figure 3.14, including the SolidWorks assembly design (A, B) and the finished rig in the simulator and with the anterior, posterior and medial Raspberry Pi cameras mounted (C, D). The holder was made from aluminium due to its machining ease, low cost, and corrosion resistant properties. All cap head screws and tapped holes were ANSI inch UNC thread 1/4" – 20 as this is the standardised screw size for camera mounting. Printed and laminated scales were placed on the adjustable parts of the holder in order to quantify and control the camera positioning. To protect the Raspberry Pi camera modules, splashproof cases were 3D printed from VeroClear® plastic using a fused-filament 3D printer (Objet30, Stratasys, USA) to protect them from PBS spray and biological tissue (Figure 3.14D).

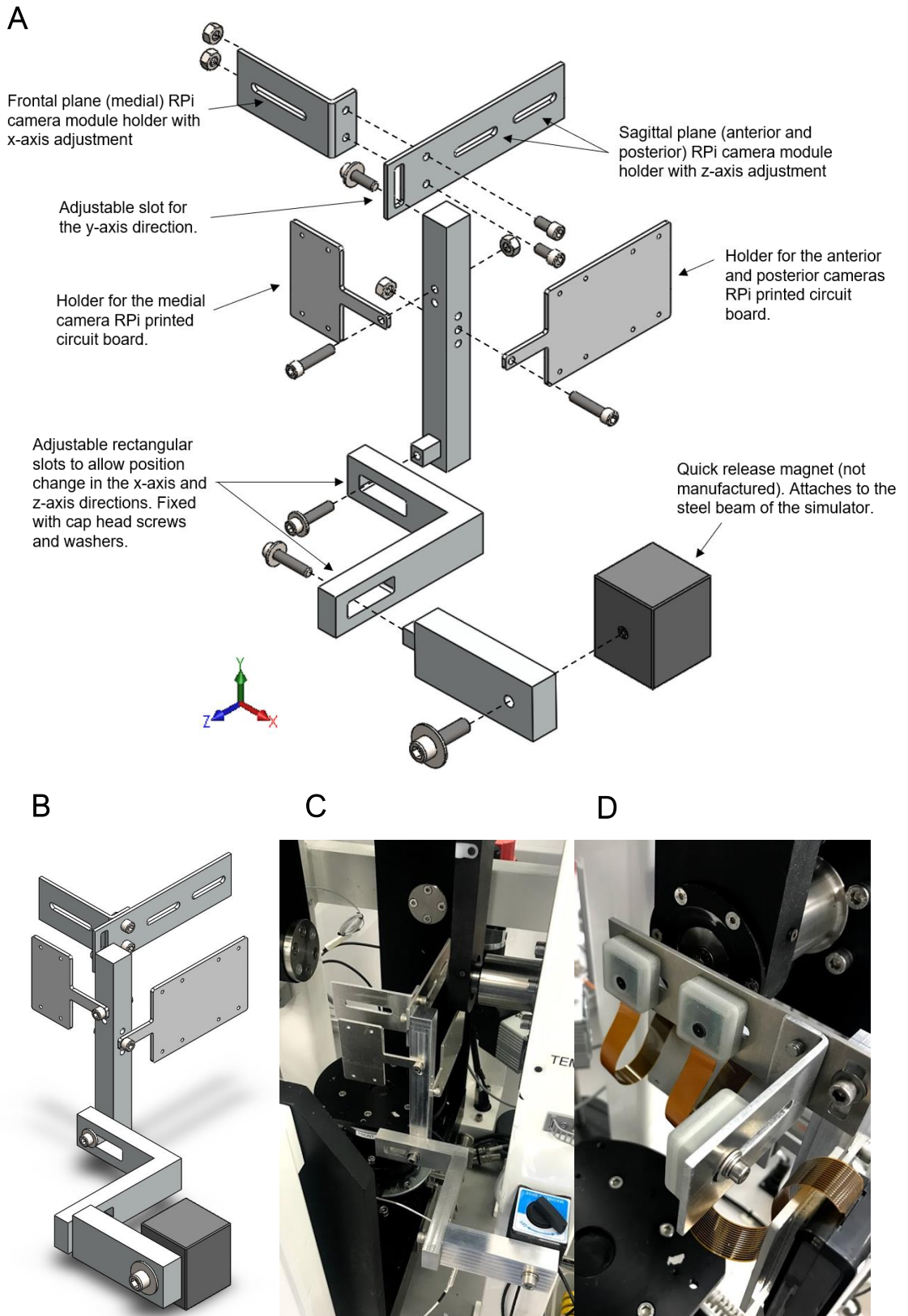


Figure 3.14. (A) Annotated exploded SolidWorks assembly and (B) complete SolidWorks assembly of the camera holder design. (C) Manufactured camera holder adhered to the simulator and (D) with the Raspberry Pi cameras mounted.

3.8 Discussion

This chapter has discussed the development of a method to measure dynamic meniscal displacement in a knee simulator. In the preliminary stages, ImageJ was used to measure the frontal plane marker position changes between frames taken from a video during a static ramping load protocol. This method was then applied to the sagittal plane, measuring position changes in the anterior and posterior regions of the meniscus. The measurement technique was then advanced to an object tracking method using MatLab. Validation experiments showed the MatLab method was more precise, with coefficient of variance's <7% (max 6.05%), and more repeatable as data processing time was reduced considerably. This was chosen over the ImageJ method to measure medial meniscus displacement experiencing dynamic flexion-extension simulator motion. The latter stages of this chapter describe the apparatus and video capture developments to suit the MatLab measurement technique and control confounding factors.

The use of markers adhered to the superior surfaces of the meniscus of cadaveric samples to identify a point of measurement has been performed in a handful of papers studying meniscal movement (Bylski-Austrow et al., 1994; Tienen et al., 2005). However, most studies take radiographical images at static states of flexion and only a handful track the movement during a continuous flexion-extension motion. In addition, the benefit of using an object tracking method is that a very small amount of tissue manipulation is required to place the pins, this allows more freedom of movement to measure dynamic displacements.

The use of video object tracking has been used in a variety of different applications from military visual surveillance systems to ecological animal population counting systems to medical imaging (Olesen et al., 2012; Kalcounis-Rueppell et al., 2013; Kamate and Yilmazer, 2015). However, to the authors knowledge, no study has used a video capture and computational object tracking method to estimate and quantify dynamic meniscal displacement.

In the next chapter, the MatLab technique and experimental set up, using the Raspberry Pi video equipment and bespoke camera rig, will be investigated further by performing sinewave motions of the anterior-posterior and tibial rotation axes on the simulator. This will aid the understanding of how rotation effects the 2D measurements and the sensitivity of the relative meniscal displacement measurement. In addition, to progress the loading protocol to include dynamic tibial motion. These further investigations will help interpretation of the data in relation to the simulator outputs and be important when progressing the method onto human specimens.

Chapter 4

Reliability Investigations of the Marker Tracking Method

4.1 Introduction

In the previous chapter an object tracking method was developed to measure the anterior-posterior and medial-lateral displacement of a moving marker in a video. This marker tracking method was validated on the medial-lateral axis using a static reliability study in section 3.6. However, the overall goal is to measure dynamic meniscus movement. Therefore, this chapter presents work which further analysed the accuracy and precision of the marker tracking method to known dynamic simulator inputs. The simulator input profiles were built up in complexity, starting by applying sinewave profiles to a solid object (dummy rig), before applying a simulated gait cycle on a porcine knee joint. The end goal was to measure dynamic meniscal displacement in the anterior, posterior, and medial meniscal regions whilst the whole knee joint was driven through a simulated gait cycle. During the simulated gait cycle, the tibia moves with the abduction-adduction, anterior-posterior and tibial rotation axes; therefore, two markers were placed at each region, one marker on the meniscus and one marker on the tibia. The key measurement was the relative displacement of the meniscus marker with respect to the tibia marker. This chapter presents a series of sub-studies prior to applying the full model to porcine and eventually human specimens, clarifying the reliability of the marker tracking method.

4.1.1 Aims and Objectives

The aim of this chapter was to establish the reliability of the marker tracking method and to aid understanding of the meniscus movement measurements obtained when complex simulator inputs are applied.

The objectives were:

1. To establish the accuracy and precision of the marker tracking method in the anterior-posterior axis using a solid plastic dummy joint;
2. to describe the effect of introducing tibial rotation on the anterior-posterior marker tracking measurements;
3. to describe the margin of error during image calibration and camera lens distortion;
4. to establish the polarity of the relative displacement between two moving markers;
5. to establish the relative meniscus displacement measurement and sample set up by performing sinewave inputs on a porcine knee joint sample with meniscal and tibial markers placed on the anterior, posterior and medial regions of the meniscus;
6. to apply a complex displacement controlled simulated gait cycle and measure the relative meniscal displacement of the anterior, posterior and medial regions of the meniscus.

4.2 Dummy Investigation: Understanding the Accuracy and Precision in Response to Sinewave Inputs

4.2.1 Rationale

This section presents work using markers adhered to a solid object (dummy) and driven through simple simulator inputs to assess the reliability of the marker tracking method. The accuracy was assessed by calculating how close the measured marker displacements were to known simulator translations. The precision was assessed by performing multiple repeats and calculating the dispersion of the measured displacements from one another.

A basic single-axis study was performed initially, only driving the anterior-posterior translation axis using a sinewave profile at different magnitudes to assess the agreement and the dispersion of the measured displacements to the known simulator translations. This study was performed to determine a baseline margin of error of the marker tracking method in the absence of additional factors such as load, and 3D motion.

A second study was performed examining the effect on the measured anterior-posterior marker displacement when applying tibial rotation. Adding tibial rotation (transverse plane) changed the depth of the marker in the video frame of both the frontal and sagittal plane cameras (moving towards and away from the lens). This moved the marker out of plane and effected the measured 2D anterior-posterior displacement in the video frame. This study was performed to understand the effect of increasing the magnitude of tibial rotation on the marker displacements in the video frame. This is useful

because the simulated gait cycle will include an amount of driven tibial rotation and the sensitivity of this on the 2D tracking system requires investigating to help characterise the measured displacements.

4.2.2 Method

4.2.2.1 Test Set Up

A dummy was manufactured consisting of a cylindrical delrin tibial base, a metal femur and a delrin floating insert to act as a meniscus (Figure 4.1A). This floating insert was able to float along the sagittal plane (anterior-posterior axis) only and allowed small amounts of rotation in the transverse plane. A green 5 mm diameter marker was adhered to the tibial base of the dummy with superglue and a small square of Velcro. The location of the marker on the tibial base was positioned medially and posteriorly at $\sim 20^\circ$ angle from the centre of the circular cross section (Figure 4.1B). This position was used so the marker could be closer to the camera lens for clarity. The tibial base diameter was large which meant if the marker was placed at the 0° on the cylindrical profile it would have been too far away to be illuminated properly. The polarities of the simulator anterior-posterior and tibial rotation axes are described in Figure 4.1C in the video frame.

A single Raspberry Pi camera was programmed and mounted in the simulator on the medial side to film the marker and a light source was placed on the simulator to illuminate the marker. A spirit level was used to ensure the camera was level. A flashing red LED light was linked to the opto-regulator of the simulator to indicate the cycle starting point in the video frame. The camera was triggered via USB through a standard web-camera application (Camera, Windows 10) and the videos were captured at 30 fps with the simulator running at a frequency of 0.5 Hz (2 second cycle duration). This frequency is half the speed of the standard frequency used in previously published work (Liu et al., 2015). This speed was necessary to reduce the motion blur of the markers in the output videos. Motion blur prevented the object-tracking bounding box adhering to the marker in the video. Reducing the frequency allowed clearer movement to be captured whilst not affecting the pattern of movement produced by the simulator.

All the videos were processed in MatLab to measure the anterior-posterior displacement of the tibial base marker during one simulator cycle (cycle 10). The pixel calibration factor was calculated as described previously (see section 3.5.2.3) to estimate the displacements in millimetres. The total measured anterior-posterior displacements for each sinewave condition were used for data analysis.

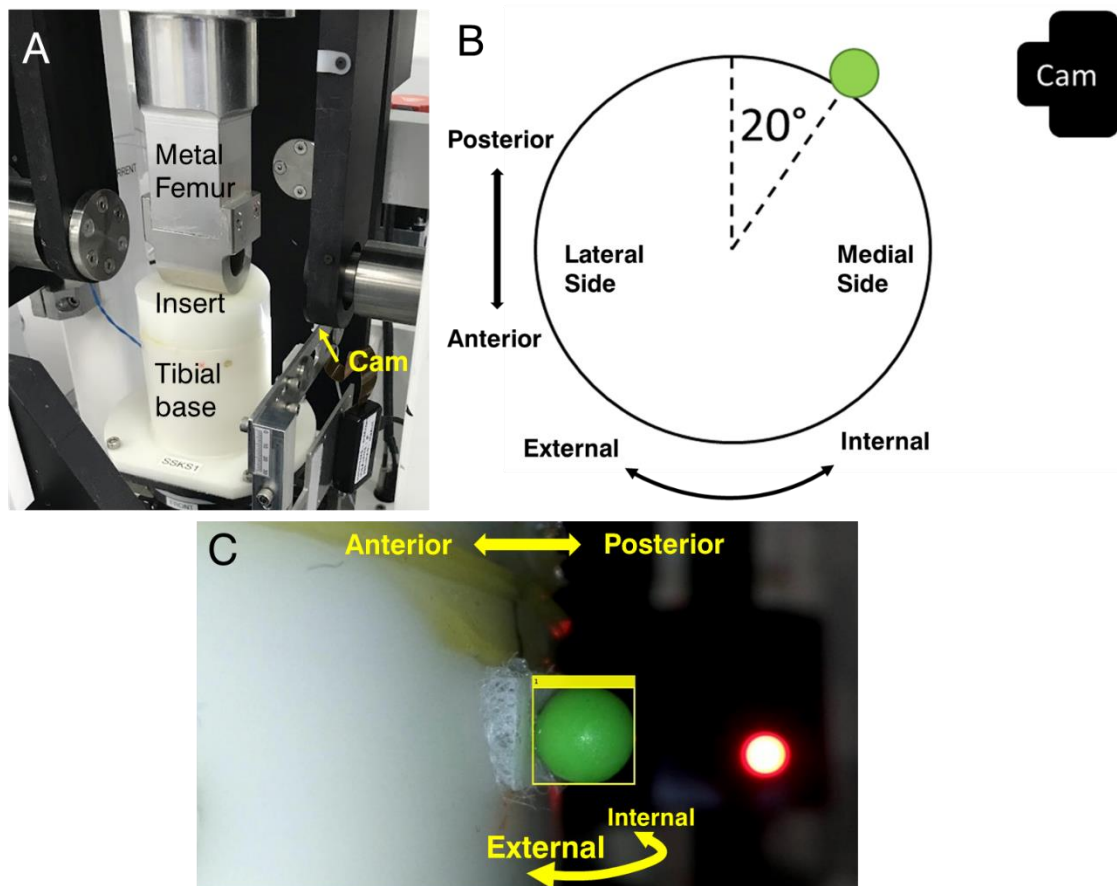


Figure 4.1.(A) Dummy study set up in the simulator. (B) Tibial base top view showing the marker position (attached to the tibial base) in relation to the camera position and the directions of the simulators driven sinewave anterior-posterior translation and internal-external rotation of the tibial base. (C) Camera frame video of the marker attached to the tibial base with labelled simulator translation and rotation axes.

4.2.2.2 Study 1: Anterior-Posterior Displacement Agreement

This study was carried out to investigate how effective the method was at measuring a moving marker in one plane. Only the anterior-posterior translation axis was driven as a sinewave profile at differing magnitudes (± 1 mm, ± 2 mm, ± 4 mm, ± 6 mm) (Figure 4.2). No load was applied, and the tibial rotation axis and the abduction-adduction axis were fixed. This study was repeated three times and the measured marker-tracking video displacement were compared to the simulators anterior-posterior translation output, which were measured with built-in optical encoder sensors. Mean percentage error (MPE) was calculated as the accuracy measure and the coefficient of variance (CV) was calculated as the precision measure of the marker tracking method.

4.2.2.3 Study 2: The Effect of Tibial Rotation on the Measured Anterior-Posterior Displacement

The sinewave profiles applied to the anterior-posterior translation and internal-external rotation axes of the simulator were used simultaneously in this study (Figure 4.2). For each of three anterior-posterior translation sinewave profiles (± 0 mm, ± 2 mm, ± 6 mm), four tibial rotation sinewave profiles ($\pm 0^\circ$, $\pm 1^\circ$, $\pm 2^\circ$, $\pm 4^\circ$) were applied. The polarities were chosen to generate anterior tibial translation and internal tibial rotation together, as this is what generally occurs with knee flexion (Shenoy et al., 2013). The abduction-adduction axis was fixed and a 500N constant axial load was applied to the dummy system during this study. This was applied because a knee specimen would always have a certain amount of axial force transmitted through the system when applying tibial rotation. Each sinewave condition combination was repeated three times and the closeness of the measured displacements were compared with each other using the coefficient of variance (CV) to further study the precision of the marker tracking method.

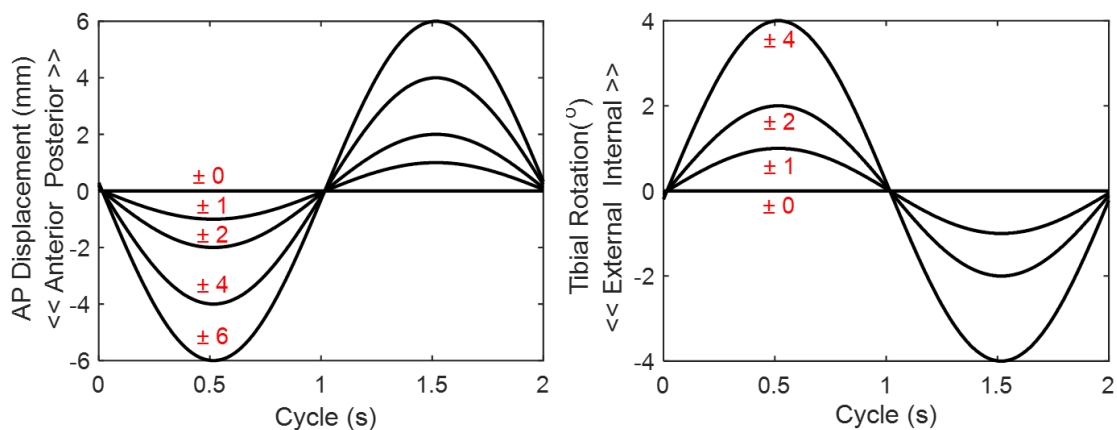


Figure 4.2. Sinewave input profiles used for the anterior-posterior (AP) translation and the internal and external tibial rotation (TR).

4.2.3 Results

4.2.3.1 Study 1: Anterior-Posterior Displacement Agreement

As shown in Table 4.1, the marking tracking measurements fell within $\pm 2\%$ of the known outputs produced by the simulator. A slight trend was observed as the MPE increased as the magnitude of each anterior-posterior sinewave condition increased. The precision of the marker tracking method was also high showing little variation between repeat measurements ($CV < 2\%$). The highest CV recorded for this study was for the sinewave condition of the smallest magnitude (± 1.0 mm: 1.31%). As shown in Figure

4.3, the marker tracking method successfully measured the moving marker with good agreement to the simulator output for each sinewave condition.

Table 4.1. Study 1 known and measured total displacements for each driven anterior-posterior (AP) sinewave case (all measurements in mm) including statistical results of mean percentage error (MPE) and coefficient of variance (CV).

AP Case	SSKS Input	SSKS Output	Marker Tracking Method			Mean (SD)	MPE (%)	CV (%)
			Trial 1	Trial 2	Trial 3			
+/- 1	2.00	1.98 (± 0.01)	1.99	1.97	2.02	1.99 (± 0.03)	- 0.97	1.31
+/- 2	4.00	3.96 (± 0.02)	3.92	3.92	3.92	3.92 (± 0.00)	- 1.03	0.00
+/- 4	8.00	7.94 (± 0.01)	7.79	7.84	7.83	7.82 (± 0.03)	- 1.49	0.33
+/- 6	12.00	11.90 (± 0.01)	11.73	11.71	11.73	11.72 (± 0.01)	- 1.51	0.08

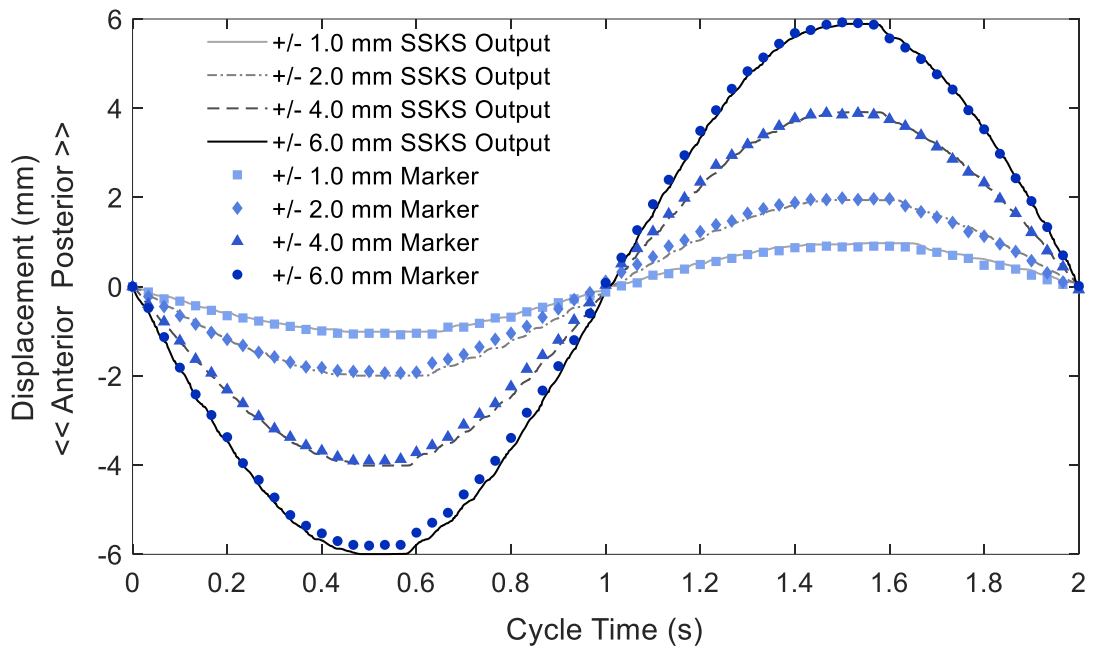


Figure 4.3. Study 1 results from repeat trial 1 showing the agreement of the marker-tracking method (blue lines) in measuring known anterior-posterior sinewave translations driven by the simulator (grey/black lines).

4.2.3.2 Study 2: The Effect of Tibial Rotation on the measured Anterior-Posterior Displacement

Even with no anterior-posterior translation applied, the tibial rotation movement created displacement of the marker along the anterior-posterior axis in the video frame (Figure 4.4A). When driven translation was applied increasing the magnitude of the tibial rotation had the effect of reducing the amount of measured anterior-posterior displacement in the video frame (Figure 4.4B).

The majority of the CV's reported in Study 2 showed an acceptable amount of precision (Table 4.2). All conditions, except for the 0 mm AP, 0° TR control condition, reported values < 10 % variation. The mean total displacement for the +/- 2 mm AP 0° TR and the +/- 6 mm AP 0° TR conditions were lower than the means reported in study 1 (AP +/- 2 mm sinewave case: 3.92 mm (study 1), 3.47 mm (study 2), - 0.45 mm; AP +/- 6 mm sinewave case: 11.72 mm (study 1), 10.85 mm (study 2), - 0.87mm).

Table 4.2. Study 2 marker tracking measured displacements and calculated coefficients of variation (CV) from three repeat trials of each driven AP translation sinewave case with associated driven tibial rotation sinewave cases (500N constant axial load applied).

<i>Driven Tibial Rotation (°)</i>	<i>Mean Total AP Displacement (mm)</i>					
	<i>AP +/- 0 mm (SD)</i>	<i>CV (%)</i>	<i>AP +/- 2 mm (SD)</i>	<i>CV (%)</i>	<i>AP +/- 6 mm (SD)</i>	<i>CV (%)</i>
± 0.0	0.07 (± 0.03)	39.1	3.47 (± 0.01)	0.2	10.85 (± 0.04)	0.4
± 1.0	0.80 (± 0.07)	9.7	3.01 (± 0.14)	4.6	10.42 (± 0.06)	0.6
± 2.0	1.37 (± 0.06)	4.7	2.47 (± 0.14)	5.8	9.65 (± 0.18)	1.9
± 4.0	2.63 (± 0.10)	3.6	1.32 (± 0.04)	2.9	8.58 (± 0.17)	1.9

4.2.4 Discussion

The aim of this section was to investigate the accuracy and precision of the marker tracking method in response to a range of sinewave profiles using a plastic dummy. A simple experiment using only one movement axis and no load (Study 1) examined how close the marker displacement, measured through the MatLab marker-tracking technique, was to a known anterior-posterior translation outputs of the simulator.

This basic study showed that the method measured planar anterior-posterior displacement within a maximum absolute value of 0.18 mm, or a mean of +/- 0.1 mm when tracking a moving simulator output, and that the measurements were reproducible

due to a low data dispersion (Table 4.1). The measured displacements also followed the movement path produced by the anterior-posterior carriage of the simulator.

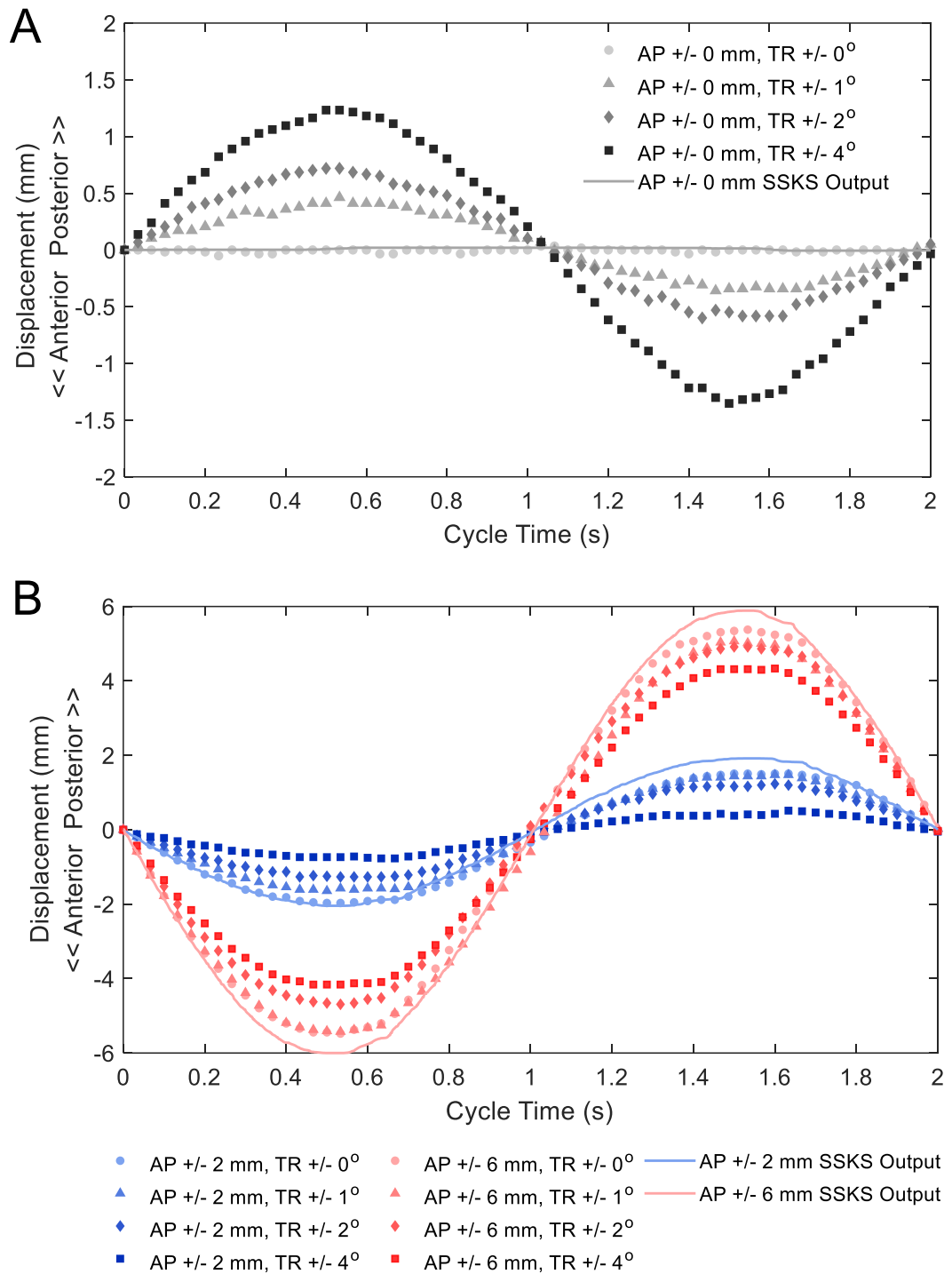


Figure 4.4. Study 2 results from repeat trial 1 showing the effect of applying tibial rotation on the anterior-posterior measurement of the marker in the video for the (A) +/- 0 mm (black/grey) AP sinewave condition and (B) the +/- 2 mm (blue) and the +/- 6 mm (red) AP conditions (500N constant load applied).

A second experiment (Study 2) was carried out during this investigation to understand the effect on the 2D marker tracking measurement when applying tibial rotation and load. When no translation was applied, the tibial rotation generated a small amount of measured anterior-posterior displacement in the video frame which followed the shape of the tibial rotation input profiles. The higher the magnitude of the applied tibial rotation sinewave case, the larger the amount of measured anterior-posterior displacement when no simulator translation was applied. Due to the polarities of the simulator, internal rotation produced posterior displacement and external rotation produced anterior displacement in the video frame. In the cases where driven anterior-posterior translation was applied (± 2 mm and ± 6 mm AP sinewave conditions), the opposite effect occurred. The measured anterior-posterior displacement in the video frame followed the direction of simulators AP carriage and the application of tibial rotation reduced the amount of measured anterior-posterior displacement in the video frame. The implications of this as a meniscus displacement measurement are discussed later in section 4.8.

Moreover, the coefficients of variation remained $< 10\%$ when motion was applied to the dummy, showing an acceptable amount of precision when measuring a moving marker. Therefore, despite the changes occurring when applying tibial rotation and moving the marker out of plane; effecting the measured 2D anterior-posterior displacement in the video frame, the marking tracking method can produce precise measurements if parameters such as camera positioning and lighting are meticulously controlled between experimental conditions. The ability to compare against experimental conditions with the developed marker tracking method relates to the overall aim of the project in devising a pre-clinical assessment, rather than producing accurate measurements in three dimensions. However, this also suggests that the marker tracking method is not particularly robust as the test set up requires tight controls and a specific environment for acceptable measurements to be obtained and compared between conditions. Herein, simulator vibrations and noise produced by the marker-tracking method meant that the CV for the fixed control condition in Study 2 (± 0 AP, $\pm 0^\circ$ TR) was high (39.1%) because small fluctuations in the signal had a larger effect on the data dispersion around the mean.

4.2.4.1 Limitations

A constant 500N load was applied during Study 2 which may have created slight vibrations in the dummy rig system affecting the measurements. In addition, any axes which were not driven were fixed at zero, meaning that the motors were working to keep

that axis at zero and creating some vibration in the system. This explains why the control condition was measured at 0.07 (+/- 0.03) mm when the target was 0.00 mm.

In addition to simulator vibration, cases with small translations or rotations were affected by the precision of the marker-tracking method. This was due to the attachment of the bounding box to the pixel area of the marker in the video frame. A pixel is the smallest element of an image and is a discrete variable, because it is not possible to measure anything in the middle of one pixel. The resolution of the marker tracking method is the pixel calibration factor (see section 3.5.2.3) meaning that the smallest possible displacement measured is limited by the size of one pixel. When the marker was held at zero, the bounding box 'flickers' between pixel boundaries, as the line cannot fall in the middle of pixel. This creates noise in the measured signal. This noise can be moderated through adequate lighting and data smoothing; however, the effect is less noticeable when measuring larger displacements (> 1.0 mm).

Lighting is a key factor to control when carrying out optical methods. Well illuminated markers allow for greater colour contrast from the background of the image generating a more accurate adherence of the bounding box to the moving marker during the blob analysis. In this study, a small trend was observed as the closeness of the measurements to the simulator outputs reduced slightly as the magnitude of each condition increased in study 1. During the larger anterior-posterior sinewave displacements (+/- 6.0 mm), the marker travelled further to the periphery of the video frame where the illumination was possibly lower than in the centre of the video frame. When the marker entered darker areas in the video more error was produced because the marker became less contrasting to the background. However, the MPE of the +/- 6.0 mm sinewave was still low at 1.51%.

4.3 Image Calibration Error

4.3.1 Rationale

A key part of the marker tracking method is calibrating all the frames in the video to the known marker diameter. The diameter of the marker was measured manually using the image tool function ('imtool') within the marker tracking script, which gave a number in pixels. The pixel calibration factor was calculated by dividing this value with the actual size of the marker (known diameter) in millimetres (Equation 3.3). The pixel calibration factor was then applied to the tracking results to give an estimate of the position data in millimetres. This estimate was dependent on the distance the camera was away from the marker and the size of the markers used. A margin of error was generated when calibrating the frames in the video in this way.

Therefore, the aims of this short study were:

- 1) To investigate the effect of overestimating or underestimating the marker pixel diameter on the measured marker displacement;
- 2) to investigate the inter and intra observer variability when measuring the diameter of the marker in the video frame using the 'imtool' function in MatLab and assessing this effect on the measurement.

4.3.2 Method

4.3.2.1 Pixel Measurement Sensitivity

This was carried out by using the +/- 6.0 mm anterior-posterior displacement sinewave results from the dummy investigation previously (see section 4.2). The 5 mm marker diameter was measured at 292 pixels by the author, this generated a pixel calibration factor of 0.0171 mm per pixel. Within the script, the marker pixel diameter (292 pixels) was manually changed to simulate overestimating and underestimating the calibration by +/- 5 pixel increments to understand the effect on the measured displacement. The known diameter of the marker (5 mm) was also changed to +/- 1 mm in this sub study which equated to a pixel calibration factor of 0.014 mm per pixel for a 1 mm underestimation and a factor of 0.020 mm per pixel for a 1 mm overestimation.

4.3.2.2 Intra-Observer and Inter-Observer Variability

To assess the differences between individual marker diameter measurement, a sample of healthy subjects familiar with computer use (n = 8; 4 males, 4 females, mean age: 28 years) took part in a marker measurement study using the 'imtool' function on the calibration image from the dummy investigation (see section 4.2). The trial was blinded to mitigate bias, meaning the subjects did not know the authors pixel measurement value (292 pixels), nor did they know what values the other subjects in the study measured. The subjects measured the 5 mm marker in the image (in pixels) three times and the mean was calculated to assess intra-observer variability. A mean was calculated across all subjects to assess inter-observer variability.

4.3.3 Results

Overestimating the marker diameter (in pixels) by + 5 pixels in the equation caused the pixel calibration factor to decrease (0.0168 mm per pixel) and therefore less displacement to be measured in the image. The total displacement of the +/- 6 mm

sinewave measurement decreased by 0.19 mm. Underestimating the marker diameter by -5 pixels increased the pixel calibration factor to 0.0174 mm per pixel, causing more displacement to be measured in the image. The total displacement of the ± 6 mm sinewave measurement increased by 0.19 mm (Figure 4.5). A calibration error of ± 5 pixels when measuring the diameter of the marker in the image created a $\pm 1.7\%$ error on the measured displacements in this analysis. Moreover, overestimating the known marker diameter (in mm) by ± 1 mm, created a $\sim \pm 20\%$ difference in displacement from the original result.

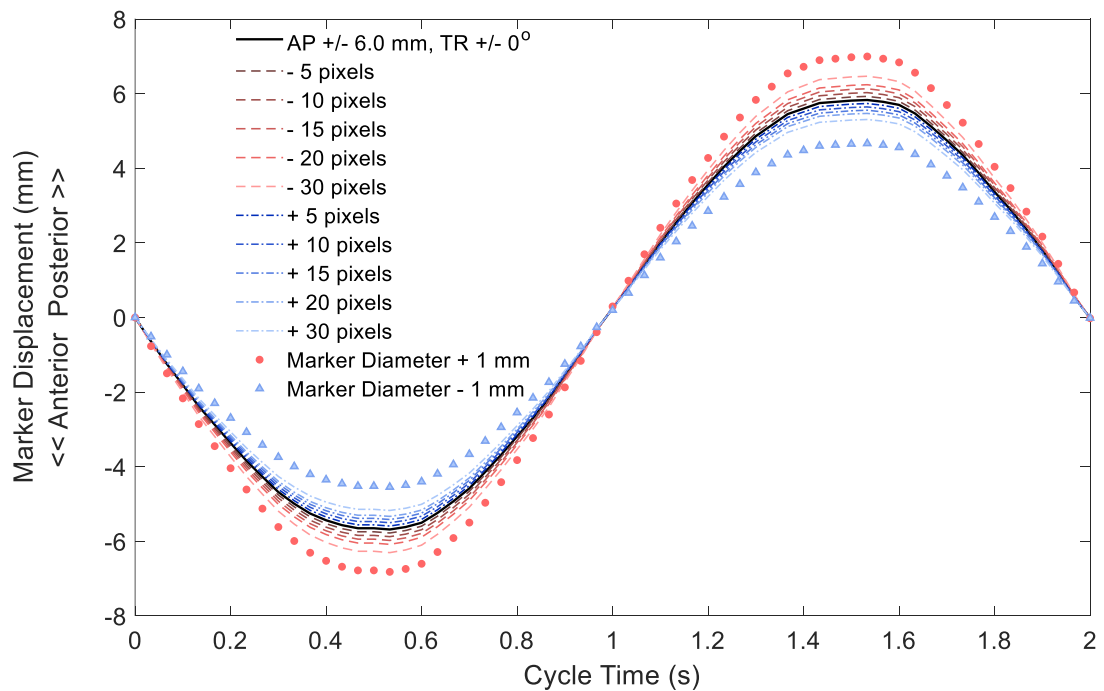


Figure 4.5. Sensitivity analysis of the marker pixel diameter calibration on the measured ± 6 mm anterior-posterior translation sinewave result from the dummy investigation (Study 1).

The mean marker diameter measurement in the image calibration was 290.92 pixels (± 2.36 SD) across the 8 subjects in the inter-observer variability study (Table 4.3). The maximum calibration measurement was 295.60 pixels and the minimum measurement was 286.50 pixels across all measurement trials of the 8 subjects. Therefore, all inter-observer measurements were with ± 4.55 pixels from this investigation. Intra-observer variability fell on average within ± 1.02 pixels of the mean measurement. The maximum range of the three repeat measurements for a subject was 4.49 pixels (subject 8) and the minimum range was 0.02 pixels (subject 4). These inter and intra observer pixel ranges were in agreement with the ± 5 pixel error generating a $\pm 1.7\%$ error in the measurement in Figure 4.5 above.

Table 4.3. Measured pixel diameters of the marker in the calibration image (Study 1) across 8 healthy subjects to assess intra and inter observer variability (All measurements in pixels).

<i>Subject</i>	<i>Image Marker Measurement 1</i>	<i>Image Marker Measurement 2</i>	<i>Image Marker Measurement 3</i>	<i>Mean</i>	<i>± SD</i>
1	289.66	292.56	291.03	291.03	1.45
2	289.50	291.06	291.03	290.53	0.89
3	295.50	295.52	295.60	295.54	0.05
4	291.00	291.02	291.02	291.01	0.01
5	288.04	288.04	289.56	288.55	0.88
6	292.52	289.52	291.02	291.02	1.50
7	288.02	286.50	286.69	287.07	0.83
8	289.53	294.02	294.00	292.52	2.59

4.3.4 Discussion

This study found that underestimating or overestimating the marker pixel diameter influenced the measured anterior-posterior displacement in the image. A higher pixel calibration factor caused more millimetres calibrated to one pixel, increasing the measured displacement. The pixel calibration factor can be increased through increasing the known diameter (numerator) or decreasing the pixel diameter (denominator) in Equation 3.3. A lower pixel calibration factor caused fewer millimetres calibrated to one pixel, decreasing the measured displacement. The opposite process creates this effect, by either decreasing the known diameter or increasing the pixel diameter.

Inter-observer variability and intra-observer variability fell within a ± 5 pixel calibration measurement error. Therefore, measurements between observers would feasibly fluctuate within ± 5 pixels, creating a potential $\pm 1.7\%$ error for a 12 mm (± 6 mm) profile from this study. The sensitivity analysis spanned to ± 30 pixels to illustrate the effect the calibration has on the results. The results from this study also stress the importance of accurately measuring the known diameter of the marker in millimetres before testing. The pixel calibration factor was dependent on the video resolution, the size of the marker and/or how far away the camera is from the marker, therefore this percentage error would be consistent for all magnitudes of displacement, providing the marker size, camera parameters and camera position were kept consistent. In addition, accurate image calibration was also dependent on a clear boundary of the marker from the background in the video frame. Adequate lighting and a contrasting marker colour would increase marker diameter measurement accuracy for image calibration.

4.4 Lens Distortion Error

4.4.1 Rationale

All camera lenses distort the world they are viewing to a certain degree and the amount of lens distortion varies between camera models (Figure 4.6). For example, action cameras used to capture sports have a field of view $\sim 180^\circ$, creating a 'barrel' distortion. Alternatively, telephoto cameras used for filming distant objects usually adopt a 'pincushion' distortion. Large amounts of lens distortion would reduce the accuracy when measuring displacements of moving objects in the video and therefore post-processing may be necessary to correct this distortion and omit this error.

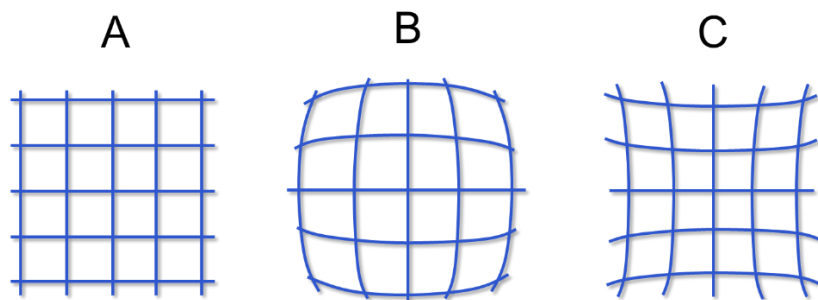


Figure 4.6. Types of lens distortion: (A) no lens distortion, (B) barrel distortion and (C) pincushion distortion.

The aim of this study was to remove any lens distortion by carrying out the intrinsic camera calibration process located within the MatLab's computer vision toolbox and to discuss the effect of performing the intrinsic calibration on the anterior-posterior sinewave results obtained during Study 1 of the dummy investigation (section 4.2.2.2).

4.4.2 Method

The intrinsic camera calibration was performed using one miniature Raspberry Pi camera programmed as a webcam. This process uses the single Camera Calibrator and the Batch Image Processor applications available within the computer vision toolbox on MatLab. Multiple images of a standard checkerboard with 25 mm sized squares were taken with the Raspberry Pi camera at different angles (Figure 4.7A). Fourteen checkerboard images were taken in total and uploaded to the Camera Calibrator application on MatLab. The intrinsic calibration was carried out showing the reprojection errors and extrinsic parameter visualisation. These outputs are for visual purposes to evaluate the accuracy of the calibration. The reprojection errors are the distance in pixels between the corners of the checker squares within each image. An acceptable overall

mean error for this calibration is < 1.0 pixel (Figure 4.7B). The extrinsic parameters estimate the positions of the camera relative to the checkerboard and vice-versa. This is useful to identify errors from checkerboard images which may need to be repeated or excluded.

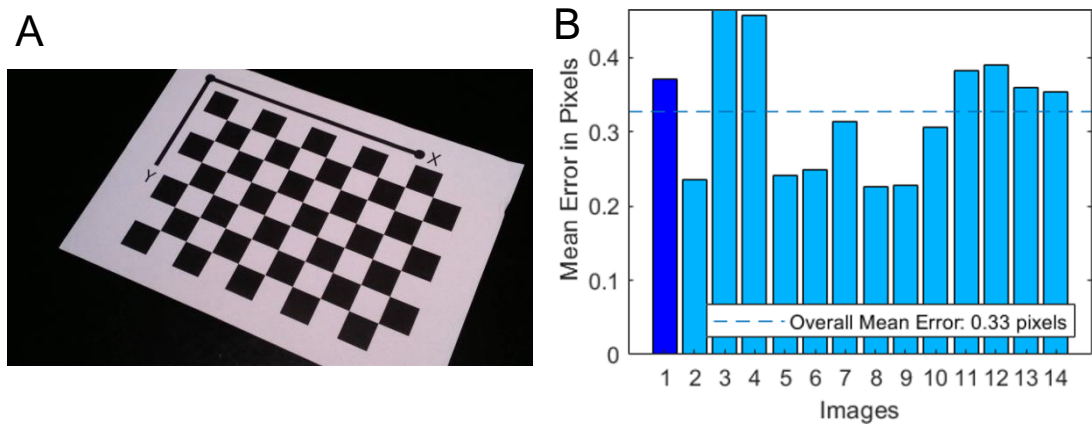


Figure 4.7. (A) An example checkerboard image and (B) the reprojection errors.

The main outputs of the calibration were contained in the structural array 'cameraParams' and exported into the workspace. This variable contained the calculated intrinsic and extrinsic camera parameters, plus the radial and tangential distortion coefficients. The camera parameters and distortion coefficients were inputted into an image function and applied to all the frames of the +/- 1.0 mm, +/- 2.0 mm and +/- 6.0 mm anterior-posterior translation sinewave condition videos from one of the study 1 trials during the dummy investigation (section 4.2.2.2). This was done by using the Batch Image Processor application (The MathWorks, 2022). The object-tracking script was then used on the videos with the applied intrinsic calibration. One cycle was extracted, and the percentage errors were calculated and compared with the previous uncalibrated results.

4.4.3 Results

The intrinsic calibration was sufficiently accurate and resulted in a mean overall reprojection error of 0.33 pixels. Comparisons between the calibrated and uncalibrated results are displayed in Figure 4.8. Images of the video frames are also illustrated to show the effect of the calibration on the lens distortion.

As shown in Table 4.4., minimal difference was found between the measured displacements (+/- 0.016 mm, maximum: 0.03 mm) from the uncalibrated and calibrated results. The calibrated measurements remained sufficiently close to the known simulator

outputs and a small difference in percentage error ($\pm 1.09\%$) was found when compared with the uncalibrated percentage errors.

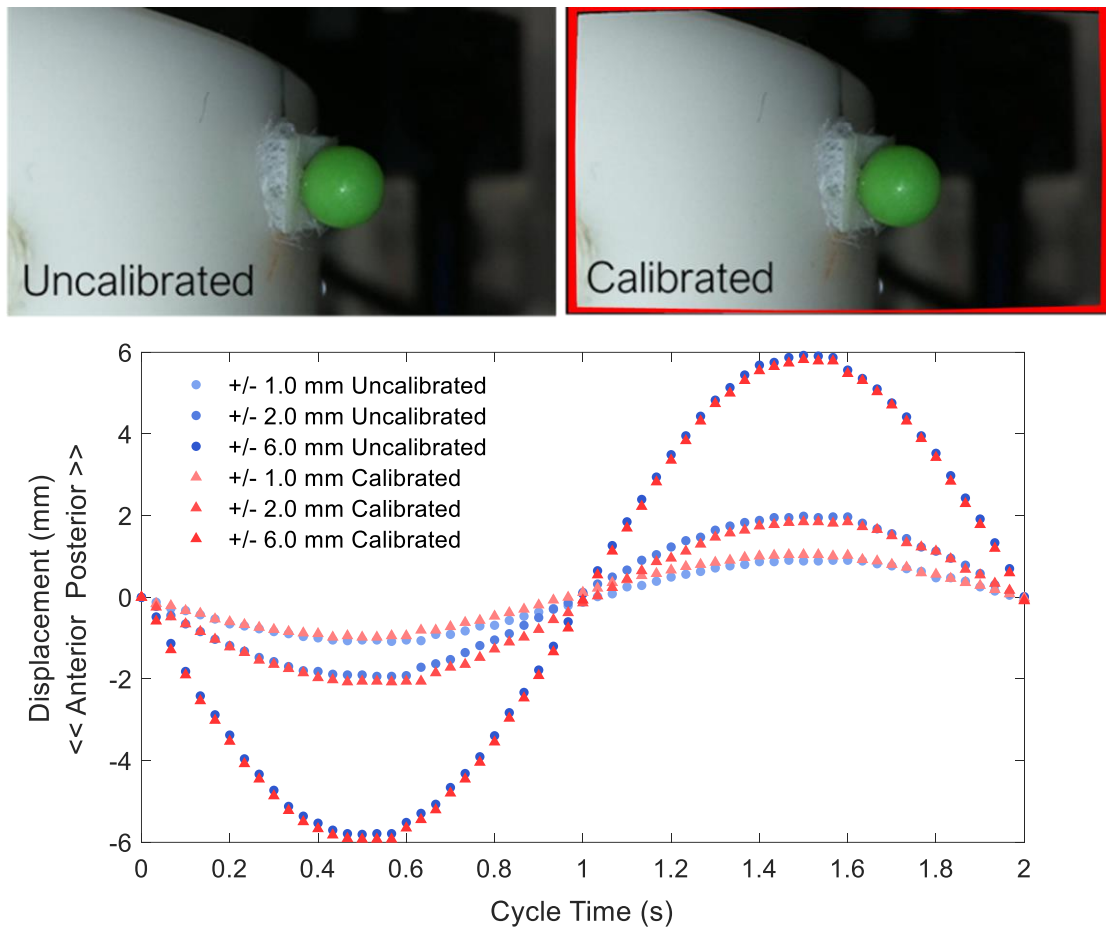


Figure 4.8. Calibrated (red) and uncalibrated (blue) anterior-posterior displacement results. Calibrated image (right) shows a narrow border (coloured red) around the edge of the frame to undistort the image using the intrinsic camera calibration method.

Table 4.4. Total displacements and percentage errors of the calibrated and uncalibrated results (all measurements in mm).

<i>Sinewave</i>	<i>SSKS Output</i>	<i>Uncalibrated</i>	<i>Uncalibrated Error (%)</i>	<i>Calibrated</i>	<i>Calibrated Error (%)</i>
± 1 mm	1.99	1.99	0.04	2.02	1.66
± 2 mm	3.94	3.92	- 0.40	3.92	- 0.40
± 6 mm	11.89	11.73	- 1.35	11.71	- 1.21

4.4.4 Discussion

The cameras chosen for this project were purposefully selected to have a short field of view of 62° to minimise lens distortion. Camera lenses will always distort the world viewed in the image in one way or another, but the purpose of this study was to understand the effect of lens distortion on the measurement by performing an intrinsic camera calibration using MatLab. The results showed generally a small difference between the displacements generated using the intrinsic calibration compared to the original uncalibrated results. However, the calibration correction is of a scale that it affects the percentage error at low displacements quite significantly but is less significant in the larger displacement cases where other forms of error dominate more so than the lens distortion.

4.5 Relative Meniscus Displacement Measurement

4.5.1 Rationale

To characterise the displacement of the meniscus during the complex motions and loads of a gait cycle, a relative measure was investigated. During a simulated gait cycle, the tibia moves with anterior - posterior translation, internal - external rotation and abduction – adduction axes. The meniscus also moves passively within the knee joint. Therefore, to understand changes in position of the meniscus, a reference was established to find the relative displacement of the meniscus in a dynamic system with multiple simultaneously moving parts. The aim of this study was to describe the displacement of the meniscus relative to the tibia by understanding the calculation and the polarity in a basic sense, using the dummy set up described previously (section 4.2.2).

4.5.2 Theory

A series of schematics were drawn out to help understand the polarity of the calculation of the tibial reference marker and the meniscus marker (Figure 4.9). The reference system of the simulators anterior (-) and posterior (+) axis in the video frame was first used to understand the direction of movements occurring. Keeping the tibial marker at zero helped establish the resulting polarity of the relative displacement (D_R) of the meniscus marker displacement (D_M) relative to the tibial marker displacement (D_T) using the calculation shown in Equation 4.1.

Equation 4.1: $D_R = D_M - D_T$

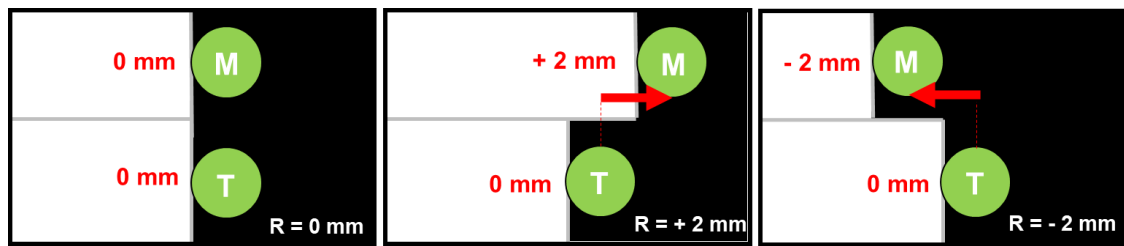


Figure 4.9. Schematics of the meniscus (M) and tibial (T) markers viewed in the video frame to understand the resultant relative displacement (R) (red arrow) of the meniscus marker relative to the tibial marker.

4.5.3 Method

This calculation was written into the MatLab tracking script and tested on the dummy described previously (see section 4.2). The camera was positioned so a marker on the floating insert (meniscus marker, M) of the dummy and a marker on the tibial base (tibial marker, T) were visible in the video frame. Grease was applied between the components to allow the floating insert to slide more easily over the tibial base. A constant 500N load was applied to the dummy and the +/- 6.0 mm anterior-posterior translation sinewave condition was repeated. The tibial rotation and abduction-adduction axes were fixed. The script simultaneously tracked the displacement of both markers over the duration of the video. The relative displacement (D_R) of the marker on the floating insert (D_M) relative to the marker on the tibial base (D_T) during one cycle was calculated within the script by applying Equation 4.1.

4.5.4 Results

The movement of the floating insert (M) in response to the tibial base (T) moving through the +/- 6 mm sinewave motion generated a peak of 4 mm posterior relative displacement (R) during the first half of the cycle and a peak of - 2 mm anterior relative displacement during the second half of the cycle. Due to the symmetry of the sinewave tibial movement used as the reference; the pattern of relative displacement reflected the same shape and magnitude as the displacement of the floating insert (M), but on the inverse side of the graph (Figure 4.10).

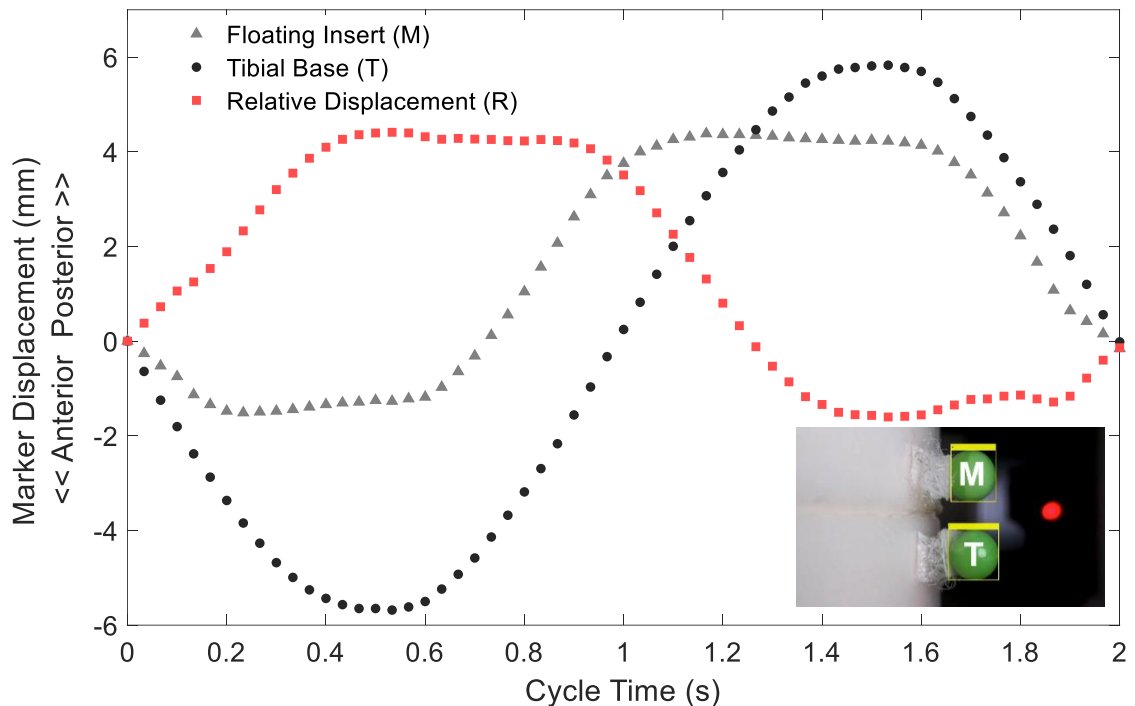


Figure 4.10. Finding the relative displacement of the meniscus marker to the tibial marker on the dummy with the simulator driving a ± 6.0 mm anterior-posterior translation sinewave profile at 0.5 Hz.

4.5.5 Discussion

A simple study using a solid body was conducted to assess the relative displacement calculation. The goal was not to emulate meniscus motion using solid body components, but to apply Equation 4.1 to the script. Due to the uniform tibial sinewave profile, the relative displacement followed a similar but inverted shape to the floating insert. The script could successfully output a relative displacement track based on this calculation. A basic subtraction was deemed sufficient for this calculation because when collecting data at the tissue level, the assumption was that the non-linear behaviours are contained within the measured displacements of the tissue withstanding dynamic loads and motions.

It is important to understand the reference systems and polarity at this point to avoid confusion when studying knee samples. There are essentially two reference systems with the same polarity: anterior (-) and posterior (+). One is the simulator reference system and the other is the tibial marker reference system. The tibial marker and the meniscus marker tracks are following the reference system of the simulator. For example, in Figure 4.10, the meniscus and tibial markers are moving negatively in the first second, meaning they are both moving anteriorly with the simulator. However, the relative displacement is following the reference system of the tibial marker, not the simulator. For example, during the first second in Figure 4.10, the relative displacement is positive (posterior) because it is relative

to the tibial marker, even though the meniscus and tibia marker are both moving anteriorly. It is important to note the meniscus marker itself is not actually moving posteriorly within the simulator's reference system, it is moving anteriorly, just less anteriorly than the tibial marker. The net effect is that the meniscus component is moving posteriorly relative to the tibial component.

4.6 Investigating the Relative Meniscus Displacement in the Anterior, Posterior and Medial regions of a Porcine Knee

4.6.1 Rationale

This research included the development of protocols to insert tibia and meniscus markers into the posterior, anterior and medial regions of a porcine knee joint sample in the simulator. The cameras were programmed and set up to track and measure the displacements of the markers and calculate the relative displacement during one sinewave cycle. This investigation was an important step in applying the method to a porcine joint sample to measure the relative meniscus displacement in the medial-lateral and the anterior-posterior directions using multiple cameras.

The aim of this study was to implement the relative displacement calculation for each meniscal region whilst applying the anterior-posterior translation and internal-external rotation sinewave conditions described previously in the dummy investigation (section 4.2.2.3). The overall goal was to apply the marker tracking method to a knee sample and examine the interactions between the meniscus and tibia marker displacement to calculate the relative displacement.

4.6.2 Method

One knee joint was dissected from the right hind leg from a 6-month year old female pig (91.3 Kg) according to the dissection and potting technique described in section 2.2.1. The capsule was retained for this study and meniscus markers were inserted into the medial (MED), anterior (ANT) and posterior (POST) regions of the medial meniscus, with corresponding tibia reference markers directly below. The sample was palpated and rotated to locate the medial meniscus with the joint capsule intact. The markers were then inserted through the joint capsule. The method for positioning the markers in each region of the meniscus is described in Figure 4.11. This method was further developed from the positioning described in section 3.4.2.3. The posterior marker was placed first by calculating the distance d from the lateral edge of the PCL (Figure

4.11A). The medial markers were placed along the posterior edge of the MCL (Hein et al., 2011; Hirose et al., 2022) and the anterior markers were placed using the same distance d , measuring from the location of the medial markers (Figure 4.11B). (Previously the anterior marker was measured from the anterior edge of the MCL, however, the width of the MCL is variable between knees, especially for human samples, so the marker positioning method was altered to account for this).

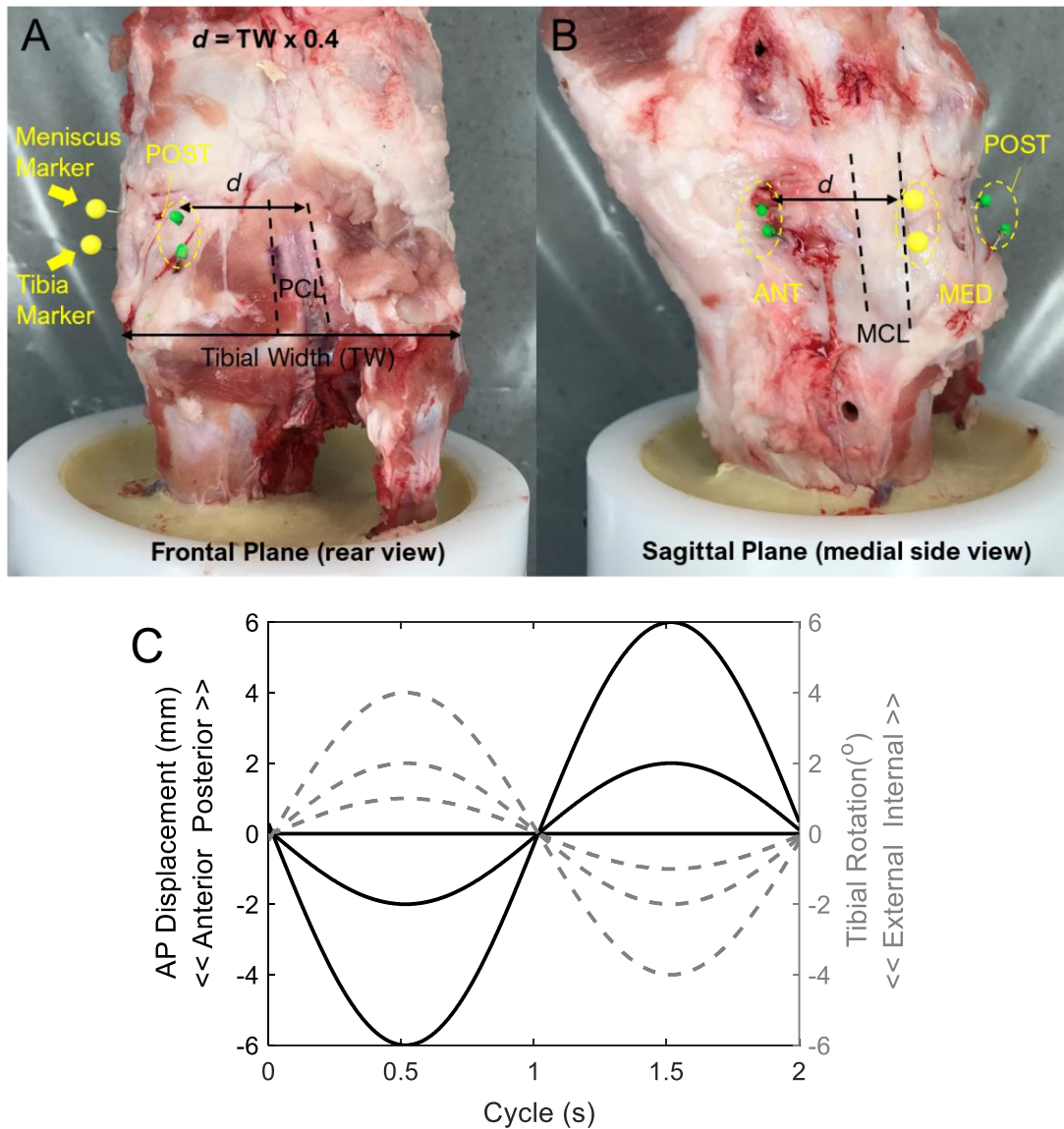


Figure 4.11. (A) Positioning of posterior (POST) meniscus and tibia markers using the equation $d = TW \times 0.4$, measuring from the lateral edge of the PCL identified through the bony prominence. (B) Positioning of the medial (MED) markers on the posterior edge of the MCL and using this to measure to the position of the anterior (ANT) markers with the distance d . (C) The anterior-posterior (AP) translation (black solid) (± 0 mm, ± 2 mm and ± 6 mm) and tibial rotation (TR) (grey dashed) ($\pm 0^\circ$, $\pm 1^\circ$, $\pm 2^\circ$ and $\pm 4^\circ$) simulator profiles used.

The markers inserted into the anterior and posterior regions were made from 2 mm diameter delrin ball bearing heads superglued to metal wire and painted green. Larger 4 mm diameter pins were used for the medial region because the medial camera was positioned further away than the anterior and posterior cameras. The positioning of these cameras with reference to the polarity of the axes of the simulator are illustrated in the previous chapter (Figure 3.13).

The same simulator sinewave profiles implemented during the dummy investigation (Study 2) earlier in this chapter were used for this study (see section 4.2.2.3). These are illustrated in Figure 4.11C. A 500N constant axial load was applied and the abduction-adduction angle was fixed during this study. The cameras were triggered to record the meniscus marker and tibial marker simultaneously during cycle 10. The tissue was sprayed with PBS and left to rest for 10 minutes with zero axial load between each kinematic condition due to repeated loading. The videos were processed in MatLab and the displacement of the marker on the meniscus was found relative to the marker on the tibia of each meniscal region and sinewave condition (see previous section 4.5).

4.6.3 Results

4.6.3.1 Meniscus and Tibia Marker Tracking

The marker tracking method was able to measure all the regional markers on the knee sample and produced displacements which oscillated in a similar sinewave motion to the simulator input profiles. The relative displacement was also implemented within the measurement technique and graphically tracked. An example of the tracked displacements for the tibia, meniscus and relative displacements, for the +/- 6.0 mm AP condition, are presented in Figure 4.12 for each meniscus region.

The ANT and POST meniscus and tibia marker displacements, measuring anterior-posterior displacement, followed a similar pattern to those reported for Study 2 in the dummy investigation (Figure 4.12A, B). The tibial marker generally moved more than the meniscus marker and higher magnitudes of tibial rotation generated similar profiles but with smaller peaks in the anterior-posterior driven cases. The tibia marker displacements best mimicked the smoothness of the applied sinewave profiles and a similar pattern to the dummy investigation. However, with no applied tibial rotation, the tibia marker only reached approximately 50% of the simulator anterior-posterior translation output, unlike that of the dummy. This is illustrated more clearly for the POST tibia results in Figure 4.13A.

In the case of the MED results, measuring medial-lateral displacement, driven anterior-posterior translation and tibial rotation generated small amounts of medial-lateral

movement of the medial meniscus and tibia markers (Figure 4.12C). Generally, applied internal rotation caused small amounts of lateral displacement and external rotation caused small amounts of medial displacement to be measured in the video frame.

4.6.3.2 Relative Displacement Tracking

The POST results were used to graphically illustrate the changes in the relative displacement from the meniscus and tibia displacement results across all the driven translations and rotation conditions. In the POST region, the tibial marker produced smoother anterior-posterior displacements following the action of the simulator profiles (Figure 4.13A). More noise and a less uniform tracking shape was associated with the meniscus marker results (Figure 4.13B) and therefore was reflected in the relative displacement results (Figure 4.13C).

During anterior simulator translation and internal rotation (0- 1 second of the cycle), the tibia and meniscus markers displaced a similar amount which created small amount relative displacement in this direction (Figure 4.13C). However, when the direction of simulator motion was shifted posteriorly and externally rotated, the meniscus marker displaced less than the tibia marker. This had a greater effect on the relative displacement and producing an anterior displacement of the meniscus marker relative to the tibia marker in the second half of the cycle (1 -2 seconds). In the case when zero anterior-posterior translation was applied by the simulator, the relative displacement in the video frame was small, meaning that the tibia and meniscus markers were measured to be moving a similar amount in the video frame. However, when $\pm 4.0^\circ$ tibial rotation was applied, a larger posterior relative displacement was measured during external tibia rotation.

Generally, the interaction between the effect of driven anterior-posterior translation and driven tibial rotation on the measured relative displacement changed between the different conditions tested. In the sagittal plane, a larger magnitude of relative displacement was measured for the POST results compared to the ANT results when driven anterior-posterior translation was applied. When zero anterior-posterior translation was applied, the applied tibial rotation incrementally increased the overall measured relative displacement for the ANT and POST results. In the frontal plane, increasing the magnitude of driven anterior-posterior translation increased the overall displacement of the medial-lateral relative displacement in the MED results, however, a 0.43 mm relative displacement was calculated during the control condition (MED, AP 0 mm, TR 0°).

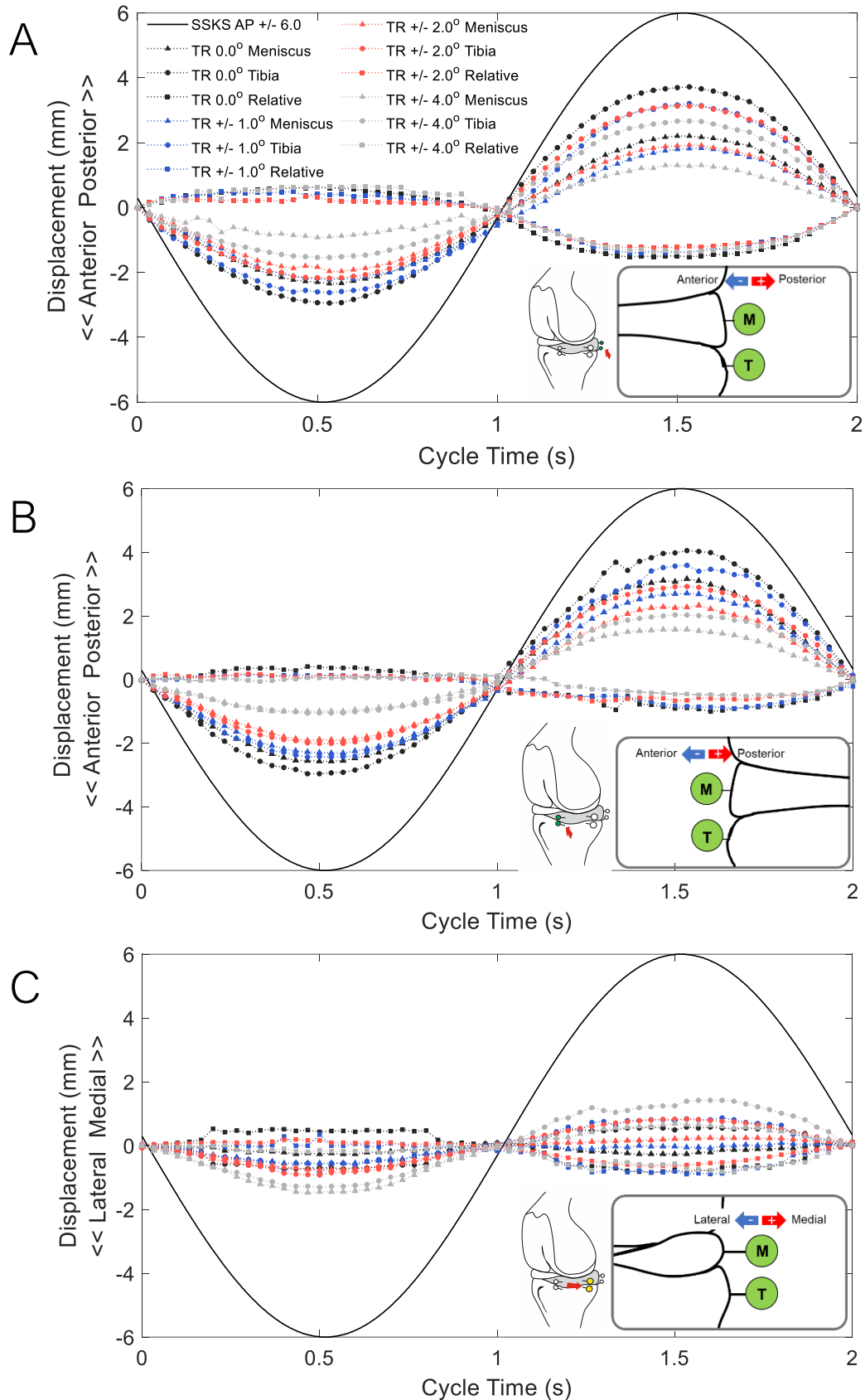


Figure 4.12. (A) POST, (B) ANT and (C) MED displacements of the meniscus marker, tibia marker and calculated relative displacement for the ± 6 mm AP sinewave condition with applied TR sinewave magnitudes of $\pm 0^\circ$ (black), $\pm 1^\circ$ (blue), $\pm 2^\circ$ (red) and $\pm 4^\circ$ (grey). Schematics indicate the marker position and the video frame polarity ($n = 1$).

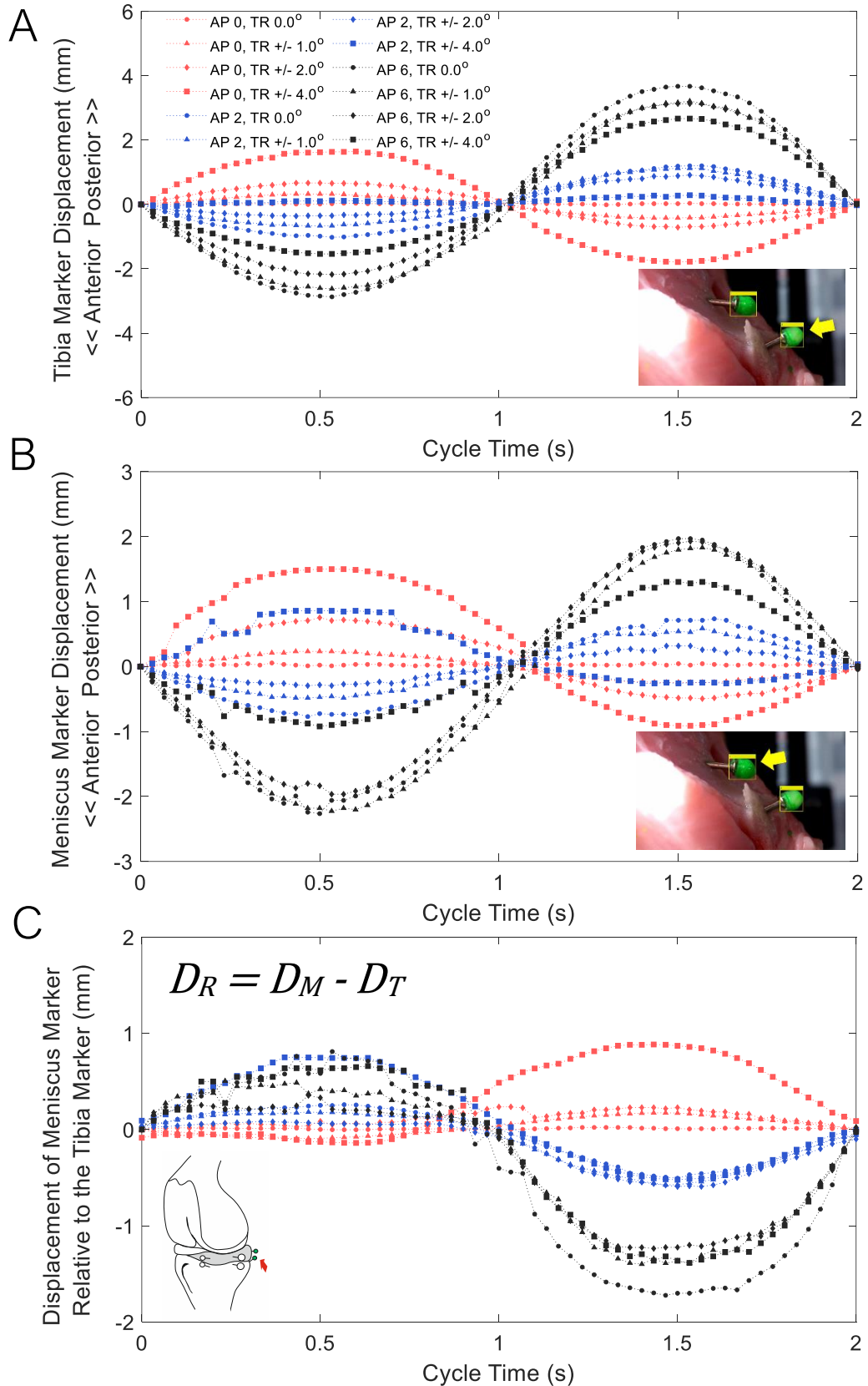


Figure 4.13. Results for the posterior (POST) meniscus region showing the measured (A) tibia marker displacements, (B) meniscus marker displacements and (C) the relative displacements (R) calculated from the equation $D_R = D_M - D_T$ for all AP (+/- 0 mm (red), +/- 2 mm (blue) and +/- 6 mm (black)) and TR (+/- 0° (circle), +/- 1° (triangle), +/- 2° (diamond) and +/- 4° (square)) sinewave conditions (n = 1).

4.6.4 Discussion

This study presents an important step in the method application to a knee sample. A method was established to place meniscus and tibia markers on the anterior, posterior and medial region of the medial meniscus with the capsule intact, and the relative displacement was measured from the meniscus and tibia marker displacements using the marker-tracking method.

The main findings from this study were that the marker-tracking method can be applied to a porcine knee sample with the capsule intact and the relative displacement can be calculated in the frontal and sagittal plane whilst the knee is moving continuously through a cyclic profile. The meniscus and tibia markers moved differently allowing the variations in relative displacements when translation and rotation were applied. The tibia marker displacements followed a similar profile smoothness to those reported during the dummy investigation, however, the magnitudes of tibia displacements were approximately 50% of the driven anterior-posterior translation when no tibial rotation was applied, this is discussed in more detail in the next sub-section. Generally, the meniscus marker moved at a slower or a similar rate and magnitude than the tibial marker and was dictated by the driven tibial motion and restricted by the anchoring root attachments and the articulation with the femoral condyles. This effected the relative displacement measurement at different points in the cycle and was able to be measured by the marker-tracking method.

It is difficult to draw any further conclusions in terms of the effect of translation and rotation on the relative displacement because the profiles used in this study involved loads, translations and rotations a porcine knee would not experience; however, these profiles were chosen to limit complexity whilst the relative displacement measurement was studied, before moving onto comparing complex gait profiles. In addition, the meniscus marker results generated more noise, this was most likely due to the capsule sliding over the meniscus locally and causing small additional movements of the pin which would have affected the measurements. In addition, uneven and low lighting on the meniscus marker compared to the tibia marker could have produced more noise in the data.

4.6.4.1 Sample Deformations

The results from the dummy investigation show a closer estimate to the driven simulator anterior-posterior movement and a more even split between the anterior displacement and posterior displacement regions of the sinewave when no tibial rotation was applied (section 4.2.3.2). In this knee study, the tibia marker displacements were around 50% lower than simulator output and higher magnitudes of posterior displacement

were measured than anterior displacement during one cycle. It is possible that a fair amount of deformation or bending of the knee sample occurred in response to the applied load and motion, as illustrated in Figure 4.14.

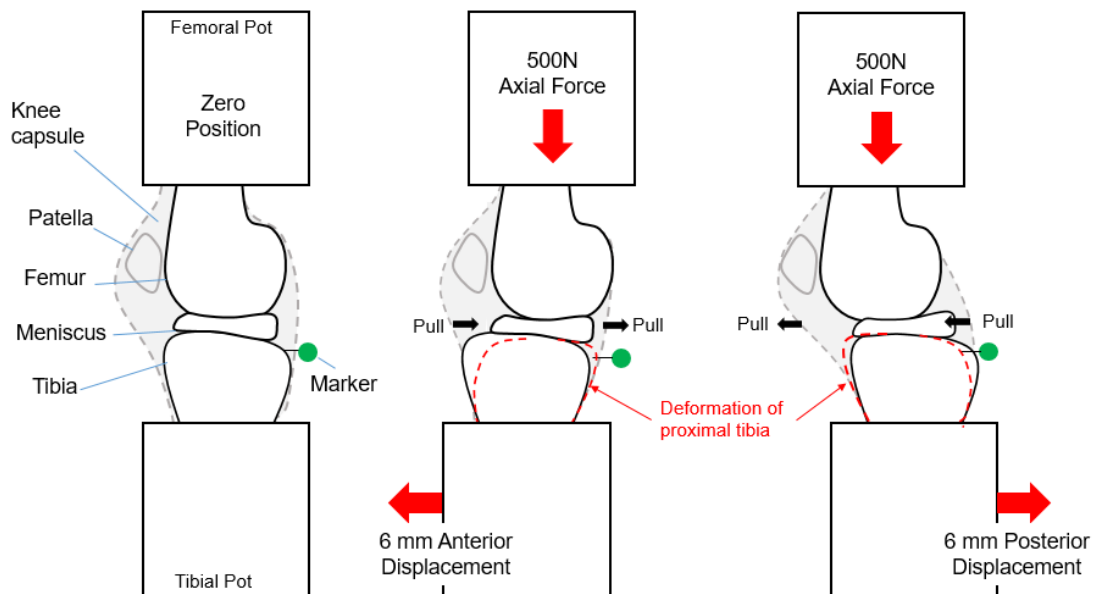


Figure 4.14. Schematic of the tibia deforming during the study and the capsule pulling in the opposite direction to resist the movement of the anterior-posterior carriage

The bone of the proximal tibia consists mainly of cancellous bone, which has a lower stiffness to allow for load bearing at the joint space level (Goldstein, 1987; Hart et al., 2017). Antagonistic pulling is probably occurring by retaining the knee capsule. The capsule of the pig knee has more soft tissue constraint in the anterior portion due to the hoffas pad, which could explain why the measured anterior displacements were lower than the posterior displacements for the tibia marker.

A short sub-study was conducted to assess the bone stiffness on the measured displacements in the video frame. Four markers were inserted at positions 10 mm apart on the tibia of the same knee sample used in this study. The +/- 6 mm anterior-posterior translation sinewave was driven and a single Raspberry Pi camera was used to record and track the displacement of each marker in the same way as the herein method. As shown in Figure 4.15, the marker in position 4 on the lowest part of the knee showed a 1.29 mm increase in total displacement compared with the marker in position 1 nearest the tibial plateau. The bone is stiffer at position 4 as more cortical bone is present. Therefore, it was likely deformation was occurring which gives confidence that this was what was happening and not a flaw or an underestimation within the marker tracking method itself and therefore the estimation of resultant relative displacement.

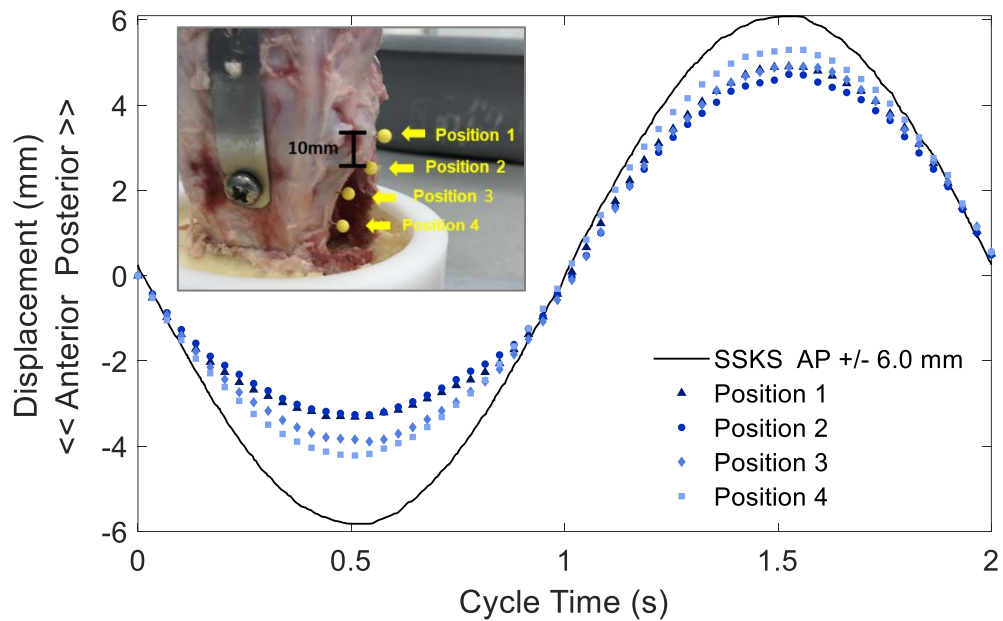


Figure 4.15. Measured displacement of four markers in four different positions along the tibia whilst simulating the +/- 6.0 AP sinewave profile (n =1).

4.7 Complex Gait Profile

A range of experiments were carried out using different simulator gait regimes including displacement control, force control and knee specific gait profiles (Liu et al., 2015; Liu et al., 2020). Simulator profiles which were programmed to move the anterior-posterior and tibial-rotation axes with force control generated sudden vibrations and shuddering of the knee joint, which made it difficult to obtain meaningful tracking results as the bounding box of the MatLab tracking script would detach from the marker in the video. Force control applies a force or a torque to the axis to facilitate translation or rotation. The constrain of natural (ligaments) or programmed (virtual) springs resist this movement. The movement of displacement control inputs was more controlled because the movement axes were responding to directly programmed displacement inputs and no springs were required to constrain the applied movement (see section 2.3). Therefore, displacement control was more suitable to apply the parameters of the marker tracking method. As previously described in section 2.3.2, a decision was made to use a modified high kinematics profile with both the anterior-posterior translation and tibial rotation axes driven and scaled to the parameters of the pig (Liu et al., 2015). This section describes the preliminary work of using the marker tracking method to measure the relative meniscal displacement in response to a gait cycle driven in the simulator.

4.7.1 Effect of Tibial Rotation on the Measured Anterior-Posterior Displacement in the Video Frame Using Gait Profile Parameters

4.7.1.1 Theoretical Model

Previously in this chapter, it has been shown during the sinewave profile experiments that when only tibial rotation (TR) is applied, without anterior-posterior translation (AP), the result on the measured AP displacement in the video frame follows a similar pattern as the TR profile but with lower peaks (section 4.2 and section 4.6). If the knee is assumed to be circular with a given radius and the marker is placed on the outside curve, directly in the centre with the camera placed on the medial side (based on a right knee), this relationship can be described using a simple mathematical model illustrated in Figure 4.16.

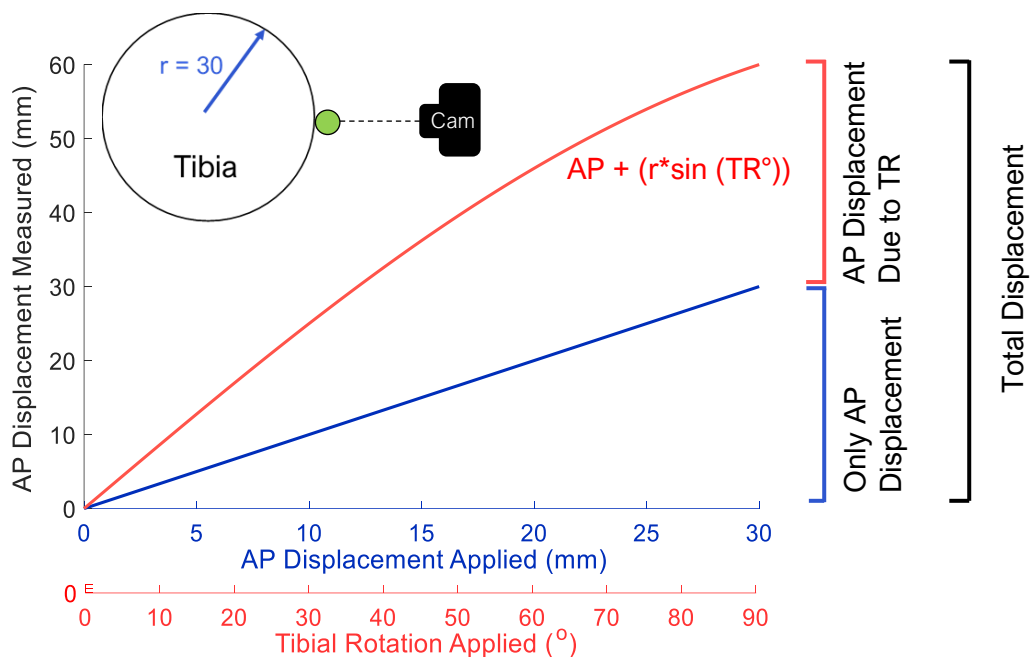


Figure 4.16. Mathematical model of the relationship between the applied AP and measured AP (blue line) with applied TR (red line) to find the total measured AP displacement in the video frame. Assumes a linear relationship between the applied and measured AP and that the tibia is circular with a radius of 30 mm.

Firstly, a simple set of TR data (0 – 90° TR, zero applied AP) was used to describe the contribution of the TR to the overall measured AP by using the trigonometry sine rule for each angle increment of TR. The larger the TR, the lower its contribution to the

measured AP displacement in the video frame. This result can therefore be described as the AP displacement due to TR (AP + TR). Secondly, a simple set of AP data was applied, ramping from 0 – 30 mm. Here the idealised situation is modelled, where the applied AP translation is equal to the measured AP displacement giving a linear relationship. The measured AP displacement from both scenarios (Applied AP + AP displacement due to TR) can be combined to give the total measured AP displacement in the video frame. An addition was deemed suitable because the two factors, rotation and translation are independent of one another and do not interact. Depending on the polarity of the AP and TR profiles, the effect on the measured AP displacement would be subtractive or additive.

This model was then applied to the AP and TR simulator input profiles from the porcine Leeds High Kinematics gait cycle described in Figure 4.17A. The TR profile with $\pm 1.6^\circ$ peaks was the one used in the porcine gait profile, however, an additional condition with $\pm 5.0^\circ$ peaks was used to understand how the measured AP displacement theoretically changes with increased TR. The relationship between the measured AP and applied AP from these simulator inputs are displayed in Figure 4.17B to show the deviation of the measured displacement from the 1-to-1 relationship when varying degrees of TR are applied. The TR profile consisting of $\pm 5.0^\circ$ presents a larger deviation from the 1-to-1 relationship compared with the $\pm 1.6^\circ$ TR condition. As shown in Figure 4.17C, the measured AP displacements were displayed across the gait cycle time to predict how the measured AP displacement in the video frame may differ across the course of one simulator cycle.

4.7.1.2 Experimental Model

An experiment was carried out to assess the theoretical model described above with the simulator inputs and a porcine knee sample. One porcine right hind leg knee joint (78.0 Kg) was dissected (see section 2.2.1) with the capsule was removed, including the collateral and cruciate ligaments. A marker was placed on the posterior region of the tibia based on the marker positioning method described previously (section 4.6.2). No load was applied during this study, and the adduction-abduction motion was fixed.

The AP gait cycle input was driven with increasing magnitudes of the TR input profile (0.0° , 1.6° , 2.0° , 3.0° , 4.0° and 5.0°), as described in Figure 4.17A with additional increments of TR. A Raspberry Pi camera was set up to record the anterior-posterior displacement of the marker in the video (measured AP). Results were processed using the marker-tracking script in MatLab and presented in Figure 4.18.

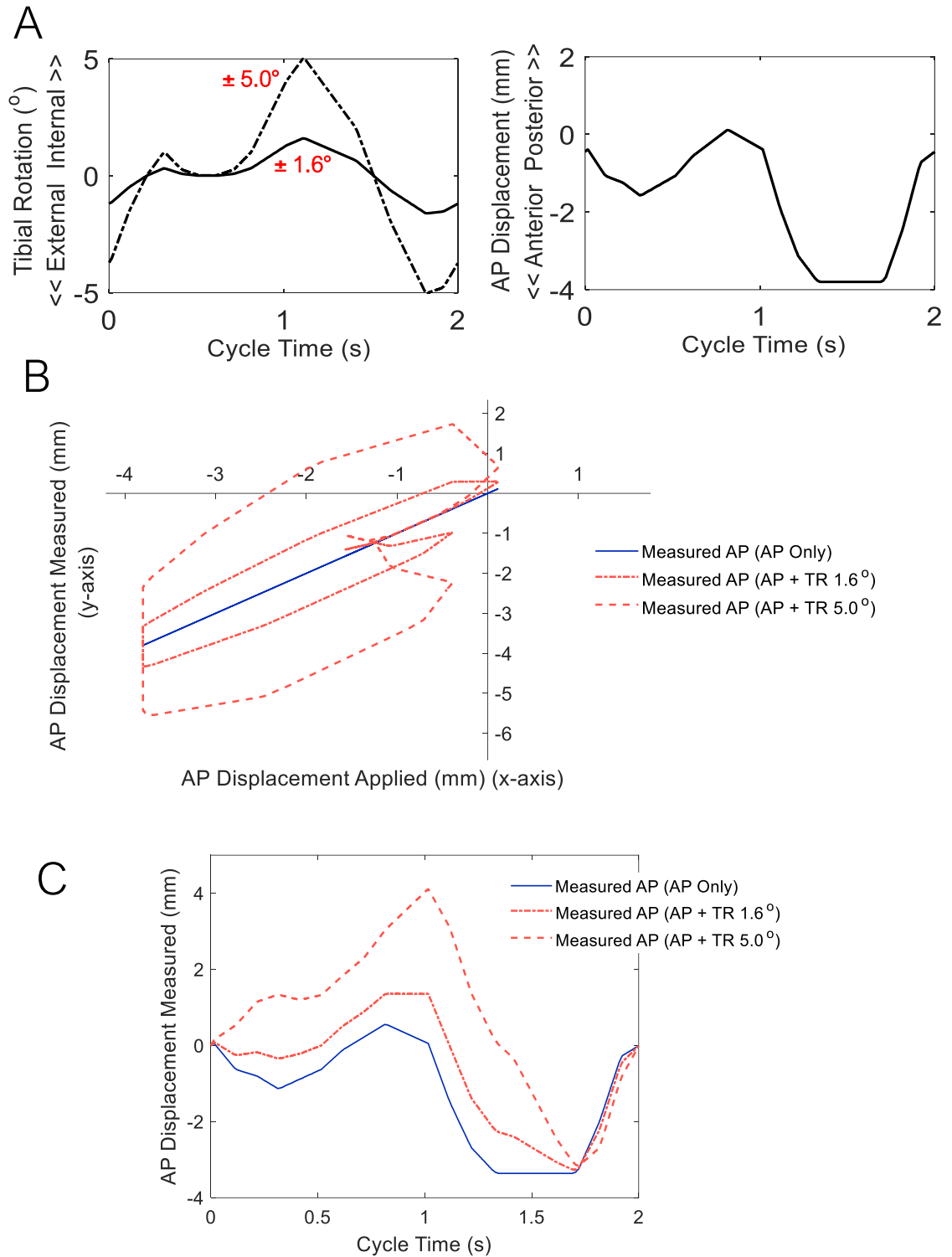


Figure 4.17. Mathematical model applied to the (A) TR and AP porcine simulator gait inputs. (B) The relationship between measured AP and applied AP (using the equation in Figure 4.16) of the AP only (blue), AP + TR 1.6° (red narrow-dashed) and AP + TR 5° (red wide-dashed). (C) Represents these variables across a gait cycle to show the predicted measured AP in the 2D video frame when TR is applied (the variables start at zero to mark the beginning of the gait cycle in the video frame).

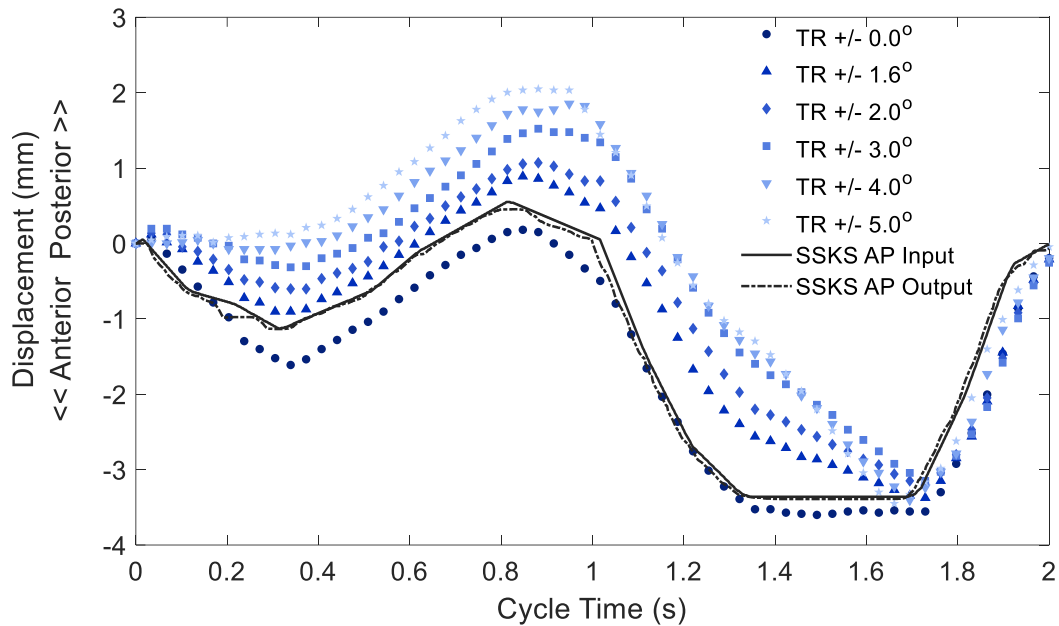


Figure 4.18. Experimental data showing the measured AP displacement of the marker in the video frame whilst increasing the magnitude of the applied TR input as the AP input was driven. In this case the AP translation input was moved to begin at zero to better compare the marker tracking measurements with the profile and assess the sensitivity of increasing the TR on the measurement ($n = 1$, porcine).

4.7.1.3 Discussion

Previously in this chapter, the relationship between TR and the measured AP in the video frame has been represented using simple sinewave inputs. With this knowledge a theoretical model was established to help describe the measured AP displacement with the application of TR when more complex gait cycle profiles are driven. This aids the interpretation of the measured AP results from complex inputs and provides further confidence in the marker tracking method. The previous sinewave study on porcine knee joints presented deformations of the tibia under abnormal loading conditions and capsular constraint (see section 4.6.4.1). In this study, no axial load was applied and the capsule was removed to emulate the assumed conditions more closely in the mathematical model.

The experimental results shown in Figure 4.18 produced a similar profile to those presented in the mathematical model in Figure 4.17C. The marker tracking method was also sensitive enough to measure AP displacements when very small increments of TR were applied, from as little as 0.4° . The most noticeable difference is the smoothing of the profile and the reduction of the maximum peak in the experimental results as compared with the theoretical results (Figure 4.17C), this was more pronounced for the $\pm 5.0^\circ$ condition than the $\pm 1.6^\circ$ condition. These differences between the experimental and theoretical model most likely occur due to the assumptions made in the model. Firstly, the

mathematical model assumes a fixed radius and a perfect cylinder instead of a tibia. Secondly, the model assumes the marker is directly in the centre of the tibial AP length, and in line with the camera, when the TR and AP are at zero.

4.7.2 Preliminary Investigation Measuring the Relative Meniscus Displacement using a Displacement Controlled Gait Profile in a Porcine Sample

4.7.2.1 Rationale

This section describes a preliminary investigation to understand the pattern of relative displacement outputs achieved from the meniscus and tibia markers of each meniscal region, for the full gait profile kinematics. This was an important step prior to performing the full porcine study, presented in the following chapter.

4.7.2.2 Method

One porcine knee joint with the capsule retained was dissected from the right-hind leg of a 6-month year old female pig (86.4 kg) and defrosted. This sample had been used for multiple studies in preliminary work so had undergone two freeze-thaw cycles in total. Markers were attached to the medial (MED), anterior (ANT) and posterior (POST) regions of the medial meniscus, with corresponding markers on the tibia, as explained previously in section 4.6.2. Three miniature cameras corresponding to each meniscal region were lined up in the simulator using the bespoke camera rig. The modified Leeds high kinematics gait cycle was performed (see section 2.3.2) with all axes driven except the abduction-adduction axis, which was left free according to previously published protocol (Liu et al., 2015). The profile was run at 0.5 Hz for 50 cycles and each camera was triggered separately but at the same cycle point and a 10-minute tissue resting period was given in between each test. The cameras were triggered to record cycle 3, 10, 25 and 50 at 30 fps. This was to see if there were any differences in the data obtained as the test proceeded and therefore cyclic loading was extended. The videos were processed in MatLab and the object-tracking script was used to measure the displacement of the meniscal and tibial markers to calculate the displacement of the meniscal marker relative to the tibial marker.

4.7.2.3 Results

The relative displacement results calculated from the meniscus and tibia marker displacements for each region from Cycle 3 are presented in Figure 4.19. Little difference

was found in the relative displacement between cycles 3, 10, 25 and 50. The results from Cycle 3 are presented. The POST and ANT results, measuring anterior-posterior displacement, presented similar result profiles for the meniscus, tibia and relative displacement results (Figure 4.19A compared to Figure 4.19B). Both sets of data showed peaks of ~ 1.5 mm of relative displacement which coincided with the peaks of the flexion and anterior translation during swing phase of the simulator gait cycle. The relative displacement was positive at this point, meaning that the meniscus marker moved in the posterior direction relative to the tibia marker, yet both the meniscus and the tibia marker were moving anteriorly with the simulator anterior-posterior translation carriage. When the knee was almost fully extended around mid-stance (0.8 seconds) the ANT meniscus marker displacement fell more anteriorly relative to the tibia marker when compared to the POST results.

The MED region results, measuring ML displacement, showed an initial peak in relative displacement of ~ 0.5 mm which coincided with the initial peak in the simulator axial force profile where heel strike occurs (Figure 4.19C). The tibia marker results followed the path of the samples abduction-adduction angle measured at cycle 50. The meniscus marker profile presents two peaks which coincide with the two axial force peaks of the gait profile. The MED results were noisier than the ANT and POST results.

4.7.3 Discussion

This short study was carried out to understand the relative meniscal displacement measurement in response to the gait cycle inputs scaled to the parameters of the pig. The relative displacement calculation (see section 4.5) was successfully carried out for each meniscal and tibia marker in the anterior, posterior and medial regions. The results showed that the displacement outputs roughly reflected the loads and motions of the applied gait inputs.

The results for the meniscus marker in the MED region were interesting because the measured displacement reflected the axial force profile applied to the knee sample. When the peaks of loading occurred during the gait cycle, the marker tracking method was able to measure the meniscus tissue moving radially and/or deforming. The results for the ANT and POST regions followed a similar pattern which was governed by the driven motion of the anterior-posterior translation and tibial rotation simulator inputs. A rounding of the peaks in the ANT and POST tibia results was measured, which is dissimilar to the measured displacement profile of the 1.6° tibial rotation condition in Figure 4.18 of the above section. This could be due to the application of load and flexion in this study, which was not applied in the previous investigation. However, it could also be due to the lighting again affecting the connection of the bounding box to the marker.

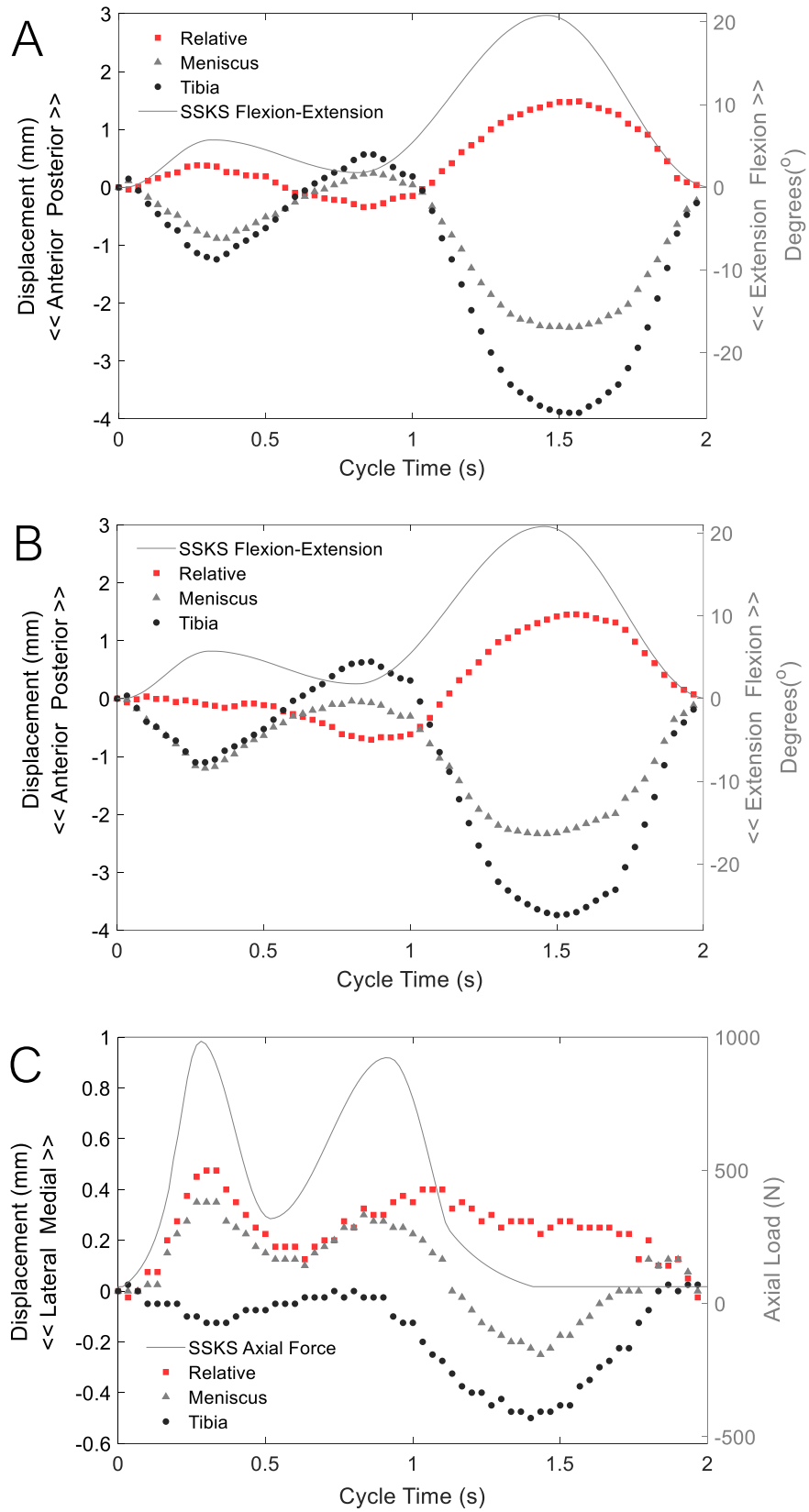


Figure 4.19. Relative (red - square), Meniscus (black – triangle) and Tibia (black – circle) displacement results across one 0.5 Hz cycle (cycle 3) for the (A) POST, (B) ANT and (C) MED meniscal regions. Knee sample tested with the capsule retained (n = 1).

Any changes in the size of this box can alter the position of the centroid of the bounding box which can therefore be reflected in the results.

Moreover, the MED results generated a fair amount of noise in the signal. As aforementioned, noise is a limitation when measuring small displacements < 1 mm with the marker tracking method. However, a more accurate signal can be achieved through developments in the lighting set up. In gait motion capture, retro-reflective markers are typically used, and the light source is positioned directly around the camera lens to illuminate the marker giving the best contrast to the background. A similar set-up was emulated for further study using the marker tracking method as shown in Figure 4.20. Three bright LED strip lights were adhered to the camera cases directly above the camera lenses and could be switched off outside the simulator. This set up ensured the light was directly illuminating the markers from the background and ensured the lighting positioning was controlled between conditions.

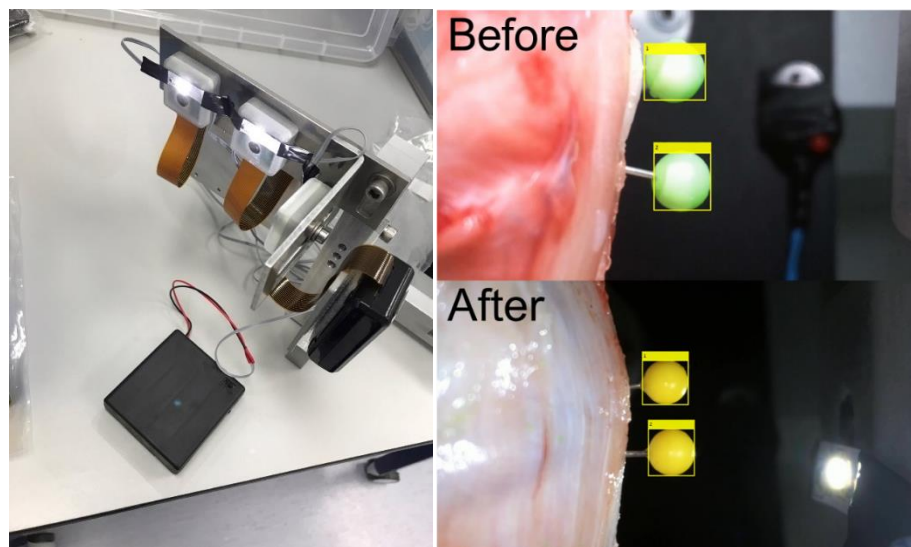


Figure 4.20. New direct LED lighting set up and video frame images showing the original lighting (before) compared with the colour contrast achieved when the new lighting set up was implemented (after)

Part of the full experimental procedure was carried out during this study, including inserting the markers and setting up the cameras. In addition, the process of dissecting the soft tissue around the markers for the capsule removed and ligaments removed conditions was also carried out in this preliminary study to establish a certain amount of methodology skill acquisition prior to beginning the porcine study in the following chapter. These conditions were not shown within the results to retain clarity as the main goal was to understand the relative displacement output. The porcine sample used for this study had been previously used in multiple investigative assessments and had also experienced an

additional freeze thaw cycle. Therefore, the integrity of the tissue was below the requirements to be included as a sample in the porcine study.

4.8 Discussion

This chapter presents an important step in method development and method acquisition by including a range of various sub-study investigations which were built-up in complexity to understand the reliability of method and its application to a porcine knee joint sample.

The dummy experiments showed that the marker-tracking technique was shown to be accurate and precise when measuring planar simulator motion with lighting and camera positioning controlled between repeat tests. Means fell within 2 % of the known simulator output with error falling within ± 0.1 mm when measuring a moving solid object in sequential sinewaves ± 1 mm to ± 6 mm in the simulator. In addition, the effects on the measurement error from an inter-observer and intra observer image calibration variation of ± 5 pixels generated 1.7 % error when moving a marker on a solid object in the simulator. The Raspberry Pi cameras had a small amount of lens distortion which generated minimal effects (maximum 0.03 mm) on the output sinewaves of ± 1 mm, ± 2 mm and ± 6 mm from the dummy investigation in the simulator. When more variables were applied to the dummy experiment including load and tibial rotation, the results were less accurate, however, a good level of precision remained. This increases the confidence in the minimum error contained within the measured displacements and is useful when comparing differences in displacement between conditions, providing factors such as lighting, and camera positioning are controlled. During application to natural knee joint samples, it is likely that this error will increase due to the addition of markers placed on pins and factors which are difficult to control, such as tissue integrity and heterogenic variability, associated with assessing the mechanics of natural tissue under complex loading conditions.

The robustness of the method is limited as conditions need to be meticulously controlled to obtain accurate and reliable results. The blob analysis function in the MatLab script relies on a clear contrast between the marker and the background to obtain higher accuracy in the tracking results. All the displacement data comes from the adherence of the bounding box to the moving marker in the video. A certain amount of noise is associated with this method due to the resolution limitation of one pixel. This noise had a larger effect on smaller applied motions where the measured movement was closer to the pixel calibration factor (resolution). However, when assessing the complex gait cycle, patterns of movement were able to be distinguished in the displacement output within \pm

0.5 mm of estimated movement. The lighting apparatus was developed to apply a more direct illumination and improve the bounding box adherence going forward which helped reduce the noise and therefore increase accuracy of the measurement.

During complex gait cycles, the knee will move in 3D because tibial rotation will occur in the transverse plane. This will influence the 2D measurement in the video frame which was investigated herein. It was found that the larger the amount of tibial rotation, the less contribution it has to the measured anterior-posterior displacement in the video frame. Characterising 3D motion using a 2D method has limitations, however, new methods should be built up in complexity. In addition, there has been newly developing research in 2D motion capture computer vision methods, allowing enhanced accessibility and ease of use (Ugbolue et al., 2013; Paternina et al., 2022). There has been previous studies looking into using singular cameras (Kinect, Microsoft, USA) to estimate 3D kinematics on solid body joint models stating fair amounts of accuracy $< 0.5^\circ$ in comparison with known measurements but larger amounts of noise in comparison to more advanced commercial gait analysis systems like OptiTrack (OptiTrack, OR, USA) (Schmitz et al., 2014; Bilezan et al., 2018). Therefore, there is scope to further develop the novel marker tracking methodology in this study by estimating 3D motions in the video (see section 7.6).

The process of inserting meniscus and tibial markers into the different regions of porcine knee samples, applying simulator profiles and triggering the cameras to obtain relative medial meniscus displacements were undertaken in this chapter. Bylski-Austrow et al. (1994) conducted an early biomechanical study using a radiographical RSA technique to assess meniscal movement during tibial rotation and translation during static $0^\circ - 30^\circ$ states of flexion and 1000 N of load in human cadaveric samples. Findings stated that anterior tibial translation moved the menisci posteriorly and visa versa, which agrees with the outcome calculated using the relative displacement calculation and the preliminary porcine knee joint investigations in this chapter. The benefit of measuring at the tissue level is that the method picks up a degree of non-linear behaviour the meniscus and the tibia experience during the gait cycle. Although the method cannot distinguish between the two, deformation and movement are contained within the measurement, and both parameters are associated with meniscal extrusion (see section 3.1). A complex gait cycle was trialled in this chapter and gave confidence that the method was able to measure the marker displacement responding to the dynamic loads and motions applied to the knee joint continuously over one gait cycle.

The next chapter includes the full study on four porcine knee joint samples where various soft tissue constraint conditions and a root tear condition will be simulated. The aim was to develop an accessible method sensitive to show a difference between an intact and a torn condition to class as a potential preclinical biomechanical investigation for meniscus interventions.

Chapter 5

Feasibility Study Assessing Dynamic Medial Meniscus Displacement using the Developed Motion Capture Method in Porcine Tibiofemoral Joints

5.1 Introduction

In the previous chapter the reliability of the marker tracking method was investigated in developmental stages. In the final sections, the marker tracking method was applied to the medial meniscus of a porcine knee sample undergoing a simulated gait cycle to measure the relative displacement of the anterior, posterior and medial meniscal regions. The work presented in this chapter is an extension of the gait cycle sub-study in section 4.7, using four porcine samples driven through the Leeds High Kinematics gait cycle and analysing the relative displacement results in response to capsular constraint conditions, medial posterior root tear severity and cyclic test duration.

5.1.1 Aims and Objectives

The overall aim of this chapter was to apply the full medial meniscus marker tracking method to four porcine knee samples prior to human knee specimen application and investigate feasibility to detect the difference in relative medial meniscus displacement between a healthy condition (capsule retained) and a damaged root tear condition (medial meniscus posterior root tear) to provide the basis for the development of a preclinical test.

The objectives were:

1. To measure the meniscus, tibia and relative displacement for the anterior, posterior and medial regions of each knee sample;
2. to simulate levels of capsular constraint and root tear severity, and measure the effect these conditions have on the relative meniscus displacement;

3. to understand the effect of cyclic test duration on the relative meniscus displacement by recording the meniscus and tibia marker displacement for cycle 3, 10, 25 and 50 for each meniscus region.

5.2 Porcine Study Methodology

5.2.1 Sample Preparation

Four porcine right knee joint samples were dissected with the knee capsule retained from the right-hind leg of four female pigs (Knee A: 82.9 kg; Knee B: 71.0 kg; Knee C: 85.3 kg; D: 85.7 kg). The samples were dissected and cemented for whole joint simulation in accordance with the protocol outlined in section 2.2.1. After dissection the samples were frozen at -22°C and left to defrost for 48 hours in the fridge (4°C) prior to testing.

Tibia and meniscus motion markers pins were pinned through the capsule into the medial, anterior and posterior regions of the medial meniscus using the method outlined in the previous chapter (section 4.6.2). In line with the set up used in the knee sinewave investigation in section 4.6, yellow 4 mm diameter pins were used for the medial region measuring medial-lateral displacement and green 2 mm diameter pins were used for the anterior and posterior regions, measuring anterior-posterior displacement (Figure 5.1).

5.2.2 Gait Profile and Camera Set Up

As previously outlined in section 4.6, the knee samples were mounted into the simulator and the three miniature Raspberry Pi cameras were held by the custom camera rig (see section 3.7.3) to view and track the meniscus and tibia markers of each meniscus region using the MatLab marker tracking script (Figure 5.1).

The Leeds High Kinematics gait cycle profile with a modified two-peak axial force scaled to the parameters of a pig was driven in displacement control at 0.5 Hz as outlined in section 2.3.2. All axes were driven except the medial-lateral axis was fixed and the abduction-adduction angle was left free to comply with that of past literature (Liu et al., 2015). For this porcine study the ramping load was changed from 10 cycles to 3 cycles, meaning that full load was applied at cycle 3. This was changed to understand differences between an early cycle of initial contact (i.e. starting walking) versus steady state gait (i.e. 50 steps). A study duration of 55 cycles was carried out for each meniscal region and each dissection/tear condition. The cameras were triggered to record data at cycle 3, 10, 25 and 50 by filtering out the cycle of interest within the data processing. To ensure the

highest image quality, the cameras were triggered individually for each 55 cycle test but capturing the same cycle number (cycle 3, 10, 25 and 50) each time for each region and condition. To account for the repeated cyclic loading, the tissue was left to rest for 10 minutes unloaded and sprayed with PBS in between each simulated 55 cycles.

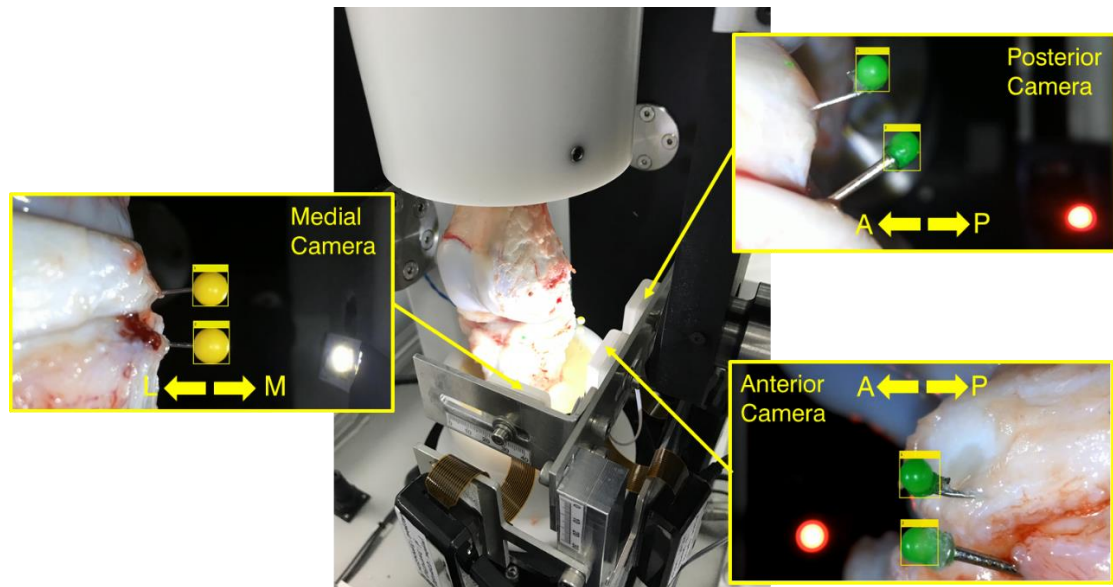


Figure 5.1 Test set up showing a porcine sample in the simulator with the medial, anterior, and posterior camera viewing the meniscus and tibia markers for each corresponding region of the medial meniscus. Screenshots of the video frame show the marker tracking bounding box and the direction of measured movement in a right knee: anterior (A) – posterior (P) and medial (M) - lateral (L).

5.2.3 Capsular Constraint and Root Tear Conditions

Sequential dissection conditions were simulated during this study which involved taking away varying degrees of soft tissues at each stage. As illustrated in Figure 5.2, the conditions were: (A) the fully intact condition with the knee capsule retained, including the patella (CAP). (B) The whole knee capsule was then resected except the cruciate and collateral ligaments (NOCAP). (C) The cruciate and collateral ligaments were then resected along with any menisco-tibial connective tissue on the medial portion of the knee as these are very closely aligned with the medial-collateral ligament. The lateral meniscus posterior menisco-tibial root was retained to match the dissection condition used in earlier studies simulating porcine tissue (NOLIG) (Liu et al., 2015).

A medial meniscus posterior root tear was then simulated in three stages of increasing severity. A scalpel was used to cut the medial meniscus posterior root 6 mm from the insertion, as previously justified in section 3.3.2.5. To develop and standardise this tear simulation, the width of the medial posterior root from Sample A was measured

with callipers, which was 13 mm. The root was cut along the superior-inferior axis 2 mm, 6 mm and 12 mm which equated to a 15%, 46% and 92% root width cut, respectively, to consider varying root widths between samples. These conditions were labelled as TORN1, TORN2, and TORN3, respectively. To ensure results are obtained, a complete tear of the root was not simulated due to the probability of the medial meniscus falling outside of the joint space as previously shown (see section 3.3.3).

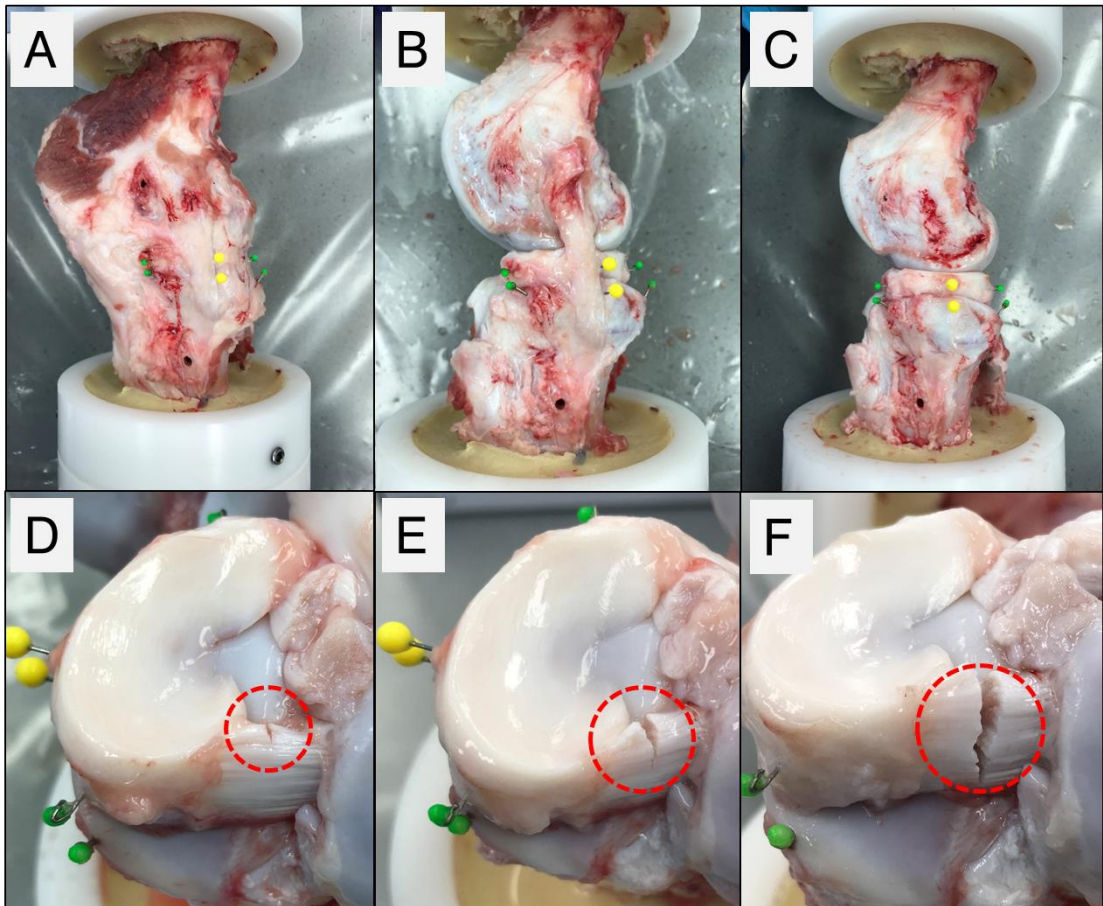


Figure 5.2. Porcine experimental conditions: (A) CAP, knee capsule intact; (B) NOCAP, knee capsule removed but ligaments retained; (C) NOLIG, collateral and cruciate ligaments removed. Medial meniscus posterior root tear conditions: (D) TORN1, 15% width tear; (E) TORN2, 46% width tear and (F) TORN3 92% width tear.

5.2.4 Data Processing and Analysis

The output videos from each test were processed in MatLab and displacement data for the meniscus and tibia markers was measured for the 2 second (0.5 Hz) duration of cycle 3, 10, 25 and 50 using the marking tracking script. Each meniscal region was calibrated using the marker diameter from the corresponding calibration image taken when the knee was unloaded and in the zero position. As explained in the previous

chapter, the relative displacement was calculated from the meniscus marker and tibia marker displacements across the period of one simulator cycle. The simulator abduction-adduction angle was left unconstrained and the output position data was analysed as each capsular constraint and root tear condition was performed.

5.2.4.1 Statistical Analysis and Comparisons

The displacement data was observed graphically for each individual sample to identify similarities and differences. The relative displacement data for cycle number 3 was statistically analysed across all the conditions for the four samples. Means, with 95% confidence intervals (95% CI), were generated from the relative displacement values at specific time-points and the range between the maximum and minimum relative displacement values during one simulator gait cycle was also calculated. Due to the outcome of the preliminary gait cycle test presented in the previous chapter (see section 4.7), these time-points were taken from the two peaks of the axial force profile for the frontal plane (medial-lateral displacement) results (Figure 5.3A), and the two peaks of the flexion-extension profile were taken for the sagittal plane (anterior-posterior displacement) results (Figure 5.3B). Using SPSS software, a Shapiro-Wilk test of normality was carried out to show approximate normal distribution in the mean relative displacement data taken from these time-points and the range. Due to the within-subjects study design, a one-way repeated measures ANOVA ($p < 0.05$) and post-hoc pairwise comparisons using Bonferroni correction were carried out to identify if there were any differences in mean relative displacements between the sequential dissection/torn conditions.

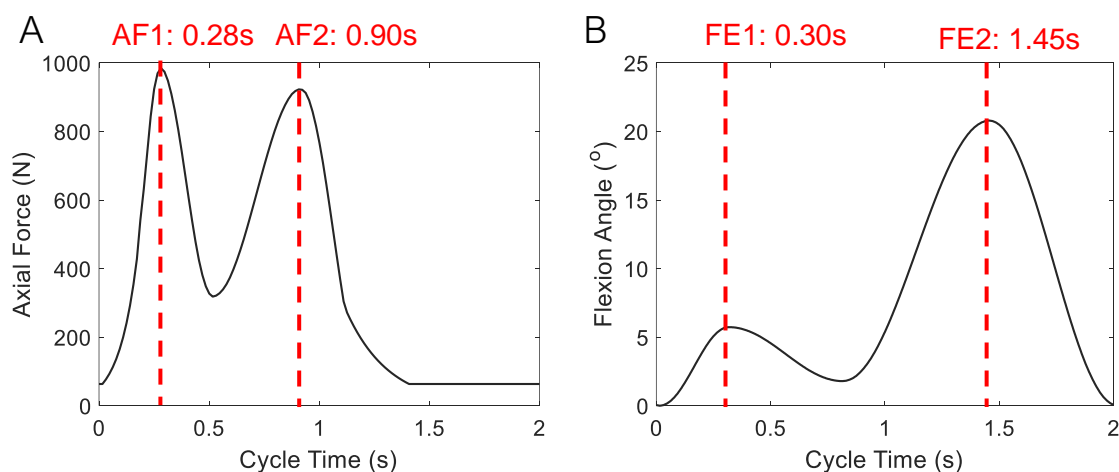


Figure 5.3 Time points from the (A) axial force (AF) and (B) flexion-extension (FE) porcine gait inputs where values were taken to generate relative displacement means for statistical analysis. Frontal plane (medial region) data uses the axial load time-points and sagittal plane (anterior region and posterior region) uses the flexion-extension time points.

5.3 Results

5.3.1 Effect of Capsular Constraint and Posterior Root Tear Severity on Relative Displacement

The displacement of the meniscus marker relative to the tibia marker (relative displacement) results for the medial, anterior and posterior regions from cycle 3 for the *CAP*, *NOCAP*, *NOLIG* and *TORN3* conditions are presented graphically in for Knees A and B in Figure 5.4 A-F and for Knees C and D in Figure 5.5 A-F.

The greatest changes in relative displacement with a root tear spanning 92% of the root width were found in the medial region (medial-lateral displacement) when compared to the other assessed conditions. As shown in Figure 5.4 A, D and Figure 5.5 A, D, all samples presented an increase in relative displacement for the *TORN3* condition compared with all other assessed conditions. Displacements measured for the *CAP*, *NOCAP*, *NOLIG*, *TORN1* and *TORN2* conditions were close to the estimated minimum measurement precision of ± 0.1 mm (mean). The maximum peak in medial relative displacement coincided with the first peak of the axial load applied during the gait cycle (AF1 0.28s time point). There were similarities in the medial region relative results for samples A, C and D, as the *CAP*, *NOCAP*, and *NOLIG* conditions medially displaced $\sim 0.20 - 0.44$ mm, which increased to ~ 1.00 mm (~ 2 fold) when the root was almost fully cut. Sample B showed more relative meniscus mobility compared with the other samples as the *CAP* condition reached a value of ~ 1.00 mm relative medial displacement at AF1, like that of the *TORN3* relative displacement measured for the other samples. However, the *TORN3* condition still showed greater relative displacement than the *CAP* condition, increasing from 0.99 mm to 1.36 mm at AF1.

In the sagittal plane, measuring anterior-posterior movement, the displacement results followed a similar two-peak shape to the flexion-extension profile of the driven gait cycle in all the assessed samples and for all the conditions (Figure 5.4 B,C, E,F and Figure 5.5 B,C, E,F). Peak relative displacement was $\sim 2.0 - 2.5$ mm during the second half of the gait cycle and only small differences occurred between the assessed dissection/root tear conditions which were inside the estimated minimum measurement precision of ± 0.1 mm. However, when the knees extended during terminal stance phase ($\sim 0.8 - 0.9$ seconds of the gait cycle), a greater amount of anterior relative displacement occurred in the anterior region (~ -0.2 mm to ~ -1.2 mm) compared with the posterior region (~ 0.2 mm to ~ -0.5 mm).

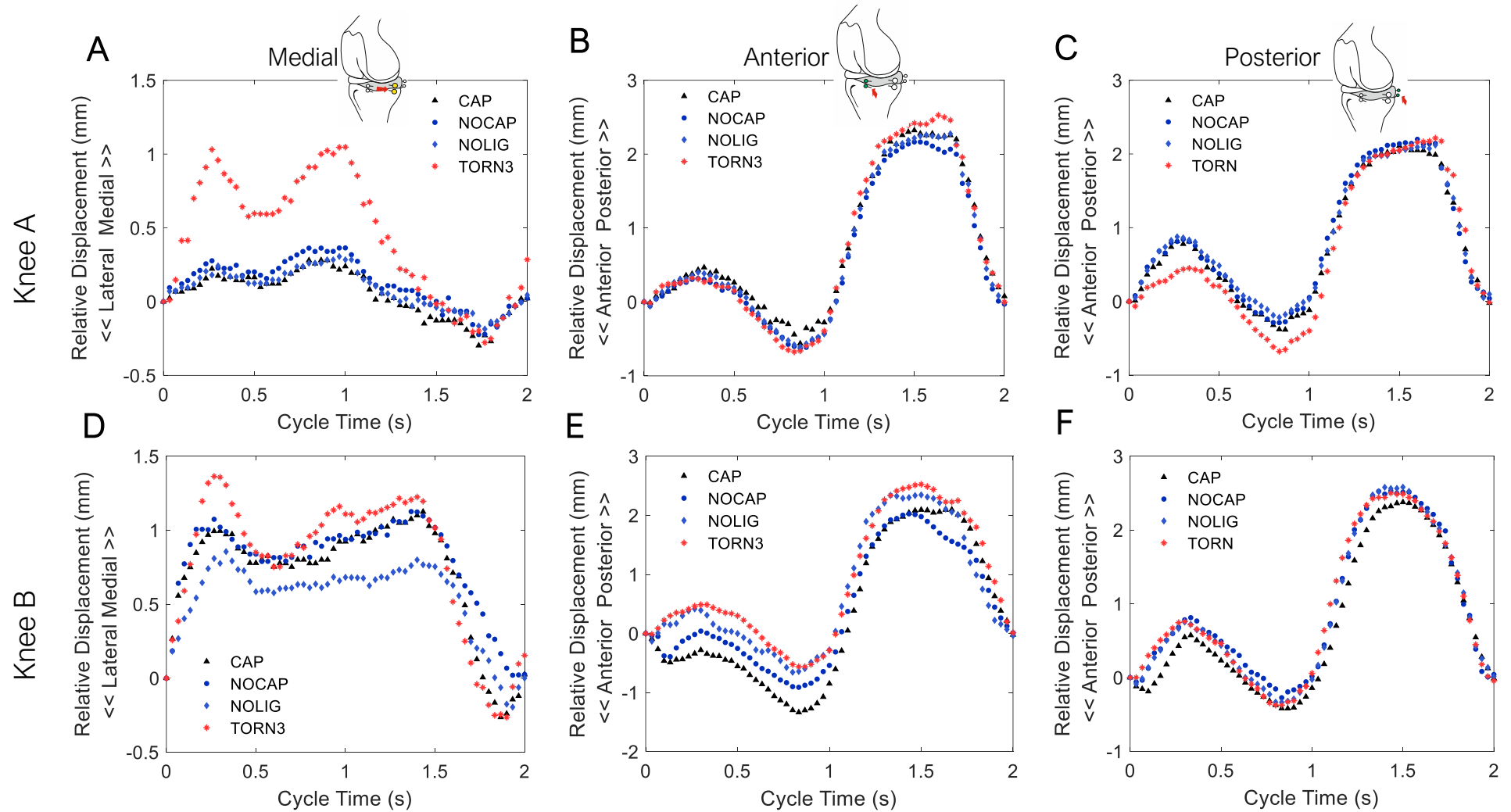


Figure 5.4 A-F. Cycle 3 relative displacement results for the medial, anterior, and posterior regions of Samples A and B (porcine).

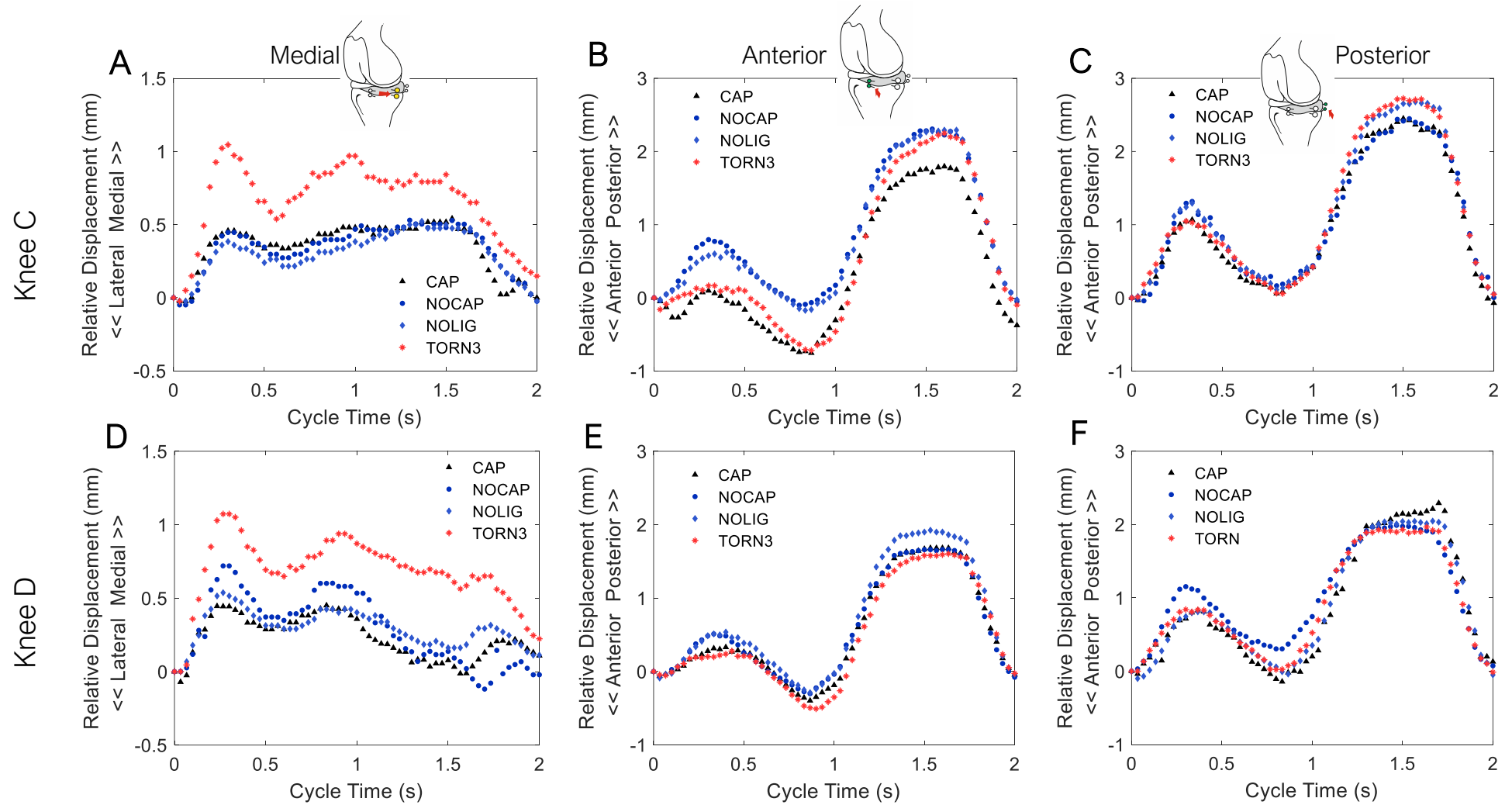


Figure 5.5 A-F. Cycle 3 relative displacement results for the medial, anterior, and posterior regions of Samples C and D (porcine).

Table 5.1 Mean relative displacements (\pm 95% CI) taken from specific gait time-points (TP) and the range (maximum-minimum) across cycle 3. All units in mm. * = significant difference from one group $p < 0.05$

<i>Meniscal Region</i>	<i>Data Type</i>	<i>CAP</i>	<i>NOCAP</i>	<i>NOLIG</i>	<i>TORN1</i>	<i>TORN2</i>	<i>TORN3</i>
<i>Medial</i>	TP: AF1	0.52 (\pm 0.53)	0.62 (\pm 0.55)	0.47* (\pm 0.40)	0.48 (\pm 0.30)	0.52 (\pm 0.34)	1.12* (\pm 0.26)
	TP: AF2	0.49 (\pm 0.35)	0.56 (\pm 0.43)	0.41* (\pm 0.25)	0.41 (\pm 0.23)	0.43 (\pm 0.22)	0.99* (\pm 0.15)
	Range	0.76 (\pm 0.66)	0.78 (\pm 0.41)	0.66 (\pm 0.42)	0.62 (\pm 0.37)	0.70 (\pm 0.38)	1.27 (\pm 0.42)
<i>Anterior</i>	TP: FE1	0.13 (\pm 0.49)	0.41 (\pm 0.50)	0.46 (\pm 0.14)	0.47 (\pm 0.18)	0.45 (\pm 0.26)	0.29 (\pm 0.23)
	TP: FE2	1.92 (\pm 0.48)	2.01 (\pm 0.42)	2.14 (\pm 0.29)	2.16 (\pm 0.27)	2.18 (\pm 0.40)	2.11 (\pm 0.67)
	Range	2.69 (\pm 0.89)	2.53 (\pm 0.69)	2.67 (\pm 0.51)	2.63 (\pm 0.25)	2.70 (\pm 0.51)	2.88 (\pm 0.66)
<i>Posterior</i>	TP: FE1	0.77 (\pm 0.33)	1.02 (\pm 0.39)	0.90 (\pm 0.37)	0.95 (\pm 0.49)	0.95 (\pm 0.49)	0.77 (\pm 0.40)
	TP: FE2	2.21 (\pm 0.27)	2.24 (\pm 0.38)	2.29 (\pm 0.51)	2.20 (\pm 0.65)	2.26 (\pm 0.64)	2.27 (\pm 0.59)
	Range	2.56 (\pm 0.32)	2.44 (\pm 0.67)	2.52 (\pm 0.69)	2.47 (\pm 0.52)	2.48 (\pm 0.71)	2.62 (\pm 0.86)

As shown in Table 5.1, the medial region (medial-lateral displacement) results presented the largest difference in relative displacement when the root was almost fully cut (*TORN3*) compared with all other tested conditions. A trend was present showing an increase in displacement from the *CAP* to the *NOCAP* conditions (AF1: + 0.10 mm; AF2: + 0.13 mm; range: + 0.02 mm). A decrease in mean relative displacement then resulted when the *NOLIG* condition was tested, and this decrease fell below the *CAP* condition baseline means (AF1: -0.05 mm; AF2: -0.08 mm; range: -0.10 mm). The mean relative displacement then increased in the medial direction from the *NOLIG* condition with increasing severity of root tear damage to exceed the capsule intact condition mean. This increase was significant between the *NOLIG* and *TORN3* conditions when the means were taken from the axial force peak time points (AF1: $p = 0.023$, AF2: $p = 0.029$).

The mean difference between the maximum and minimum relative displacement values across cycle 3 (range) increased by 0.51 mm in the presence of a severe root tear (*TORN3*) compared with the capsule intact condition (*CAP*). No statistical significance was found between the dissection/root tear conditions when the mean relative

displacement ranges were analysed. However, a near significance ($p = 0.057$) was found between the *NOLIG* and *TORN3* conditions.

In the sagittal plane, the anterior and posterior region results showed no significantly different means between the conditions at either peak flexion time points or for the range. During the first flexion peak during the gait cycle (FE1, time-point) the mean relative displacement for the posterior region reached $\sim 2x$ that of the anterior region for all tested conditions. During the second flexion peak in the gait cycle, the mean relative displacement for the posterior region reached a value of $\sim 0.2\text{mm}$ more than the anterior region at FE2 time-point. The mean range data for the anterior and posterior region relative displacement results were similar and fell between $\sim 2.5 - 3.0$ mm during cycle 3.

5.3.2 Meniscus and Tibia Marker Tracking

In terms of the measured meniscus marker and tibia marker displacements used to calculate the relative displacement, an example of these tracking results is shown for Sample A in Figure 5.6 for the *CAP* and *TORN3* conditions. All the meniscus marker and tibia marker tracking results are presented in Appendix E. Generally, across all samples, the tibia marker of medial region measuring medial-lateral displacement, followed the action of the unconstrained (free) adduction-abduction angle of the simulator during the gait cycle and the meniscus marker displacements reflected the two peaks of the axial load profile during the first half of the gait cycle (Figure 5.6 A). During swing phase the action of the other driven axes affected the 2D measurement by creating a measured lateral displacement of the meniscus marker. Changes in the measured relative displacement of the medial region during the presence of a root tear was generally caused by increases in the meniscus marker displacement.

In the sagittal plane (Figure 5.6 B and C), the tibia marker displacements of the anterior and posterior region were similar across the conditions and the samples, reflecting the driven tibial rotation and anterior-posterior translation simulator axes as assessed previously (see section 4.7.1). Slight changes in tibia marker displacements were measured in the presence of a root tear compared with the capsule intact condition. The difference between the maximum and minimum posterior region tibia displacements increased from 3.91 mm (*CAP*) to 4.49 mm (*TORN3*) (Figure 5.6B). Anterior region tibia displacements increased from 3.71 mm (*CAP*) to 4.23 mm (*TORN3*) (Figure 5.6C). The meniscus marker displacements in the sagittal plane followed a similar action to the tibial marker displacements but at a lower magnitude generating a predominant relative displacement in the posterior direction, as described in the above section. Small changes were measured for the meniscus marker between the capsule and root tear conditions in the sagittal plane and are reflected in the relative results described above.

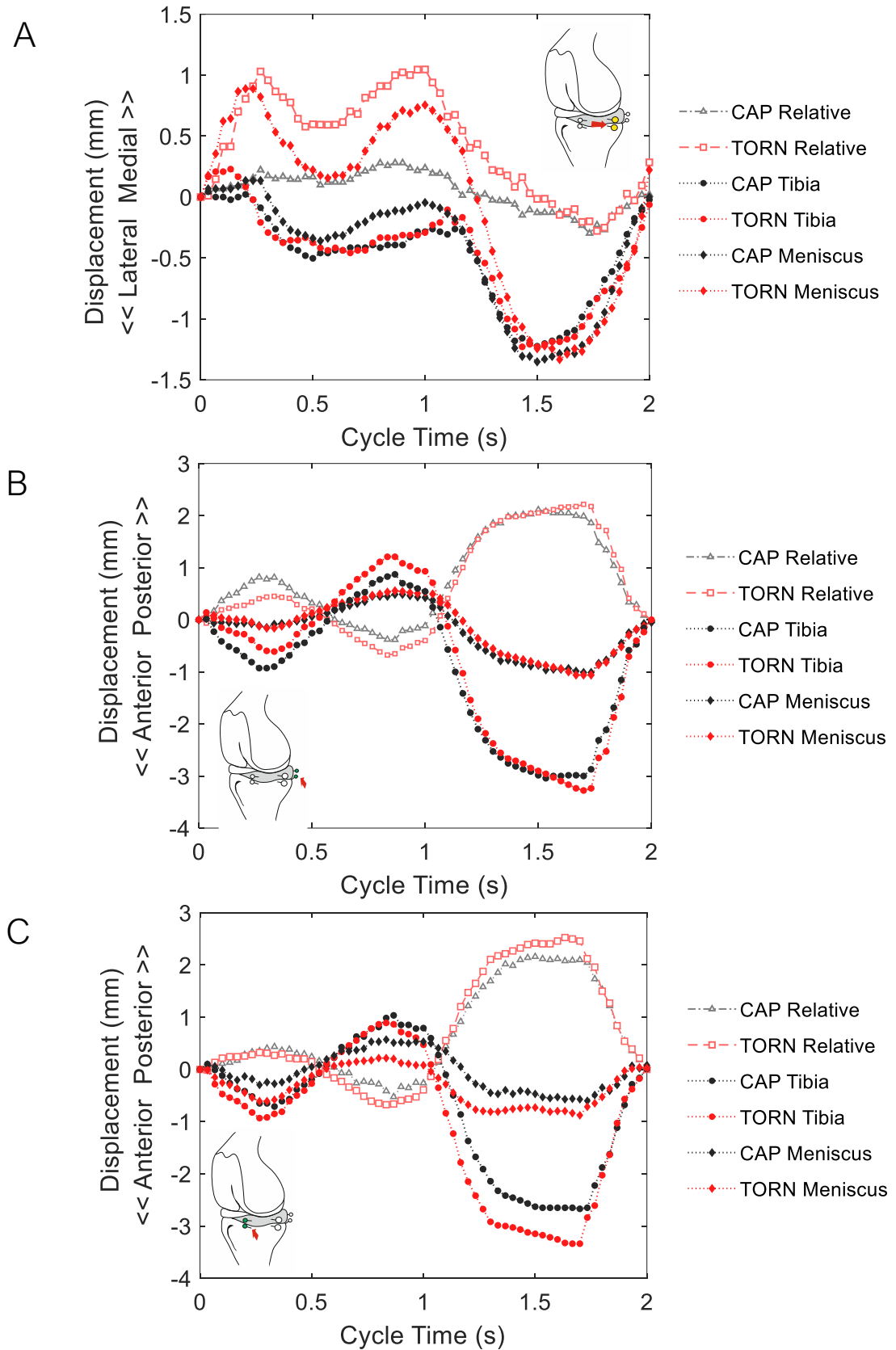


Figure 5.6. Sample A representative example of the meniscus marker, tibia marker and calculated relative displacement results for the (A) medial, (B) posterior and (C) anterior region of the CAP and TORN3 conditions for across cycle 3 (porcine).

5.3.3 Simulator Adduction – Abduction Position

Changes in the adduction-abduction angle were measured in the medial tibia marker displacement results. All knees had a unique profile of adduction-abduction output during the simulated gait cycle, causing a unique tibial marker displacement. A representative example between Sample B and Sample C, which showed different adduction adduction profiles during the experiment is presented in Figure 5.7. In the presence of a severe tear, the adduction-abduction angle tended to offset or shift but retained a similar profile reflected in the tibia marker displacements, as shown for Sample B (Figure 5.7A). However, in Sample C, (Figure 5.7 B) where the adduction-abduction arm swing was near zero, the tibia marker displaced in small amounts and slightly reflected deformations caused by the applied two-peak axial force profile. In the presence of a severe tear the tibial marker displacement decreased in both directions to near zero and the two peaks disappeared (Figure 5.7 B).

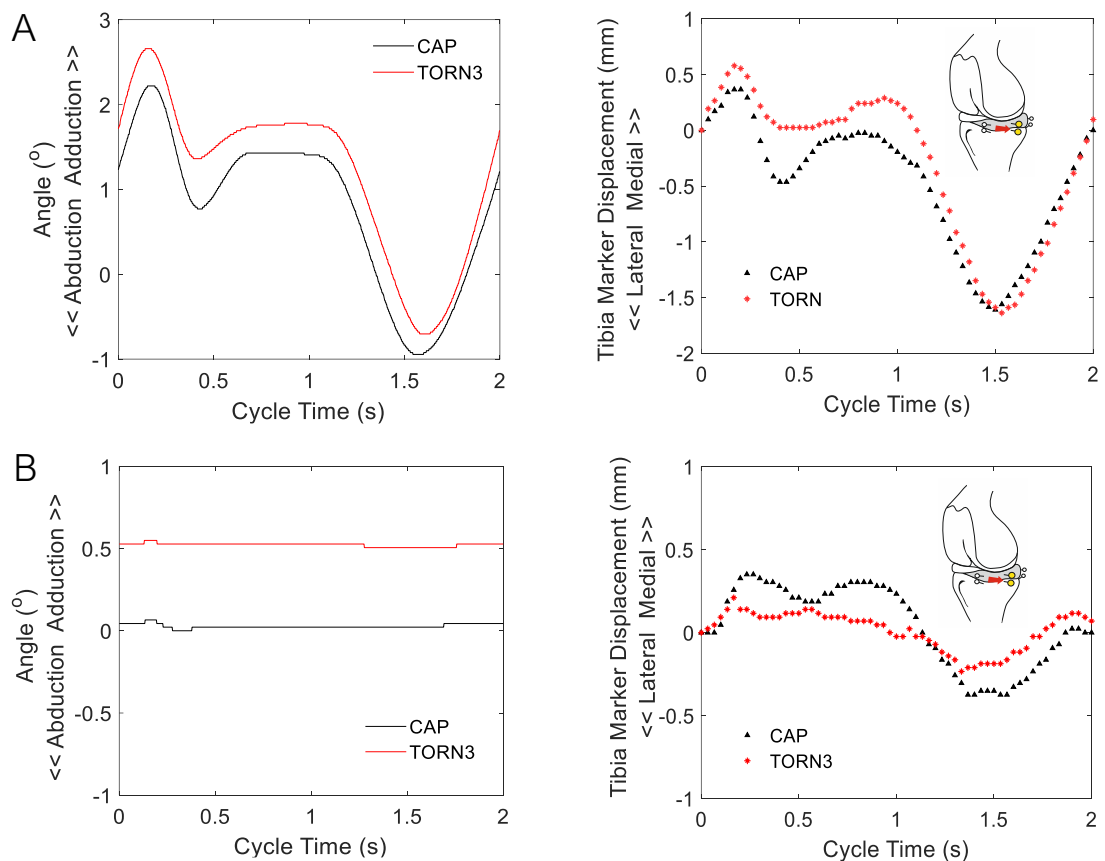


Figure 5.7. Comparative example of varying adduction-abduction angle between samples showing the simulator output and tibia marker displacement results during cycle 3 for (A) Sample B and (B) Sample C (porcine).

5.3.4 Effect of Cyclic Test Duration on Relative Displacement

In the sagittal plane, no substantial trends were found for the cyclic test duration, which presented little effect on the relative displacement results for all the conditions. As shown in Figure 5.8 for Sample C, changes in the relative displacements were observed and fell within 0.05 – 0.2 mm (~10 %) of each other as the duration of the test increased between cycle 3, cycle 10, cycle 25 and cycle 50. In addition, these values generally fell within the minimum measurement error of +/- 0.1 mm. However, a larger difference of 0.5 mm was found in the anterior region CAP condition profile between cycle 3 and the other measured cycles, although this was only found for Sample C.

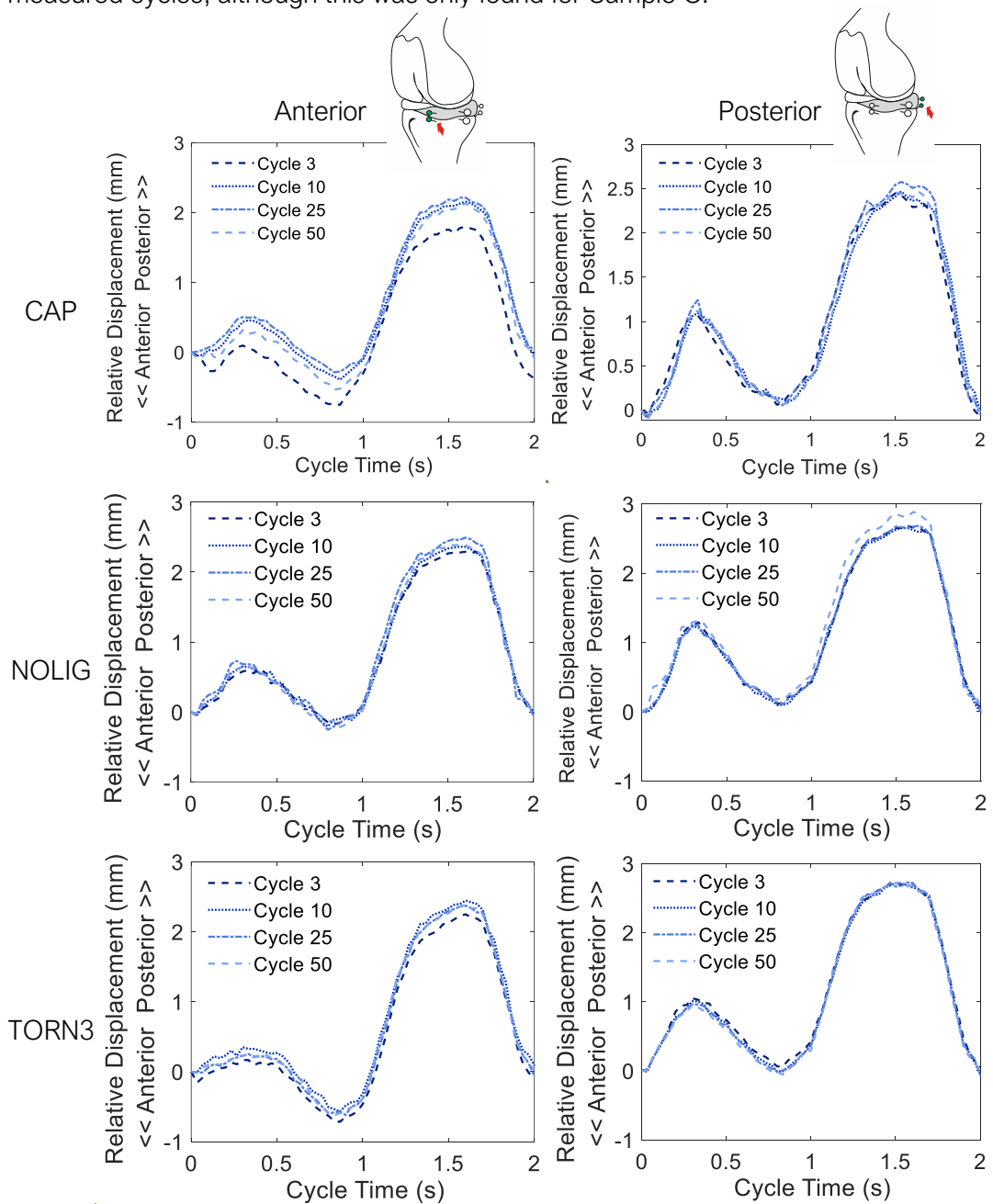


Figure 5.8. Sample C anterior and posterior region relative displacement results for cycle 3, 10, 25 and 50 for the CAP, NOLIG and TORN3 conditions (porcine).

In the frontal plane, no substantial trends were found for the relative displacements across the cyclic test duration (cycle 3, cycle 10, cycle 25 and cycle 50) for the *CAP*, *NOCAP*, *NOLIG*, *TORN1* and *TORN2* conditions. Small changes of 0.02 - 0.15 mm (mean ~15%) fell within the minimum error of +/- 0.1 mm of the method. For the *TORN3* condition, the relative displacement coinciding at timepoint AF1 decreased on average by 26.25% (0.29 mm) from cycle 3 to cycle 50. The change in the difference between the maximum and minimum relative values (range) decreased on average by 12.6 % between cycle 3 and cycle 50. This trend was found across all samples (Figure 5.9 A, B, C and D). Most of this decrease in the medial-lateral relative displacement had occurred by cycle 10.

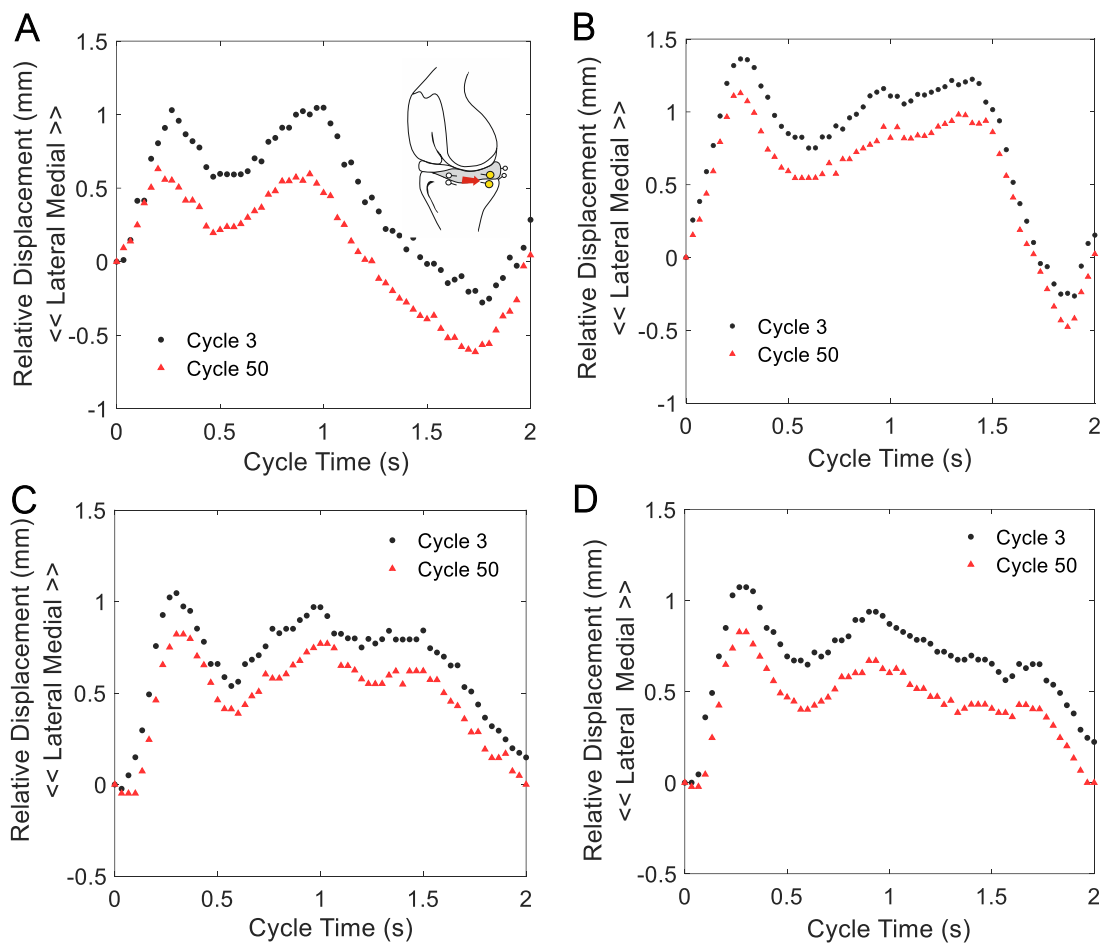


Figure 5.9. Medial region TORN3 relative displacement results for cycle 3 and cycle 50 for all tested porcine knee samples A-D (corresponding graphs to each sample).

5.4 Discussion

The work in this chapter presents an important step in developing the experimental model by assessing the feasibility of the meniscus tracking model using the marker tracking method on four porcine whole-joint samples, prior to assessing the model on

human knee specimens. Due to the anatomical differences between the porcine and the human knee, few data comparisons are possible with previously published literature at this stage, however, the main goal was to develop the model on porcine knee joints and investigate the feasibility to detect the difference in displacement between a healthy and a damaged medial meniscus state.

5.4.1 Main Findings

- The main finding from this study was that the experimental model using the novel motion capture system was able to measure relative meniscal displacement for all three (anterior, posterior and medial) meniscal regions;
- the largest changes in relative displacement occurred in the medial region measuring medial-lateral displacement measurement and reflected the first load peak in the applied dynamic axial force of the gait profile. The most severely torn condition (*TORN3*) showed increased displacement in the medial direction by ~ 2 fold compared to the other experimental conditions, however, this was mostly not statistically significant;
- statistical significance was found using a repeated measured one way ANOVA only between the NOLIG and *TORN3* conditions in the medial region for Cycle 3 when the AF1 and AF2 time-point means were analysed from the four porcine samples;
- no significant differences were found for the anterior and posterior region results; however, the displacement profile reflected the two peak shape of the applied gait flexion-extension;
- cycle duration influenced the medial region *TORN3* results which presented a mean decrease in peak relative displacement of 0.29 mm at AF1 between Cycle 3 and Cycle 50 for all knee samples throughout the experiment.

5.4.2 Evaluation of the Motion Capture Method to Assess Biomechanical Changes with Root Tear Injury

5.4.2.1 Frontal Plane, Medial-Lateral Displacement

The novel motion capture was able to measure the relative displacement throughout a dynamic simulated gait cycle applied to the porcine knee joints. This study found the meniscus moved more medially relative to the tibial marker in the presence of a severe root tear. Despite the displacement of the tibial marker which was governed predominantly by the abduction-adduction angle, which was left free during the gait

profile, this change in relative displacement was measurable with the novel motion capture method and was brought about by increases in the magnitude of the meniscus marker displacement with a root tear. In addition, the two peaks of the axial force profile coincided with two peaks in the measured displacements of the meniscus marker and in some cases (where adduction-abduction angle was small) the tibia marker. The measured data reflected the action of the medial meniscus and the root attachments responding to the applied dynamic axial load and changes were detectable when the root was severely torn, affecting the load transmitted through the meniscus and therefore the tibia.

The motion capture method was able to detect a medial offset or extrusion of the meniscus marker relative to the tibia marker during the first few cycles of the test duration. The peak relative displacement of the medial region was higher during cycle 3 than for cycle 10, cycle 25 and cycle 50 for all knee samples, whereas the range (maximum – minimum value) did not change. The cycle 3 data included both the increase in relative displacement and the extrusion of the medial meniscus. By cycle 10, the meniscus had found a position, limited to further extrusion by the small part of the posterior root still attached and continued to move in the cyclic steady-state manor, producing a similar relative displacement range. Because the displacement data for each cycle is filtered to begin at zero at the start of the gait cycle, this offset of the whole meniscus was not directly measured in the results but could be assessed through screen shots taken from cycle 3 and cycle 50 (Figure 5.10).

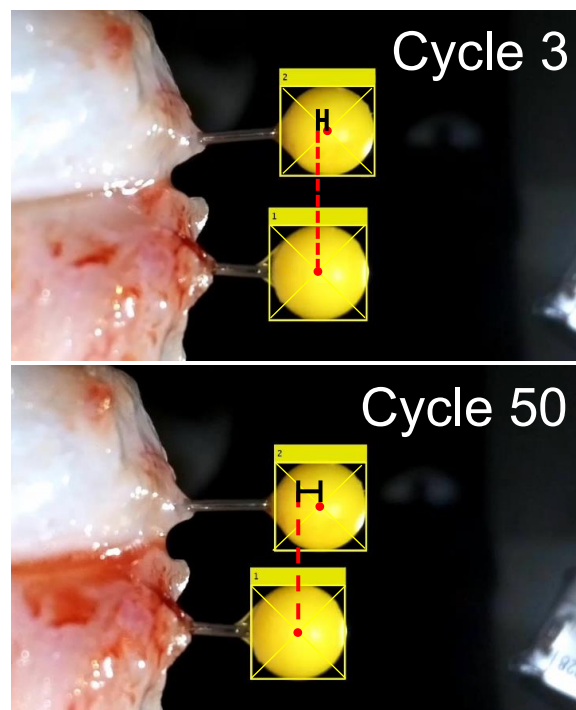


Figure 5.10. Porcine sample A TORN3 condition screenshots for cycle 3 and cycle 50 showing the extrusion measured between the centroid of the meniscus (2) and tibia (1) markers.

Although the most severely root tear condition produced increased relative displacement in the frontal plane compared to the other experimental conditions, this difference was only statistically significant with the *NOLIG* condition during Cycle 3 and when the AF1 and AF2 timepoint means were taken. The *NOLIG* condition moved the least in the medial-lateral direction, compared to the soft-tissue constrained *CAP* and *NOCAP* conditions. This trend was shown across all the samples and potentially is counter intuitive, with one expecting more movement of the medial meniscus without the medial meniscus-MCL ligamentous constraint (Paletta et al., 2020). However, this is likely an effect of the sequential loading bias throughout the experiment affecting the water retention of the tissue, the stiffness, and the movement; rather than the measurement technique itself. The meniscus adopts time-dependent tissue mechanics and water retention is vital for its load dissipating functions (Özkaya et al., 2017). Even though a 10 minute resting period with PBS spray between each test was given, it was almost impossible to retain adequate water retention and tissue integrity of the meniscus throughout this study design and remains a key limitation of the experimental model.

In addition, the use of statistical techniques for such a low sample number are not particularly useful and can only allude to measured trends. A physical change is evident in the meniscus when root damage is caused and this can be measured using the developed model, however what is observed experimentally is challenging to show statistically and remains a further challenge for the future. It is also important to note that the precision of the marker tracking method from the reliability investigations in Chapter 4 was approximately ± 0.1 mm affecting the comparison between measured displacements in this study. However, at this stage only the feasibility of the dynamic meniscus tracking model was assessed; application to human specimens involves applying higher magnitudes of load and motion which may produce and larger displacements further away from the thresholds of the marker tracking method precision.

5.4.2.2 Sagittal Plane, Anterior-Posterior Displacement

The results for the anterior and posterior meniscal regions measuring anterior-posterior displacement in the sagittal plane presented no substantial differences in relative displacement between the capsule and root tear conditions and with cyclic test duration. However, for both regions the relative meniscal displacement results were similar in shape and magnitude with the peaks coinciding with the peaks of the flexion-extension profile. Slight differences were observed, as the anterior region results showed more anterior relative displacement during terminal stance phase (~40% - 50% gait cycle) where almost full extension occurs. The second peak of the axial force is applied during this phase

causing tibia deformation, radial deformation of the meniscus and/or soft tissue movement affecting pin motion.

Physical changes in the anterior-posterior displacement of the meniscus were observed during the most severely torn condition, however, the meniscus tracking method was not able to measure these changes in this plane due to the 2D nature and the controlled driven nature of the anterior-posterior carriage and the tibial rotation axes of the gait-profile dominating the motion. The effect of tearing the root was that the meniscus extruded medially toward the sagittal plane cameras. This meant that in the video frame the meniscus marker appeared slightly larger than the tibial marker as it was closer to the camera. This was considered in the image calibration for the meniscus marker, however, did not change the measured displacements between the conditions a great amount. It is also possible that even with a cut spanning 92% of the root width, the meniscus still retained a fair amount of anterior-posterior displacement ability responding to the driven gait profile.

5.4.3 Limitations

Limitations of the marker tracking method such as displacement occurring due to pin motion have been previously described and still apply during this study. Further limitations to note during this development work is as aforementioned, a bias in the order of tested conditions caused by repetitive cyclic loading and the degradation of the tissue with experiment duration. The total experiment duration per sample was around 72 hours after defrosting meaning that the final experimental condition had a lower tissue quality than the first condition; affecting the measured displacements. In addition, as it was not possible to complete all the conditions in one working day, the samples were kept in the fridge overnight in PBS soaked tissue. This potentially allowed more rehydration time prior to testing certain conditions such as the *NOCAP* condition which was typically carried out in the morning of day two.

5.4.4 Summary

The experimental model has been developed on porcine specimens and applied dynamic load and motion profiles of the simulator gait cycle were able to be characterised through the meniscus, tibia and relative displacements measured with the motion capture method. A measurable difference in relative displacement was found between the fully intact and a severely torn condition in the medial region throughout the study, however; this difference was not statistically significant when assessing a low sample size. A limitation of sequential loading causing a systematic bias and effecting levels of tissue

hydration throughout the experiment were difficult to avoid using this type of experimental model. However, meniscal extrusion in the damaged state was also observed over the course of cyclic test duration and few changes in relative displacement between the conditions were measured in the sagittal plane regions. Overall, this study has given confidence that the marker tracking measurement technique is sensitive to obtain meniscal kinematic data during a gait cycle and the lack of statistical strength likely amounts to factors of the methodology which are difficult to control when assessing natural tissues. The next chapter will now adapt and apply this experimental model to human whole knee joint specimens.

Chapter 6

Application of the Motion Capture Method to Assess Dynamic Medial Meniscus Displacement in Human Knee Specimens

6.1 Introduction

In the previous chapter, a feasibility study of the experimental model was performed using the novel motion capture system on porcine specimens. In this chapter the clinical relevance of the experimental model was advanced through applying the marker tracking system to measure medial meniscus kinematics in human cadaveric knee joint specimens undergoing a dynamic gait cycle in a mechanical simulator. The development process involved adapting aspects of the methodology described in the previous chapter to account for larger specimen dimensions, larger amounts of driven motion and differences in tissue integrity. In addition to meniscal root damage cases, a medial meniscus allograft transplantation (MAT) was additionally performed on $n = 3$ samples to assess the efficacy of the experimental model in response to an intervention condition.

6.1.1 Aim and Objectives

The aim of this chapter was to apply the marker tracking method to human cadaveric knee specimens and measure the anterior-posterior displacement and medial-lateral displacement of the medial meniscus during a simulated gait cycle. With the overall goal to assess whether the precision of the method will allow the differentiation of medial meniscus displacement with and without a root tear in human specimens

The objectives were:

1. To adapt the porcine experimental model to be able to measure the displacement of the meniscus marker and tibia marker pinned to the medial, anterior and posterior regions of a human knee specimen undergoing a simulated gait cycle;

2. to calculate the relative anterior-posterior displacement and medial-lateral displacement from the measured meniscus and tibia marker displacements of the corresponding meniscal region in human knee specimens;
3. to investigate the effect of capsule constraint conditions and varying severities of a medial posterior root tear on the relative medial meniscus displacement of human knee specimens;
4. to understand the effect of cyclic test duration on the relative displacement measured at the medial, anterior, and posterior marker regions;
5. to understand the effect of applying a meniscus allograft transplantation (MAT) intervention condition on the measured relative meniscus displacement.

6.2 Method Adaptations for Human Specimens

The transition from porcine to human specimens required adaptations to the experimental model to account for the larger human specimen size as well as the greater variability in size compared to porcine knee specimens. In addition, human knee specimens included left and right knee joints, therefore the experimental model was adapted to be applicable to both. The camera rig was initially set up for right knees as the right hind leg of pigs were ordered to the laboratory as the standard animal model. In addition, the modified Leeds high kinematics gait profile was driven at full load and full motion for human specimens, whereas the gait profile parameters used for porcine specimens were scaled down to a third. The camera parameters were optimised to allow effective marker tracking and displacement measurement during human knee simulation.

6.2.1 Camera Rig Adaptations

To adapt the model for left and right knee specimens, two additional parts were manufactured for the camera rig which was previously described in section 3.7.3. In order to allow the position of the magnet attaching the rig to the simulator to be adjusted, the vertical component was manufactured with a slot cut and an additional cuboid component was manufactured to attach the vertical component to the existing 'L' shaped component (Figure 6.1A). This allowed the motion capture system to be compatible to measure the meniscus kinematics of left knee specimens with the abduction-adduction (AA) axis constrained using the attachable/detachable AA arm, if necessary (Figure 6.1B). Further developments also included adaptations to the component holding the anterior and posterior cameras. A new part was manufactured to allow for the larger human knee size and variations in tibial slope (Figure 6.1C and D). Washers were also used to increase the amount of space between the joint space and the cameras.

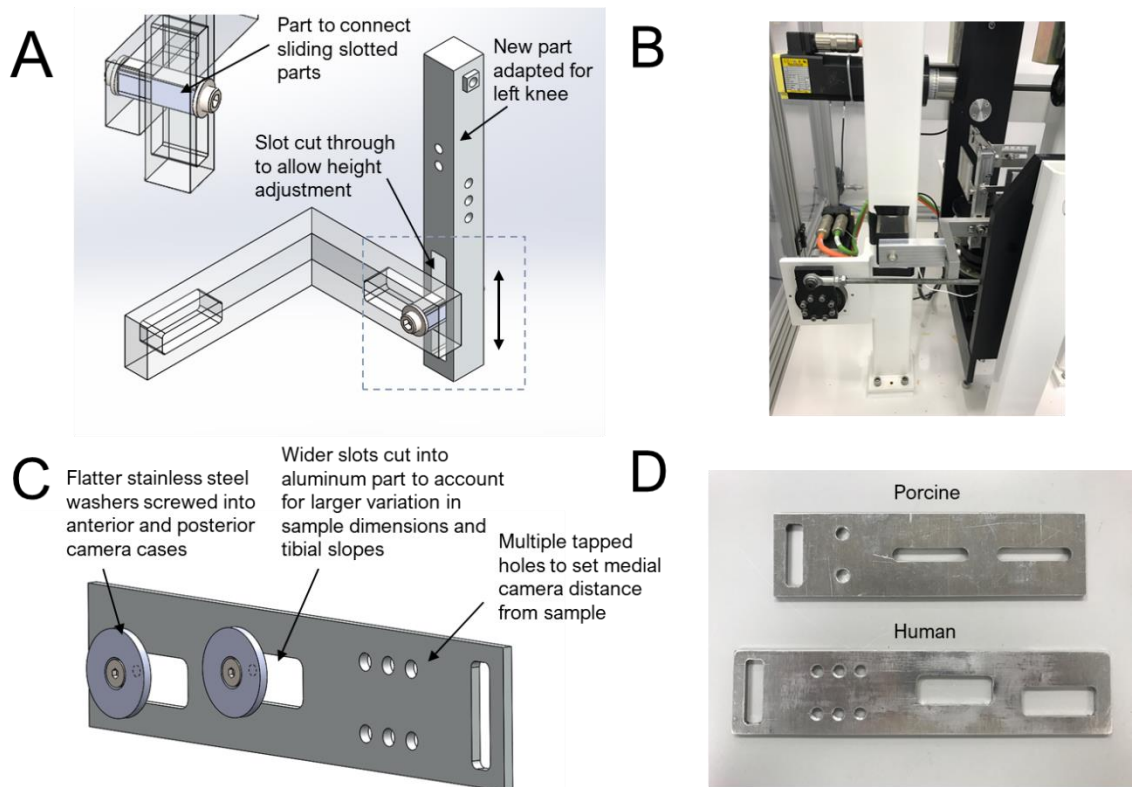


Figure 6.1. Camera rig adaptations to enable compatibility with human specimens. (A) SolidWorks models of newly manufactured parts for left knee specimens. (B) Image of manufactured parts allowing attachment of the abduction-adduction arm during left knee testing. (C) SolidWorks assembly of human anterior and posterior camera attachment. (D) Manufactured human component and comparison with the porcine component.

6.2.2 Camera Triggering in Python

During the human knee study, the profile was driven at the same speed (0.5 Hz) as in the porcine study, however, the markers were moving through larger driven translations within the same time frame, creating more motion blur. During the porcine study the cameras were programmed as USB web cameras (UVC gadgets) and triggered using a standard computer camera application (Windows Camera). The limitation of this method was that the cameras could only trigger at 30 fps. This frame rate was suitable for porcine specimens; however, a higher frame rate was required for human specimens especially for the anterior and posterior cameras which were situated closest to the anterior and posterior markers. Details of the Raspberry Pi camera programming and python triggering scripts are described in Appendix D. A python script was written and executed which enabled the cameras to record a 6 second video at 90 frames per second at a reduced resolution (1290 x 720 pixels). Multiple motion tests were carried out using this script to find the best adjustment between resolution and frame rate to minimise the motion blur of

a moving marker in a video. This new camera triggering method was then trialled using a human knee specimen and deemed successful as clear tracking of the meniscus and tibia markers was achieved for all three cameras and meniscus regions. A live feed was used to align the markers within the video frame and a 1 second calibration video at the same resolution were achieved by running scripts on Python. An open source file transfer application (WinSCP) was used to transfer calibration and video files from the Raspberry Pi camera microSD card to the laptops local drive.

6.2.3 Marker Pin Development

The marker pins were adapted because the human meniscus tissue was difficult to penetrate compared with the porcine meniscus. The human markers were made from 23 gauge (0.6 mm) syringe tips cut with pliers and superglued to 2 mm stainless steel ball bearing heads with a tapped hole. The heads were primed with metal primer paint and painted bright green with petrol resistant paint. Adhering stainless steel pins and heads was difficult due to the surface finish and irregular shapes, therefore using a ball bearing with a tapped hole allowed for a stronger bond reducing the risk of the head falling off the pin. Syringes were required for human specimens as the metal wire (used previously for porcine) was not sharp enough to penetrate the tibia or the stiff posterior horn of the medial meniscus (Makris et al., 2011). The diameter was measured after painting as the layers of paint on the ball bearing increased the diameter to approximately 3 mm which was used for the anterior and posterior camera image calibration.

6.3 Human Study Methodology

6.3.1 Sample Preparation

Fresh-frozen human knee specimens ($n = 10$) were dissected, aligned and cemented for knee simulation from the left and right legs of deceased donors (mean age: 50 years; mean BMI: 23.75; sex: 6 male, 4 female) according to the protocol described in section 2.2.2. All samples were MRI scanned prior to dissection and assessed by a trained colleague to examine the bone quality, menisci quality and alignment measurements such as the tibial width and epicondylar axis (see section 2.2.2.3). All samples had experienced one freeze-thaw cycle for MRI scanning prior to testing. One sample had been previously simulated in a separate study and had experienced an extra freeze-thaw cycle compared to the other samples. This sample was used for method development for the MAT procedure described in section 6.6. The human knee specimens were dissected with the capsule retained and marker pins were inserted into the medial, anterior and posterior

regions of the medial meniscus with corresponding reference markers on the tibial plateau directly below. The same marker positioning used for the porcine study was used for the human specimens (see section 4.6.2). The capsule in human knee specimens was thicker than porcine knee capsule, therefore, a small scalpel incision was made in the capsule to prevent the motion of the pin being dominated by the capsule stiffness. In addition, the insertion of the medial gastrocnemius tendon and the direct arm of the semimembranosus tendon covered the posterior aspect of the medial condyle and tibial plateau. Therefore, these tendons were carefully excised to position the posterior markers into the meniscus and the tibial plateau. In some samples it was difficult to locate the posterior aspect of the MCL to place the medial markers due to the thick connective tissue and the ligaments consistency with the connective capsular tissue. In this case, the pin was inserted on the medial aspect of the medial meniscus in line with the centre of rotation (COR) hole drilled during alignment (see section 2.2.2.5).

6.3.2 Developments to the Capsular Constraint and Root Tear Conditions

The dissection and root tear conditions used to examine human knee specimens were initially the same as those applied to the porcine experimental model described in the previous chapter (*CAP*, *NOCAP*, *NOLIG*, *TORN1*, *TORN2* and *TORN3*) (see section 5.2.3). A total of 4 human samples were assessed using the initial conditions (*CAP*, *NOCAP*, *NOLIG*, *TORN1*, *TORN2* and *TORN3*), however, problems such as fractures, simulator tuning issues and insecure cement fixation occurred in all specimen experiments. These initial conditions nonetheless provided an important period of method development and acquisition; however, the dissection and root tear conditions for the human study were then changed to *intact*, *capsule removed*, *partial tear* and *complete tear*. These alterations were necessary for the following reasons:

- to perform the MAT procedure as some remaining connective tissue was left around the medial meniscus periphery to attach the sutures;
- to retain clinical relevance of the type and extent of the tear as a complete tear has been commonly observed in the medial meniscus posterior root (LaPrade et al., 2015);
- to further reduce the risk of fracture by reducing the number of loaded conditions on the sample throughout the duration of the full experiment.

As illustrated in Figure 6.2, the revised conditions were: (A) *Intact*: the same as the previous capsule retained condition. (B) *Capsule removed*: included the excision of the collateral and cruciate ligaments, however, some connective tissue was retained around the medial meniscus perimeter for the MAT procedure to be carried out. (C) *Partial tear*: a scalpel was used to perform a cut spanning 50% of the medial meniscus posterior root. This cut was performed as close as possible to the root insertion to retain more of the root for the MAT procedure. (D) *Complete tear*: a scalpel was used to cut the full width of the medial meniscus posterior root through, whilst retaining some connective tissue on the peripheral border to prevent the damaged meniscus falling out of the joint space and to allow attachment for the MAT sutures.

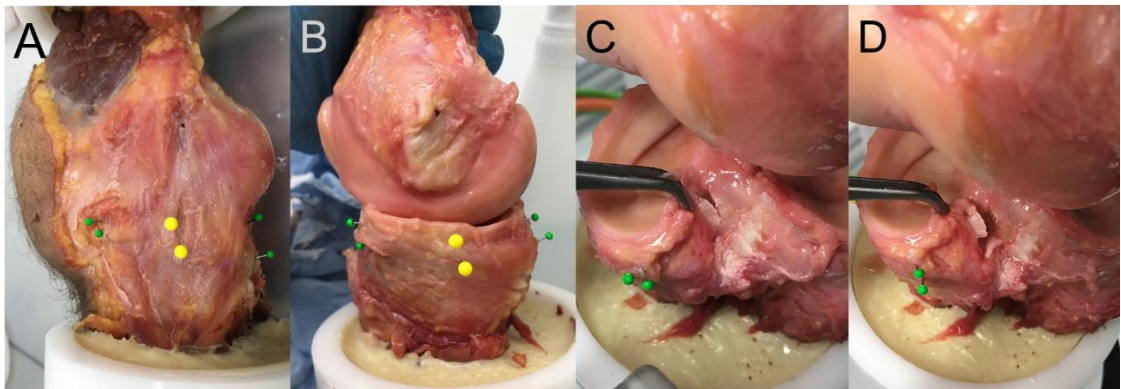


Figure 6.2. Revised human study dissection/torn conditions: (A) Intact, knee capsule fully intact. (B) Capsule removed, knee capsule and ligaments excised. (C) Partial root tear, medial posterior root tear at the insertion spanning 50% of the root width. (D) Complete root tear, 100% of root width.

6.3.2.1 Sample Overview

All the fresh--frozen human samples which were simulated are described in Table 6.1 with details of the conditions assessed (initial and revised), experimental issues and MRI scan notes. Once the conditions were revised, a total of $n = 4$ successful human samples with the *intact*, *capsule removed*, *partial tear* and *complete tear* conditions were studied and a total of $n=3$ samples were studied with the MAT procedure.

Table 6.1. Details of tested human samples and assessed initial and revised conditions.

Sample ID	Age	Sex	BMI	MRI Scan Notes	Initial Conditions						Comments
					CAP	NOCAP	NOLIG	TORN1	TORN2	TORN3	
RTKN2910	55	F	15.36	Meniscal horn tears, lateral meniscus extrusion	✓	✓	✓	✓	✗	✗	Low BMI and incorrect root tear simulation
LTKN1393	50	F	21.46	Posterior horn tears in both menisci	✗	✗	✗	✗	✗	✗	Sample fractured during pre-test tuning
LTKN1333	22	M	28.88	Good cartilage, bone density and menisci	✗	✗	✗	✗	✗	✗	Data collected but incorrect simulator input
LTKN1162	35	M	21.85	Good cartilage, bone density and menisci	✗	✗	✓	✓	✓	✓	Error in bone cement fixation initially
Sample ID	Age	Sex	BMI	MRI Scan Notes	Revised Conditions					Comments	
					Intact	Capsule Removed	Partial Tear	Complete Tear	Allograft (MAT)		
LTKN1017	56	M	20.78	Anterior root attachment of medial meniscus torn	✓	✓	✓	✓	✓		
LTKN0812	54	M	20.52	Mild meniscus degeneration	✓	✓	✓	✓	✗		
RTKN1064	61	M	30.87	Medial meniscus extruded in the anterior portion	✓	✓	✓	✓	✗		
LTKN2083	64	M	30.82	Small medial meniscus tears and degeneration	✓	✓	✓	✓	✗	Sample fractured during allograft condition	
RTKN1952	48	F	20.67	Signs of meniscus degeneration / OA	✗	✓	✗	✓	✓	Large AA oscillation: sample realigned	
LTKN1409	58	F	26.25	*previously simulated*	✗	✓	✗	✓	✓	*previously simulated*	

6.3.3 Gait Profile and Camera Set Up

The modified Leeds high kinematics gait profile at full load and position parameters was used for human specimens, with the abduction-adduction axis left free to move, as described in section 2.3.2. The miniature cameras were set up in the camera rig to video the corresponding marker regions for right and left human knee specimens as shown in Figure 6.3. For left knee specimens the polarity of anterior-posterior displacement and medial-lateral displacement was inverted in the videos and therefore the graphical polarity was also inverted compared to right knees. This is explained further in section 6.3.5.2.

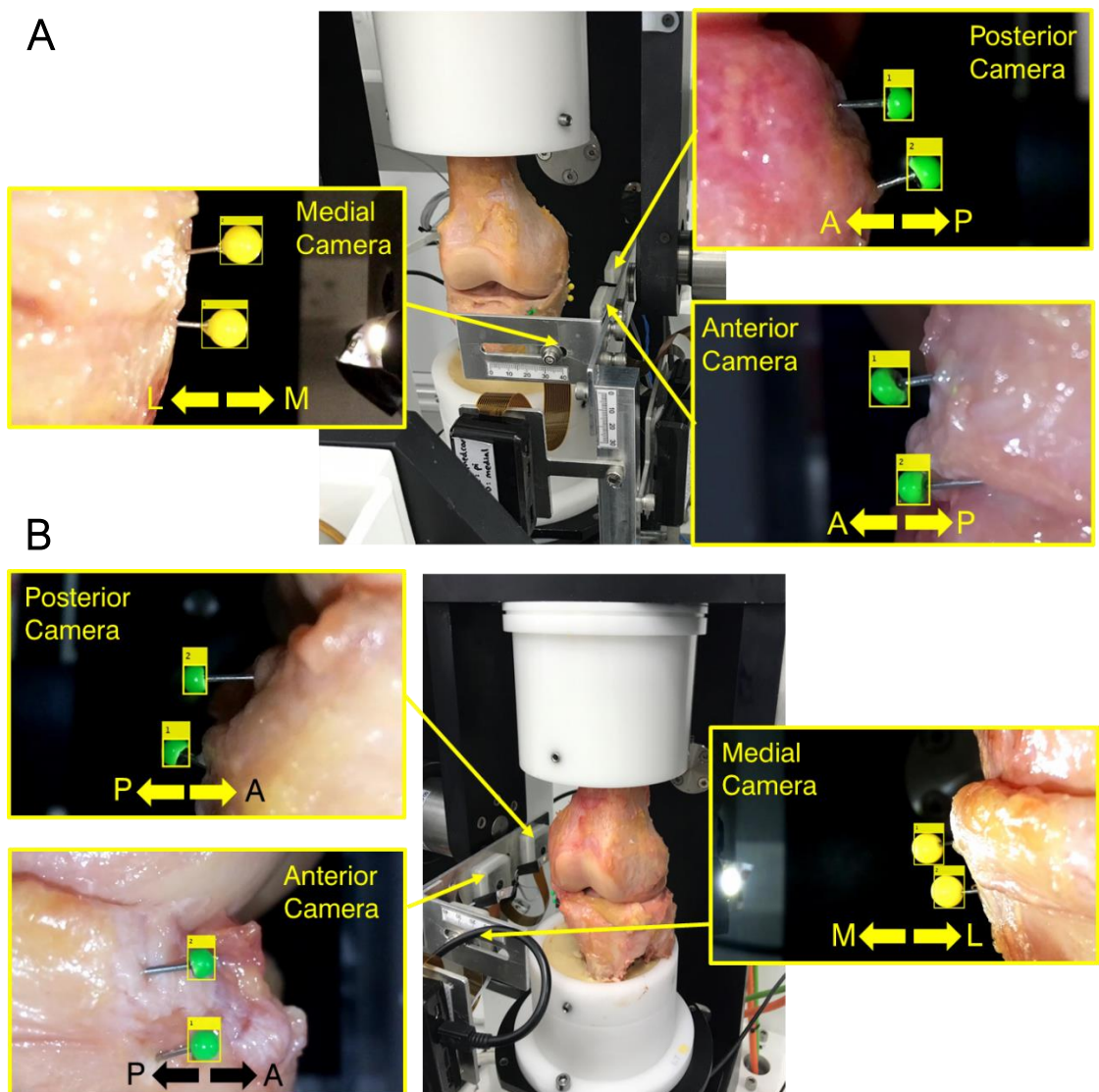


Figure 6.3. Human study test set up showing the differences in anterior-posterior (AP) and medial-lateral (ML) image measurement polarity with a (A) right and (B) left knee.

6.3.4 Data Collection Procedure

The meniscus tracking data collection procedure for each condition is illustrated in Figure 6.4. The human specimens were at higher risk of fracture due to the tissue integrity and the higher forces applied through the simulator; therefore, the axial load was ramped up over the first 10 gait cycles of the test. The first set of meniscus tracking data was measured for cycle 10 when full load was applied. The second set of meniscus tracking measurements were taken at cycle 50 to assess if there were changes in the displacements over time. These parameters were adapted for human specimens because the results of the porcine study showed minimal differences between cycle 10-50 suggesting two time points would be suitable for human samples, whilst also reducing the risk of fracture.

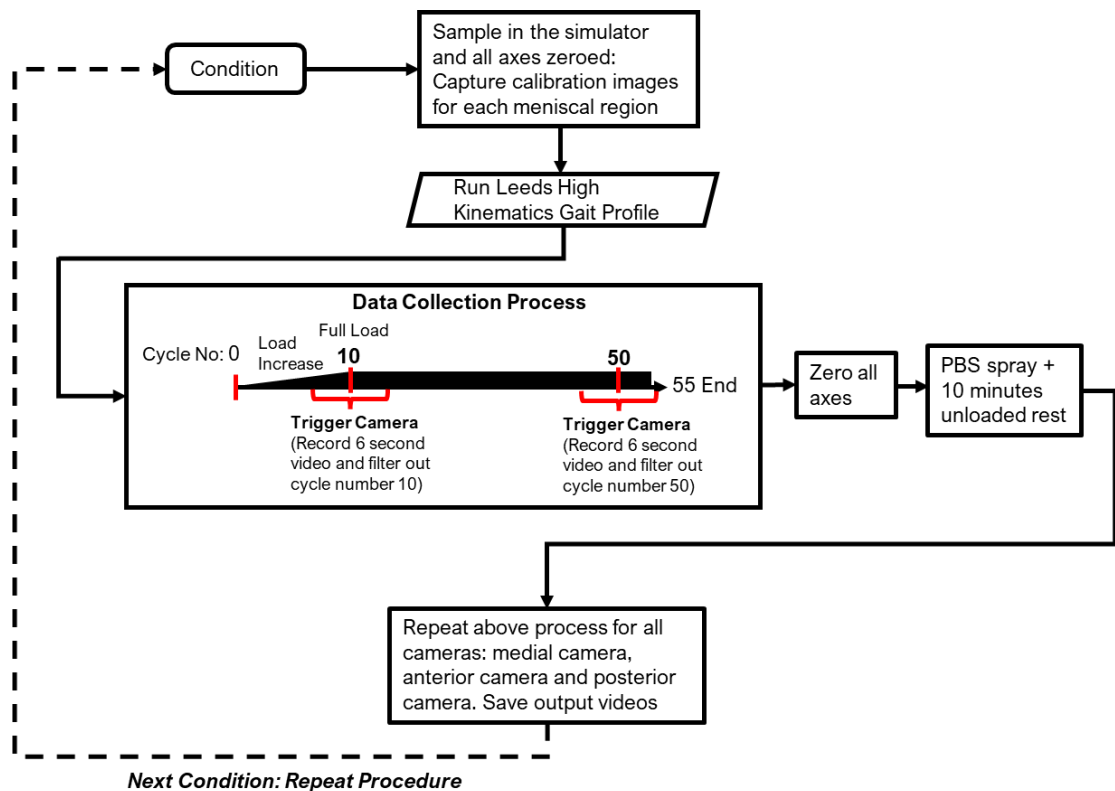


Figure 6.4. Data collection procedure repeated for all three meniscus regions (anterior, posterior and medial) during each of the four dissection/root tear condition (a total of 12 repeats for each sample).

6.3.5 Data Processing and Analysis

The human displacement data was processed from the Cycle 10 and Cycle 50 Raspberry Pi output videos from each dissection/torn condition and each camera using

the marker tracking method on MatLab. The output data was the anterior-posterior displacement and medial-lateral displacement of the tibia and meniscus markers, plus the calculated relative meniscus displacement for both these directions.

Due to the increased frame rate of the anterior and posterior cameras used to assess human specimens, the duration of one human gait cycle in the video increased from 60 frames (at 30 fps) to anywhere in the region of 130 – 150 frames (at 90 fps); equating to the number of data points. This was found to be irregular and most likely dependent on the computational hardware sharing the bandwidth through multiple USB ports, as a larger amount of processing power was required to trigger at 90 fps. However, to solve this problem, an extra line of interpolation code was written to ensure all the data points in one filtered gait cycle were 150, to allow for clearer data comparisons between the conditions.

6.3.5.1 Effect of Cyclic Test Duration

Maximum differences in relative displacement throughout the duration of the data collection process were small between the conditions. The largest difference was +/- 0.5 mm throughout the gait cycle between the *intact* and *complete tear* conditions for Cycle 10 and Cycle 50 during the human study. This differed from the porcine study, where there was a consistent medial shift observed for each sample's most severely torn condition (*TORN3*) condition throughout the duration of the test. Cycle 3 was the first cycle assessed in the porcine study design; however, as aforementioned, this was altered to Cycle 10 in the human study to prevent the risk of fracture. Problems with pin tissue adherence also occurred with increasing cyclic test duration during human specimen investigation. The decision was therefore made to discuss the Cycle 10 results in this chapter.

6.3.5.2 Left vs Right Knee Polarity

Data processing for left and right knee samples followed the same process, however, because the camera system was inverted as illustrated previously in Figure 6.3, the output displacement data polarity was also inverted (Table 6.2).

6.3.5.3 Statistical Analysis and Comparisons

The same statistical analysis was carried out for human specimens as previously described for porcine specimens (see section 5.2.4). Using SPSS software, a Shapiro-Wilk test of normality was carried out to show approximate normal distribution in the relative

displacement data. A repeated measures one-way ANOVA ($p < 0.05$) was used to compare the relative displacement means of $n = 4$ samples, between the *intact*, *capsule removed*, *partial tear* and *complete tear* conditions. The means were taken from the range (difference between maximum and minimum value during the gait cycle) and at specific time points during the gait cycle, relating to the peaks in the axial force profile (AF1, 0.28 seconds, AF2 0.90 seconds) for medial-lateral displacement, and the peaks in the flexion-extension profile (FE1, 0.3 seconds, FE2, 1.45 seconds) for anterior-posterior displacement. The 95% confidence intervals (95% CI) were also calculated to understand the level of uncertainty around the relative displacement estimations.

Table 6.2. Description of the opposing measurement polarity in the video frame for left and right human knees in relation to the medial-lateral and anterior-posterior motion directions.

<i>Plane</i>	<i>Marker Location / Region</i>	<i>Motion Directions</i>	<i>Right Knee Polarity</i>	<i>Left Knee Polarity</i>
Frontal	Medial Region	Medial	+ ve	- ve
		Lateral	- ve	+ ve
Sagittal	Anterior Region	Posterior	+ ve	- ve
		Anterior	- ve	+ ve
	Posterior Region	Posterior	+ ve	- ve
		Anterior	- ve	+ ve

6.3.6 Study Design Summary

A summary of the methodology and the flow of work is illustrated in Figure 6.5, showing how the human knee specimens were partitioned into the different method development studies (Development Study, Tear Study and MAT study). The next section discusses the results of four human specimens (Tear Study in Figure 6.5) assessed with the medial posterior root completely torn. Discussed in the latter half of this chapter is the MAT intervention study comprising of $n=3$ human specimens (MAT Study in Figure 6.5) (see section 6.6).

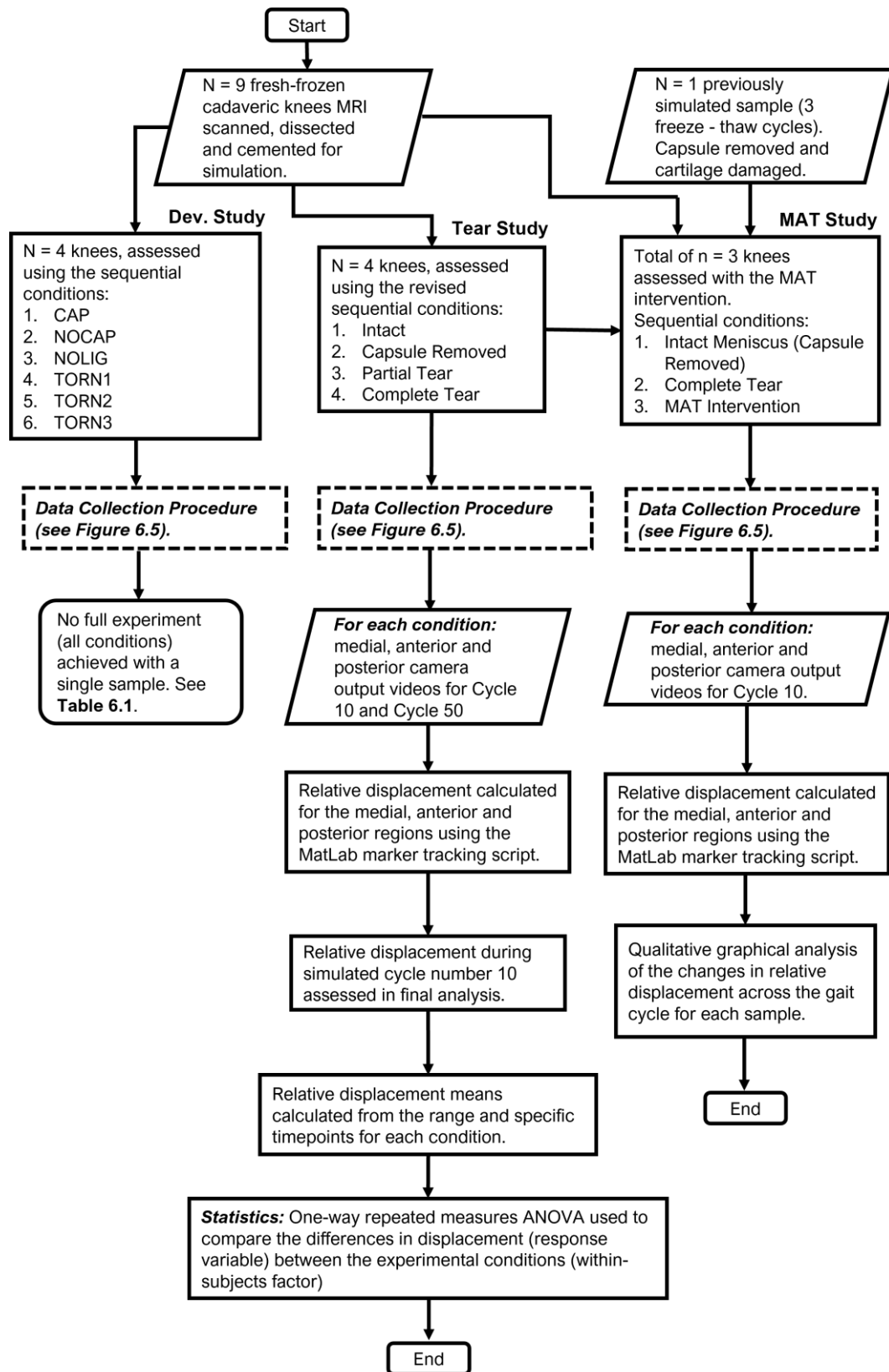


Figure 6.5. Human study design flow chart showing the fragmenting of the scanned human knee samples into three different studies (Development Study, Tear Study and MAT study) and the analysis of the outcome tracking data.

6.4 Tear Study Results

6.4.1 Relative Displacement Individual Sample Detail

The relative meniscus displacements for each region (medial, anterior, and posterior) across cycle 10 are presented for each human sample in Figure 6.6 and Figure 6.7. Values are described in absolute terms to provide consistency between left and right samples. All displacements described in this section are the displacement of the meniscus marker relative to the tibial (reference) marker.

6.4.1.1 Medial-lateral Displacement in the Frontal Plane, One Region

In the frontal plane (medial region), the displacement was unique between each sample. There was a greater difference in medial-lateral displacement between the conditions for sample LTKN1017 and LTKN0812 (Figure 6.6A,D) compared with RTKN1064 and LTKN2083 (Figure 6.7 A,D).

For sample LTKN1017, the largest difference between tissue states occurred in the second half of the cycle between the *complete tear* case and all other conditions. Specifically, the displacement approximately doubled compared to the other conditions, peaking at 3.05 mm (Figure 6.6A). There were other, smaller differences between the tissue states which were nonetheless of a larger scale than the assumed measurement error of ± 0.1 mm. The *capsule removed* and *partial tear* conditions had lower displacement (~ 1 mm lower) during the first half of the gait cycle in comparison to both the *intact* and *complete tear* conditions.

For sample LTKN0812, the largest difference between the conditions occurred in the last three quarters of the gait cycle (0.5 s – 2.0 s) between the *complete tear* case and all other conditions. During the first quarter of the gait cycle, small differences near the boundaries of the assumed measurement error occurred between all the conditions, displacing similarly by ~ 1 mm during this period. Thereafter, the displacement profile of the *complete tear* case became uncoupled from that of the *intact*, *capsule removed* and *partial tear* conditions. The *complete tear* case peaked at 1.75 mm during the second half of the gait cycle (Figure 6.6D). The *capsule removed* and *partial tear* conditions displaced in the opposite direction by a peak difference of ~ 1.5 mm compared with the *intact* condition results.

Both samples RTKN1064 and LTKN2083 followed a similar pattern of displacement throughout the gait cycle and differences between the tissue states for RTKN1064 and LTKN2083 were smaller than the *complete tear* conditions of LTKN1017 and LTKN0812. The largest difference between the *intact* and *complete tear* conditions was approximately

+/- 0.50 mm throughout the gait cycle for both RTKN1064 and LTKN2083. For the *intact* case, displacement peaked at ~ 1 mm throughout the gait cycle for both samples. During the second half of the gait cycle, the *complete tear* case for both samples had a lower displacement than *capsule removed* and *partial tear conditions*. During the second half of the gait cycle, the peak displacement for the *capsule removed* and *partial tear* conditions was ~ 2.3 mm for RTKN1064 (Figure 6.7A) and ~ 1.3 mm for LTKN2083 (Figure 6.7D).

6.4.1.2 Anterior-Posterior Displacement in the Sagittal Plane, Two Regions

In the sagittal plane, each sample presented a unique profile of anterior-posterior displacement throughout the gait cycle for both the posterior region (Figure 6.6 C, F; Figure 6.7 C,F) and anterior region (Figure 6.6 B,E; Figure 6.7 B,E). There was a predominant posterior direction of relative displacement across all samples and conditions throughout the gait cycle. In addition, displacements typically reached a higher magnitude for the anterior region than the posterior region for each sample.

Anterior Region

In most cases, the displacement for the anterior region followed the same shaped profile throughout the gait cycle for the *capsule removed*, *partial tear* and *complete tear* conditions. For LTKN1017, the *intact* case produced the largest amount of displacement peaking at 6.5 mm during the second half of the gait cycle. All the other conditions (*capsule removed*, *partial tear* and *complete tear*) peaked around ~ 5 mm during the second half of the gait cycle. Differences between the *capsule removed*, *partial tear* and *complete tear* conditions were close to the measurement error threshold of +/- 0.1 mm for anterior-posterior relative displacement (Figure 6.6B).

Sample LTKN0812 presented the largest magnitude of anterior-posterior displacement compared with all other samples. The largest differences in the anterior region were found for the *complete tear* condition, where peak displacement was approximated half (~ 5 mm) that measured for the *intact*, *capsule removed* and *partial tear* conditions (~10 mm) during the second half of the gait cycle (Figure 6.6E). Differences between the *capsule removed*, *partial tear* and *complete tear* conditions were close to the measurement error threshold.

For sample RTKN1064, the largest difference occurred during the first half of the gait cycle for the *intact* case, which presented ~ 2 mm lower peaks in displacement, compared with the *capsule removed*, *partial tear* and *complete tear* conditions. The same effect for the *intact* case was also present in the second half of the gait cycle, showing a plateau in the peak (~ 6 mm) as compared to the shallower double-peaked profile (~ 9

mm) shown for the *capsule removed*, *partial tear* and *complete tear* conditions (Figure 6.7 B). Smaller differences occurred between these conditions of around ± 1 mm, which fell outside of the estimated measurement error.

In a similar way to sample RTKN1064, sample LTKN2083 *intact* condition displacement plateaued slightly during the second half of the gait cycle, however reached a peak displacement of ~ 5.5 mm; similar to the *capsule removed* and *partial tear* conditions. The *complete tear* case showed a reduction of ~ 1 mm during the second half of the gait cycle, as compared with the other conditions (Figure 6.7E).

Posterior Region

For samples LTKN1017 and LTKN0812, the largest difference occurred for the *complete tear* case, presenting a reduction of peak displacement of around half that measured for *intact* condition during the second half of the gait cycle (Figure 6.6 C, F). Completely tearing the root also caused the displacement to become disjointed from the profile shown for the *intact*, *capsule removed*, and *partial tear* conditions. There were smaller differences in displacement between the *intact*, *capsule removed*, and *partial tear* conditions which exceeded the estimated level of precision of the method. Sample LTKN0812 also showed higher relative mobility in the posterior region than all other samples (Figure 6.6F).

For samples RTKN1064 and LTKN2083, the largest difference occurred in the *complete tear* case. Sample RTKN1064 showed a reduction in peak displacement of ~ 1 mm compared with the other conditions during the second half of the gait cycle (Figure 6.7 C). For LTKN2083, the *complete tear* condition showed an atypical pattern compared with the other conditions during the first half of the gait cycle. A small peak of 0.81 mm in displacement occurred in the opposite (anterior) direction and the displacement oscillated approximately ± 1 mm around zero (Figure 6.7 F). For samples RTKN1064 and LTKN2083 a similar pattern of displacement occurred for the *intact*, *capsule removed* and *partial tear* conditions during the gait cycle. The displacement for these samples showed a narrower singular peak of 4.75 mm (RTKN1064) and 4.33 mm (LTKN2083) during the second half of the gait cycle (Figure 6.7 C, F).

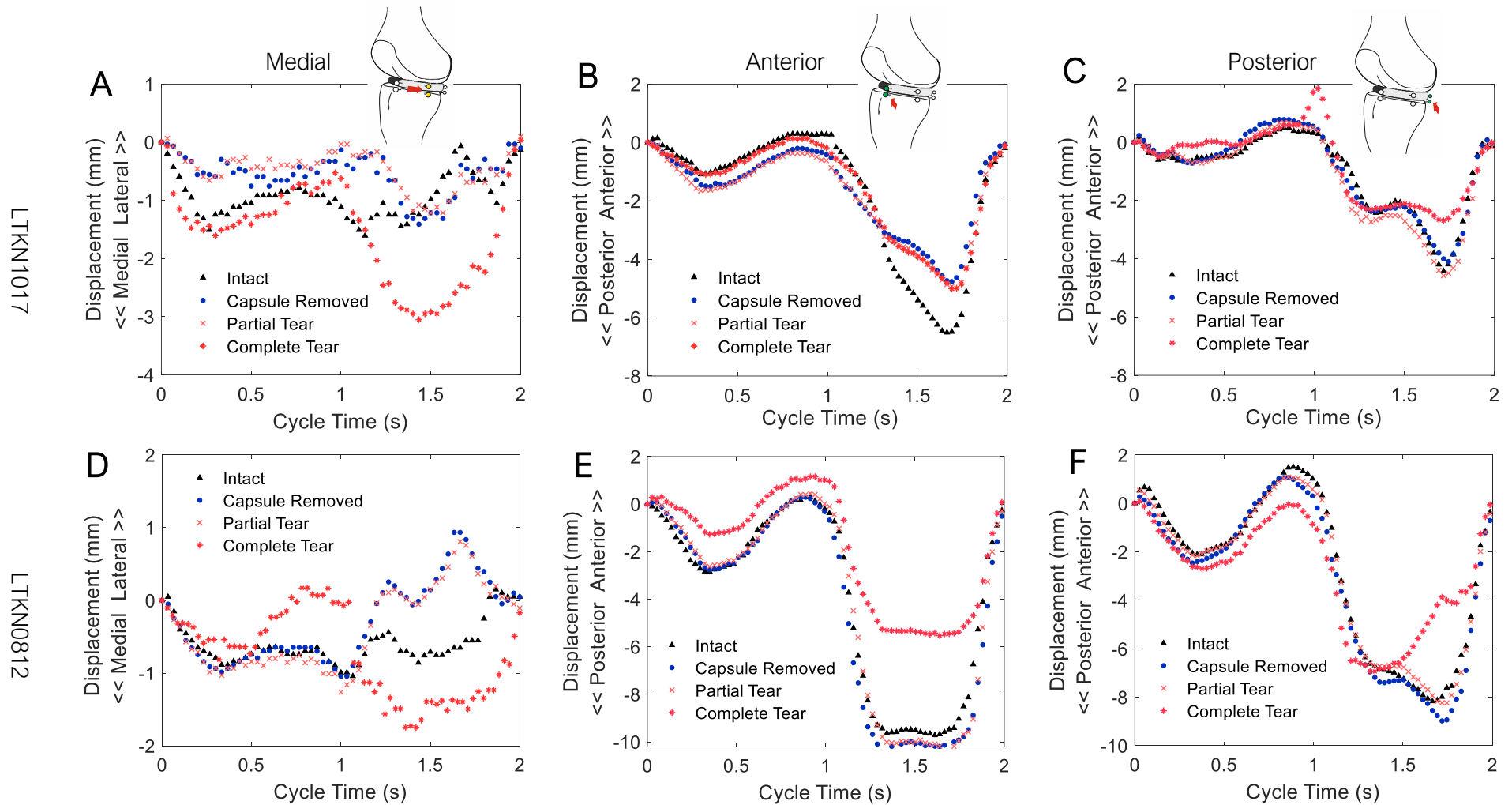


Figure 6.6. Measured cycle 10 relative displacement for the medial, anterior and posterior regions of (A-C) LTKN1017 and (D-F) LTKN0812 (human).

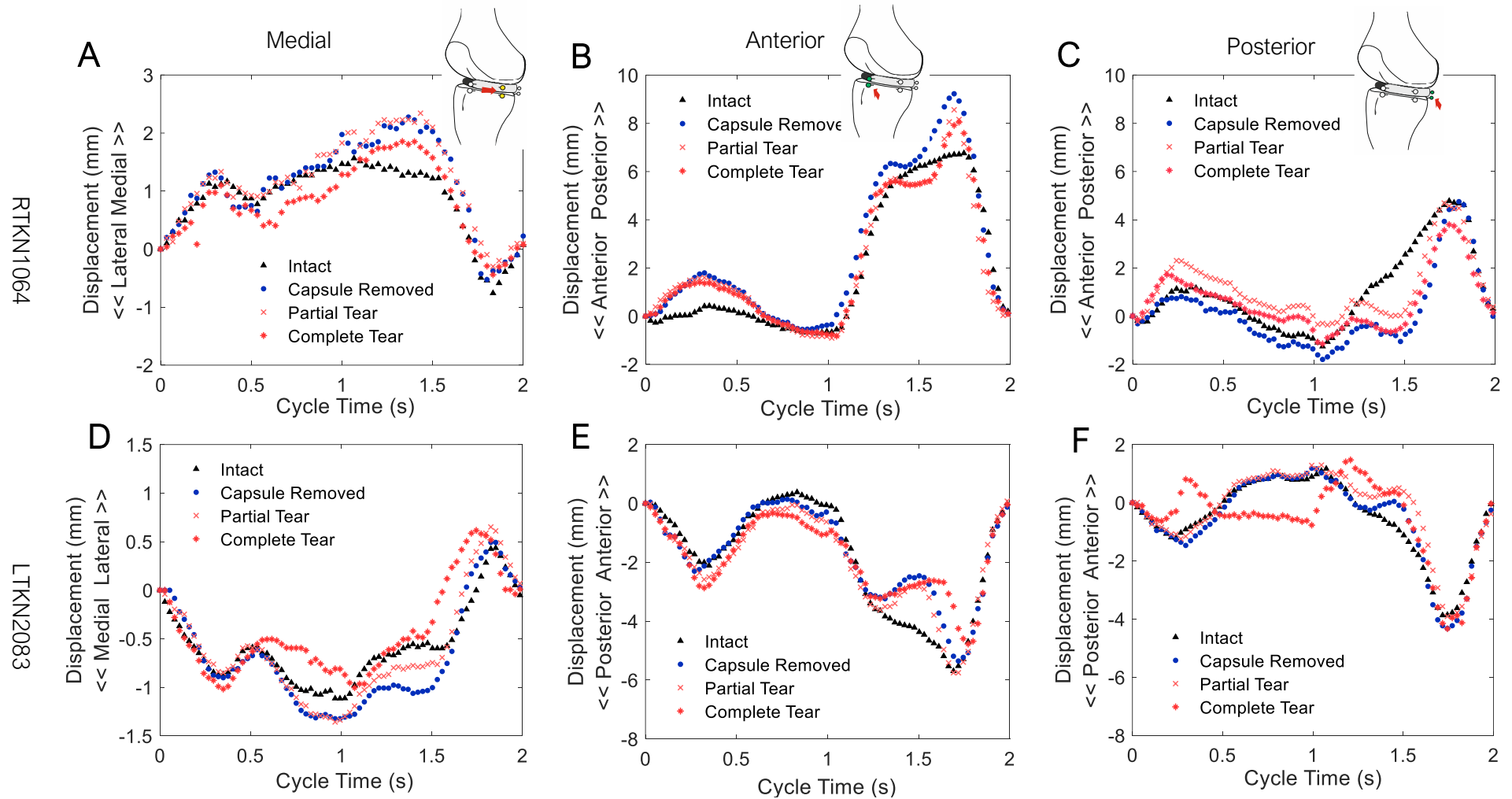


Figure 6.7. Measured cycle 10 relative displacement for the medial, anterior and posterior regions of (A-C) RTKN1064 and (D-F) LTKN2083 (human).

6.4.2 Relative Displacement Summary

No statistically significant differences ($p > 0.05$) were found between the *intact*, *capsule removed*, *partial tear* and *complete tear* conditions using the repeated measures one-way ANOVA on means taken from relative displacement values at specific timepoints and the range (max – min value during one cycle) as shown in Table 6.3. Generally, the mean anterior-posterior relative displacement taken from the maximum – minimum range slightly decreased with root damage in the sagittal plane. Between the intact and complete root tear condition the anterior region mean range reduced by ~ 1.2 mm; and in the posterior region by ~ 0.8 mm.

Table 6.3. Mean relative displacements (\pm 95% CI) taken from specific gait time-points (TP) and the range (maximum-minimum) for cycle 10. All units in millimetres (all cases $p > 0.05$)

<i>Meniscal Region</i>	<i>Data Type</i>	<i>Intact</i>	<i>Capsule Removed</i>	<i>Partial Tear</i>	<i>Complete Tear</i>
<i>Medial</i>	TP: AF1	1.02 (\pm 0.47)	0.91 (\pm 0.48)	0.89 (\pm 0.42)	0.98 (\pm 0.63)
	TP: AF2	1.02 (\pm 0.42)	0.97 (\pm 0.78)	1.07 (\pm 0.88)	0.58 (\pm 0.71)
	Range	1.67 (\pm 0.75)	2.01 (\pm 0.93)	2.01 (\pm 0.87)	2.24 (\pm 0.99)
<i>Anterior</i>	TP: FE1	1.54 (\pm 1.69)	1.98 (\pm 0.74)	1.97 (\pm 0.68)	1.56 (\pm 1.36)
	TP: FE2	6.17 (\pm 3.71)	5.56 (\pm 5.40)	5.47 (\pm 5.10)	4.34 (\pm 2.02)
	Range	7.60 (\pm 2.71)	7.68 (\pm 4.69)	7.76 (\pm 4.39)	6.43 (\pm 2.87)
<i>Posterior</i>	TP: FE1	1.12 (\pm 0.81)	1.31 (\pm 1.22)	1.48 (\pm 1.14)	0.75 (\pm 2.22)
	TP: FE2	2.95 (\pm 4.38)	2.18 (\pm 5.83)	2.19 (\pm 5.21)	1.94 (\pm 5.32)
	Range	6.43 (\pm 3.53)	6.76 (\pm 3.67)	6.30 (\pm 3.25)	5.62 (\pm 1.83)

The largest decrease in mean relative displacement occurred during the second flexion peak in the sagittal plane, with the mean values reported at FE2 time-point decreasing by ~ 2 mm (anterior region) and ~ 1 mm (posterior region). The mean medial –

lateral relative displacement range slightly increased with each dissection/torn condition from 1.67 mm to 2.24 mm between the intact and the completely torn condition respectively. There was no clear trend identified in mean relative displacements between the conditions when values were taken at the AF1 and AF2 time-points from the medial region markers.

6.4.3 Tibia and Meniscus Marker Displacements

6.4.3.1 Medial-lateral Translation in the Frontal Plane, One Region

The relative displacement results for each sample were governed by the meniscus marker and tibia marker displacements (see Appendix F).

A relationship was observed between the raw displacements of the medial tibial marker and the abduction-adduction angle of the tibiofemoral joint measured by the simulator (Figure 6.8). The pattern of abduction-adduction angle varied between samples and governed the behaviour of the tibial marker displacement. For samples where the abduction-adduction angles had smaller magnitudes in the intact case, the capsule removal and cutting of the meniscus root typically generated increased abduction-adduction angles, and therefore also increased tibial marker movement.

For samples LTKN1017 and LTKN0812, the meniscus marker produced a similar shaped profile as the tibia marker; largely governed by the abduction-adduction angle. Changes in the relative displacement between the conditions occurred predominantly due to changes in the meniscus marker displacement. When the root was completely torn, the meniscus displacement became disjointed from the typical pattern observed for the *intact*, *capsuled removed* and *partial tear* conditions. During the second half of the gait cycle, a reduction in the peak meniscus marker displacement occurred for both samples of ~1.5 - ~2 mm for the *complete tear* condition, roughly half that of the other conditions (Appendix F).

For samples RTKN1064 and LTKN2083, simulator adduction-abduction increased as tissue was dissected and the root was cut, causing an increase in tibia displacement and meniscus displacement. The changes in meniscus and tibia marker displacement between the conditions were more random and oscillated more for LTKN2083 than RTKN1064. The peaks and troughs of the meniscus displacement coincided at similar points throughout the gait cycle for the *intact*, *capsule removed* and *partial tear* conditions, whereas the *complete tear* condition did not follow this pattern (Appendix F).

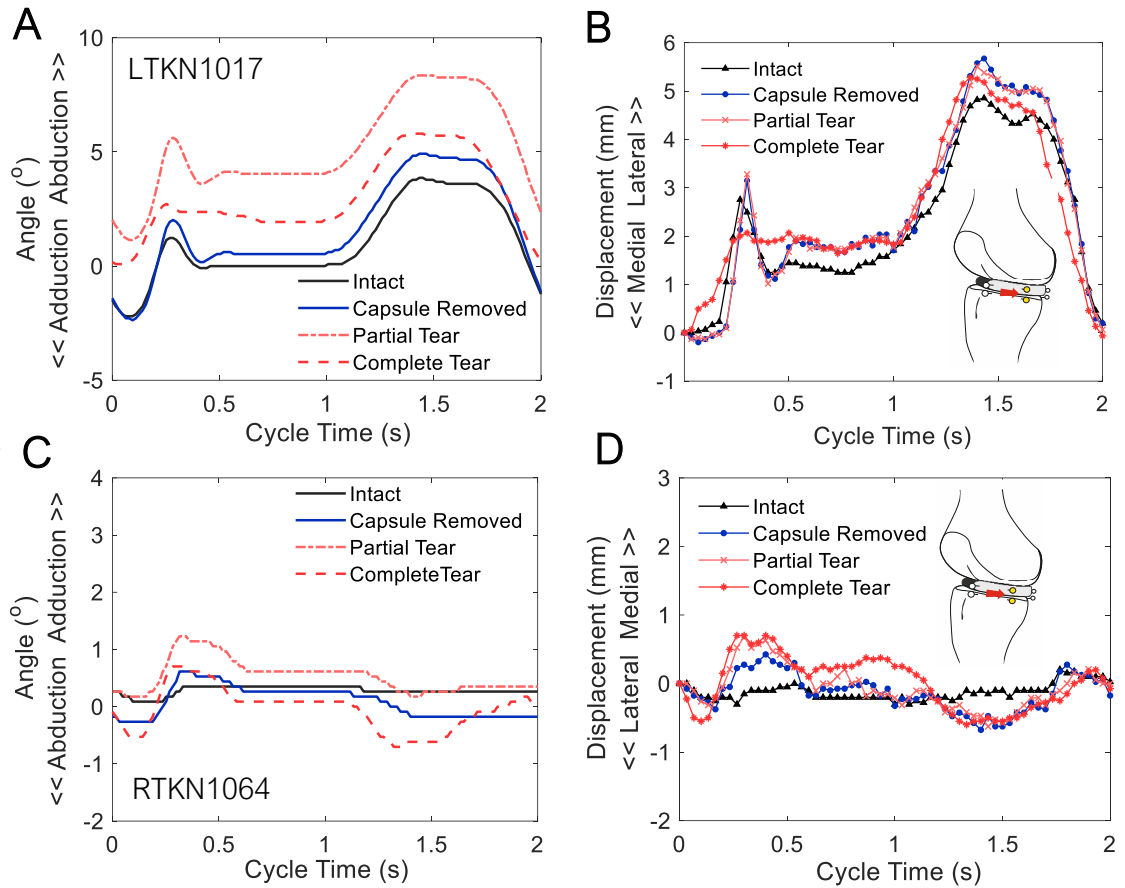


Figure 6.8. Representative example of the comparison between the simulator abduction-adduction output and measured medial region tibial marker displacement for (A, B) LTKN1017 and (C, D) RTKN1064 (human).

6.4.3.2 Anterior-Posterior Translation in the Sagittal Plane, Two Regions

The tibial marker moved in a similar way throughout the gait cycle for both the anterior and posterior regions. The tibia marker followed the combined action of the driven anterior-posterior carriage and the driven tibial rotation of the simulator, moving predominantly anteriorly with the tibial carriage, and peaking at ~10 mm in the second half of the gait cycle. Small differences between the conditions were found in the tibia displacement for the anterior region results, however, in the posterior region slight changes in the tibia displacement were measured between the *intact* and the *complete tear* conditions (Figure 6.9).

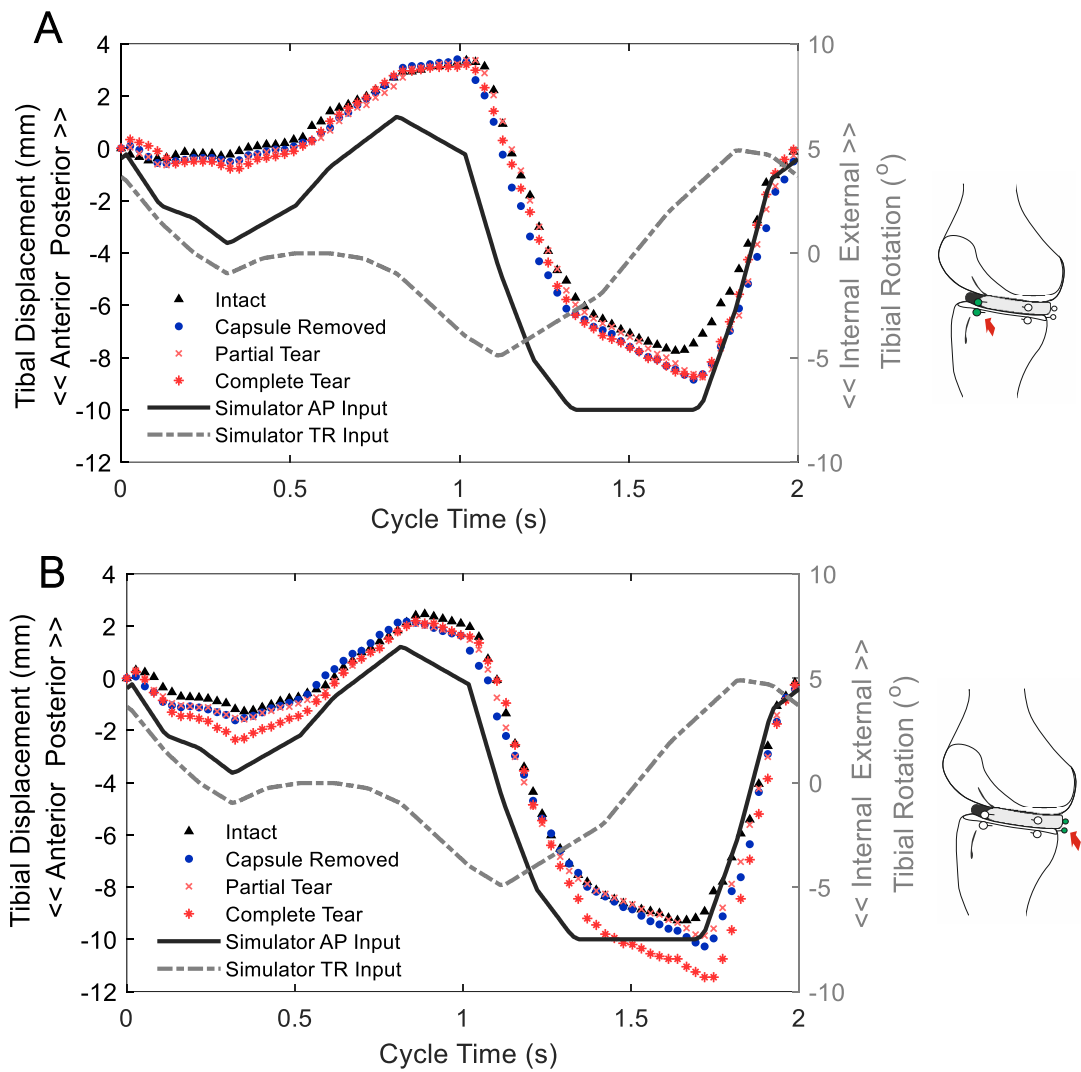


Figure 6.9. Human sample LTKN0812 representative example of the (A) anterior region and (B) posterior region tibial marker displacement in relation to the anterior-posterior (AP) translation and tibial rotation (TR) gait profile inputs. The left-knee tibial marker polarity was inverted to match the polarity of the anterior-posterior (AP) simulator input.

Changes in the relative displacement between the conditions largely occurred due to changes in the meniscus displacement. For sample LTKN0812, the largest differences in the anterior region were observed for the *complete tear* condition, which had increased meniscus displacement, peaking at 3.31 mm during the second half of the gait cycle in the opposed direction than the other conditions. In addition, the *complete tear* profile changed and mimicked the triangular shape of the anterior displacement peak of the tibia marker displacement during the second half of the gait cycle. This effect was also observed in the posterior region results for LTKN0812, where the *complete tear* increased meniscus displacement by 6.63 mm, a ~7-fold increase from the *intact* condition displacement,

during the second half of the gait cycle. The profile again emulated the triangular shape of the tibial displacement during second half of the gait cycle.

The posterior region meniscus displacement for the *intact*, *capsule removed* and *partial tear* conditions for LTKN1017, RTKN1064 and LTKN2023 followed a similar smoothness and pattern to the applied flexion-extension gait profile. For LTKN1017, the *complete tear* condition did not present large increases in magnitude compared with the other conditions, but the profile became disjointed from the typical pattern measured for the *intact*, *capsule removed* and *partial tear* conditions.

Sample LTKN2083 showed an atypical spike in meniscus marker displacement for the *complete tear* condition, locally peaking from 0.27 mm to 3.88 mm during the first half of the gait cycle at ~ 0.30 seconds. An increase of 1.96 mm was also present at this same time-point in the tibia displacement results for LTKN2083 (Appendix F).

6.5 Tear Study Discussion

6.5.1 Main Findings

The main findings from this study were:

- the motion capture method was able to be applied to human knee specimens experiencing a simulated gait cycle;
- the relative displacement results were unique to each individual sample;
- the specific patterns and magnitudes of meniscus, tibia and relative displacement created high variation between samples and therefore no statistically significant trends between the conditions were found;
- completely tearing the root generally presented a reduction in the anterior-posterior relative displacement and an increase in the medial-lateral relative displacement, compared with the *intact*, *complete tear* and *partial tear* conditions;
- in some cases, changes to both the tibia displacement and the meniscus displacement occurred when tissue was dissected or the root was damaged, which overall had little effect on the relative displacement.

6.5.2 Limitations

Several limitations were present during this study. As previously mentioned, a low sample size greatly reduces the power of this study. From the MRI scans, all knee specimens showed a variable amount of meniscus damage and cartilage degeneration

prior to testing. This was difficult to control due to the tissue availability, however, it was deemed more important if the sample had a consistent bone density and quality to allow confidence in applying the full load gait cycle without fracture. In addition, due to the differences in condylar geometry, the centre of rotation alignment and cementing procedure was difficult to keep consistent between samples because the epicondylar axis of the femur is usually at an angle (Yin et al., 2015), but during the cementing procedure this is set to 0° to line-up with the rotational axis of the simulator. This could have created more of a tilt in some samples more than others and potentially adding to the differences in femoral and tibial contact and adduction-abduction angle.

As previously mentioned, a certain amount of measured displacement is possibly caused by motion of the pin, however, there was a larger amount of pin motion with the knee capsule intact compared to the other conditions. This questions the validity of the knee capsule intact condition as the control to base the other condition measurements off and it is possible the condition with the capsule removed maybe a more reliable control.

In addition, the measurements in this study were taken from cycle 10, not cycle 3 as undertaken in the porcine study. Due to human tissue availability and cost, the methodology was adapted to reduce the risk of the human specimen fracturing by ramping the axial load over a longer period. However, this could have meant any offset/extrusion of the meniscus with a complete root tear could have occurred before cycle 10 was measured in the human study. Hence minimal changes were observed with cyclic test duration in this study as seen in the porcine results.

The revised conditions used in this study were implemented to allow the MAT intervention condition to be performed to be carried out after the root was completely torn. However, this meant that it was difficult to control the amount of connective tissue remaining when the complete root tear was performed. This meant that some samples might have had more connective tissue attached to the tibia than other samples affecting the amount of measured displacement.

6.5.3 Sample Variation

There was a large amount of variation between the assessed samples and no statistically significant trends were found (p values > 0.05) between relative displacement means calculated from the range and specific timepoints across the gait cycle using a repeated measures one-way ANOVA. Human specimen simulation studies are difficult to draw statistically significant trends with the sample sizes typically available for cadaveric research. However, human specimen variability has been previously reported in a cadaveric knee simulation study, where a specimen-specific gait profile was developed

using force controlled gait inputs and virtual springs to provide a close match to the natural soft tissue constraint (Liu et al., 2020). During this thesis investigation, each knee axis was driven to the same gait parameters using displacement control, regardless of specimen size, soft tissue constraint or injury condition. This simulation model was chosen to assess the application of the marker-tracking methodology by limiting the number of variables to isolate the changes relating to the relative medial meniscus displacement and allow for easier comparisons between the conditions. However, these gait parameters may not have been appropriate for human specimens due to the variability which occurs across many factors such as sex, age, BMI, tibia / femur geometry, walking gait, knee alignment etc. The porcine knee samples in the previous chapter were taken from pigs of a similar age, sex and weight, therefore, using a regular displacement-controlled gait profile generated similar magnitudes and patterns of meniscus displacement between all the samples, as compared to the human study.

Moreover, unlike the porcine study, the peaks of the simulated gait profile axial force and flexion-extension profiles were less so reflected within the human relative displacement results. These differences are most likely due to differences in anatomical knee geometry, tissue mechanics and sample age affecting the tissue integrity and not the sensitivity of the marker tracking method. In two knee samples, the meniscus marker displacement in the posterior region followed a similar smoothness and profile to the applied flexion-extension profile. This suggests the anterior-posterior displacement of the medial meniscus was closely connected to the action of the femoral condyles. A recent study using dynamic MRI methods reported that meniscus kinematics are governed by the interactions between the femoral and tibial interactions of the knee joint (Yamamoto et al., 2021). Further study could focus on applying specimen specific force-controlled gait profiles to assess specimen specific meniscus displacement and meniscus interventions going forward.

6.5.4 Intact / Healthy Medial Meniscus Displacement

Due to the novelty of this work, it is difficult to directly compare dynamic medial meniscus displacement results to the findings reported in previous publications. The methods used to assess dynamic meniscus displacement in previous literature are predominantly radiographical, such as MRI or RSA. The loading regimes typically applied are a weight bearing or unloaded squat motion, or passive full range of motion (ROM) femoral flexion. In addition, the locations where the meniscus body movement were directly measured from also varied. To provide a visual validation the novel methodology developed throughout this thesis, Table 6.4 summarises previously published intact (no injury or intervention conditions applied) medial meniscus displacement values reported

during dynamic *in-vivo* and *in-vitro* radiographical studies of knee joint motion measuring meniscus displacement. The bottom row shows the mean peak findings of the herein human tear study's intact (capsule retained) results. The peak relative displacement values (in absolute terms) were taken across the gait cycle for the medial, anterior and posterior region results from the intact capsule condition and a mean of these peaks was calculated for each region ($n = 4$). Even though the findings highlighted in Table 6.4 are not directly comparable due to differences in loading regimes, measurement equipment and measurement locations. The comparisons show the human study findings of this thesis were within a similar range of medial meniscus displacements reported from dynamic *in-vivo* and *in-vitro* cadaveric studies within the literature, where the measurements were taken in a similar area in the meniscus body.

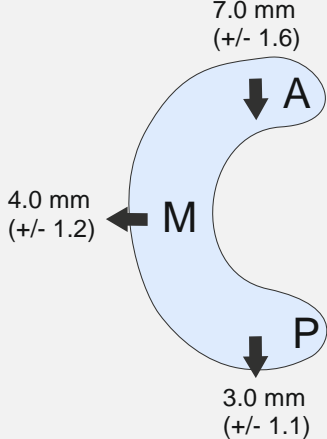
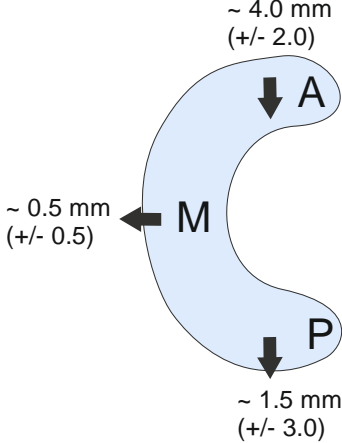
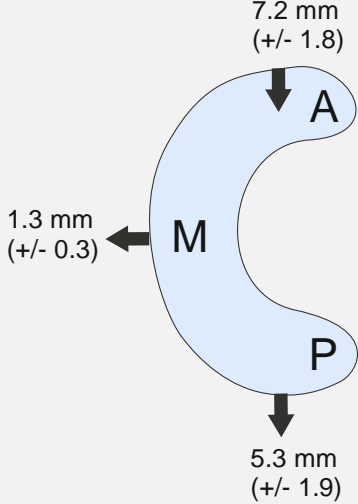
In addition, consistent with previously published literature, the relative displacement of the medial meniscus posterior region generally moved less than the medial meniscus anterior region for each sample, due to the higher stiffness and shorter root attachment site of this region (Thompson et al., 1991; Bylski-Austrow et al., 1994; Vedi et al., 1999; Yamamoto et al., 2021). Moreover, Table 6.4 highlights the variation in meniscus displacement measurement location across the literature. For example, Hamamoto et al. (2004) measured from the inside edge of the meniscal body and obtained larger values than the other studies where measurements were taken from predominantly the outer peripheral edge or within the meniscal body. Measuring on the inside edge potentially reflects more deformation being in close contact with the condyles, whereas measuring around the peripheral edge maybe more restricted by soft tissue constraint. Nonetheless, this was the first study to apply dynamic physiological load to cadaveric samples and assess medial meniscus displacement with simultaneously applied gait parameters.

6.5.5 Knee Capsule Constraint

There are mixed reports in the literature as to whether the knee capsule effects medial meniscus biomechanics. Some studies have shown that damaging the meniscotibial ligament increases measured medial meniscus extrusion, both in cadaveric investigation and clinical studies (Krych, Bernard, Leland, et al., 2020; Paletta et al., 2020), whereas other studies have not found a significant effect (De Maeseneer et al., 2002; Vrancken et al., 2014). In this study, the knee capsule was cut away in stages to assess the sensitivity of the motion capture method and the effect of the capsule medial meniscus movement. Removing the capsule had minimal effect on the relative displacement measurement in the porcine study, however, in the human study, a change in displacement occurred between the intact and capsule removed conditions, but this change was difficult to draw conclusions from and varied greatly between samples.

Table 6.4. Comparison of dynamic intact (healthy) human medial meniscus displacement (mean +/- SD) from previously published *in-vivo* and *in-vitro* radiographical studies with the tear study results of this thesis (bottom row). The arrows illustrate the measurement locations and the direction of displacement of the medial meniscus during the various experiments.

Study	Method	Loading Regime	Medial Meniscus Displacement
Thompson et al. (1991)	Cadaveric MRI	N = 5 knee specimens Full passive ROM unloaded flexion (110° -130°)	<p>7.0 mm (+/- 0.7) Anterior Region 3.2 mm (+/- 1.3) Posterior Region</p>
Vedi et al. (1999)	In-vivo MRI	N = 14 healthy male subjects 0 – 90° flexion squat Weight bearing	<p>7.1 mm (+/- 2.5) Anterior Region 3.6 mm (+/- 2.3) Medial Region 3.9 mm (+/- 1.8) Posterior Region</p>
Hamamoto et al. (2004)	In-vivo MRI	N = 20 healthy subjects (10 male, 10 female) 0° - 147° (mean) full ROM flexion Unloaded, subjects lying in the prone position	<p>16.8 mm (+/- 2.9) Anterior Region 8.9 mm (+/- 2.9) Posterior Region</p>

Vrancken et al. (2014)	Cadaveric RSA	<p>N = 6</p> <p>Simulated 0 - 90° squat</p> <p>357N – 1000N axial load</p> <p>3.4Nm IE tibial torque</p> <p>67N tibial drawer load</p>	 <p>7.0 mm (+/- 1.6)</p> <p>4.0 mm (+/- 1.2)</p> <p>3.0 mm (+/- 1.1)</p>
Vrancken et al. (2016)	Cadaveric RSA	<p>N = 5</p> <p>Simulated 0 - 90° squat</p> <p>357N – 1000N applied load</p> <p>3.4Nm IE tibial torque</p> <p>67N tibial drawer load</p>	 <p>~ 4.0 mm (+/- 2.0)</p> <p>~ 0.5 mm (+/- 0.5)</p> <p>~ 1.5 mm (+/- 3.0)</p>
This Thesis	Cadaveric motion capture	<p>N= 4</p> <p>Simulated gait cycle</p> <p>Maximum load: 2600N</p> <p>Maximum flexion 60°</p> <p>Mean peaks and direction of motion taken from the relative meniscus displacement during a simulated gait cycle</p>	 <p>7.2 mm (+/- 1.8)</p> <p>1.3 mm (+/- 0.3)</p> <p>5.3 mm (+/- 1.9)</p>

6.5.6 Root Tear Injury and Meniscal Extrusion

Characterising the dynamic displacement of the injured meniscus has not been studied to great extent. The developed methodology measured trends in relative displacement when the meniscus was subject to severe root damage, however, rather

than a clear increase in relative displacement throughout the gait cycle and also throughout the cyclic test duration (extrusion), as seen within the porcine study medial region results (see section 5.3), the human results produced more complex changes in relative meniscus displacement when the medial posterior root was cut and the creation of a dynamic injury model of traumatic pathological meniscal extrusion was difficult to achieve.

In most cases the *complete tear* condition brought about the largest differences in relative displacement compared with the *intact*, *capsule removed* and *partial tear conditions*. LTKN1017 and LTKN0812 showed ~ 2-fold increases in medial region relative displacement during the second half (swing phase) of the gait cycle compared with the intact condition. LTKN1017 reached peak values of 3 mm relative displacement in the medial direction which agrees with clinical diagnosis reports of pathological meniscus extrusion measured on frontal plane radiographs (see section 1.5.2). However, this was not consistent and for other samples the relative displacement did not change greatly when severe root damage was applied. In these cases, changes in displacement were measured for both the tibia and the meniscus marker results across the gait cycle, when severe root damage was applied. Due to the nature of the relative displacement calculation, if the magnitude of tibial displacement increased in one direction and the amount of meniscus displacement increased in the same direction; the effect on the relative displacement was minor. The validity of using the tibia marker as a reference was questioned as a result. However, part of the novelty of this dynamic experimental model involved including the moving tibia as a reference to measure the relative meniscus movement. The adduction-abduction arm of the simulator could be fixed in future experiments to control this variation, however, applying too much constraint to a simulated cadaveric knee may increase the risk of fracture. Perhaps in future investigations of the motion capture method, assessing the relative displacement of the meniscus with reference to the simulator tibial outputs maybe considered to maintain a regular reference between conditions.

Furthermore, in other cases tearing the root completely did not generate large changes in relative displacement magnitude but became disconnected from the typical pattern of displacement observed for the *intact*, *capsule removed* and *partial tear conditions*. In addition, the root tear conditions had a larger effect on the anterior-posterior displacement of the medial meniscus, as compared with the findings of the porcine study. When the medial meniscus posterior root was completely torn, the amount of measured relative displacement tended to decrease in the anterior-posterior direction. This maybe counter intuitive, as one may expect increased movement with damage (Ikeuchi et al., 1998; Hein et al., 2011; Ozeki et al., 2020; Paletta et al., 2020). The tibial anterior-posterior displacement carriage was driven during this study, causing only small changes

in the anterior-posterior tibia marker displacement to occur between the conditions. Most of the change in relative displacement came from the increased meniscus marker displacement, which followed a similar pattern and shape as the tibia displacement with severe root damage. The effect was less overall relative displacement as the meniscus displacement became less responsive to the action of the femoral condyles and was taken by the driven action of the tibia. It was possible that without the constraint of the root, the meniscus became unconnected and was moved passively by the action of the tibia. In addition, the recoverability of the medial meniscus was disrupted with root damage during the cyclic nature of knee simulation.

Walczak et al. (2021) measured dynamic medial meniscus extrusion in cadaveric knee samples using an LVDT during an unloaded 0° - 90° passive flexion experiment with the posterior root detached. The LVDT was positioned posteriorly on the meniscus, near the site of the root tear injury. The results showed a non-linear relationship between increasing flexion angle and medial meniscus extrusion. When the root was detached, the medial meniscus extruded to maximum displacement (3.5 mm) by 50° flexion, with the highest rate of displacement occurring within the first 30° of flexion. Thereafter, from 50° to 90° flexion, medial meniscus extrusion plateaued. In clinic, Karpinski et al. (2019) assessed the dynamic changes of the extruded medial meniscus in a group of patients with diagnosed meniscus extrusion against a healthy patient group. MRI scans were taken with patients in the supine position followed by another MRI scan with the patient upright and load bearing. The change in extrusion was measured between the MRI scans and despite the extrusion group having significantly increased medial meniscus displacement in the supine position, the change in extrusion was significantly less than the healthy group. Furthermore, an *in-vivo* MRI study found less anterior-posterior medial meniscal movement when correlated with grade of cartilage abnormality of medial compartment and therefore a high chance of associated meniscus extrusion (Kawahara et al., 2001).

The findings from this human tear study and those discussed in the studies above may be in support of the simultaneous functionality of the meniscus; suggesting that during dynamic movement, the damaged meniscus displaced less than the intact meniscus because the load bearing function has been disrupted. On the other hand, it should be stressed that no definitive conclusions on human medial meniscus behaviour can be drawn due to various associated limitations such as study sample size mentioned above and in the next chapter, however, the novel methodology developed showed it was possible to assess meniscus injury under functional conditions in human knee joint specimens.

6.6 Meniscus Allograft Transplantation (MAT) Study

A medial meniscus allograft transplantation (MAT) was performed on three samples to assess the efficacy of the experimental model in response to an intervention condition in comparison to an intact meniscus and a damaged (completely torn root) condition.

6.6.1 MAT Methodology

As previously shown in Table 6.1, the MAT procedure was performed on n=3 samples in total (LTKN1017, RTKN1952 and LTKN1409). One sample (LTKN1409) had previously undergone long duration wear testing (48 hours) and had osteochondral plugs removed from the femoral condyles, however, the results were included as part of the human intervention method development process. The conditions studied for each sample in the MAT study were the intact meniscus (same as the capsule removed condition) the completely torn medial posterior root (complete tear) and the allograft intervention condition (MAT) described in the next section. Due to the uncertainty of the intact knee capsule condition disturbing the pin motion and affecting the measurement, and the absence of this condition in two of the three samples, this condition was not included in the MAT study.

6.6.1.1 MAT Procedure

The MAT procedure was performed by a trained colleague after assessing the completely torn condition for each sample. The procedure is described in steps 1 – 6 in Figure 6.10. (1) The medial meniscus was cut out with a scalpel, leaving the connective tissue of the meniscus rim attached to the tibia and cutting the medial meniscus anterior root at the insertion site. (2) The remaining anterior and posterior horns of the removed medial meniscus graft were sutured with vertical loop sutures and a securing overlock. A rim suture was also placed on the graft body. (3) Tibial tunnels were then drilled from the original positions of the medial meniscus anterior and posterior root insertion sites. A 3.5 mm cannulated drill was used and guided through an arthroscopic ACL drill guide (Smith & Nephew, Memphis, TN, USA). The drill guide ensured the anterior and posterior tibial tunnels exited the bone in the same location anteriorly though the proximal tibia (anterior tibia drill site). (4) Guide sutures attached to eyelet guide wires were fed through the anterior tibia drill site and the loops of the guide sutures appeared at the anterior and posterior root insertion sites on the tibial plateau. (5) The trailing horizontal limbs of the medial meniscus graft horn sutures and rim suture were held around the horn and rim guide sutures. The eyelet guide wires were then pulled back through the tibial tunnels, so

the graft horn sutures appeared through the anterior tibia drill site. (6) The horn and rim sutures were secured, and multiple mattress sutures were used to secure the graft to the rim around the perimeter. Figure 6.11 shows images of the completed MAT produce on two samples.

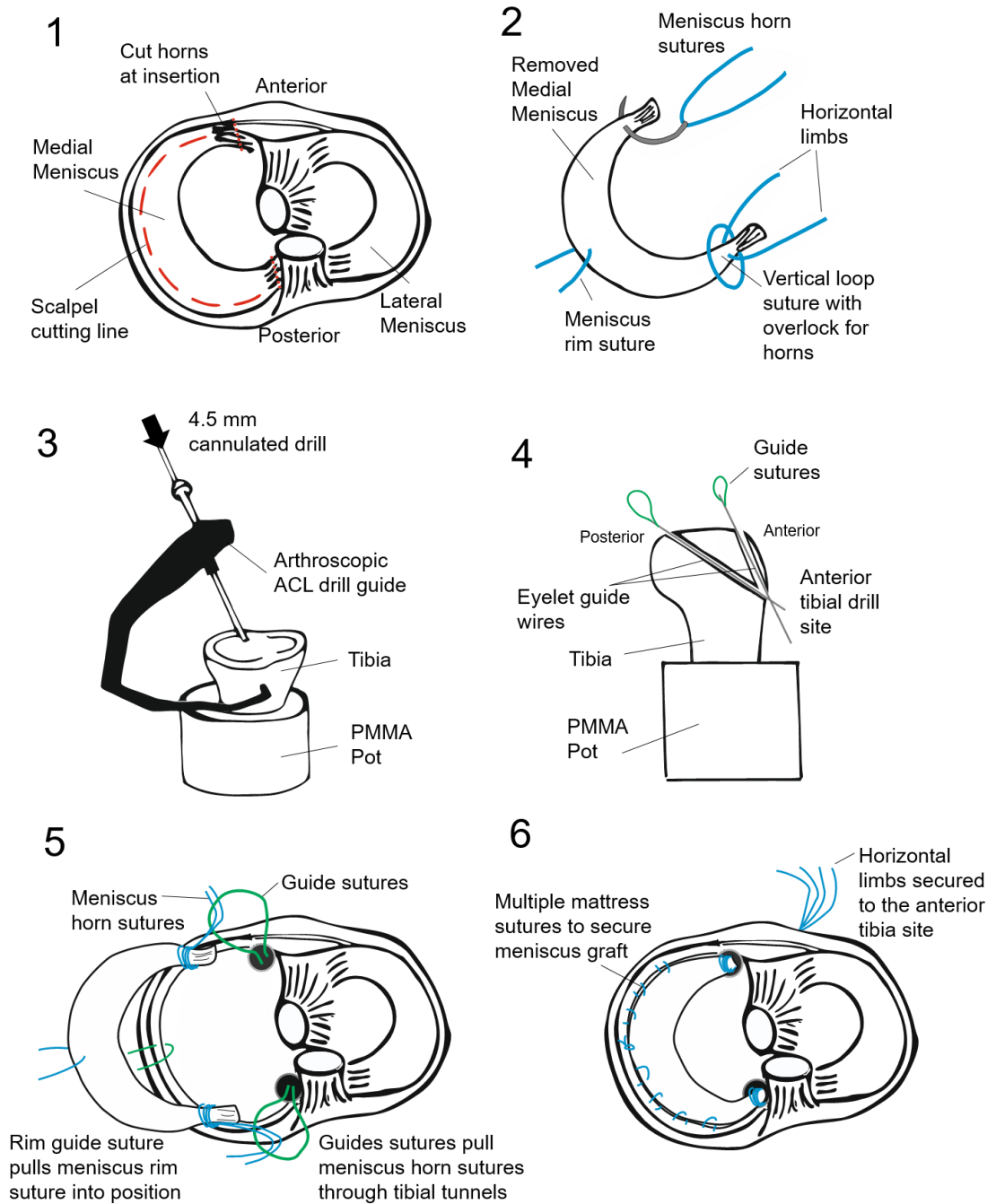


Figure 6.10. MAT intervention procedure in steps 1-6.

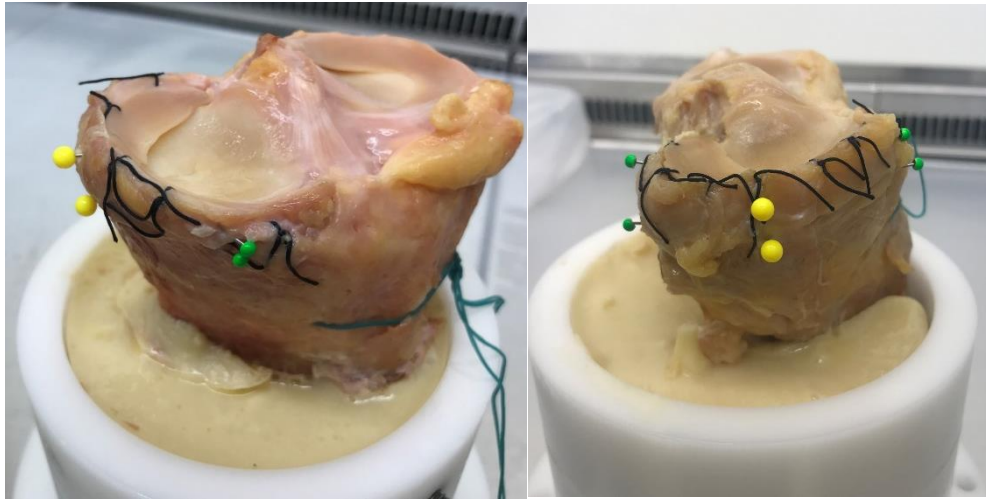


Figure 6.11. Complete MAT procedure on two human samples.

6.6.1.2 Data Analysis

The same simulated gait profile and protocol described earlier in this chapter were used for the MAT study (see section 6.3). The medial-lateral relative displacement (medial region) and anterior-posterior relative displacement (anterior region and posterior region) were processed for the intact meniscus, complete root tear and MAT intervention conditions. Due to the conclusions of the human tear study and the low sample size, statistical analysis was not performed for the MAT study. The relative displacement between the conditions was compared graphically for each sample and meniscal region. A discrete analysis incorporating the relative movement direction of all three meniscus regions in a pictograph-like schematic was also carried out in this study. The aim of this robust analysis was to understand whether the direction of movement changed between the conditions, regardless of the magnitude of measured relative displacement. The simulated gait cycle was split into four 0.5 second quarters to carry out the directional analysis. The medial, anterior and posterior region graphical relative displacement results were assessed and an estimate of the predominant direction of relative movement (medial-lateral or anterior-posterior) was given for each region at each 0.5 second period.

6.7 MAT Study Results

6.7.1 Relative Displacement Summary

The magnitude and profile of relative displacement were unique to each human knee sample and no consistent trends were measured when the MAT intervention was applied (Figure 6.12 and Figure 6.13).

6.7.1.1 Medial-lateral Displacement in the Frontal Plane, One Region

For sample LTKN1409, the *MAT* condition increased the displacement throughout the gait cycle compared to the *intact meniscus* and *complete tear* conditions. The largest peak difference was 0.95 mm compared to the *intact meniscus* in the second half of the gait cycle. The *complete tear* condition reduced the displacement by ~ 0.5 mm compared with the *intact meniscus* during the first half of the gait cycle. The peak in the second half of the gait cycle emulated a triangular shape, which was not present in the *intact meniscus* and *MAT* conditions (Figure 6.12A).

For sample LTKN1017, the *MAT* condition increased displacement compared with the *intact meniscus* condition, peaking at 2.56 mm during the second half of the gait cycle. However, the *MAT* condition reduced the displacement by ~ 0.5 mm compared to the *complete tear* condition; bringing displacement slightly closer to that of the *intact meniscus* (Figure 6.13A).

For RTKN1952, the *MAT* condition showed a reduction of 0.66 mm during the first half of the gait cycle compared with the *intact meniscus* condition. The displacement for the *intact meniscus* and *complete tear* conditions were similar throughout the gait cycle, with differences falling within the assumed measurement error (Figure 6.13D).

6.7.1.2 Anterior-posterior Displacement in the Sagittal Plane, Two Regions

For both the anterior and posterior regions, the *MAT* condition for LTKN1409 produced a ~ 1.96 mm higher displacement during the second half of the gait cycle, compared with the *intact meniscus*. However, the *complete tear* condition reduced the amount of displacement by ~ 1.85 mm compared to the *intact meniscus* at this time-point (Figure 6.12 B, C).

In the posterior region, the *complete tear* altered the pattern of displacement and became unconnected to the pattern shown for the *intact meniscus* during the first half of the gait cycle. However, the *MAT* procedure corrected this, following a similar pattern to the *intact meniscus* but displacing at a ~ 1 mm higher magnitude in the first half (Figure 6.12C).

For sample LTKN1017, in the anterior region, the *MAT* intervention increased the displacement by ~ 1 mm and created a plateau in the profile throughout the middle section of the gait cycle when compared with the *intact meniscus* and *complete tear* conditions. Small differences of 0.5 mm in displacement between the *intact meniscus* and *complete tear* conditions occurred throughout the gait cycle (Figure 6.13B). In the posterior region, the *MAT* condition increased displacement by 2.43 mm compared with the *intact meniscus* condition, peaking at ~ 6 mm in the second half of the gait cycle. The opposite

effect was measured for the complete tear condition which presented a peak reduction of ~ 1.5 mm from the *intact meniscus* condition in the second half of the gait cycle (Figure 6.13C).

For RTKN1952, in the anterior region, the *MAT* condition showed increased displacement of approximately 0.70 – 1.50 mm more than the *intact meniscus* during the first half of the gait cycle. During the second half of the gait cycle, displacement decreased by 1.82 mm and 2.29 mm for both the *complete tear* and the *MAT* condition, respectively, compared to the *intact meniscus* condition (Figure 6.13E). In the posterior region, a similar result to LTKN1409 was found for RTKN1952, as the *MAT* procedure corrected the increase in displacement measured for the *complete tear* condition during the first half of the gait cycle, causing the *MAT* condition to follow a similar pattern to the *intact meniscus* within the assumed measurement error during the first half of the gait cycle. However, during the second half of the gait cycle the *MAT* condition reduced the displacement compared to the *intact meniscus* condition by 1.75 mm, whereas the *complete tear* and *intact meniscus* displaced at a similar magnitude during this period (Figure 6.13F).

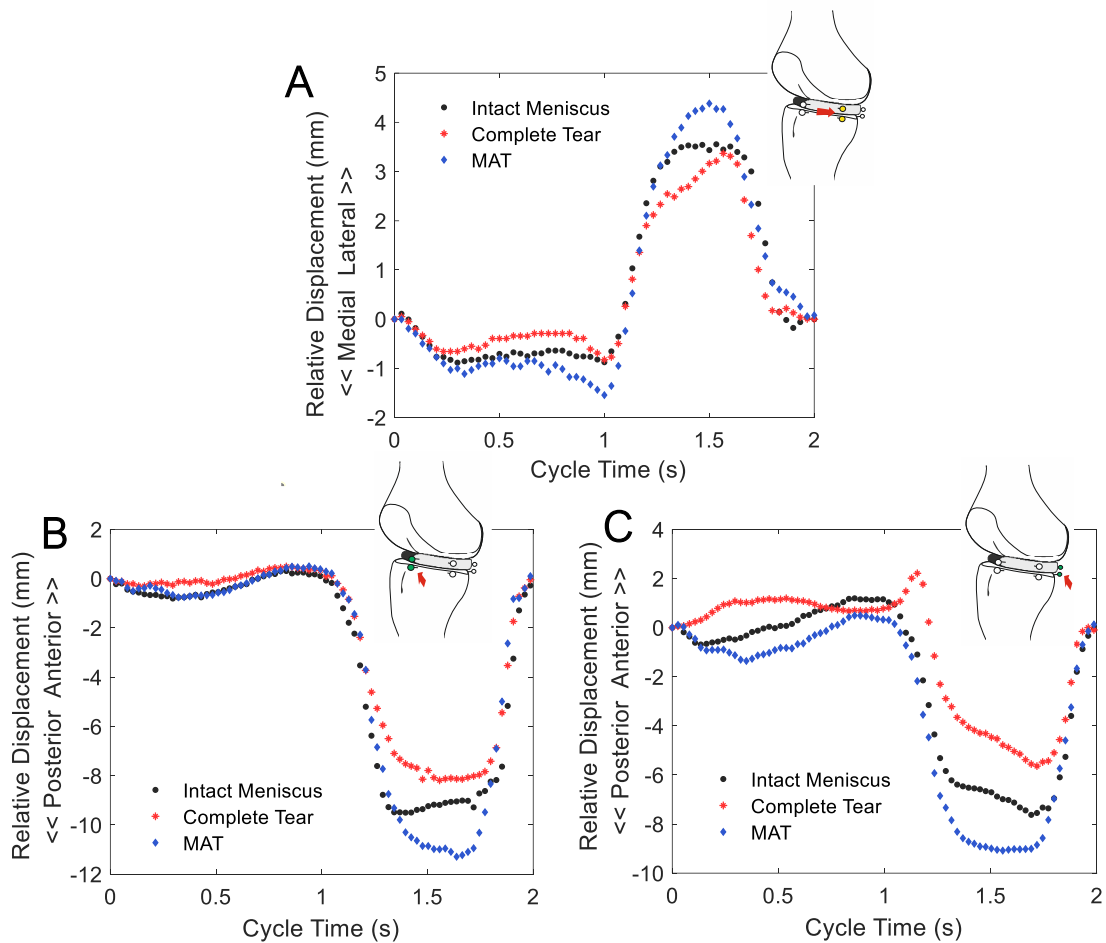


Figure 6.12. Human sample LTKN1409 relative displacement results for the (A) medial, (B) anterior and (C) posterior regions across one simulated gait cycle.

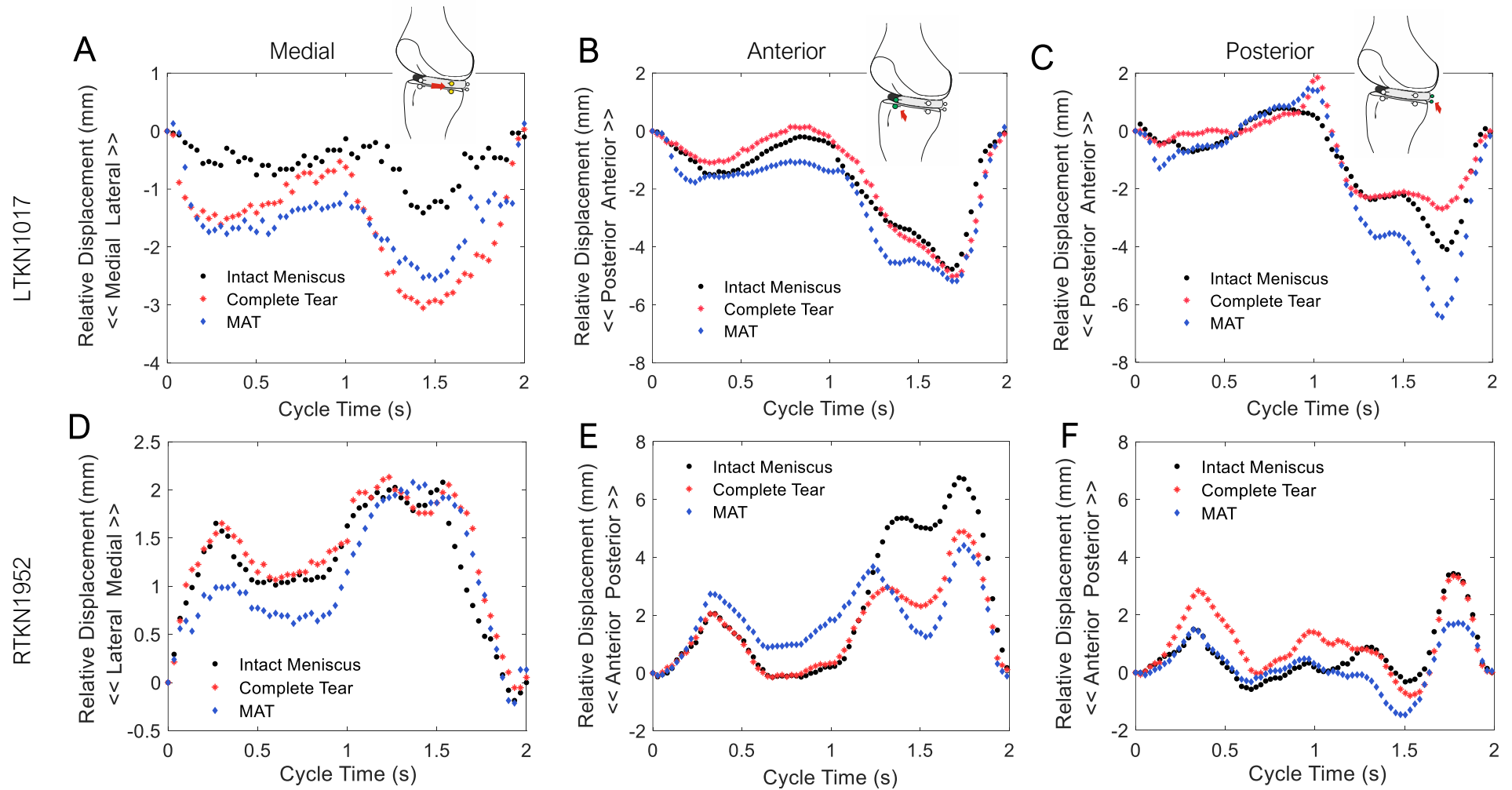


Figure 6.13. Relative displacements for the medial, anterior and posterior regions of (A-C) LTKN1017 and (D-F) RTKN1952 (human).

6.7.2 Relative Displacement Directional Analysis

Samples LTKN1017 and LTKN1409 showed a similar direction pattern of anterior-posterior meniscus motion for the *intact meniscus* condition (Figure 6.14 and Figure 6.15A). This followed a pattern of posterior movement between 0 - 0.5 seconds, anterior movement between 0.5 – 1.0 seconds, posterior movement between 1.0 – 1.5 seconds and anterior movement between 1.5 – 2.0 seconds; roughly following the periods of gait cycle flexion (posterior movement) and extension (anterior movement).

When the root was completely torn, LTKN1049 and LTKN1017 showed a change in the direction of anterior-posterior movement during the first half of the gait cycle, when most of the load was applied. The posterior region, near the site of the root tear, moved in the anterior direction between 0 - 0.5 seconds for both samples (Figure 6.14 and Figure 6.15A). However, the effect continued for LTKN1409 into the next period between 0.5 - 1.0 seconds, where the posterior region also moved in the posterior direction when the femur extended.

The direction of movement in the anterior region between 0 – 0.5 seconds was unclear and approximately zero for LTKN1409 (Figure 6.14). When the MAT procedure was carried out, the changes in the directional movement were restored to the intact meniscus movement in the first 0 – 0.5 seconds of the gait cycle for both LTKN1409 and LTKN1017 (Figure 6.14 and Figure 6.15A). During 0.5 – 1.0 seconds, the direction of the posterior region was restored for LTKN1409, however, the direction of the anterior region for LTKN1017 changed from an anteriorly inclined movement to a plateaued displacement. There were no clear changes in the direction of medial-lateral movement between the conditions of LTKN1409 and LTKN1017 found during this analysis.

The directional movement of the medial meniscus for sample RTKN1952 was different to the other samples and more difficult to generalise within the four gait cycle periods (Figure 6.15B). However, the *intact meniscus* directional movement for sample RTKN1952 was similar in the first 0 - 0.5 seconds of the gait cycle; moving posteriorly and medially. The *MAT* condition presented changes in the measured direction of relative movement compared to the *intact meniscus* during multiple periods of the gait cycle (0.5 – 2.0 seconds).

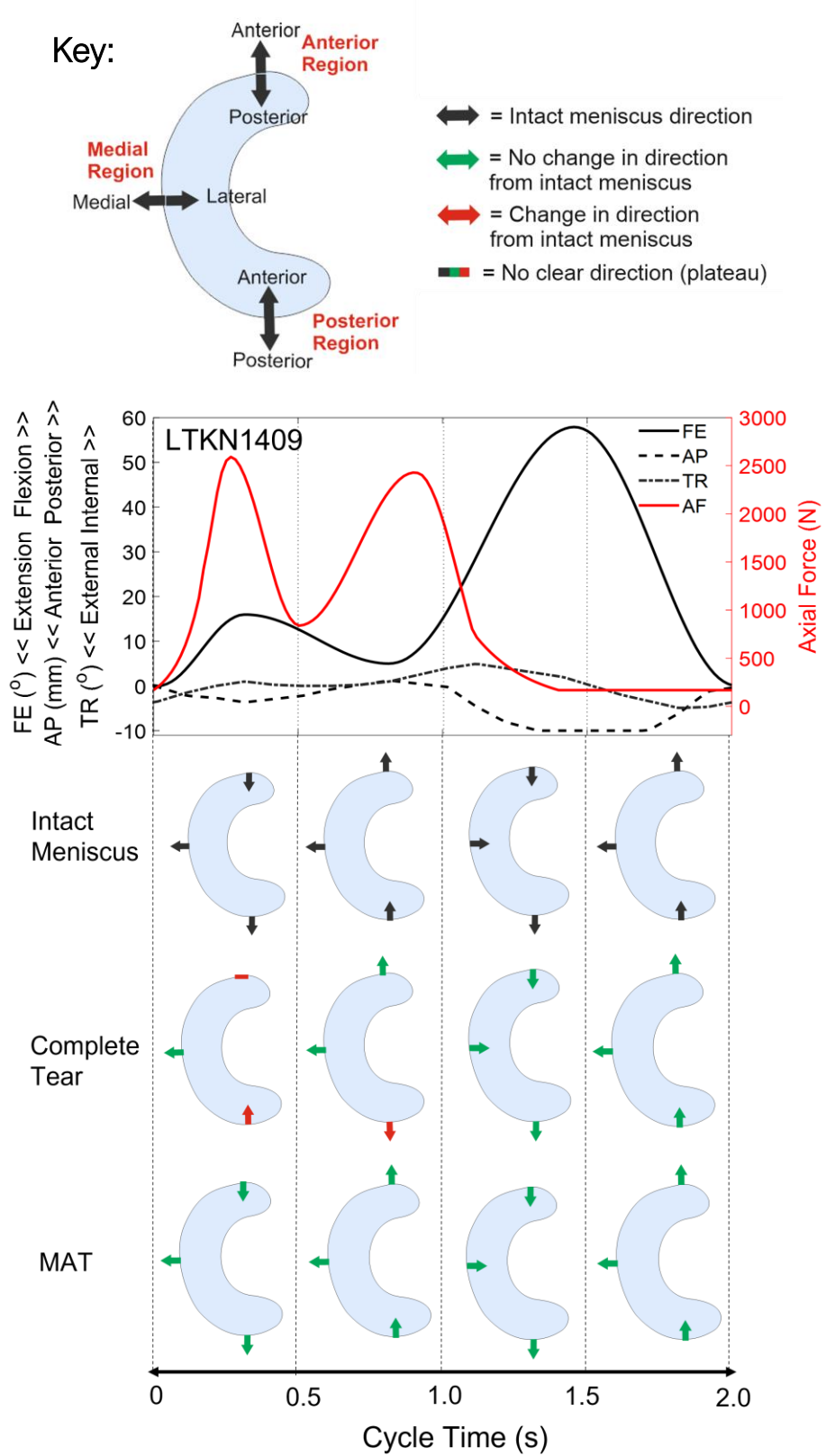


Figure 6.14. Medial meniscus directional analysis for human sample LTKN1409, showing the driven axes of the simulated gait cycle and schematics of the estimated direction of regional relative displacement for each 0.5 second gait cycle period. See key at the top.

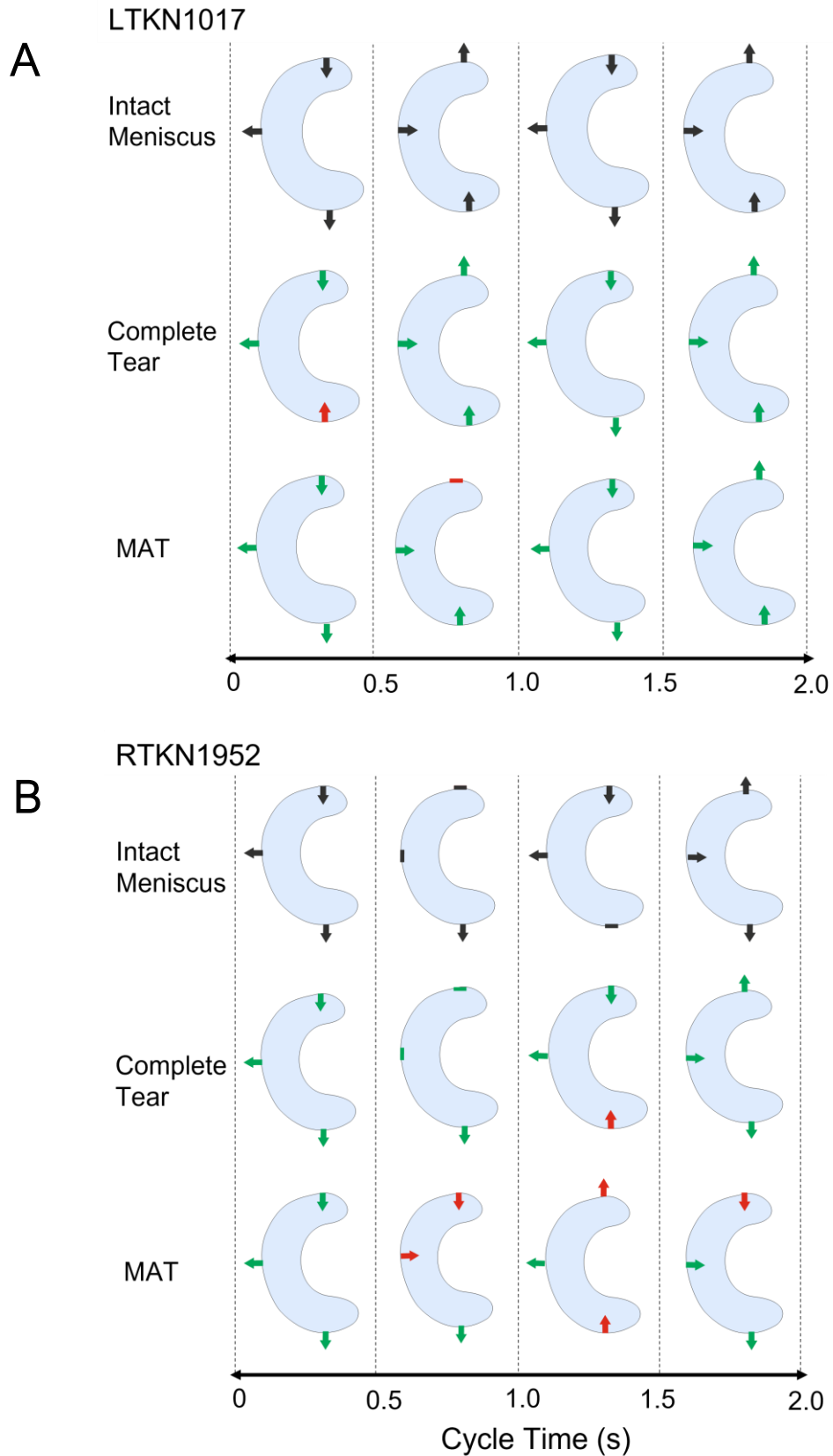


Figure 6.15. Medial meniscus directional analysis for human sample (A) LTKN1017 and (B) RTKN1952, showing the schematics of the estimated direction of regional relative displacement for each 0.5 second gait cycle period. See key on previous page.

6.8 MAT Study Discussion

The main purpose of this study was to understand if an intervention could be assessed with the novel motion capture experimental model; to form the basis of a pre-clinical biomechanical assessment.

6.8.1 Main Findings

The main findings were:

- The motion capture model was able to measure the relative displacement of the medial meniscus with an MAT intervention applied throughout the duration of a simulated gait cycle;
- each sample presented a unique pattern of relative displacement;
- the relative movement of the MAT intervention varied between each sample when compared with the *intact meniscus* and *complete tear* conditions;
- when observing discrete directional changes between the conditions, the *MAT* condition roughly corrected the anterior-posterior movement of LTKN1409 and LTKN1017 after a *complete tear*, to move in a similar direction to that of the *intact meniscus* condition.

6.8.2 Limitations

The limitations for the intervention study are mostly consistent with those described previously. Sample LTKN1409 was previously long-term wear tested in lubricant and had undergone one more freeze-thaw cycle than the other samples. Poor tissue quality for this sample may have affected the meniscus kinematics, however, using this sample was an important step in initially assessing the feasibility of the intervention experimental model. The MAT procedure was undertaken by a trained colleague; however, it was difficult to control this positioning between samples, especially when pulling the sutures to secure the graft to the tibia. Using a trained orthopaedic surgeon in future studies would help reduce possible inconsistencies with the MAT procedure. Moreover, there were instances when the marker pins fell out of position due to the nature of performing the MAT procedure. Using the marker positioning method, the markers pins were reattached after the MAT procedure had been carried out, however, small changes in these pin locations could have affected the results.

6.8.3 Effect of the MAT Intervention

The use of an MAT in clinic remains controversial, despite it being the gold standard for total meniscus replacement. Previous biomechanical studies have shown positive outcomes in terms of contact areas and contact pressures with an MAT in comparison to a meniscectomy, especially with bone plug surgical fixation techniques (Kim et al., 2013; Brial et al., 2019; Ambra et al., 2019). However, the restoration of native meniscus biomechanics remains unclear and dynamic displacement analysis of the allograft transplanted meniscus has not been studied to great extent. In Vrancken et al. (2016) RSA was used to assess dynamic medial-lateral and anterior-posterior translation for the native medial meniscus, a polyurethane total meniscal implant and an MAT in cadaveric samples experiencing a dynamic squat loading regime. The implant and the MAT performed similarly, showing a significant increase in posterior and medial translation compared to the native meniscus. The researchers concluded that the implant or the MAT could not restore the native meniscal function as increased meniscal mobility alludes to increases in abnormal cartilage loading.

Herein, the goal of the MAT intervention was to bring the relative displacement of the medial meniscus across the gait cycle closer to that measured for the intact meniscus condition than the completely torn root condition. In general, it was difficult to draw conclusions on the effectiveness of the MAT procedure in comparison with the other conditions due to the limitations of the methodology. However, some trends were identified which could be examined further in future study. In most cases, the relative anterior-posterior displacement increased throughout the gait cycle when the MAT intervention was examined in comparison with the intact meniscus. As shown in Appendix F, the measured anterior-posterior meniscus displacement of LTKN1409 and LTKN1017 was usually lower than that of the other conditions. This effect could have been because the MAT procedure caused the meniscus autograft to be affixed too tightly to the tibia, restricting the meniscus marker movement, and therefore increasing the relative displacement with respect to the tibia marker.

Due to the novelty of this work, it is difficult to know what effect a ~ 2 mm increase in relative meniscus displacement would have on the knee joint clinically. However, a change in movement direction in relation to a control measurement possibly suggests abnormality in motion and therefore loading through the knee joint. In this analysis, when observing directional changes between the conditions, the MAT condition roughly corrected the sagittal plane movement of LTKN1409 and LTKN1017 to be similar to that of the *intact meniscus*. On the other hand, sample RTKN1952 generated more changes in direction with an MAT applied than a complete tear. This was potentially due to the variation in the suture tensioning of the complex MAT suture procedures between samples, which was carried out by a researcher, not a clinician. It was therefore difficult to

draw conclusions into the effectiveness of the MAT intervention, however, the directional analysis included in this study is an important step in understanding the holistic movement of the medial meniscus throughout the gait cycle, and if this changes when a damaged and intervention condition are assessed. So far within this project, the relative displacements of each meniscus region (medial, anterior and posterior) have been analysed individually to one another. This analysis additionally shows how the relative displacement data may be used with each other as a set of coordinates to visualise movement of the meniscus.

Differences in the displacement results between knee samples could be attributed to limiting factors of the experimental procedure such as variation in the suturing fixation, knee specimen quality and low sample size. However, what was possible to establish was that the methodology was able to measure relative displacement in the medial-lateral and anterior-posterior directions with an MAT intervention applied and compared with the healthy and a torn case. However, in terms of the marker-based motion capture methodology, further developments would have to focus on the challenge of ensuring correct locations of marker pins on the reinserted meniscus graft.

Chapter 7

Overall Discussion

7.1 Research Rationale

The meniscus is a dynamic tissue; the ligamentous root attachments and specialised shape allow the meniscus to move and deform with knee load and motion. This allows the meniscus to adopt simultaneous mechanical functionality of load transmission and knee stability, to protect the articular cartilage from damage and stabilise the knee; the latter function could be comparable to that of an extra ligament (Fairbank, 1948; Walker and Erkman, 1975; Shrive et al., 1978).

Pathological meniscus extrusion occurs when the meniscus adopts an abnormal position and is usually the result of a traumatic root tear injury. This disrupts the load transmitting function of the meniscus, leading to accelerated cartilage degeneration and associated osteoarthritis (Costa et al., 2004; Gajjar et al., 2021). Therefore, meniscus displacement, which incorporates both the deformation and movement of the meniscus with the application of knee joint load and motion is an important metric to assess in preclinical investigations of meniscus interventions. However, functional biomechanical assessment of the meniscus has not been studied to great extent. Most biomechanical cadaveric studies assess meniscus biomechanics and meniscus interventions using static or quasi-static loading regimes. These regimes do not properly apply the simultaneous shear, compressive and tensile forces the meniscus experiences *in-vivo*. There are only a handful of studies which measure dynamic meniscus displacement to investigate meniscus function. To the authors knowledge, meniscus displacement has not yet been measured continuously throughout a physiologically loaded simulated gait cycle *in-vitro*.

This research aimed to fill these gaps in knowledge through developing a novel methodology to assess dynamic displacement of the meniscus relative to the tibia in the frontal (medial-lateral displacement) and sagittal (anterior-posterior displacement) planes of human cadaveric knee joints undergoing a simulated gait cycle, with applied physiological load and motion parameters. Therefore, establishing a potential experimental model to assess the biomechanics of meniscus interventions pre-clinically.

7.1.1 Aims

1. To develop a novel method to measure dynamic meniscus displacement in a human tibiofemoral joint undergoing a simulated gait profile in the knee simulator.
2. To develop a pre-clinical biomechanical model measuring meniscus displacement to assess the effects of meniscus extrusion and the efficacy of a meniscus intervention in comparison with a healthy and a damaged (root tear) condition.

7.2 Main Findings

7.2.1 Development of the Marker Tracking Methodology

A MatLab video marker-tracking technique using an object detection code was incrementally developed from preliminary studies using a simple ImageJ screenshot technique whilst applying simplified loading conditions to porcine medial meniscus in the frontal plane and sagittal plane. Further developments included reliability assessments which estimated the minimum measurement error of the MatLab marker tracking method to be within ± 0.1 mm accuracy when compared to known displacements of a marker on a solid plastic body moved by the simulator's anterior-posterior translation output. Other forms of error were investigated, such as the inter-observer and intra-observer variability when calibrating the video to display the tracking results in millimetres and not pixels. Observer variation was found to be within the band of ± 5 pixels in 8 subjects generating a possible 1.7% measurement error. Camera lens distortion was also investigated using an intrinsic camera calibration; however, this was found to have small effects (max 0.03 mm) on the marker-tracking measurement. However, these values were dependent on conditions such as camera position, marker position/size and lighting. In addition, the application to knee specimens would also affect these values due to differences in material properties and 3D tibial rotation during the gait cycle.

The finalised motion capture method using the MatLab marker-tracking technique estimated the continuous displacement of moving coloured marker throughout the duration of one simulated gait cycle, run at 2 seconds speed (0.5 Hz) per cycle. Three Raspberry Pi cameras illuminated with LED lights were programmed to capture the anterior-posterior displacement (anterior and posterior region) and medial-lateral displacement (medial region) of the medial meniscus. Each region had a marker pinned into the medial meniscus and a reference marker on the tibial plateau. The relative meniscus displacement was used as the main outcome measure to characterise the displacement of the meniscus marker relative to the tibial marker.

7.2.2 Feasibility Assessment of the Experimental Model on Porcine Samples

The feasibility and verification of using the motion capture method as a pre-clinical experimental model was assessed on porcine knee specimens ($n = 4$). The novel methodology was able to detect a 2-fold increase in medial-lateral relative displacement (medial region) during the simulated gait cycle (cycle 3) when the medial meniscus posterior root was cut most severely (92% of the root width (*TORN3*), 6 mm from the insertion), compared to all other assessed conditions, however; this was not strongly statistically significant. In addition, there was evidence of the medial meniscus with a 92% root tear moving radially, or extruding, throughout the duration of each 50 cycle test. Small differences in relative displacement were detected between the capsule dissection conditions (*CAP*, *NOCAP* and *NOLIG*) and the initial root cuts spanning 15% and 46% of the root width (*TORN1* and *TORN2*). In the sagittal plane (anterior and posterior regions), little differences were detected between the dissection and root tear conditions. However, the relative meniscus displacement profile roughly reflected the kinematic flexion-extension input profile of the simulated gait cycle.

7.2.3 Assessment of the Experimental Model on Human Knee Joint Specimens

The experimental model was then applied to human knee samples ($n = 4$) with root tear injury and human knee samples ($n = 3$) with a meniscus allograft transplantation (MAT) intervention. The model was slightly adapted from the porcine investigation to be able to assess larger human knee samples and incorporate the MAT procedure. Minimal differences in relative displacement or all regions were found with cyclic test duration in the human tear study. The relative displacement in the medial-lateral and anterior-posterior directions was found to be unique to each human sample, generating a large amount of variation when comparing sample means together. The most prominent differences in relative displacement occurred for the most severely torn condition with most cases showing a decrease in anterior-posterior relative displacement throughout the gait cycle, compared with the intact condition.

An MAT intervention was assessed in three human specimens against an intact meniscus condition (knee capsule and ligaments removed) and the completely torn root condition. These findings showed variable effects of the MAT intervention on the relative displacement of the medial meniscus. In some cases, the MAT intervention corrected the direction of anterior-posterior relative displacement to follow a similar pattern to the intact meniscus condition. A discrete directional analysis of all three medial meniscus regions was carried out throughout the four quarters of the gait cycle to assess this. However, it was difficult to control the amount of connective tissue remaining in the completely torn

conditions or the tensioning of the sutures in the MAT, which could have provided more constraint in some knees than others.

7.3 The Technical Challenge of the Motion Capture Method

The technical challenge of this thesis was designing a measurement system that was low-cost and small enough to be able to fit into a high-load knee wear simulator and be able to withstand loads of up to 2600 N during simulated human gait. In addition, to allow the knee joint to be able to move freely throughout the applied gait cycle without too much manipulation to the tissue. The system also had to provide a sufficient level of accuracy and precision to be sensitive to measure changes in tissue states of the medial meniscus to model meniscal extrusion, root tear injury and meniscus interventions. A camera-based motion-tracking method was chosen because this allowed free movement of the knee in the simulator, allowing dynamic physiological gait parameters to be applied. This method also allowed manipulation of the knee capsule conditions as the marker pins could be pinned directly into the meniscus through the capsule and the capsule dissected around the pins to maintain the marker positions.

In recent years, advanced 3D coordinate measuring systems have been applied to biomechanical meniscus studies (Daney et al., 2019; Hirose et al., 2022). Daney et al. (2019) assessed meniscus extrusion using a portable probe coordinate measuring device in 10 cadaveric knee joints in the intact, root tear, and sutured repaired states. The knees were assessed under 1000 N axial load and 0° and 90° static flexion angles. Hirose et al. (2022) used a commercial motion capture system with optical cameras and retroreflective markers on the porcine lateral meniscus to understand the displacement changes which occur in the anterior-posterior direction when the meniscus was subject to varying severities of a mid-body radial tear. A robot arm was used to apply a continuous flexion range from 20° to 90° at a constant load of 100 N, however the data was captured at 30° and 60° flexion with an applied higher load of 300 N. Although these methods have high accuracy, the knees were assessed under statically loaded conditions at specific flexion angles and/or at lower than physiological loads. The meniscus moves and deforms to withstand the compressive, shear and tensile forces experienced *in-vivo* and ideally biomechanics should be assessed in this way.

Dynamic cadaveric investigation of meniscus displacement has been assessed previously using radiographical methods such as roentgen stereographic analysis (RSA) and MRI (Thompson et al., 1991; Bylski-Austrow et al., 1994; Vrancken et al., 2014). Displacement measurement probes have also been used throughout a continuous unloaded flexion range of motion (Walczak et al., 2021). However, in these studies lower

loads are usually applied (up to 1000 N) to protect cadaveric samples. The measurement of *in-vitro* cadaveric meniscus displacement during dynamic simulated gait has not been reported previously within the literature. However, the motion capture system developed within this project was able to measure relative medial meniscus displacement under physiological gait conditions in human knee joints, reaching loads of ~ 2600 N.

Moreover, the developed motion capture system was low-cost and used resources available in the institute with additional purchasing and manufacture costs amounting to ~ £300. The system was also compact and able to measure marker displacement at a minimum distance of ~ 30 mm away from the sample, making it accessible for a variety of other tissue-level displacement applications within the wider research field. Developing resourceful and accessible measurement systems which are low cost are striking interest within the research community.

However, a trade-off occurs as lower cost generally comes with a lower level of method precision, which was true for this project. Hirose et al. (2022) stated the accuracy of the commercial motion capture system when assessed using the robot arm was +/- 0.041 mm and acceptable under the researchers self-proposed threshold of < 1.00 mm. Error estimations of +/- 0.1 mm were found when this projects novel marker tracking method was assessed using known translations of the simulator and a moving marker on a solid body. However, it was likely this error threshold increased when assessing natural knee joints with the motion capture technique in this thesis, due to addition of 3D tibial motion, material properties of biological tissues and movement associated with the pin. On the other hand, this research showed that this level of error was acceptable to obtain relative medial meniscus displacement estimations from porcine and human knee joint samples during a simulated gait cycle, because characteristics of the applied axial force and flexion-extension profiles were reflected in the relative displacement data. In addition, when intact (capsule retained) results from the human tear study were compared to published *in-vivo* and *in-vitro* studies assessing dynamic meniscus displacement during flexion activities, the mean peak values fell within in a similar range (see section 6.5.4). Findings which showed little statistical strength were more likely to do with factors associated with the experimental procedure, rather than the motion capture method.

On the other hand, a trade-off with robustness also emerges as speed of simulation, camera positioning and lighting were imperative to control between each condition to obtain clear and comparable tracking results, whereas commercially available systems are more versatile to apply to different situations. Expensive commercial motion capture systems also have the capability of obtaining 3D measurements, although these systems would not be compatible to operate in such a small sample area of the knee simulator. Herein, the motion capture system was developed in 2D assessing two important anatomical planes of motion at three meniscus regions of the knee (frontal plane, medial-

lateral displacement; sagittal plane, anterior-posterior displacement). However, this system has scope for further developments, including 3D estimations and simultaneous triggering (see section 7.6).

7.4 Evaluation of the Experimental Model as a Preclinical Assessment

The pre-clinical biomechanical assessment of meniscus interventions is lacking within the literature and is one of the key reasons there has only been a handful of total meniscus replacements or tissue-engineered alternatives pass clinical trials. The primary goal of developing the developed experimental model was to understand if a difference could be measured between a healthy, damaged and an intervention state. A methodology sensitive to these three conditions gives confidence in using the model as a preclinical assessment for meniscus interventions.

Meniscus displacement was governed by both the action of the tibial motion, the femoral motion and the applied axial load. Liu et al. (2020) found that each human knee specimen adopted a specimen specific spring constraint when imitating natural soft tissue constraint during force-controlled knee simulation, this led to the generation of specimen specific gait profiles. In a similar way, meniscus displacement may also specimen specific and perhaps assessing each knee individually using force controlled parameters maybe more appropriate going forward.

The response of the human medial meniscus with severe root tear injury was more complex when subject to cyclic loading regimes. In most cases a reduced relative anterior-posterior meniscus displacement was found with a complete root tear. It was possible that with the application of cyclic load the meniscus recoverability had reduced as a new position was found due to the injury, generating less overall relative displacement during a gait cycle. Clinical radiographical investigations in patients with medial meniscus extrusion have shown that the change in extrusion between supine and upright MRI scans was significantly lower than healthy patients, despite having significantly higher meniscus displacement statically (Karpinski et al., 2019) (see section 6.5.6).

Variable effects of an MAT were found during this investigation; however, the novel data fuelled original analyses into the pattern or direction of relative displacement throughout the gait cycle, rather than just assessing the magnitude. A discrete directional analysis was used for the MAT study, where the gait cycle was divided into quarters and the direction of displacement was analysed for the root tear injury and the MAT against the intact meniscus relative displacement results. In some cases, the MAT corrected the direction of the displacement to be similar to that of the intact condition at different points

throughout the gait cycle, despite increased magnitudes of relative displacement being measured with MAT (section 6.8).

The findings of this research have shown the motion capture methodology had the capability to be sensitive to assess soft tissue constraint, root tears and MAT conditions. However, the effect on biomechanics remains inconclusive and difficult to evaluate from the variation which occurred between human samples and due to limitations surrounding the experimental procedure, explained in the following section. However, this research has provided insights into medial meniscus function in response to root injury and intervention, promoting avenues for further study.

The relative displacement measurement contains both factors: deformation and movement of the meniscus and the tibial plateau. Deformation describes the change in shape of the meniscus and movement describes the sliding motion. These factors are influenced by the application of load and motion to the knee joint, which were applied simultaneously during the simulated gait cycle.

It was possible that an interplay of deformation and movement of the meniscus occurred. In some regions, the displacement measurement may reflect the meniscus deforming, in other regions, meniscal movement may dominate. It was interesting to note that in the porcine study, the first peak in the measured medial-lateral relative displacement generally coincided with the first peak of the applied axial load (see section 5.3). The meniscus marker tracking reflected the two-peaks of the axial force profile, whereas the tibia marker tracked the motion of the action of the abduction-adduction rotation as a translation (see Appendix E). When the root was severely torn, the increase in medial displacement at the first axial load peak was potentially a result of increased movement, possibly dominating deformation. During the human study, displacement peaks coinciding with the applied load and motion parameters were less prominent and varied between samples. This difference could be attributed to a range of factors such as the sample age, knee alignment, different meniscus tissue properties and pre-existing tissue degeneration.

In summary, it was difficult to deduce whether the method was most sensitive to load or motion without isolating these parameters and conducting further sensitivity analyses. Perhaps assessing the interplay between healthy meniscus deformation and movement could provide a deeper analysis of the measurement and meniscus biomechanics. Computational modelling could provide the potential to further explore the deformation and movement interplay contained within the measurement.

Moreover, the novel data produced gives insight into the positional behaviour of the medial meniscus which holds great value in computational investigations. Due to the complexity and heterogeneity of the meniscus, meniscus behaviour is only broadly

characterised in computational studies, therefore, this data could be used to aid the validation of computational finite element analysis models.

7.5 Limitations

7.5.1 Limitations of the Motion Capture Method

7.5.1.1 Marker Location

The motion marker pins were only placed on the anterior, posterior and medial peripheral regions of the medial meniscus. Therefore, meniscus and tibia displacements were only measured at these points, disregarding displacement occurring in other areas of the meniscal body and tibial plateau during gait. However, from previous literature, these locations seemed the most prominent areas to characterise meniscus movement.

7.5.1.2 Marker Pin Movement

The marker pins were inserted through the capsule into the meniscus body. There was potentially a small amount of pin movement reflected in the displacement results due to disturbance by the surrounding capsule; however, it was difficult to analyse how much this pin movement was contributing to the data. However, pins were required to enable insertion through the knee capsule and maintain marker position as tissue was dissected away to examine the dissection/root tear conditions. In future study, the fixation of the marker pins could be developed to minimise as much pin movement as possible.

7.5.1.3 Two-Dimensional Analysis

The developed motion capture method was only able to obtain 2D measurements (x and y) from the cameras. Changes occurring in the z plane can give an idea of what is happening rotationally to the meniscus during gait and with injury or intervention. However, multiple markers were placed on three different meniscal regions to assess two key movement directions to characterise movement. In addition, there is a large interest developing 2D products to obtain results due to the simplicity and accessibility. However, the benefit of this methodology is that it is scalable and has the potential to include 3D calculations into the code.

7.5.2 Limitations of the Experimental Procedure

7.5.2.1 Sample Size

Small sample sizes of 3-4 knees were used for each of the studies carried out in this thesis. A low sample size gives low statistical power to the study, and it could be that the knees assessed were outliers of the general population. However, this was mainly due to the high cost and low availability of cadaveric knee specimens.

7.5.2.2 Tissue Hydration and Degeneration

The sequential process of applying the repeated cyclic loading conditions meant that systematic bias existed during the experimental model. The biomechanical behaviour of the meniscus changes as repeated loading continues, due to the loss of water retention and increasing degeneration of the dehydrated tissue. This was a difficult factor to control and meant that the conditions were likely applied with the tissue in different states. Future study could implement a preconditioning programme before each loading test, or longer rehydration periods to try and control this factor.

7.5.2.3 Concomitant Injury of the Knee

The knee joint is an intricate system where injury to one area of the knee affects other areas and applying root tear injury to the knee joint will ultimately change the kinetics during gait. In this study the same displacement-controlled gait inputs were used to assess each knee joint regardless of size, age, alignment and regardless of the dissection, root tear and intervention conditions. Walking gait is unique to each person and a person would likely not be able to walk in the same way if root injuries occurred. However, this was necessary initially to isolate the conditions with the same input for easier comparisons relating to changes in meniscus displacement and assessment of the methodology.

7.5.2.4 Connective Tissue Control

It was difficult to control the amount of connective tissue remaining between the samples for each of the conditions, and how tight to pull the sutures when implementing the MAT procedure. This meant that some samples may have had more constraint than other samples for certain conditions, affecting the results. Future study could benefit from using an experienced orthopaedic surgeon to implement the intervention procedure and minimise inconsistencies.

7.5.2.5 Knee Alignment and Cementing Procedure

The natural knee simulation alignment and cementing methodology was based on previously developed and published methods (Liu et al., 2015; Bowland et al., 2018; Liu et al., 2020), however, there are associated limitations. The method for determining the centre of rotations (CORs) on the medial and lateral condyles was done using the bony landmarks (epicondyles) of the LCL and MCL insertions, without quantitative input or details of the natural mechanical or anatomical axes (see section 2.2.1.3 and 2.2.2.5). In the human study, MRI scans were used to assess the bone quality prior to simulation. The measurements on the MRI scans helped determine the size and epicondylar axis angle of the joint, but the lack of information on the true mechanical and anatomical axis of the leg (due to the donor sample arriving as just the knee area) made it difficult to use these measurements effectively. Moreover, the variation in knee joint size, age, condylar shape and tissue quality made it difficult for this method to be standardised across the samples. In addition, the COR holes had to facilitate the simulators COR axis to enable simulation, and not necessarily the natural COR axis of the knee joint. Therefore, an amount of variation exists during the alignment and cementing procedure and likely influences the results. However, this error was difficult to measure but could be analysed in future analysis of the cementing methodology.

7.6 Recommendations for Future Motion Capture Method

Developments – 3D Estimations

Previous studies in literature have reported the pattern of meniscus movement when subject to internal/external tibial rotation (Bylski-Austrow et al., 1994; Tienen et al., 2005). The novel motion capture methodology developed in this thesis measured medial-lateral and anterior-posterior displacement of the meniscus and tibial markers in the frontal and sagittal planes, therefore, changes occurring in the transverse plane are unknown. However, the methodology has scalable potential to further estimate medial meniscus movement in 3D; measuring the changes which may occur in the transverse plane (internal/external tibial rotation) with injury and intervention. There are couple of methods in which these 3D estimations could be achieved in future developments. These are illustrated in Figure 7.1 A and B.

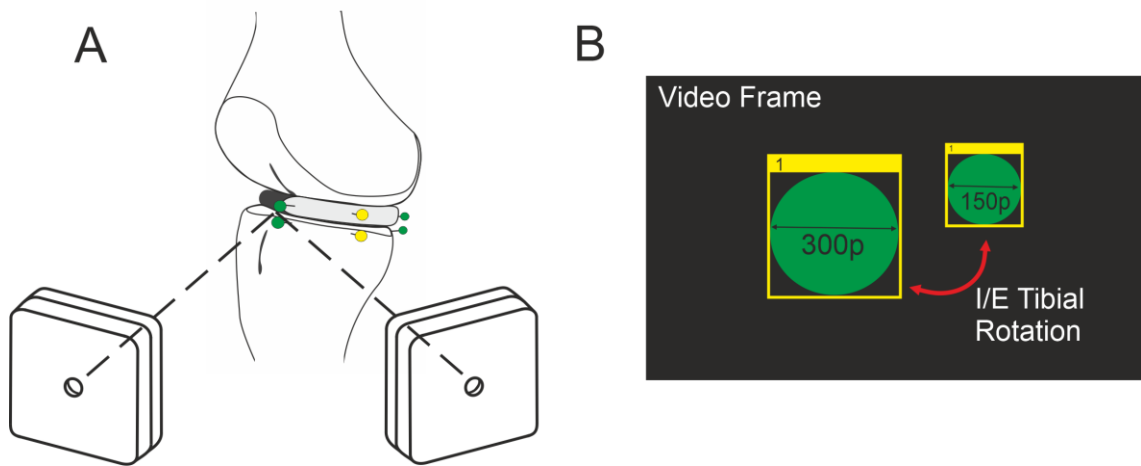


Figure 7.1. Future developments of the motion capture methodology to estimate 3D changes in meniscus movement with internal/external (I/E) tibia rotation. (A) Camera triangulation. (B) Estimation of changing distance of the marker away from the camera lens using the width of the marker in pixels (p).

Camera triangulation is a mathematical reconstruction method whereby the 3D position of an object on two different images can be estimated in space (Figure 7.1 A) (Hartley and Zisserman, 2003). This method would require a stereo camera set up and accurately measured distances/angles, however, this could be included into the MatLab script. The online Matlab documentation includes information on how to use the software's built in 'triangulate' functions to obtain 3D estimates (Lourakis, 2023).

The second 3D method uses the same camera set-up of the current motion capture method and would require a few more parameters to be calculated within the code. The blob analysis function used to detect objects in an image finds the centroid of the object but also the width of the bounding box, so this can be tracked throughout the video. As show in Figure 7.1 B, when the marker is closer to the camera lens, the width of bounding box (p = pixels) will increase, and when the marker is further away, the width of the bounding box will decrease. This method would estimate the change in depth of the marker based on the width of the marker in each video frame. An estimation of the distance of the marker away from the camera would have to be made initially; this is possible using MatLab's camera calibration tool (The MathWorks, 2022).

7.7 Conclusion

The meniscus adopts simultaneous functionality; however, functional biomechanical assessment of the meniscus is lacking in the literature. In this thesis, a novel motion capture method was designed, developed, verified and validated to assess dynamic medial meniscus displacement in the medial-lateral and anterior-posterior directions of cadaveric knees experiencing a simulated gait cycle. The knees were also assessed in conjunction with varying levels of knee capsule constraint, medial meniscus posterior root tear injury and a meniscus allograft transplantation. Limitations associated with the experimental procedure prevented statistically strong conclusions to be found, however, the developed methodology provides a potential tool to assess dynamic meniscus displacement preclinically, and further study could provide useful insights into the native biomechanical function of the medial meniscus and the changes that occur with injury and intervention. The novel displacement data may also be beneficial as a validation for computational models of the medial meniscus. In addition, the practical applications of the motion capture system may stretch further than the bounds of meniscus tracking and the knee joint. Providing a low-cost and convenient estimation of tissue-level mechanics to a variety of applications suitable for marker-based tracking.

References

- Abdelgaid, A., Fisher, J. and Jennings, L.M. 2022. Understanding the differences in wear testing method standards for total knee replacement. *Journal of the Mechanical Behavior of Biomedical Materials*. **132**(April), p.105258.
- Abraham, A.C., Edwards, C.R., Odegard, G.M. and Donahue, T.L.H. 2011. Regional and fiber orientation dependent shear properties and anisotropy of bovine meniscus. *Journal of the mechanical behavior of biomedical materials*. **4**(8), pp.2024–2030.
- Achtnich, A., Petersen, W., Willinger, L., Sauter, A., Rasper, M., Wörtler, K., Imhoff, A.B. and Diermeier, T. 2018. Medial meniscus extrusion increases with age and BMI and is depending on different loading conditions. *Knee Surgery, Sports Traumatology, Arthroscopy*. **26**(8), pp.2282–2288.
- Ahmed, A. and Burke, D. 1991. In-vitro measurement of static contact pressure distribution in synovial joints. *Mechanics Computing in 1990's and Beyond*. **105**(August), pp.579–583.
- Ahmed, I., Khatri, C., Parsons, N., Hutchinson, C.E., Staniszewska, S., Price, A.J. and Metcalfe, A. 2020. Meniscal tear outcome (METRO) review: A protocol for a systematic review summarising the clinical course and patient experiences of meniscal tears in the current literature. *BMJ Open*. **10**(8), pp.1–5.
- Alhalki, M.M., Howell, S.M. and Hull, M.L. 1999. How Three Methods for Fixing a Medial Meniscal Autograft Affect Tibial Contact Mechanics. *The American Journal of Sports Medicine*. **27**(3), pp.320–328.
- Allaire, R., Muriuki, M., Gilbertson, L. and Harner, C.D. 2008. Biomechanical consequences of a tear of the posterior root of the medial meniscus: similar to total meniscectomy. *Journal of Bone and Joint Surgery*. **90**(9), pp.1922–1931.
- Allen, A.A., Caldwell, G.L. and Fu, F.H. 1995. Anatomy and biomechanics of the meniscus. *Operative Techniques in Orthopaedics*. **5**(1), pp.2–9.
- Ambra, L.F., Mestriner, A.B., Ackermann, J., Phan, A.T., Farr, J. and Gomoll, A.H. 2019. Bone-Plug Versus Soft Tissue Fixation of Medial Meniscal Allograft Transplants: A Biomechanical Study. *American Journal of Sports Medicine*. **47**(12), pp.2960–2965.
- Andrews, S.H.J., Adesida, A.B., Abusara, Z. and Shrive, N.G. 2017. Current concepts on structure–function relationships in the menisci. *Connective Tissue Research*. **58**(3–4), pp.271–281.
- Arnoczky, S.P., Cook, J.L., Carter, T. and Turner, A.S. 2010. Translational Models for Studying Meniscal Repair and Replacement: What They Can and Cannot Tell Us. *Tissue Engineering Part B: Reviews*. **16**(1), pp.31–39.
- Ateshian, G.A. 2009. The role of interstitial fluid pressurization in articular cartilage lubrication. *Journal of Biomechanics*. **42**(9), pp.1163–1176.
- Athanasίου, K.A. and Sanchez-Adams, J. 2009. *Engineering the Knee Meniscus* [Online]. Morgan & Claypool. Available from: <http://www.morganclaypool.com/doi/abs/10.2200/S00186ED1V01Y200903TIS001>.
- B Morrison, J. 1970. The Mechanics of the Knee Joint in Relation to Normal Walking. *Journal of biomechanics*. **3**(1), pp.51–61.
- Baratz, M.E., Fu, F.H. and Mengato, R. 1986. Meniscal tears: The effect of meniscectomy and of repair on intraarticular contact areas and stress in the human knee. A

- preliminary report. *American Journal of Sports Medicine*. **14**(4), pp.270–275.
- Barnett, P.I., Fisher, J., Auger, D.D., Stone, M.H. and Ingham, E. 2001. Comparison of wear in a total knee replacement under different kinematic conditions. *Journal of Materials Science: Materials in Medicine*. **12**(10–12), pp.1039–1042.
- Baudet, A., Morisset, C., D'Athis, P., Maillefert, J.F., Casillas, J.M., Ornetti, P. and Laroche, D. 2014. Cross-talk correction method for knee kinematics in gait analysis using Principal Component Analysis (PCA): A new proposal. *PLoS ONE*. **9**(7), pp.1–7.
- Bayliss, L.E., Culliford, D., Monk, A.P., Glyn-Jones, S., Prieto-Alhambra, D., Judge, A., Cooper, C., Carr, A.J., Arden, N.K., Beard, D.J. and Price, A.J. 2017. The effect of patient age at intervention on risk of implant revision after total replacement of the hip or knee: a population-based cohort study. *The Lancet*. **389**(10077), pp.1424–1430.
- Bedi, A., Kelly, N., Baad, M., Fox, A.J.S., Ma, Y., Warren, R.F. and Maher, S.A. 2012. Dynamic contact mechanics of radial tears of the lateral meniscus: Implications for treatment. *Arthroscopy - Journal of Arthroscopic and Related Surgery*. **28**(3), pp.372–381.
- Bilesan, A., Owlia, M., Behzadipour, S., Ogawa, S., Tsujita, T., Komizunai, S. and Konno, A. 2018. Marker-based motion tracking using Microsoft Kinect. *IFAC-PapersOnLine*. **51**(22), pp.399–404.
- Bowland, P. 2016. *Biotribology of osteochondral grafts in the knee*. [Online] University Of Leeds. Available from: <https://etheses.whiterose.ac.uk/>.
- Bowland, P., Ingham, E., Fisher, J. and Jennings, L.M. 2018. Development of a preclinical natural porcine knee simulation model for the tribological assessment of osteochondral grafts in vitro. *Journal of Biomechanics*. **77**(August), pp.91–98.
- Boxheimer, L., Lutz, A.M., Treiber, K., Goepfert, K., Crook, D.W., Marincek, B. and Weishaupt, D. 2004. MR Imaging of the Knee: Position Related Changes of the Menisci in Asymptomatic Volunteers. *Investigative Radiology*. **39**(5), pp.254–263.
- Brial, C., McCarthy, M., Adebayo, O., Wang, H., Chen, T., Warren, R. and Maher, S. 2019. Lateral Meniscal Graft Transplantation: Effect of Fixation Method on Joint Contact Mechanics During Simulated Gait. *American Journal of Sports Medicine*. **47**(10), pp.2437–2443.
- Brockett, C.L., Abdelgaied, A., Haythornthwaite, T., Hardaker, C., Fisher, J. and Jennings, L.M. 2016. The influence of simulator input conditions on the wear of total knee replacements: An experimental and computational study. *Proceedings of the Institution of Mechanical Engineers, Part H: Journal of Engineering in Medicine*. **230**(5), pp.429–439.
- Brophy, R.H., Cottrell, J., Rodeo, S.A., Wright, T.M., Warren, R.F. and Maher, S.A. 2010. Implantation of a synthetic meniscal scaffold improves joint contact mechanics in a partial meniscectomy cadaver model. *Journal of Biomedical Materials Research - Part A*. **92**(3), pp.1154–1161.
- Buckwalter, J.A., Saltzman, C. and Brown, T. 2004. The impact of osteoarthritis: implications for research. *Clinical Orthopaedics and Related Research (1976-2007)*. **427**, pp.S6–S15.
- Bullough, P.G., Munuera, L., Murphy, J. and Weinstein, A.M. 1970. The strength of the menisci of the knee as it relates to their fine structure. *The Journal of bone and joint surgery. British volume*. **52**(3), pp.564–567.

- Bylski-Austrow, D.I., Ciarelli, M.J., Kayner, D.C., Matthews, L.S. and Goldstein, S.A. 1994. Displacements of the menisci under joint load: An in vitro study in human knees. *Journal of Biomechanics*. **27**(4), pp.421–431.
- Bytyqi, D., Shabani, B., Lustig, S., Cheze, L., Karahoda Gjurgjeala, N. and Neyret, P. 2014. Gait knee kinematic alterations in medial osteoarthritis: Three dimensional assessment. *International Orthopaedics*. **38**(6), pp.1191–1198.
- Chevrier, A., Nelea, M., Hurtig, M.B., Hoemann, C.D. and Buschmann, M.D. 2009. Meniscus structure in human, sheep, and rabbit for animal models of meniscus repair. *Journal of Orthopaedic Research*. **27**(9), pp.1197–1203.
- Churchill, D.L., Incavo, S.J., Johnson, C.C. and Beynon, B.D. 1998. The transepicondylar axis approximates the optimal flexion axis of the knee. *Clinical orthopaedics and related research*. (356), pp.111–118.
- Costa, C.R., Morrison, W.B. and Carrino, J.A. 2004. Medial Meniscus Extrusion on Knee MRI: Is Extent Associated with Severity of Degeneration or Type of Tear? *American Journal of Roentgenology*. **183**(1), pp.17–23.
- Crema, M.D., Roemer, F.W., Felson, D.T., Englund, M., Wang, K., Jarraya, M., Nevitt, M.C., Marra, M.D., Torner, J.C., Lewis, C.E. and Guermazi, A. 2012. Factors associated with meniscal extrusion in knees with or at risk for osteoarthritis: The multicenter osteoarthritis study. *Radiology*. **264**(2), pp.494–503.
- D Lima, D.D., Patil, S., Steklov, N., Slamini, J.E. and Colwell, C.W. 2005. The Chitranjan Ranawat Award: In Vivo Knee Forces after Total Knee Arthroplasty. *Clinical Orthopaedics and Related Research*. **440**, pp.45–49.
- Daney, B.T., Aman, Z.S., Krob, J.J., Storaci, H.W., Brady, A.W., Nakama, G., Dornan, G.J., Provencher, M.T. and LaPrade, R.F. 2019. Utilization of Transtibial Centralization Suture Best Minimizes Extrusion and Restores Tibiofemoral Contact Mechanics for Anatomic Medial Meniscal Root Repairs in a Cadaveric Model. *American Journal of Sports Medicine*. **47**(7), pp.1591–1600.
- Debieux, P., Jimenez, A.E., Novaretti, J.V., Kaleka, C.C., Kriscenski, D.E., Astur, D.C., Obopilwe, E., Tamburini, L.M., Muench, L.N., Cote, M.P., Cohen, M. and Coyner, K.J. 2021. Medial meniscal extrusion greater than 4 mm reduces medial tibiofemoral compartment contact area: a biomechanical analysis of tibiofemoral contact area and pressures with varying amounts of meniscal extrusion. *Knee Surgery, Sports Traumatology, Arthroscopy*. **29**(9), pp.3124–3132.
- Deponti, D., Giancamillo, A. Di, Scotti, C., Peretti, G.M. and Martin, I. 2015. Animal models for meniscus repair and regeneration. *Journal of Tissue Engineering and Regenerative Medicine*. **9**(5), pp.512–527.
- Englund, M., Guermazi, A. and Lohmander, S.L. 2009. The Role of the Meniscus in Knee Osteoarthritis: a Cause or Consequence? *Radiologic Clinics of North America*. **47**(4), pp.703–712.
- Englund, M., Guermazi, A., Roemer, F.W., Aliabadi, P., Yang, M., Lewis, C.E., Torner, J., Nevitt, M.C., Sack, B. and Felson, D.T. 2009. Meniscal tear in knees without surgery and the development of radiographic osteoarthritis among middle-aged and elderly persons: The multicenter osteoarthritis study. *Arthritis and Rheumatism*. **60**(3), pp.831–839.
- Fairbank, T.J. 1948. Knee joint changes after meniscectomy. *The Journal of bone and joint surgery. British volume*. **30**(4), pp.664–670.
- Favenesi, J.A., Shaffer, J.C. and Mow, V.C. 1983. Biphasic mechanical properties of knee

meniscus. *Trans Orthop Res Soc.* **8**, p.57.

- Feucht, M.J., Kühle, J., Bode, G., Mehl, J., Schmal, H., Südkamp, N.P. and Niemeyer, P. 2015. Arthroscopic Transtibial Pullout Repair for Posterior Medial Meniscus Root Tears: A Systematic Review of Clinical, Radiographic, and Second-Look Arthroscopic Results. *Arthroscopy.* **31**(9), pp.1808–1816.
- Fithian, D.C., Kelly, M.A. and Mow, V.C. 1990. Material properties and structure-function relationships in the menisci. *Clinical orthopaedics and related research.* (252), pp.19–31.
- Forster, H. and Fisher, J. 1996. The influence of loading time and lubricant on the friction of articular cartilage. *Proceedings of the Institution of Mechanical Engineers. Part H, Journal of engineering in medicine.* **210**(2), pp.109–119.
- Fox, A.J.S., Bedi, A. and Rodeo, S.A. 2012. The Basic Science of Human Knee Menisci: Structure, Composition, and Function. *Sports Health.* **4**(4), pp.340–351.
- Fukubayashi, T., Torzilli, P.A., Sherman, M.F. and Warren, R.F. 1982. An in vitro biomechanical evaluation of anterior-posterior motion of the knee. Tibial displacement, rotation, and torque. *Journal of Bone and Joint Surgery.* **64**(2), pp.258–264.
- Furumatsu, T., Okazaki, Yuki, Okazaki, Yoshiki, Hino, T., Kamatsuki, Y., Masuda, S., Miyazawa, S., Nakata, E., Hasei, J., Kunisada, T. and Ozaki, T. 2019. Injury patterns of medial meniscus posterior root tears. *Orthopaedics and Traumatology: Surgery and Research.* **105**(1), pp.107–111.
- Gajjar, S.M., Solanki, K.P., Shanmugasundaram, S. and Kambhampati, S.B.S. 2021. Meniscal Extrusion: A Narrative Review. *Orthopaedic Journal of Sports Medicine.* **9**(11), pp.1–10.
- Goertzen, D.J., Budney, D.R. and Cinats, J.G. 1997. Methodology and apparatus to determine material properties of the knee joint meniscus. *Medical Engineering & Physics.* **19**(5), pp.412–419.
- Goldstein, S.A. 1987. The mechanical properties of trabecular bone: Dependence on anatomic location and function. *Journal of Biomechanics.* **20**(11–12), pp.1055–1061.
- Grassi, A., Zaffagnini, S., Marcheggiani Muccioli, G.M., Benzi, A. and Marcacci, M. 2014. Clinical outcomes and complications of a collagen meniscus implant: A systematic review. *International Orthopaedics.* **38**(9), pp.1945–1953.
- Hamamoto, K., Tobimatsu, Y. and Zabinska-Uroda, K. 2004. Magnetic resonance imaging evaluation of the movement and morphological changes of the menisci during deep knee flexion. *Journal of Physical Therapy Science.* **16**(2), pp.143–149.
- Hamill, J., Knutzen, K. and Derrick, T. 2015. *Biomechanical Basis of Human Movement* 4th ed. Philadelphia, PA: Lippincott Williams & Wilkins.
- Hart, N.H., Nimphius, S., Rantalainen, T., Ireland, A., Siafarikas, A. and Newton, R.U. 2017. Mechanical basis of bone strength: Influence of bone material, bone structure and muscle action. *Journal of Musculoskeletal Neuronal Interactions.* **17**(3), pp.114–139.
- Hartley, R. and Zisserman, A. 2003. *Multiple View Geometry in Computer Vision* 3rd ed. Cambridge University Press.
- Hasan, J., Fisher, J. and Ingham, E. 2014. Current strategies in meniscal regeneration. *Journal of Biomedical Materials Research - Part B Applied Biomaterials.* **102**(3), pp.619–634.

- Hein, C.N., Deperio, J.G., Ehrensberger, M.T. and Marzo, J.M. 2011. Effects of medial meniscal posterior horn avulsion and repair on meniscal displacement. *Knee*. **18**(3), pp.189–192.
- Heinlein, B., Kutzner, I., Graichen, F., Bender, A., Rohlmann, A., Halder, A.M., Beier, A. and Bergmann, G. 2009. ESB clinical biomechanics award 2008: Complete data of total knee replacement loading for level walking and stair climbing measured in vivo with a follow-up of 6-10 months. *Clinical Biomechanics*. **24**(4), pp.315–326.
- Hirose, T., Mae, T., Ogasawara, I., Yamakawa, S., Nakata, K., Ohori, T., Tsujii, A. and Okada, S. 2022. Meniscal Displacement and Loss of Load-Transmission Function After Radial Tear of the Lateral Meniscus in a Porcine Model: New Insights Into the Functional Dynamics of the Injured Meniscus. *American Journal of Sports Medicine*. **50**(7), pp.1850–1857.
- Hollister, A.M., Jatana, S., Singh, A.K., Sullivan, W.W. and Lupichuk, A.G. 1993. The axes of rotation of the knee. *Clinical orthopaedics and related research*. (290), pp.259–268.
- Höpker, W.W., Angres, G., Klingel, K., Komitowski, D. and Schuchardt, E. 1986. Changes of the elastin compartment in the human meniscus. *Virchows Archiv. A, Pathological anatomy and histopathology*. **408**(6), pp.575–592.
- van Houtem, M., Clough, R., Khan, A., Harrison, M. and Blunn, G.W. 2006. Validation of the soft tissue restraints in a force-controlled knee simulator. *Proceedings of the Institution of Mechanical Engineers, Part H: Journal of Engineering in Medicine*. **220**(3), pp.449–456.
- Hsieh, H.H. and Walker, P.S. 1976. Stabilizing mechanisms of the loaded and unloaded knee joint. *The Journal of bone and joint surgery. American volume*. **58**(1), pp.87–93.
- Hulet, C., Menetrey, J., Beaufils, P., Chambat, P., Djian, P., Hardy, P., Potel, J.-F., Servien, E., Seil, R., French Arthroscopic Soc, S.F.A., French Arthroscopic, S. and The French Arthroscopic, S. 2015. Clinical and radiographic results of arthroscopic partial lateral meniscectomies in stable knees with a minimum follow up of 20 years. *Knee Surgery, Sports Traumatology, Arthroscopy*. **23**(1), pp.225–231.
- Ikeuchi, K., Sakoda, H., Sakaue, R., Tsuji, K. and Tomita, N. 1998. A new method for accurate measurement of displacement of the knee menisci. *Proceedings of the Institution of Mechanical Engineers, Part H: Journal of Engineering in Medicine*. **212**(3), pp.183–188.
- ISO-14243-3 2014. *Implants for Surgery. Wear of Total Knee-Joint Prostheses. Loading and Displacement Parameters for Wear-Testing Machines with Displacement Control and Corresponding Environmental Conditions for Test*.
- Jeong, H.-J., Lee, S.-H. and Ko, C.-S. 2012. Meniscectomy. *Knee Surgery & Related Research*. **24**(3), pp.129–136.
- Jia, T., Sun, N.L. and Cao, M.Y. 2008. Moving object detection based on blob analysis *In: Proceedings of the IEEE International Conference on Automation and Logistics, ICAL 2008*, pp.322–325.
- Johnson, T., Andriacchi, T.P. and Laurent, M.P. 2000. Development of a Knee Wear Test Method Based on Prosthetic in Vivo Slip Velocity Profiles *In: Orthopaedic Research Society Conference 12-15 March 2000* [Online]. Orlando, Florida, USA: [Online], p.1. Available from: www.ors.org/Transactions.
- Kalcounis-Rueppell, M., Parrish, T. and Pauli, S. 2013. Application of Object Tracking in Video Recordings to the Observation of Mice in the Wild. *Springer Proceedings in*

Mathematics and Statistics. **64**, pp.105–115.

- Kamate, S. and Yilmazer, N. 2015. Application of Object Detection and Tracking Techniques for Unmanned Aerial Vehicles. *Procedia Computer Science*. **61**, pp.436–441.
- Karpinski, K., Diermeier, T., Willinger, L., Imhoff, A.B., Achtnich, A. and Petersen, W. 2019. No dynamic extrusion of the medial meniscus in ultrasound examination in patients with confirmed root tear lesion. *Knee Surgery, Sports Traumatology, Arthroscopy*. **27**(10), pp.3311–3317.
- Kawahara, Y., Uetani, M., Fuchi, K., Eguchi, H., Hashmi, R. and Hayashi, K. 2001. MR assessment of meniscal movement during knee flexion: correlation with the severity of cartilage abnormality in the femorotibial joint. *Journal of computer assisted tomography*. **25**(5), pp.683–690.
- Kean, C.O., Brown, R.J. and Chapman, J. 2017. The role of biomaterials in the treatment of meniscal tears. *PeerJ*. **5**(10), pp.1–26.
- Kikawada, T. 2023. Color Marker based Object Tracking. *The MathWorks Inc.* [Online], Online. [Accessed 22 January 2023]. Available from: <https://www.mathworks.com/matlabcentral/fileexchange/65816-color-marker-based-object-tracking>.
- Kim, D.H., Lee, G.C., Kim, H.H. and Cha, D.H. 2020. Correlation between meniscal extrusion and symptom duration, alignment, and arthritic changes in medial meniscus posterior root tear: research article. *Knee Surgery and Related Research*. **32**(1), pp.1–8.
- Kim, E., Kim, Y.J., Cha, J.G., Kim, M.Y., Lee, D.H., Cho, S.G. and Kim, R.S. 2015. Kinematic change of the meniscus and the tibiofemoral joint space in asymptomatic volunteers using a wide bore 3T closed MRI system. *Skeletal Radiology*. **44**(10), pp.1441–1451.
- Kim, J.G., Lee, Y.S., Bae, T.S., Ha, J.K., Lee, D.H., Kim, Y.J. and Ra, H.J. 2013. Tibiofemoral contact mechanics following posterior root of medial meniscus tear, repair, meniscectomy, and allograft transplantation. *Knee Surgery, Sports Traumatology, Arthroscopy*. **21**(9), pp.2121–2125.
- Kim, J.H., Chung, J.H., Lee, D.H., Lee, Y.S., Kim, J.R. and Ryu, K.J. 2011. Arthroscopic suture anchor repair versus pullout suture repair in posterior root tear of the medial meniscus: A prospective comparison study. *Arthroscopy - Journal of Arthroscopic and Related Surgery*. **27**(12), pp.1644–1653.
- Kim, J.H., Lee, S., Ha, D.H., Lee, S.M., Jung, K. and Choi, W. 2018. The effects of graft shrinkage and extrusion on early clinical outcomes after meniscal allograft transplantation. *Journal of Orthopaedic Surgery and Research*. **13**(1), p.181.
- Krause, W.R., Pope, M.H., Johnson, R.J. and Wilder, D.G. 1976. Mechanical changes in the knee after meniscectomy. *The Journal of bone and joint surgery. American volume*. **58**(5), pp.599–604.
- Krych, A.J., Bernard, C.D., Kennedy, N.I., Tagliero, A.J., Camp, C.L., Levy, B.A. and Stuart, M.J. 2020. Medial Versus Lateral Meniscus Root Tears: Is There a Difference in Injury Presentation, Treatment Decisions, and Surgical Repair Outcomes? *Arthroscopy - Journal of Arthroscopic and Related Surgery*. **36**(4), pp.1135–1141.
- Krych, A.J., Bernard, C.D., Leland, D.P., Camp, C.L., Johnson, A.C., Finnoff, J.T. and Stuart, M.J. 2020. Isolated meniscus extrusion associated with meniscotibial ligament abnormality. *Knee Surgery, Sports Traumatology, Arthroscopy*. **28**(11),

pp.3599–3605.

- Krych, A.J., Johnson, N.R., Mohan, R., Dahm, D.L., Levy, B.A. and Stuart, M.J. 2018. Partial meniscectomy provides no benefit for symptomatic degenerative medial meniscus posterior root tears. *Knee Surgery, Sports Traumatology, Arthroscopy*. **26**(4), pp.1117–1122.
- Kurosawa, H., Fukubayashi, T. and Nakajima, H. 1980. Load-bearing mode of the knee joint: physical behavior of the knee joint with or without menisci. *Clinical Orthopaedics and Related Research*. (149), pp.283–290.
- Kutzner, I., Heinlein, B., Graichen, F., Bender, A., Rohlmann, A., Halder, A., Beier, A. and Bergmann, G. 2010. Loading of the knee joint during activities of daily living measured in vivo in five subjects. *Journal of Biomechanics*. **43**(11), pp.2164–2173.
- Kwon, H., Brown, W.E., Lee, C.A., Wang, D., Paschos, N., Hu, J.C. and Athanasiou, K.A. 2019. Surgical and tissue engineering strategies for articular cartilage and meniscus repair. *Nature reviews. Rheumatology*. **15**(9), pp.550–570.
- Lafortune, M.A., Cavanagh, P.R., Sommer, H.J. and Kalenak, A. 1992. Three-dimensional kinematics of the human knee during walking. *Journal of Biomechanics*. **25**(4), pp.347–357.
- Laible, C., Stein, D.A. and Kiridly, D.N. 2013. Meniscal repair. *Journal of the American Academy of Orthopaedic Surgeons*. **21**(4), pp.204–213.
- Lamb, J.N. and Guy, S.P. 2016. Soft tissue knee injuries. *Surgery (Oxford)*. **34**(9), pp.453–459.
- LaPrade, C.M., James, E.W., Cram, T.R., Feagin, J.A., Engebretsen, L. and Laprade, R.F. 2015. Meniscal Root Tears: A Classification System Based on Tear Morphology. *The American Journal of Sports Medicine*. **43**(2), pp.363–369.
- Lechner, K., Hull, M.L. and Howell, S.M. 2000. Is the circumferential tensile modulus within a human medial meniscus affected by the test sample location and cross-sectional area? *Journal of Orthopaedic Research*. **18**(6), pp.945–951.
- Lee, D.-H., Lee, B.-S., Kim, J.-M., Yang, K.-S., Cha, E.-J., Park, J.-H. and Bin, S.-I. 2011. Predictors of degenerative medial meniscus extrusion: radial component and knee osteoarthritis. *Knee Surgery, Sports Traumatology, Arthroscopy*. **19**(2), pp.222–229.
- Lee, D.H. 2018. Incidence and Extent of Graft Extrusion following Meniscus Allograft Transplantation. *BioMed Research International*., pp.1–11.
- Lee, D.W., Ha, J.K. and Kim, J.G. 2014. Medial Meniscus Posterior Root Tear: A Comprehensive Review. *Knee Surgery & Related Research*. **26**(3), pp.125–134.
- Lee, S.J., Aadalén, K.J., Malaviya, P., Lorenz, E.P., Hayden, J.K., Farr, J., Kang, R.W. and Cole, B.J. 2006. Tibiofemoral Contact Mechanics After Serial Medial Meniscectomies in the Human Cadaveric Knee. *The American Journal of Sports Medicine*. **34**(8), pp.1334–1344.
- Lee, S.K., Yang, B.S., Park, B.M., Yeom, J.U., Kim, J.H. and Yu, J.S. 2018. Medial meniscal root repair using curved guide and soft suture anchor. *CiOS Clinics in Orthopedic Surgery*. **10**(1), pp.111–115.
- Leroy, A., Beaufils, P., Faivre, B., Steltzlen, C., Boisrenoult, P. and Pujol, N. 2017. Actifit® polyurethane meniscal scaffold: MRI and functional outcomes after a minimum follow-up of 5 years. *Orthopaedics and Traumatology: Surgery and Research*. **103**(4), pp.609–614.

- Liu, A., Ingham, E., Fisher, J. and Jennings, L.M. 2019. Development of a pre-clinical experimental simulation model of the natural porcine knee with appropriate ligamentous constraints. *PLoS ONE*. **14**(5), pp.1–14.
- Liu, A., Jennings, L.M., Ingham, E. and Fisher, J. 2015. Tribology studies of the natural knee using an animal model in a new whole joint natural knee simulator. *Journal of Biomechanics*. **48**(12), pp.3004–3011.
- Liu, A., Sanderson, W.J., Ingham, E., Fisher, J. and Jennings, L.M. 2020. Development of a specimen-specific in vitro pre-clinical simulation model of the human cadaveric knee with appropriate soft tissue constraints. *PLoS ONE*. **15**(10 October), pp.1–15.
- LORD Corp. MircoStrain 2013. *M-DVRT Microminiature Displacement Sensor*. Williston, VT, USA.
- Lourakis, M. 2023. Stereo Triangulation. *MATLAB Central File Exchange*. [Online]. [Accessed 27 January 2023]. Available from: <https://www.mathworks.com/matlabcentral/fileexchange/67383-stereo-triangulation>.
- De Maeseneer, M., Shahabpour, M., Vanderdood, K., Van Roy, F. and Osteaux, M. 2002. Medial meniscocapsular separation: MR imaging criteria and diagnostic pitfalls. *European Journal of Radiology*. **41**(3), pp.242–252.
- Makris, E.A., Hadidi, P. and Athanasiou, K.A. 2011. The knee meniscus: Structure-function, pathophysiology, current repair techniques, and prospects for regeneration. *Biomaterials*. **32**(30), pp.7411–7431.
- Marzo, J.M. and Gurske-DePerio, J. 2009. Effects of Medial Meniscus Posterior Horn Avulsion and Repair on Tibiofemoral Contact Area and Peak Contact Pressure With Clinical Implications. *The American Journal of Sports Medicine*. **37**(1), pp.124–129.
- Masuda, S., Furumatsu, T., Okazaki, Y., Kodama, Y., Hino, T., Kamatsuki, Y., Miyazawa, S. and Ozaki, T. 2018. Medial meniscus posterior root tear induces pathological posterior extrusion of the meniscus in the knee-flexed position: An open magnetic resonance imaging analysis. *Orthopaedics & Traumatology: Surgery & Research*. **104**(4), pp.485–489.
- McCann, L., Ingham, E., Jin, Z. and Fisher, J. 2009. Influence of the meniscus on friction and degradation of cartilage in the natural knee joint. *Osteoarthritis and Cartilage*. **17**(8), pp.995–1000.
- McCann, L., Udofia, I., Graindorge, S., Ingham, E., Jin, Z. and Fisher, J. 2008. Tribological testing of articular cartilage of the medial compartment of the knee using a friction simulator. *Tribology International*. **41**(11), pp.1126–1133.
- McDermott, I.D. and Amis, A.A. 2006. The consequences of meniscectomy. *JOURNAL OF BONE AND JOINT SURGERY-BRITISH VOLUME*. **88B**(12), pp.1549–1556.
- McDermott, I.D., Masouros, S.D. and Amis, A.A. 2008. Biomechanics of the menisci of the knee. *Current Orthopaedics*. **22**(3), pp.193–201.
- McDevitt, C.A. and Webber, R.J. 1990. The ultrastructure and biochemistry of meniscal cartilage. *Clinical orthopaedics and related research*. (252), pp.8–18.
- McEwen, H.M.J., Barnett, P.I., Bell, C.J., Farrar, R., Auger, D.D., Stone, M.H. and Fisher, J. 2005. The influence of design, materials and kinematics on the in vitro wear of total knee replacements. *Journal of Biomechanics*. **38**(2), pp.357–365.
- McMurray, T.P. 1942. The semilunar cartilages. *British Journal of Surgery*. **29**(116), pp.407–414.

- Mohamadi, A., Momenzadeh, K., Masoudi, A., Walley, K.C., Ierardi, K., Ramappa, A., DeAngelis, J.P. and Nazarian, A. 2021. Evolution of knowledge on meniscal biomechanics: a 40 year perspective. *BMC Musculoskeletal Disorders*. **22**(1), pp.1–13.
- Mononen, M.E., Jurvelin, J.S. and Korhonen, R.K. 2013. Effects of radial tears and partial meniscectomy of lateral meniscus on the knee joint mechanics during the stance phase of the gait cycle—A 3D finite element study. *Journal of Orthopaedic Research*. **31**(8), pp.1208–1217.
- Mow, V.C., Kuei, S.C., Lai, W.M. and Armstrong, C.G. 1980. Biphasic creep and stress relaxation of articular cartilage in compression? Theory and experiments. *Journal of biomechanical engineering*. **102**(1), pp.73–84.
- Mow, V.C. and Lai, W.M. 1980. Recent Developments in Synovial Joint Biomechanics. *SIAM Review*. **22**(3), pp.275–317.
- Muzaffar, N., Orth, M.S., Kirmani, O., Ahsan, M., Orth, M.S., Ahmad, S. and Orth, M.S. 2015. Meniscal Extrusion in the Knee : Should only 3 mm Extrusion be Considered Significant ? An Assessment by MRI and Arthroscopy. . **9**(2), pp.17–20.
- Navasartian, D.J. and DeBerardino, T.M. 2018. Meniscus Root Repair. *Operative Techniques in Sports Medicine*. **26**(4), pp.238–245.
- NiBIB 2023. Ultrasound. *National Institute of Biomedical Imaging and Bioengineering*.
- Nogueira-Barbosa, M.H., Gregio-Junior, E., Lorenzato, M.M., Guermazi, A., Roemer, F.W., Chagas-Neto, F.A. and Crema, M.D. 2015. Ultrasound assessment of medial meniscal extrusion: A validation study using MRI as reference standard. *American Journal of Roentgenology*. **204**(3), pp.584–588.
- Nordin, M. and Frankel, V.H. 2001. *Basic biomechanics of the musculoskeletal system* 3rd ed. London; Philadelphia; Lippincott, Williams & Wilkins.
- Olesen, O.V., Paulsen, R.R., Højgaard, L., Roed, B. and Larsen, R. 2012. Motion tracking for medical imaging: A nonvisible structured light tracking approach. *IEEE Transactions on Medical Imaging*. **31**(1), pp.79–87.
- Ozeki, N., Koga, H., Matsuda, J., Kohno, Y., Mizuno, M., Katano, H., Tsuji, K., Saito, T., Muneta, T. and Sekiya, I. 2020. Biomechanical analysis of the centralization procedure for extruded lateral menisci with posterior root deficiency in a porcine model. *Journal of Orthopaedic Science*. **25**(1), pp.161–166.
- Özkaya, N., Leger, D., Goldsheyder, D. and Nordin, M. 2017. Mechanical Properties of Biological Tissues *In: Fundamentals of Biomechanics: Equilibrium, Motion, and Deformation* [Online]. Cham: Springer International Publishing, pp.361–387. Available from: https://doi.org/10.1007/978-3-319-44738-4_15.
- Palanca, M., Tozzi, G. and Cristofolini, L. 2016. The use of digital image correlation in the biomechanical area: A review. *International Biomechanics*. **3**(1), pp.1–21.
- Paletta, G.A., Crane, D.M., Konicek, J., Piepenbrink, M., Higgins, L.D., Milner, J.D. and Wijdicks, C.A. 2020. Surgical Treatment of Meniscal Extrusion: A Biomechanical Study on the Role of the Medial Meniscotibial Ligaments With Early Clinical Validation. *Orthopaedic Journal of Sports Medicine*. **8**(7), pp.1–8.
- Paletta, G.A., Manning, T., Snell, E., Parker, R. and Bergfeld, J. 1997. The effect of alligraft meniscal replacement on intraarticular contact area and pressures in the human knee: A biomechanical study. *American Journal of Sports Medicine*. **25**(5), pp.692–698.

- Paternina, M.A., Singh, A., Raipur, N., Padhy, I.S., Viswakumar, A., Rajagopalan, V., Ray, T., Gottipati, P. and Parimi, C. 2022. Development of a Robust, Simple, and Affordable Human Gait Analysis System Using Bottom-Up Pose Estimation With a Smartphone Camera. *Frontiers in Physiology*. **12**, pp.1–11.
- Paxton, E.S., Stock, M. V and Brophy, R.H. 2011. Meniscal repair versus partial meniscectomy: a systematic review comparing reoperation rates and clinical outcomes. *Arthroscopy: The Journal of Arthroscopic & Related Surgery*. **27**(9), pp.1275–1288.
- Perey, O. 1962. Follow-up results of meniscectomy with regard to the working capacity. *Acta Orthopaedica*. **32**(1–4), pp.457–460.
- Peters, T.J. and Smillie, E.S. 1972. Studies on the Chemical Composition of the Menisci of the Knee Joint with Special Reference to the Horizontal Cleavage Lesion. *Clinical Orthopaedics and Related Research*®. **86**.
- Petersen, W., Forkel, P., Feucht, M.J., Zantop, T., Imhoff, A.B. and Brucker, P.U. 2014. Posterior root tear of the medial and lateral meniscus. *Archives of Orthopaedic and Trauma Surgery*. **134**(2), pp.237–255.
- Petersen, W. and Tillmann, B. 1995. Age-related blood and lymph supply of the knee menisci: a cadaver study. *Acta Orthopaedica*. **66**(4), pp.308–312.
- Petersen, W. and Tillmann, B. 1998. Collagenous fibril texture of the human knee joint menisci. *Anatomy and embryology*. **197**(4), pp.317–324.
- Proctor, C.S., Schmidt, M.B., Whipple, R.R., Kelly, M.A. and Mow, V.C. 1989. Material properties of the normal medial bovine meniscus. *Journal of orthopaedic research*. **7**(6), pp.771–782.
- Reinders, J., Sonntag, R., Vot, L., Gibney, C., Nowack, M. and Kretzer, J.P. 2015. Wear testing of moderate activities of daily living using in vivo measured knee joint loading. *PLoS ONE*. **10**(3), pp.9–11.
- Reynolds, R.J., Walker, P.S. and Buza, J. 2017. Mechanisms of anterior-posterior stability of the knee joint under load-bearing. *Journal of Biomechanics*. **57**, pp.39–45.
- Roemer, F.W., Zhang, Y., Niu, J., Lynch, J.A., Crema, M.D., Marra, M.D., Nevitt, M.C., Felson, D.T., Hughes, L.B., El-Khoury, G.Y., Englund, M. and Guermazi, A. 2009. Tibiofemoral joint osteoarthritis: Risk factors for MR-depicted fast cartilage loss over a 30-month period in the multicenter osteoarthritis study. *Radiology*. **252**(3), pp.772–780.
- Roos, H., Laurén, M., Adalberth, T., Roos, E.M., Jonsson, K. and Lohmander, L.S. 1998. Knee osteoarthritis after meniscectomy: prevalence of radiographic changes after twenty-one years, compared with matched controls. *Arthritis & Rheumatology*. **41**(4), pp.687–693.
- Rowe, P.J., Myles, C.M., Walker, C. and Nutton, R. 2000. Knee joint kinematics in gait and other functional activities measured using flexible electrogoniometry: How much knee motion is sufficient for normal daily life? *Gait and Posture*. **12**(2), pp.143–155.
- Sanchez-Adams, J., Willard, V.P. and Athanasiou, K.A. 2011. Regional variation in the mechanical role of knee meniscus glycosaminoglycans. *Journal of applied physiology (Bethesda, Md. : 1985)*. **111**(6), pp.1590–1596.
- Schillhammer, C.K., Werner, F.W., Scuderi, M.G. and Cannizzaro, J.P. 2012. Repair of lateral meniscus posterior horn detachment lesions: A biomechanical evaluation. *American Journal of Sports Medicine*. **40**(11), pp.2604–2609.

- Schmitz, A., Ye, M., Shapiro, R., Yang, R. and Noehren, B. 2014. Accuracy and repeatability of joint angles measured using a single camera markerless motion capture system. *Journal of Biomechanics*. **47**(2), pp.587–591.
- Schneider, C.A., Rasband, W.S. and Eliceiri, K.W. 2012. NIH Image to ImageJ: 25 years of image analysis. *Nature Methods*. **9**(7), pp.671–675.
- Scholes, C., Houghton, E.R., Lee, M. and Lustig, S. 2015. Meniscal translation during knee flexion: what do we really know? *Knee Surgery, Sports Traumatology, Arthroscopy*. **23**(1), pp.32–40.
- Schumacher, B.L., Schmidt, T.A., Voegtline, M.S., Chen, A.C. and Sah, R.L. 2005. Proteoglycan 4 (PRG4) synthesis and immunolocalization in bovine meniscus. *Journal of Orthopaedic Research*. **23**(3), pp.562–568.
- Seedhom, B.B. 1979. Transmission of the load in the knee joint with special reference to the role of the menisci. Part I. Anatomy, analysis and apparatus. *Engineering in Medicine*. **8**(4), pp.207–219.
- Selvik, G. 1989. Roentgen stereophotogrammetry: A method for the study of the kinematics of the skeletal system. *Acta Orthopaedica*. **60**(S232), pp.1–51.
- Setton, L.A., Guilak, F., Hsu, E.W. and Vail, T.P. 1999. Biomechanical factors in tissue engineered meniscal repair. *Clinical Orthopaedics and Related Research*. **367**(SUPPL.), pp.254–272.
- Shemesh, M., Shefy-Peleg, A., Levy, A., Shabshin, N., Condello, V., Arbel, R. and Gefen, A. 2020. Effects of a novel medial meniscus implant on the knee compartments: imaging and biomechanical aspects. *Biomechanics and Modeling in Mechanobiology*. **19**(6), pp.2049–2059.
- Shenoy, R., Pastides, P.S. and Nathwani, D. 2013. (iii) Biomechanics of the knee and TKR. *Orthopaedics and Trauma*. **27**(6), pp.364–371.
- Shoemaker, S.C. and Markolf, K.L. 1986. The role of the meniscus in the anterior-posterior stability of the loaded anterior cruciate-deficient knee. Effects of partial versus total excision. *Journal of Bone and Joint Surgery*. **68**(1).
- Shrive, N.G., O'Connor, J.J. and Goodfellow, J.W. 1978. Load-bearing in the knee joint. *Clinical Orthopaedics and Related Research*. (131), pp.279–287.
- Siemieniuk, R.A.C., Harris, I.A., Agoritsas, T., Poolman, R.W., Brignardello-Petersen, R., Van de Velde, S., Buchbinder, R., Englund, M., Lytvyn, L., Quinlan, C., Helsingen, L., Knutsen, G., Olsen, N.R., Macdonald, H., Hailey, L., Wilson, H.M., Lydiatt, A. and Kristiansen, A. 2018. Arthroscopic surgery for degenerative knee arthritis and meniscal tears: a clinical practice guideline. *British journal of sports medicine*. **52**(313), pp.1–7.
- Sihvonen, R., Paavola, M., Malmivaara, A., Itala, A., Joukainen, A., Nurmi, H., Kalske, J., Jarvinen, T.L.N. and Finnish Degenerative Meniscal Lesion Study, G. 2013. Arthroscopic Partial Meniscectomy versus Sham Surgery for a Degenerative Meniscal Tear. *New England Journal of Medicine*. **369**(26), pp.2515–2524.
- Stewart, T.D. and Hall, R.M. 2006. (iv) Basic biomechanics of human joints: Hips, knees and the spine. *Current Orthopaedics*. **20**(1), pp.23–31.
- Sturnieks, D.L., Besier, T.F., Mills, P.M., Ackland, T.R., Maguire, K.F., Stachowiak, G.W., Podsiadlo, P. and Lloyd, D.G. 2008. Knee joint biomechanics following arthroscopic partial meniscectomy. *Journal of Orthopaedic Research*. **26**(8), pp.1075–1080.
- Sutton, L.G., Werner, F.W., Haider, H., Hamblin, T. and Clabeaux, J.J. 2010. In vitro

- response of the natural cadaver knee to the loading profiles specified in a standard for knee implant wear testing. *Journal of Biomechanics*. **43**(11), pp.2203–2207.
- Swamy, N., Wadhwa, V., Bajaj, G., Chhabra, A. and Pandey, T. 2018. Medial meniscal extrusion: Detection, evaluation and clinical implications. *European Journal of Radiology*. **102**, pp.115–124.
- Sweigart, M.A., Zhu, C.F., Burt, D.M., Deholl, P.D., Agrawal, C.M., Clanton, T.O. and Athanasiou, K.A. 2004. Intraspecies and interspecies comparison of the compressive properties of the medial meniscus. *Annals of Biomedical Engineering*. **32**(11), pp.1569–1579.
- Takroni, T., Laouar, L., Adesida, A., Elliott, J.A.W. and Jomha, N.M. 2016. Anatomical study: comparing the human, sheep and pig knee meniscus. *Journal of Experimental Orthopaedics*. **3**(1), p.35.
- Taylor, W.R., Heller, M.O., Bergmann, G. and Duda, G.N. 2004. Tibio-femoral loading during human gait and stair climbing. *Journal of Orthopaedic Research*. **22**(3), pp.625–632.
- The MathWorks 2022. Measuring Planar Objects with a Calibrated Camera - MATLAB & Simulink - MathWorks UK. [Accessed 22 June 2022]. Available from: <https://uk.mathworks.com/help/vision/ug/measuring-planar-objects-with-a-calibrated-camera>.
- The MathWorks Inc. 2017. Multiple Object Tracking - MATLAB & Simulink - MathWorks UK. [Accessed 16 July 2020]. Available from: <https://uk.mathworks.com/help/vision/examples/motion-based-multiple-object-tracking.html>.
- The MathWorks Inc. 2023. Segment Image and Create Mask Using Color Thresholder. *The MathWorks Inc.* [Online]. [Accessed 3 April 2023]. Available from: <https://www.mathworks.com>.
- Thompson, W.O., Thaete, F.L., Fu, F.H. and Dye, S.F. 1991. Tibial meniscal dynamics using three-dimensional reconstruction of magnetic resonance images. *The American Journal of Sports Medicine*. **19**(3), pp.210–216.
- Thorup, V.M. 2007. Biomechanical gait analysis of pigs. *Animal*. **1**(5), pp.708–715.
- Tienen, T.G., Buma, P., Scholten, J.G.F., Van Kampen, A., Veth, R.P.H. and Verdonchot, N. 2005. Displacement of the medial meniscus within the passive motion characteristics of the human knee joint: An RSA study in human cadaver knees. *Knee Surgery, Sports Traumatology, Arthroscopy*. **13**(4), pp.287–292.
- Tissakht, M. and Ahmed, A.M. 1995. Tensile stress-strain characteristics of the human meniscal material. *Journal of Biomechanics*. **28**(4), pp.411–422.
- Tsujii, A., Nakamura, N. and Horibe, S. 2017. Age-related changes in the knee meniscus. *The Knee*. **24**(6), pp.1262–1270.
- Ugbohue, U.C., Papi, E., Kaliarntas, K.T., Kerr, A., Earl, L., Pomeroy, V.M. and Rowe, P.J. 2013. The evaluation of an inexpensive, 2D, video based gait assessment system for clinical use. *Journal of Electromyography and Kinesiology*. **23**(4), pp.483–489.
- Vaquero-Picado, A. and Rodríguez-Merchán, E.C. 2018. Arthroscopic repair of the meniscus: Surgical management and clinical outcomes. *EFORT Open Reviews*. **3**(11), pp.584–594.
- Vedi, V., Williams, A., Tennant, S.J., Spouse, E., Hunt, D.M. and Gedroyc, W.M.W. 1999. Meniscal movement - An in-vivo study using dynamic MRI. *Journal of Bone and Joint Surgery*. **81**(1), pp.10–15.

Surgery. **81B**(1), pp.37–41.

- Verdonk, P., Beaufils, P., Bellemans, J., Djjan, P., Heinrichs, E.L., Huysse, W., Laprell, H., Siebold, R. and Verdonk, R. 2012. Successful treatment of painful irreparable partial meniscal defects with a polyurethane scaffold: Two-year safety and clinical outcomes. *American Journal of Sports Medicine*. **40**(4), pp.844–853.
- Verdonk, P.C.M., Verstraete, K.L., Almqvist, K.F., De Cuyper, K., Veys, E.M., Verbruggen, G. and Verdonk, R. 2006. Meniscal allograft transplantation: long-term clinical results with radiological and magnetic resonance imaging correlations. *Knee Surgery, Sports Traumatology, Arthroscopy*. **14**(8), pp.694–706.
- Vrancken, A.C.T., Buma, P. and Van Tienen, T.G. 2013. Synthetic meniscus replacement: A review. *International Orthopaedics*. **37**(2), pp.291–299.
- Vrancken, A.C.T., Eggermont, F.E., Tienen, T.G. van, Hannink, G.J., Buma, P., Janssen, D.W. and Verdonschot, N.J. 2016. Functional biomechanical performance of a novel anatomically shaped polycarbonate urethane total meniscus replacement. *Knee Surgery, Sports Traumatology, Arthroscopy*. **24**(5), pp.1485–1494.
- Vrancken, A.C.T., Hannink, G., Madej, W., Verdonschot, N., Van Tienen, T.G. and Buma, P. 2017. In Vivo Performance of a Novel, Anatomically Shaped, Total Meniscal Prosthesis Made of Polycarbonate Urethane: A 12-Month Evaluation in Goats. *American Journal of Sports Medicine*. **45**(12), pp.2824–2834.
- Vrancken, A.C.T., van Tienen, T.G., Hannink, G., Janssen, D., Verdonschot, N. and Buma, P. 2014. Releasing the circumferential fixation of the medial meniscus does not affect its kinematics. *Knee*. **21**(6), pp.1033–1038.
- Walczak, B.E., Miller, K., Behun, M.A., Sienkiewicz, L., Stokes, H.H., McCabe, R. and Baer, G.S. 2021. Quantifying the differential functional behavior between the medial and lateral meniscus after posterior meniscus root tears. *PLoS ONE*. **16**(11 November), pp.1–12.
- Walker, P.S., Arno, S., Bell, C., Salvadore, G., Borukhov, I. and Oh, C. 2015. Function of the medial meniscus in force transmission and stability. *Journal of Biomechanics*. **48**(8), pp.1383–1388.
- Walker, P.S. and Erkman, M.J. 1975. The role of the menisci in force transmission across the knee. *Clinical Orthopaedics*. **109**, pp.184–192.
- Wasserstein, D., Dwyer, T., Gandhi, R., Austin, P.C., Mahomed, N. and Ogilvie-Harris, D. 2013. A matched-cohort population study of reoperation after meniscal repair with and without concomitant anterior cruciate ligament reconstruction. *American Journal of Sports Medicine*. **41**(2), pp.349–355.
- Wenger, A., Wirth, W., Hudelmaier, M., Noebauer-Huhmann, I., Trattng, S., Bloecker, K., Frobell, R.B., Kwok, C.K., Eckstein, F. and Englund, M. 2013. Meniscus body position, size, and shape in persons with and persons without radiographic knee osteoarthritis: Quantitative analyses of knee magnetic resonance images from the osteoarthritis initiative. *Arthritis and Rheumatism*. **65**(7), pp.1804–1811.
- Whipple, R.R., Wirth, C.R. and Mow, V.C. 1985. Anisotropic and zonal variations in the tensile properties of the meniscus. *Trans. Orthop. Res. Soc.* **10**, p.367.
- Wilharm, A., Hurschler, C., Dermitas, T. and Bohnsack, M. 2013. Use of Tekscan K-scan sensors for retropatellar pressure measurement avoiding errors during implantation and the effects of shear forces on the measurement precision. *BioMed Research International*, pp.1–7.

- Yamamoto, T., Taneichi, H., Seo, Y. and Yoshikawa, K. 2021. MRI-based kinematics of the menisci through full knee range of motion. *Journal of Orthopaedic Surgery*. **29**(2), pp.1–8.
- Yao, J., Lancianese, S.L., Hovinga, K.R., Lee, J. and Lerner, A.L. 2008. Magnetic resonance image analysis of meniscal translation and tibio-menisco-femoral contact in deep knee flexion. *Journal of Orthopaedic Research*. **26**(5), pp.673–684.
- Yin, L., Chen, K., Guo, L., Cheng, L., Wang, F. and Yang, L. 2015. Identifying the functional flexion-extension axis of the knee: An in-vivo kinematics study. *PLoS ONE*. **10**(6), pp.1–11.
- Zhang, A.L., Miller, S.L., Coughlin, D.G., Lotz, J.C. and Feeley, B.T. 2015. Tibiofemoral contact pressures in radial tears of the meniscus treated with all-inside repair, inside-out repair and partial meniscectomy. *The Knee*. **22**(5), pp.400–404.
- Zhou, Z.R. and Jin, Z.M. 2015. Biotribology: Recent progresses and future perspectives. *Biosurface and Biotribology*. **1**(1), pp.3–24.

Appendix A – Literature Table

Study	Meniscus Injury / Intervention	Samples	Loading Regime	Outcome Measures		Soft Tissue Constraint	Main Findings
				Contact Mechanics	Tibial Kinematics		
Paletta et al. 1997	Total Meniscectomy and MAT (Lateral Meniscus)	Cadaveric N = 10 Age range: 22 – 48 yrs	Quasi-static	Not measured	Not measured	Capsule and ligaments mostly intact with incisions to apply pressure film/ conditions	41% - 64% increase in contact area with MAT vs total meniscectomy. 17 – 23% decrease in contact area with MAT vs intact
			Max Load: 1800N Fixed flexion: 0°, 30°, 60° All other axes unconstrained				
Allaire et al. 2008	Posterior Root Tear - Trans-tibial tunnel repair - total meniscectomy (Medial Meniscus)	Cadaveric N = 9 Age range: 24 – 54 yrs	Quasi-static	Not measured	Registration blocks and 3D models. (Performed on n = 6 samples due to technical malfunctions)	Capsule and ligaments mostly intact with < 1 cm incisions to apply conditions	Root tear mean contact pressures increased by 25.4%. Not sig. different to meniscectomy condition. Restored with tunnel repair. Kinematics: external rotation, anterior translation, adduction (varus) angle increased with root tear
			Custom Testing Jig Max Load: 1000N Fixed flexion: 0°, 30°, 60°, 90° All other axes unconstrained				
Marzo and Gurske – DePerio, 2009	Posterior root tear and tibial tunnel repair (medial meniscus)	Cadaveric N = 8	Static	Not measured	Not measured	Main ligaments intact. Anterior capsulotomy and menisco-tibial/femoral ligaments cut to insert sensors	24.4% increase in medial contact pressure and 20.2% decrease in medial contact area with root tear. Repair results similar to intact
			Max Load: 1800N Fixed flexion: 0° All other axes fixed				
Brophy et al. 2010	Partial meniscectomy and synthetic scaffold (Actifit) (Lateral meniscus)	Ovine N = 6	Dynamic	Not measured	Not measured	Capsule removed. Ligaments intact. Osteotomy around LCL insertion to detach and reattach the partial meniscectomy and replacement conditions.	Meniscus manipulation influenced mean and peak contact pressures throughout gait. Synthetic scaffold reduced mean and peak contact pressures compared to partial meniscectomy.
			Knee simulator TKR gait profile scaled to a sheep. Max load: 300N Max flexion: 35° AP force and TR torque driven. 10 gait cycles at 0.5 Hz (10 th cycle used)				

Study	Meniscus Injury / Intervention	Samples	Loading Regime	Contact Mechanics	Outcome Measures		Soft Tissue Constraint	Main Findings
					Meniscus Displacement	Tibial Kinematics		
Hein et al. 2011	Posterior horn avulsion and tibial tunnel repair (medial meniscus)	Cadaveric N = 7 Age range: 64 – 80 yrs	Static Max Load: 1800N Fixed flexion: 0° All other axes fixed	Not measured	3 x LVDT's positioned at the anterior, middle and posterior peripheral meniscus locations	Not measured	Most of the capsule was retained. Capsulotomies were performed to access the anterior and posterior horns.	Avulsed condition in the middle location showed significantly increased displacement (3.28 mm) compared with the intact and repaired. Repair restored meniscus displacements close to intact condition.
Bedi et al. 2012	Radial Tears, Suture Repair and Partial Meniscectomy (Lateral Meniscus)	Cadaveric N = 6	Dynamic Simulated Gait Cycle Max Load: 2100N Max flexion: 15° AP force and TR torque driven 20 cycles, 0.5 Hz	Tekscan pressure sensors Results taken at 15% and 45% peaks	Not measured	Not measured	Main ligaments intact. Anterior capsulotomy and menisco-tibial/femoral ligaments cut to insert sensors	Significant effect of most severe (90% width) radial tears and partial menis-ectomy on peak contact pressures vs intact condition at 45% gait.
Schill- hammer et al. 2012	Posterior horn detachment and tibial tunnel repair (lateral meniscus)	Cadaveric N = 8 Age range: 25 – 89 yrs	Dynamic Simulated Gait cycle. Scaled to 1/3 Max load: ~1000N Max flexion: ~20° AP force and TR torque driven Free ML and AA 5 slow gait cycles performed, 20s duration per cycle	Tekscan pressure sensors	Not measured	Resultant AP displacement and tibial rotation recorded	Main ligaments intact. Anterior capsulotomy and menisco-tibial/femoral ligaments cut to insert sensors	Tear caused maximum peak pressure to sig. increase from 2.8MPa to 4.2MPa in lateral compartment - repair decreased to 2.9MPa. No sig differences in tibial rotations/ translations.

Study	Meniscus Injury / Intervention	Samples	Loading Regime	Outcome Measures			Main Findings
				Contact Mechanics	Meniscus Displacement	Tibial Kinematics	
Kim et al. 2013	Posterior root tear, tunnel repair, meniscectomy and MAT (Medial Meniscus)	Cadaveric N = 10	Quasi-static Max load: 300N Fixed flexion: 0°, 30°, 60°, 90° All other axes unconstrained	Novel digital pressure sensor (Pliance-X germany)	Not measured	Not measured	Repaired posterior roots improved mean contact mechanics vs meniscectomy but this effect decreased as flexion increased. Repair or MAT did not restore back to intact conditions
Vrancken et al. 2014	Medial Meniscus detachment and reattachment of MCL	Cadaveric N = 6 Age range: 75 – 90 yrs	Dynamic Simulated squat (scaled down) Max load: 1000N Max flexion: 90° 3.4Nm tibial torque 67N AP force	Not measured	Rotengen Stereo - grammatic analysis (RSA)	Not measured	Results showed that releasing the fixation of the MM and MCL did not affect meniscal motion, as did suturing the meniscus back to the capsule again
Vrancken et al. 2016	Total Meniscectomy, replacement and MAT (Medial Meniscus)	Cadaveric N = 5 Age range: 70 – 88 yrs	Dynamic Simulated squat (scaled down) Max load: 1000N Max flexion: 90° 3.4Nm tibial torque 67N AP load	Tekscan pressure sensors (90° flexion statically)	RSA	Not measured	PCU implant showed similar results to allograft (reduced contact pressures as compared to meniscectomy) but unable to restore function of the native. Implant and allograft more mobile than the native condition.
Brial et al. 2019	MAT fixation techniques and meniscectomy. (Lateral Meniscus)	Cadaveric N = 6	Dynamic Simulated gait Max Load: 2100N Max flexion: 15° 0.5 Hz for 20 cycles AP force, TR torque driven AA and ML unconstrained	Tekscan pressure sensors (Results taken at 15% and 45% load peaks)	Not measured	ML and AP positions during gait cycle	Both MAT fixation methods improved contact mechanics compared to meniscectomy

Study	Meniscus Injury / Intervention	Samples	Loading Regime	Contact Mechanics	Outcome Measures		Soft Tissue Constraint	Main Findings
					Meniscus Displacement	Tibial Kinematics		
Ozeki et al. 2019	Posterior root tear, capsule detachment, and centralisation (suture anchor) repair (Lateral Meniscus)	Porcine N = 6	Static Max load: 200N Flexion: 0° All other axes constrained	Tekscan pressure sensors	Measurement method not specified but distance between two markers measured pre and during applied load	Not measured	Majority of posterior and anterior capsule removed. Most ligaments retained except LCL, resected to insert sensors.	Centralisation suture procedure restored lateral meniscus extrusion and contact pressures closer to intact condition as compared to root tear condition
Daney et al. 2019	Posterior root tears and trans tibial pull out / centralisation suture repair. Anatomic and Non-anatomic positions (medial meniscus)	Cadaveric N = 10 Age range: 35 - 65 yrs	Quasi-Static Instron E1000 Max load: 1000N Fixed flexion angles: 0°, 30°, 60°, 90° All other axes fixed.	Tekscan pressure sensors	3D coordinate measuring device (CMM) (ROMER Absolute Arm; Hexagon Manufacturing Intelligence) at 0° and 90°	Not measured	Capsule removed, ligaments retained.	Root tear condition generated the highest contact pressures and amount of extrusion measured at the MCL compared with all other conditions. Anatomic repair positioning restored near native contact mechanics and extrusion vs non-anatomic positioning
Paletta et al. 2020	Medial meniscotibial ligament detachment and suture anchor repair (medial meniscus)	Cadaveric N = 6 Mean age: 60 +/- 7 yrs	Pre loading + Static E1000 Instron Measurements taken in full extension + 10 Nm varus moment after 100 dynamic 0° - 90° FE cycles with 2.2 Kg load	Not measured	Ultrasound 12 mHz linear probe (GE Healthcare)	Not measured	Capsule intact. Damage and repairs performed arthroscopically	Meniscotibial ligament has a contributing role in meniscal stability. Mean and absolute extrusion increased with detachment and reduced with repair. However, still significantly increased from baseline (intact).

Study	Meniscus Injury / Intervention	Samples	Loading Regime	Contact Mechanics	Outcome Measures Meniscus Displacement	Tibial Kinematics	Soft Tissue Constraint	Main Findings
Walczak et al. 2021	Posterior root tear (Lateral and Medial Meniscus)	Cadaveric N = 11 Age range: 36 – 84 yrs	Axial compression Max load: 1800N Fixed flexion: 0°, 30°, 45°, 60°, 90° Dynamic rotation: 0° to 100° no load	Not measured	LVDT probe	Not measured	Capsule and ligaments mostly intact with < 1 cm incisions to create root tears	Root tears increase extrusion for both menisci. Medial meniscus extruded more than the lateral meniscus with a root tear.
Debieux et al. 2021	Meniscus Extrusion and contact area relationship Centralisation repair (Medial Meniscus)	Cadaveric N = 10 Age range: 43 – 60 yrs	Quasi-Static Instron E1000 Max load: 1000N Fixed flexion angles: 0°, 30°, 60°, 90° All other axes fixed.	Tekscan pressure sensors	Not measured as an outcome measure. Traction device pulled suture to pull the meniscus centrifugally to set extrusion value	Not measured	Mostly removed. Femoral osteotomy to access medial compartment	With roots intact, increased medial meniscus extrusion significantly decreased contact area. Greatest impact > 4 mm extrusion. Suture repair was sufficient at restoring contact area.
Hirose et al. 2022	Radial body tear of the lateral meniscus	Porcine N = 8	Robotic arm preconditioning cycles of 20° - 90° FE with 100N load. 300N load applied at 30° and 60° FE where results were taken. Max load: 300N Fixed flexion: 0° and 30°	Resultant force measured using a force-moment sensor	Reflective Markers and Motion capture (OptiTrak)	Not measured	Ligaments intact but most of the capsule removed to adhere markers to the meniscus body.	Most severe (90% width) radial body tear showed movement at the tear site and reduction in transmitted force.

Appendix B – Ethical Approval



**Health Research
Authority**

East Midlands - Leicester South Research Ethics Committee

The Old Chapel
Royal Standard Place
Nottingham
NG1 6FS

13 August 2018

Dr Louise Jennings
Associate Professor of Medical Engineering
University of Leeds
School of Mechanical Engineering
University of Leeds
Leeds
LS2 9JT

Dear Dr Jennings

Study title:	Optimising knee therapies through improved population stratification and precision of the intervention
REC reference:	18/EM/0224
Protocol number:	N/A
IRAS project ID:	239594

Thank you for your letter of 10 August 2018 responding to the Proportionate Review Sub-Committee's request for changes to the documentation for the above study.

The revised documentation has been reviewed and approved by the sub-committee.

We plan to publish your research summary wording for the above study on the HRA website, together with your contact details. Publication will be no earlier than three months from the date of this favourable opinion letter. The expectation is that this information will be published for all studies that receive an ethical opinion but should you wish to provide a substitute contact point, wish to make a request to defer, or require further information, please contact please contact hra.studyregistration@nhs.net outlining the reasons for your request.

Under very limited circumstances (e.g. for student research which has received an unfavourable opinion), it may be possible to grant an exemption to the publication of the study.

Confirmation of ethical opinion

On behalf of the Committee, I am pleased to confirm a favourable ethical opinion for the above research on the basis described in the application form, protocol and supporting documentation as revised.

Conditions of the favourable opinion

The REC favourable opinion is subject to the following conditions being met prior to the start of the study.

Management permission must be obtained from each host organisation prior to the start of the study at the site concerned.

Management permission should be sought from all NHS organisations involved in the study in accordance with NHS research governance arrangements. Each NHS organisation must confirm through the signing of agreements and/or other documents that it has given permission for the research to proceed (except where explicitly specified otherwise).

Guidance on applying for HRA and HCRW Approval (England and Wales)/ NHS permission for research is available in the Integrated Research Application System, at www.hra.nhs.uk or at <http://www.rdforum.nhs.uk>.

Where a NHS organisation's role in the study is limited to identifying and referring potential participants to research sites ("participant identification centre"), guidance should be sought from the R&D office on the information it requires to give permission for this activity.

For non-NHS sites, site management permission should be obtained in accordance with the procedures of the relevant host organisation.

Sponsors are not required to notify the Committee of management permissions from host organisations.

Registration of Clinical Trials

All clinical trials (defined as the first four categories on the IRAS filter page) must be registered on a publically accessible database. This should be before the first participant is recruited but no later than 6 weeks after recruitment of the first participant.

There is no requirement to separately notify the REC but you should do so at the earliest opportunity e.g. when submitting an amendment. We will audit the registration details as part of the annual progress reporting process.

To ensure transparency in research, we strongly recommend that all research is registered but for non-clinical trials this is not currently mandatory.

If a sponsor wishes to request a deferral for study registration within the required timeframe, they should contact hra.studyregistration@nhs.net. The expectation is that all clinical trials will be registered, however, in exceptional circumstances non registration may be permissible with prior agreement from the HRA. Guidance on where to register is provided on the HRA website.

It is the responsibility of the sponsor to ensure that all the conditions are complied with before the start of the study or its initiation at a particular site (as applicable).

Ethical review of research sites

The favourable opinion applies to all NHS sites taking part in the study, subject to management permission being obtained from the NHS/HSC R&D office prior to the start of the study (see “Conditions of the favourable opinion” above).

Approved documents

The documents reviewed and approved by the Committee are:

<i>Document</i>	<i>Version</i>	<i>Date</i>
Covering letter on headed paper	1	10 August 2018
Letter from sponsor		
Participant information sheet (PIS)	Version 4	30 April 2018
Participant information sheet (PIS)	4	02 May 2017
REC Application Form [REC_Form_26062018]		26 June 2018
Research protocol or project proposal	Version 1	04 April 2018
Summary CV for Chief Investigator (CI)		01 May 2018

Statement of compliance

The Committee is constituted in accordance with the Governance Arrangements for Research Ethics Committees and complies fully with the Standard Operating Procedures for Research Ethics Committees in the UK.

After ethical review

Reporting requirements

The attached document “After ethical review – guidance for researchers” gives detailed guidance on reporting requirements for studies with a favourable opinion, including:

- Notifying substantial amendments
- Adding new sites and investigators
- Notification of serious breaches of the protocol
- Progress and safety reports
- Notifying the end of the study

The HRA website also provides guidance on these topics, which is updated in the light of changes in reporting requirements or procedures.

Feedback

You are invited to give your view of the service that you have received from the Research Ethics

Service and the application procedure. If you wish to make your views known please use the feedback form available on the HRA website:

<http://www.hra.nhs.uk/about-the-hra/governance/quality-assurance>

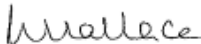
We are pleased to welcome researchers and R & D staff at our RES Committee members' training days – see details at <http://www.hra.nhs.uk/hra-training/>

18/EM/0224

Please quote this number on all correspondence

With the Committee's best wishes for the success of this project.

Yours sincerely



pp

**Mr John Aldridge
Chair**

Email: NRESCommittee.EastMidlands-LeicesterSouth@nhs.net

Enclosures: *"After ethical review – guidance for researchers"*

Copy to: *NHS Research Ethics Officer*

Appendix C – Standard Operating Procedure: MATLAB Object Tracking Script



SOP.01.07.I
Revision 1

SOP.01.07.I Standard Operating Protocol MATLAB Object Tracking Script for Meniscus Tracking

Author: Genevieve Pounds

Date: 29th March 2023

Revision: 1

1.0 RATIONALE

This standard operating procedure is used to collect displacement data from videos of coloured markers attached to the meniscus and tibia, during natural knee joint simulation. The procedures outlined in this document should be carried out in the preparation room of the Tissue Engineering Laboratory or Bioengineering laboratory, School of Mechanical Engineering, University of Leeds.

2.0 RESPONSIBILITY

It is the responsibility of the researcher to ensure that all test procedures outlined in this document are carried out in accordance with these instructions. This procedure involves working with electronics and code. The researcher should ensure they are familiar with all the procedures covering meniscus tracking in the iMBE laboratories, particularly disposal techniques. Contact a member of iMBE technical support to arrange demonstration or to seek assistance

3.0 ASSOCIATED DOCUMENTS

SOP.01.07.H Camera Programming for Meniscus Tracking

4.0 MATERIALS

- Input video files: saved video files (eg: mp4 format) from data collection
- Calibration Image (still image of markers at a zero position to calibrate)
- Known diameter / size of markers eg: 2 mm

- Live Scripts: **MultipleMarkerTrackingScript.mlx** – This can track one or more objects (of the same colour) in a video at the same time.

MATLAB documentation: <https://uk.mathworks.com/help/vision/ug/motion-based-multiple-object-tracking.html>

Colour segmentation and Blob Analysis Examples:

https://uk.mathworks.com/help/vision/examples.html?category=computer-vision-with-simulink&tid=CRUX_topnav

5.0 EQUIPMENT

Computer with MATLAB installed

Download MATLAB toolboxes:

- Computer Vision Toolbox
- Image Processing Toolbox

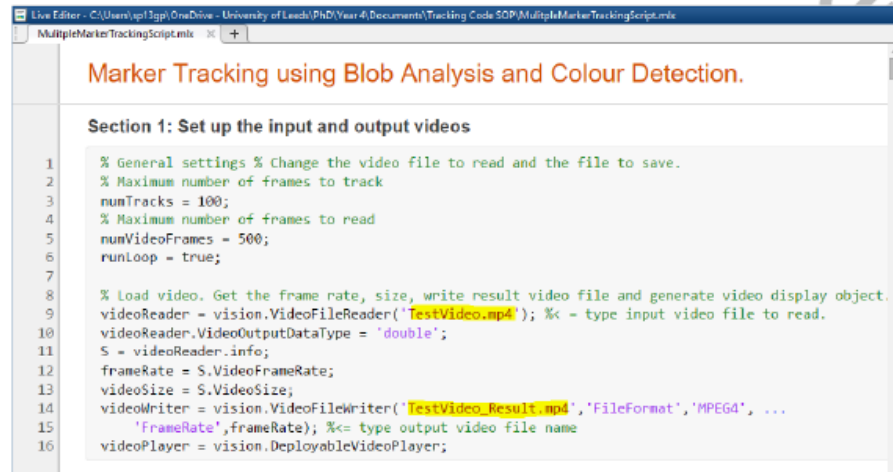
6.0 PROCEDURE

1. Step 1: Read the input video parameters (eg: frame rate and resolution) and set up the output video of the tracking result using 'vision.VideoFileReader' and 'vision.VideoFileWriter' functions.

- 1.1. Take a video of one or more moving coloured markers. This is your input video.
- 1.2. Save the input video to a folder in a preferred format (eg: mp4) and save tracking script (see materials section 4.0) to the same folder. Open MatLab and locate this folder in the directory (on the left of the screen).
- 1.3. Open the script and in **line 9** type the input video file name (within the quotation marks) in the first section (eg: 'TestVideo.mp4'). In **line 14**, change the output video name to the desired resultant output video name (make sure different to input video name, otherwise it will overwrite the original video) (**Figure 1**)

- 1.4. Click **'Run Section'** on the top toolbar of the Live Editor tab. Variables should appear in the workspace, including the 'frameRate' and 'videoSize' from the input video. The 'videoPlayer' and 'videoWriter' have also been set up to output the results in due course.

** Make sure video input file is labelled correctly to avoid errors.*



```

Live Editor - C:\Users\j3gpl\OneDrive - University of Leeds\PhD\Year 4\Documents\Tracking Code SOP\MultipleMarkerTrackingScript.mlx
MultipleMarkerTrackingScript.mlx
Marker Tracking using Blob Analysis and Colour Detection.

Section 1: Set up the input and output videos

1  % General settings % Change the video file to read and the file to save.
2  % Maximum number of frames to track
3  numTracks = 100;
4  % Maximum number of frames to read
5  numVideoFrames = 500;
6  runLoop = true;
7
8  % Load video. Get the frame rate, size, write result video file and generate video display object.
9  videoReader = vision.VideoFileReader('TestVideo.mp4'); %< - type input video file to read.
10 videoReader.VideoOutputDataType = 'double';
11 S = videoReader.info;
12 frameRate = S.VideoFrameRate;
13 videoSize = S.VideoSize;
14 videoWriter = vision.VideoFileWriter('TestVideo_Result.mp4', 'FileFormat', 'MPEG4', ...
15   'FrameRate', frameRate); %<= type output video file name
16 videoPlayer = vision.DeployableVideoPlayer;
  
```

Figure 1. The first section of the script highlighting the areas to type the names of your input and output videos in mp4 format. After running this section, information from the input video should appear in the workspace on the right of the screen.

2. Step 2: Identify the markers in the first frame of the video by using the colour thresholder application.

- 2.1. In section 2 of the script at **line 21**, delete the '%' at the beginning of the line and press 'Run Section'. This will open the Colour Thresholder Application in a separate window (**Figure 2**)

Section 2: Create a Mask function to detect the coloured markers.

```

17 % Read Frame 1
18 frame = step(videoReader);
19
20 %% Create a mask function using the colour thresholder app.
21 colorThresholder(frame); % <- comment line out after performing once on a video file.
22
23 % Use HSV option and toggle the colour wheel so the marker colour is only showing. Toggle the
24 % saturation and contrast bars to isolate the colour marker even more. Click export and
25 % 'export as function' and save. File default name is 'Mask.m'.
26
27 % Display frame 1 and the colour thresholded image.
28 subplot(1, 2, 1)
29 imshow(frame)
30
31 % May need to remove disturbances from the frame if the markers are not contrasting enough.
32 mask = Mask(frame); %<= insert name of colour threshold function file here.
33 mask = imopen(mask, strel('square',6));
34 mask = imfill(mask, 'holes');
35
36 subplot(1, 2, 2)
37 imshow(mask)
38
39 % Reset video loading
40 videoReader.reset;

```

Figure 2. In section 2, delete the '%' in front of the 'colorThresholder(frame)' line (highlighted) and press 'Run Section' on the top toolbar

- 2.2. In the Colour Thresholder Application, select the HSV (Hue, Saturation, Value) colour space button.
- 2.3. Using this colour space, toggle the H, S and V parameters on the right of the window to segment out the marker colour from the background colours in the video frame (eg: green). When finished, click Export > Export Function (**Figure 3**)
- 2.4. An untitled script file containing these colour segmentation parameters will appear in the editor window in MatLab. Click '**Save As**' > name as '**Mask.m**' to the current folder. This is the Mask file containing the segmentation parameters. (as default it will be shown as: createMask.m).

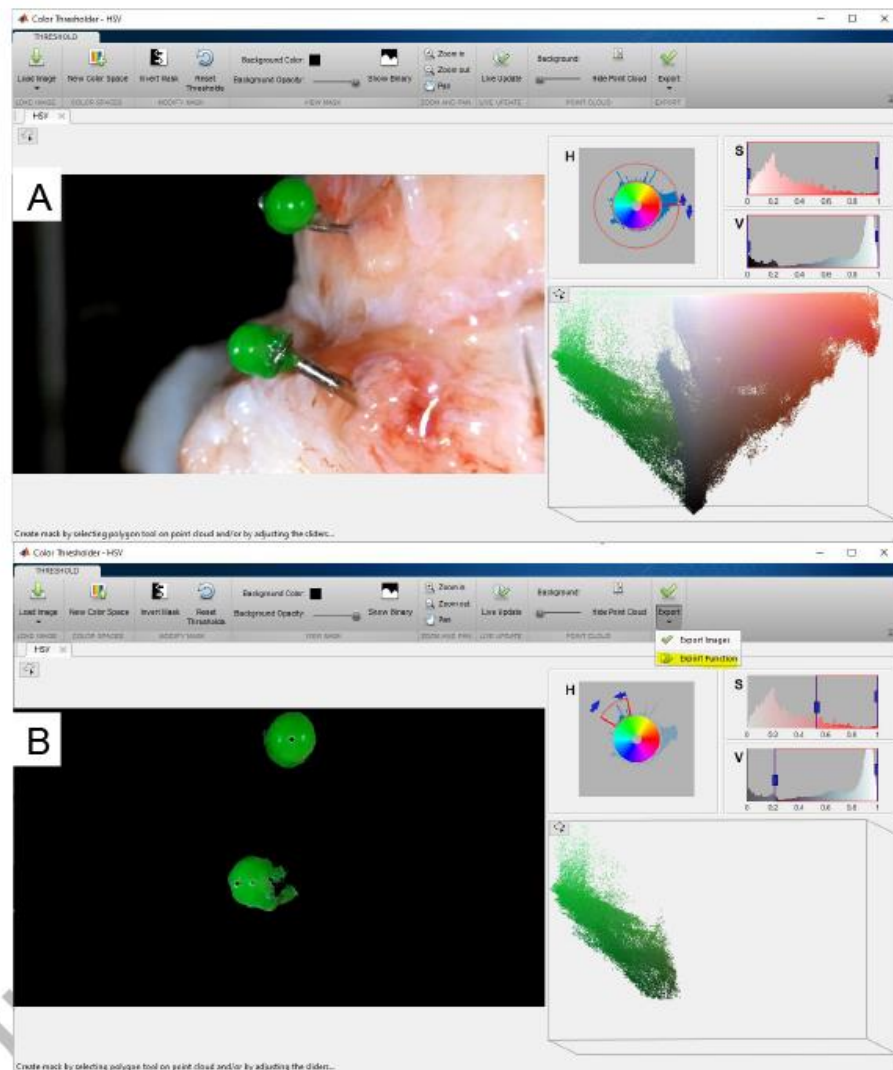


Figure 3. In the HSV colour space of the colour thresholder application. (A) The screen layout with the first frame of the video. (B) View after toggling the H, S and V parameters on the right side of the screen to segment the green colour of the markers out from all other colours.

- 2.5. Return to section 2 of the script and insert a '%' at the beginning of **line 21** to stop the colour thresholder app from opening again (as we have already completed this step).
- 2.6. In **line 32**, make sure the '*mask = Mask(frame)*' is named the same as the **Mask.m** file recently saved.
- 2.7. Click '**Run Section**' again.
- 2.8. An image output will appear (**Figure 4**) showing the first frame in the video and the segmented colour mask file as a binary image. The pixels associated with the marker colour (eg: green) have been assigned '1' and the pixels associated with the background (i.e. not the marker) have been assigned '0' in this binary overlay.

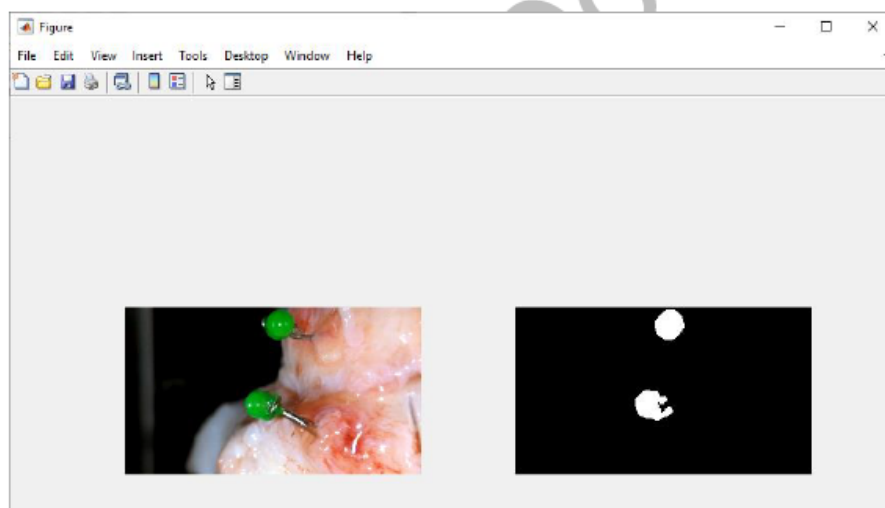


Figure 4. Colour thresholding output showing the first frame in the video and the binary image of the marker colour segmentation.

3. Step 3: Set the blob analysis parameters for object tracking

- 3.1. Scroll down to section 3 (**Figure 5**) and click 'Run Section'.
- 3.2. The 'MinimumBlobArea' (line 46) can be changed to only detect certain sized objects in the video. i.e. this is currently set to detect objects larger than a 600 pixel area.
- 3.3. 'centroidLog' (line 63) is an empty spreadsheet/matrix of NaN cells. This will be where the x and y coordinates of each blob centroid will be deposited as the tracking is applied to all the frames of the video

```

Section 3: Create blob analysis object.
41 % Create object for blob analysis
42 % Create an object for blob analysis (center point / boundary box)
43 blobAnalyser = vision.BlobAnalysis('AreaOutputPort', false, ...
44     'CentroidOutputPort', true, ...
45     'BoundingBoxOutputPort', true, ...
46     'MinimumBlobArea', 600, ...
47     'ExcludeBorderBlobs', true);
48
49 %% Initialise tracks (creates an array of tracks. Each track is a structure representing a
50 % moving object in a video. The purpose of the structure is to maintain the
51 % state of a tracked object. Structure contains following fields:
52
53 tracks = struct ( ...
54     'id', {}, ... % ID.
55     'bbox', {}, ... % Bounding box in the current frame (for display).
56     'kalmanFilter', {}, ... % Kalman filter for this object tracking.
57     'age', {}, ... % Age, number of frames since track was first detected.
58     'totalVisibleCount', {}, ... % Total number of frames in which the track was detected.
59     'consecutiveInvisibleCount', {}); % Number of consecutive frames for which the track
60 % was not detected (invisible).
61
62 nextId = 1; % ID of the next track.
63 centroidLog = nan(numTracks, 2*numVideoFrames); %'empty' matrix of 100 x 1000 NaN
64 BBoxLog = nan(numTracks, 2*numVideoFrames);
65 frameCount = 1;

```

Figure 5. Section 3 of the script to set the blob analysis parameters.

4. **Step 4: Run the object tracking loop. This section attaches a box (blob) around the markers in the video assigned with the pixel allocation '1' from the binary image overlay (Mask file). This is applied to the first frame in the video and then the loop applies these parameters to all the frames in the video whilst deploying a video player to observe the tracking.**

- 4.1. Scroll down to section 4 and input the 'Mask' file name into line 71 (**Figure 6**).

```

Section 4: Marker Detection and Tracking (Video Player Deployed)
66 while (runLoop && ~isDone(videoReader))
67     frame = step(videoReader); % Detect objects in the frame from functions performed above.
68
69     % Detect moving objects (areas): Binary matrix 'mask': 1 is foreground (coloured marker) an
70     % background.
71     mask = Mask(frame); %<= insert name of colour threshold (mask) funtion here.
72
73     % Centre point/bounding box detection on mask:
74     [centroids, bboxes] = step(blobAnalyser, mask);
75
76     % Predict the position in the current frame from the previous frame.
77     % Predict new locations of existing tracks using the kalman filter:
78     for i = 1:length(tracks) %returns length of largest array dimension in tracks.
79         bbox = tracks(i).bbox;
80         predictedCentroid = int32(predict(tracks(i).kalmanFilter)); % Predicts the current loca
81         tracks(i).bbox = [predictedCentroid - bbox(3:4)/2, bbox(3:4)]; % Shifts the bounding bo
82         % centre is at the predicted location.
83     end
84

```

Figure 6. Running the tracking loop section. Change the highlighted area (line 71) to the name of the save Mask file (see section 2.4 in this document).

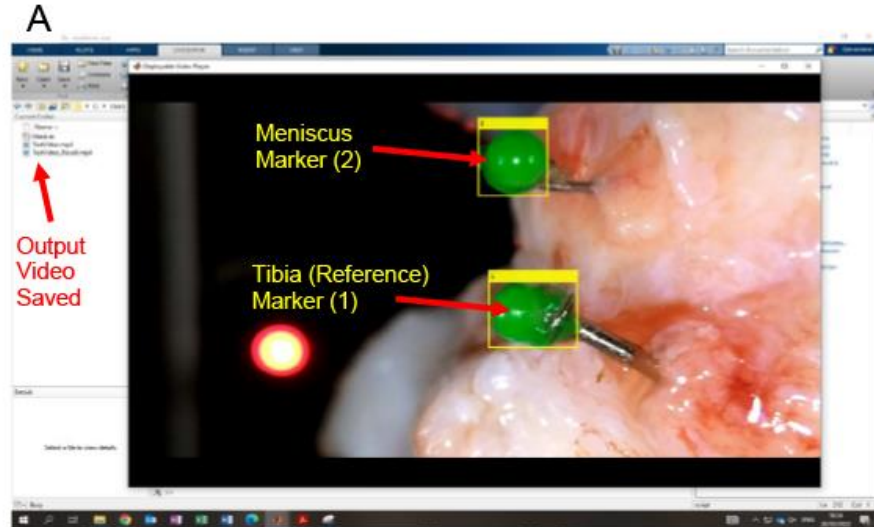
- 4.2. Click 'Run Section' (deploys a video player pop up – wait until the full video is processed, the output video will save concurrently) (**Figure 7A**)

- 4.3. As this loop is running, the x and y coordinates of the centre of the numbered yellow boxes (attached to the markers) are deposited into the spreadsheet 'CentroidLog' (**Figure 7B**)

N.B. This section can take a few minutes (depending on the size of the video).

If errors occur check:

- *The minimum blob area value is large enough?*
- *Colour throughout video – does the lighting change?*
- *Do the markers leave the video frame at any point during the video?*



B

x axis pixel coordinates (odd column numbers)

y axis pixel coordinates (even column numbers)

etc...

First Marker (eg: Tibia Marker is no.1 in this case)

Second Marker (i.e. Meniscus Marker is no.2 in this case)

	1	2	3	4	5	6	7	8	9	10	11
1	776	535	757	534	746	533	737	533	737	532	734
2	902	16	897	12	896	11	892	10	893	12	893
3	NaN	NaN	NaN	NaN	NaN	NaN	NaN	NaN	NaN	NaN	NaN
4	NaN	NaN	NaN	NaN	NaN	NaN	NaN	NaN	NaN	NaN	NaN

Figure 7. (A) Screenshot of the tracking loop in section 4 running with the video player pop up. The blob analysis assigns and numbers yellow boxes around the objects associated with the segmented colour throughout all the frames in the video. (B) Image of the centroidLog variable and how the X and Y pixel values are deposited as the section 4 runs.

5. Step 5: Filter out the marker x and y pixel coordinates from the centroidLog file.

- 5.1. In section 5, change lines 226 and 229 to the correct numeric marker labels (eg: 1 or 2) from the tracking output (**Figure 8**).
- 5.2. Click 'Run Section' (This extracts the x and y pixel data from CentroidLog and puts the data into column arrays)

```

Section 5: Filter Out the Marker Pixel Tracks from CentroidLog
223 % Run sections above and look at numbered blobs of interest in the video. Filter these rows of
224 % interest out of the centroidLog data (not the predicted tracks). Use rmissing
225 % function to exclude remaining NaNs in the data.

Marker (eg: Meniscus)
226 centroidLogM = rmissing((centroidLog(2,:))); % <= number of marker track (filter to centroid log row)
227 x = centroidLogM(:, 1: 2: end)'; % Reads odd numbers in row as x position in centroid log
228 y = centroidLogM(:, 2: 2: end)'; % Reads even numbers in row as y position

Reference Marker (eg: Tibia)
229 centroidLogT = rmissing((centroidLog(1,:)));
230 Tx = centroidLogT(:, 1: 2: end)'; % Reads odd numbers in row as x position in centroid log
231 Ty = centroidLogT(:, 2: 2: end)'; % Reads even numbers in row as y position

```

Figure 8. Section 5: filter out the X and Y tracking tracks into variables. Remember to change the highlighted numbers to the correctly assigned object numbers in the video.

6. Step 6: Calibrate the video to get displacement data in millimetres using the input calibration image (see materials section 4.0)

- 6.1. In section 6, go to line 236 and input the name of the calibration image file.
- 6.2. In line 237, make sure the 'imtool' function has no '%' in front of it (**Figure 9A**)
- 6.3. Click 'Run Section' – This will open the 'imtool' application in a new window. In this application, click the ruler icon on the toolbar and measure the diameter of the two markers (eg: meniscus and tibia) in pixels (**Figure 9B**)
- 6.4. Got back to section 6 in the code and input these values into the corresponding lines (lines 241 and 242). Make sure the known marker diameter (eg: 2 mm) is inputted correctly above (lines 239 and 240)
- 6.5. Lastly insert a '%' before the imtool function on line 237 (**Figure 9C**)
- 6.6. Click 'Run Section' to update the calibration factors

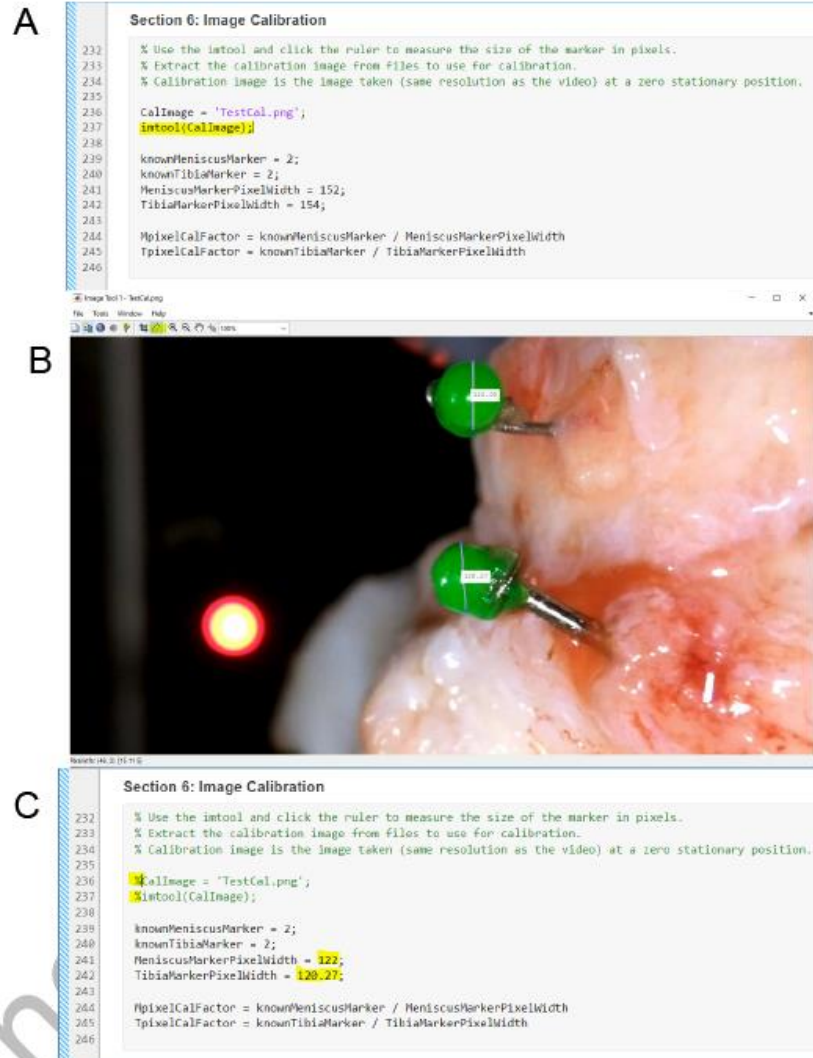


Figure 9. Section 6 image calibration. (A) Input the correct calibration image file name into line 236 and click run section to open the imtool application. (B) Screenshot of the imtool application with the marker diameters measured using the ruler icon in the top left of the screen. (C) Input the corresponding marker diameters into lines 241 and 242 of section 6 of the script. Put a '%' before lines 236 and 237 before running section 6 again and updating the calibration factor parameters (make sure the known marker diameters (lines 239 and 240) are correct eg: 2 mm).

7. Step 7: Process the calibrated graphical outputs (in millimetres) of the X and Y position throughout the video duration.

7.1. In section 7, click 'Run Section' (Figure 10)

7.2. Two output graphs should appear, one for the X positions changes and one for the y positions changes (with calibration applied) (Figure 11)

```

Section 7: Graphs of temporal changes
Estimated X Values
247 figure;
248 t = ((@(size(centroidLogI,2)/2-1))/frameRate)'; %size returns a row vector who's elements are the same length of the
249 % corresponding dimensions for centroidLogI then divided by the video frame rate.
250
251 % Find the change in position for x coordinates of the marker and multiply by pixel calibration factor:
252 changeX = (x - x(1,1))*TpixelCalFactor;
253 TibiaChangeX = (Tx - Tx(1,1))*TpixelCalFactor;
254
255 % Graph the result:
256 plot(t,changeX);
257 hold on;
258 plot(t, TibiaChangeX);
259 title('Marker Position');
260 xlabel('Video Time (s)');
261 ylabel('X Displacement (mm)');
262 legend('Meniscus x-axis', 'Tibia x-axis')
263 hold off

Estimated Y values
264 % Find the change in position for y coordinates of the marker and multiply by pixel calibration factor:
265 changeY = (y - y(1,1))*TpixelCalFactor;
266 changeY = (changeY - 2*changeY); % < = invert the y data because the image axis is flipped by default.
267 TibiaChangeY = (Ty - Ty(1,1))*TpixelCalFactor;
268 TibiaChangeY = (TibiaChangeY - 2*TibiaChangeY); % < = invert the y data because the image axis is flipped by default.
269
270 % Graph the result:

```

Figure 10. Section 7 of the script to process the temporal changes of the x and y parameters for each marker throughout the video duration.

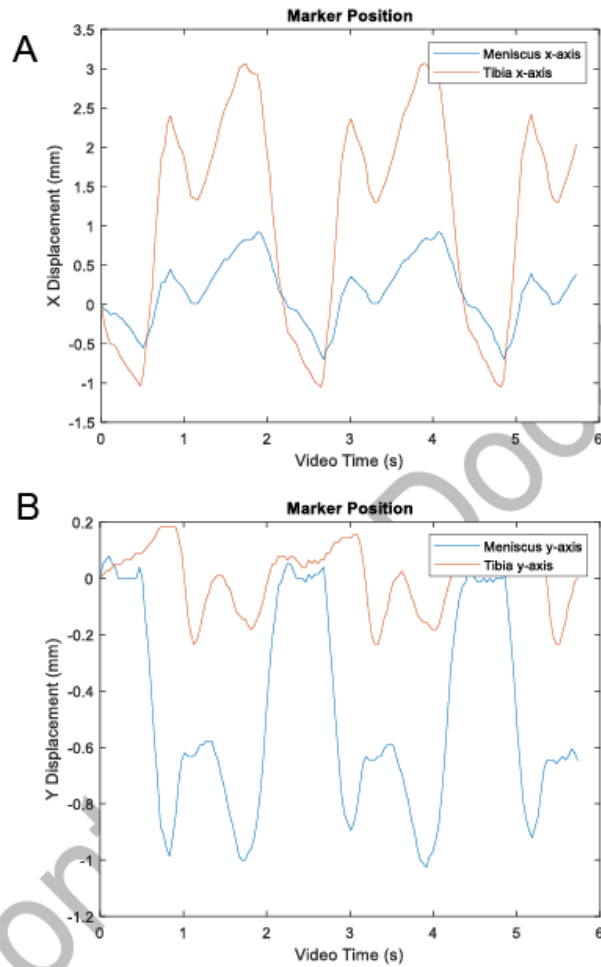


Figure 11. Example outputs from section 7 showing the calibrated (A) X-axis displacement and the (B) Y-axis displacement of the meniscus (blue lines) and tibia (orange lines) markers throughout the duration of the video.

8. Step 8: Extract one cycle and calculate the relative displacement.

To extract a section of this graph (e.g: a gait cycle) you need to know the duration of your gait cycle eg: 2 seconds and roughly where the gait cycle begins (eg: using a flashing light or a counter in the image).

You also need to know how many frames (frame rate) there are in this cycle period. Eg: 2 second duration gait cycle filmed with a camera at 30 frames per second = 60 frames. Therefore, ~ 60 data points need to be extracted from the start of the cycle.

8.1. Go to **line 282** of section 8 and input the numbered data points which span the cycle you would like to extract (**Figure 12**) (use the video duration variable 't' in the workspace to help get the row numbers of the cycle).

8.2. For example, in **Figure 12**, data points 30 to 60 were extracted as the variable 'cycle'. The total number of data points between these cells is 61 frames (there is a small amount of video lag time vs real world time) and is therefore updated in the variable 'CyclePercent2' (This defines the x-axis of the new filtered graph). The results in the new graph were filtered to start from a displacement of 0 at the beginning of the cycle.

8.3. Click 'Run Section'

N.B. A 2 second cycle time won't fall perfectly in the results output due to camera recording lags (Figure 13A). However, this is filtered out in the final graphical output (Figure 13B).

Section 8: Extract data from One Cycle

```

281 % Extract the array of rows (n:n) for one cycle as a new variable changeX2.
282 cycle = (30:90);
283
284 changeX2 = changeX(cycle);
285 changeX2Diff = (changeX2 - changeX2(1,1));
286 TibiaChangeX2 = TibiaChangeX(cycle); %<---
287 TibiaChangeX2Diff = (TibiaChangeX2 - TibiaChangeX2(1,1));
288 CyclePercent2 = linspace(0,2,61);
289
290 changeY2 = changeY(cycle);
291 changeY2Diff = (changeY2 - changeY2(1,1));
292 TibiaChangeY2 = TibiaChangeY(cycle);
293 TibiaChangeY2Diff = (TibiaChangeY2 - TibiaChangeY2(1,1));

```

Figure 12. Section 8. Change the highlighted areas to extract the data points spanning one gait cycle from the output signals displayed in Figure 11.

9. Step 9: Scroll to Section 9 and generate a new graph with the filtered cycle results and the calculated relative displacement results.

- 9.1. Click 'Run Section' to generate the graphical outputs for both the X and Y tracking results and the relative displacement (**Equation 1** and **Figure 13**). Don't forget to put the polarity of the displacement on the graphs to help understand the direction of the movement of the markers.

Equation 1. $D_R = D_M - D_T$

relative displacement (D_R)

other marker displacement (eg: meniscus) (D_M)

reference marker displacement (eg: Tibia) (D_T)

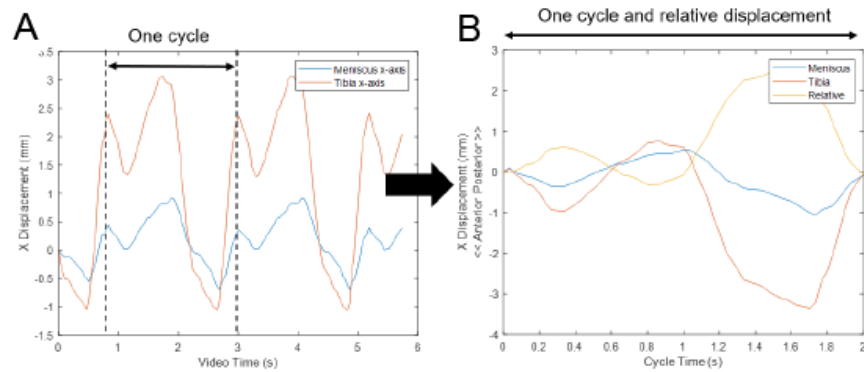


Figure 13. (A) X-displacement results cycle filtering process from section 8. (B) Output graph with the relative displacement (yellow line) results included over the duration of the cycle.

10. SAVE the workspace and the graphical outputs

Appendix D - Standard Operating Procedure: Camera Programming for Meniscus Tracking



SOP.01.07.H
Revision **2**

SOP.01.07.H Standard Operating Protocol Camera Programming for Meniscus Tracking

Author: Genevieve Pounds

Date: 29.03.23

Revision: 2

1.0 RATIONALE

This standard operating procedure is applied to the programming of miniature cameras used for meniscus tracking when simulating natural knee joints. The procedures outlined in this document should be carried out in the preparation room of the Tissue Engineering Laboratory or Bioengineering laboratory, School of Mechanical Engineering, University of Leeds.

2.0 RESPONSIBILITY

It is the responsibility of the researcher to ensure that all test procedures outlined in this document are carried out in accordance with these instructions. This procedure involves working with electronics and code. The researcher should ensure they are familiar with all the procedures covering meniscus tracking in the iMBE laboratories, particularly disposal techniques. Contact a member of iMBE technical support to arrange demonstration or to seek assistance

3.0 ASSOCIATED DOCUMENTS

SOP.01.07.E Single Station Knee Simulator 2 and 3
SOP.01.07.F Single Station Knee Simulator 4
SOP.06.01 Preparation of Porcine Knee Joints for use in the SSKS
SOP.11.24 Preparation of human knee samples for models of meniscus interventions including dynamic contact mechanics
SOP.01.07.I MATLAB Object Tracking Script

4.0 MATERIALS

Helpful resources to support this documentation:

<https://www.raspberrypi.com/documentation/accessories/camera.html>

<https://www.tomshardware.com/uk/>

<http://www.davidhunt.ie/raspberry-pi-zero-with-pi-camera-as-usb-webcam/>










<https://randomnerdtutorials.com/video-streaming-with-raspberry-pi-camera/>

5.0 EQUIPMENT

The equipment required to is described and illustrated in Table 1.

- A smart phone with a hotspot internet connection is required.

Table 1. Equipment required for meniscus tracking

3 x RPi v2 camera modules with lens adjuster		3 x Micro SD cards (minimum 16GB)	
3 x RPi Zero W CPU		3 x RPi Zero Camera Cases	
3 x RPi Zero Camera Adaptor		3 x Micro USB to USB cables	
1 x adjustable camera rig compatible with the single station knee simulator		1 x Standard Laptop (Eg: Dell Latitude)	
3 x 3D printed VeroClear push fit camera casings			

6.0 PROCEDURE

1. Set up the Raspberry Pi Hardware and Software

- 1.1. Connect the camera hardware together as shown in **Figure 1** to form one Raspberry Pi (RPi) Camera Unit. Be careful not to touch the metal parts of the circuit board or camera and remember to keep the units in anti-static bags when not in use



Figure 1. One Raspberry Pi camera unit with v2 camera, RPi zero CPU and casing

- 1.1. Download Raspbian OS (Lite version) on the SD card. This might require a SD-card to USB adapter if the laptop does not have an SD card socket built in. Website link to find Raspbian: <https://www.raspberrypi.org/software/>.

N.B. If using a university computer, you will need to send a ticket to IT and fill out a 'Local_Administrative_Privileges_template' form to download Raspbian Imager

- 1.2. Download the Imager Application from the link and within the Raspbian Imager application click > Raspberry Pi OS (other) > Raspberry Pi OS Lite (32-bit) > Click the settings cog at the bottom right of the window.

- 1.3. In the settings area you can enable the: hostname (*raspberrypi*), enable ssh, set username (*pi*) and password (*raspberrypi*) and connect to your mobile phone hotspot (**Figure 2**).

- 1.4. Save the settings and write the software to the SD card. Click 'Write'.

N.B. This takes a few minutes to write the software to the SD card

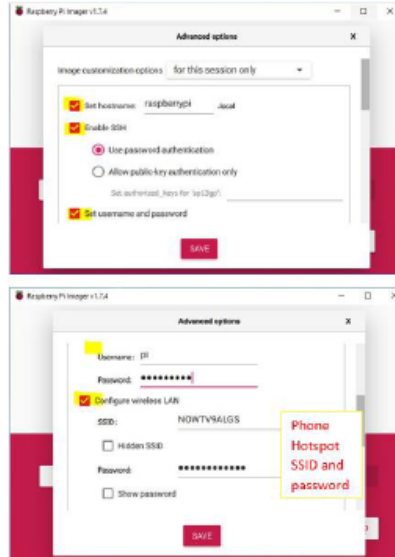


Figure 2. Applying advanced options when write the new version of Raspberry Pi OS Lite to the SD card. Make sure the SSID and password of the phone hotspot are entered.

2. Set up each Raspberry Pi Camera Unit as a headless connection via ssh (secure shell) and USB

- 2.1. After completing section 1 above, open the SD card files (Boot D:) and create a new empty text file (delete the .txt file extension) and name it '*ssh*' to allow remote access
- 2.2. Open the file 'config.txt' in the root directory of the SD card (Boot D:). Type the line: '*dtoverlay=dwc2*' at the bottom of the text and save.
- 2.3. Open the file 'cmdline.txt' and type the line: '*modules-load=dwc2,g-ether*' at the end and click save (Figure 3)

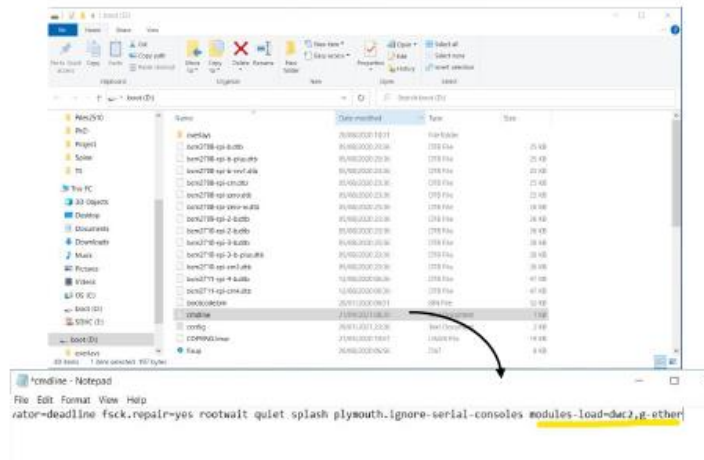


Figure 3. Opening the cmdline.txt file and adding the following line to the text.

- 2.4. Next safely remove the SD card and put it into the Raspberry Pi Camera Unit SD socket.
- 2.5. Restart the laptop.
- 2.6. Connect the laptop to the phone hotspot SSIS and password (***in order for a successful initial connection to be made, both the laptop and the Raspberry Pi need to be on the same network***)
- 2.7. Using a micro-USB to USB cable, connect the Raspberry Pi camera unit to the laptop via the USB port, not the power port (**Figure 4**).

N.B. It takes a few minutes for the laptop to detect the Raspberry Pi. A 'USB device malfunctioned' message might pop up, but shortly followed by a positive connection beep sound. This means the connection has been successful.

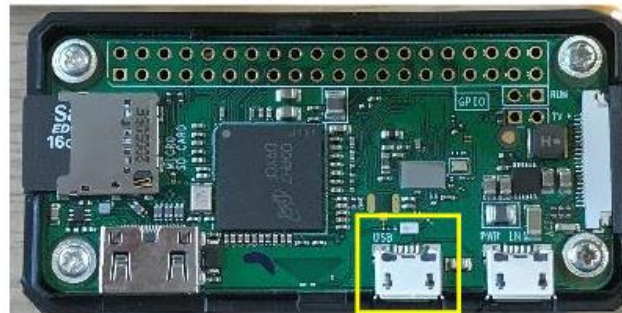


Figure 4. USB port on Raspberry Pi zero.

2.8. Following a successful USB connection open the windows Command Prompt and login using **ssh pi@raspberrypi** followed by the password: **raspberrypi** and enter

N.B. when typing the password, it will be invisible

2.9. The connection should now be successful between the laptop and the raspberry pi operating system. The RPi Camera Unit can now be controlled via command prompt

2.10. To allow for a more intuitive set up and avoid confusion between cameras, change the hostname and password as follows:

2.10.1. Type '**sudo raspi-config**' into the command prompt, this will open the configuration GUI (**Figure 5**)

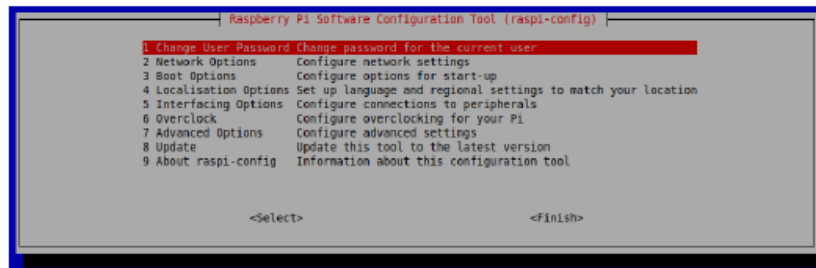


Figure 5. RPi configuration tool window (raspi-config)

2.10.2. Select '1 Change User Password'

2.10.3. Type the new password '**anterior**', press enter

2.10.4. Select '2 Network Options'

2.10.5. Select 'N1 Hostname'

2.10.6. Type the new hostname '**antcam**', press enter

2.10.7. Click reboot to save the settings (the RPi will turn off and disconnect. Unplug and replug the USB cable then open command prompt and type: **ssh pi@antcam** followed by the new password and enter (**Figure 6**)

N.B. the password is always invisible when logging in.


```

Command Prompt - ssh pi@antcam
Microsoft Windows [Version 10.0.19041.1110]
(c) Microsoft Corporation. All rights reserved.

C:\Users\genev>ssh pi@antcam
pi@antcam's password:

```

Figure 6. Login with the above via command prompt

2.11. Repeat all the steps above to set up each RPi Camera Unit

2.11.1. Change the login credentials for each RPi Camera Unit to make each camera easier to identify as indicated in Table 2.

Table 2. Login credentials to assign to each RPi Camera Unit

	Anterior camera	Posterior Camera	Medial Camera
Hostname	antcam	postcam	medcam
Username	pi	pi	pi
password	anterior	posterior	medial

Camera triggering methods (webcam or python)

Videoin and tracking meniscus markers is possible through two different triggering methods: as a webcam through a standard camera application or by using a python script. For porcine samples, the cameras were all used as webcams due to the lower magnitudes of motion. For human samples, the medial camera remained as a webcam, but the anterior and posterior cameras were triggered through python. The current set up for human knee samples using all three camera is described in **Figure 7**.

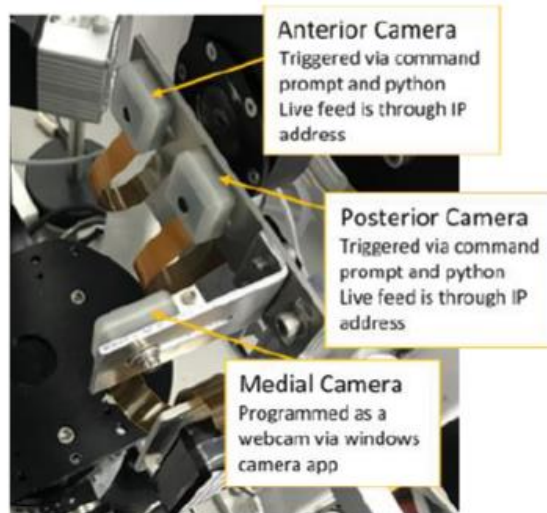


Figure 7. Camera positioning set up and triggering methods for human samples

Enabling the camera to be viewed as a webcam (Section 3) is easy because a standard camera application (eg: Windows Camera) can be used to view a live feed and also record in 1920 x 1080 HD as an .mp4 file and take images at the click of a button. However, the camera settings are limited to 30 frames per second. Meaning filming faster movement can create motion blur of the marker in the video. The medial camera is set further away from the markers than the anterior and posterior cameras, therefore, viewing this camera as a webcam at 30fps is suitable to capture movement of the marker for human samples.

Triggering the RPi Camera Units through python (Section 4) allows for a wider array of camera settings and configurations to be used, including filming at a higher frame rate (eg: 90 frames per second) to capture faster movement (or more movement within the same time frame). This method allows for higher clarity of marker movement in the video when testing human samples. However, this method is more complex as the process is not all contained in the same application. A live-feed of the camera will have to be enabled by connecting to the cameras IP

addresses through python and then viewing through a browser (Section 5). The cameras themselves will be triggered by writing python scripts for video capture and/or image capture.

3. Triggering the cameras as a webcam (UVC gadget)

3.1. Connect the RPi Camera Uni via USB and connect via ssh as explained previously in section 2.7

3.2. Type in the following lines of code:

```
pi@antcam:~ $ sudo apt-get update
pi@antcam:~ $ sudo apt-get install git
pi@antcam:~ $ cd /home/pi
pi@antcam:~ $ git clone https://github.com/climberhunt/uvc-gadget.git
pi@antcam:~ $ cd uvc-gadget/
pi@antcam:~ $ ls
pi@antcam:~ $ sudo cp piwebcam.service /etc/systemd/system/
pi@antcam:~ $ sudo systemctl enable piwebcam
pi@antcam:~ $ sudo nano /boot/cmdline.txt
```

(This opens the cmdline text file. Change the last line from)

```
modules-load=dwc2,g-ether
```

to

```
modules-load=dwc2,libcomposite
```

Then click Ctrl+X and then click Y to save this file and exit
Continue by adding the following lines:

```
pi@antcam:~ $ cd /home/pi/uvc-gadget
pi@antcam:~ $ make

pi@antcam:~ $ sudo ln -s
/lib/systemd/system/getty@.service/etc/systemd/system/getty
.target.wants/getty@ttyGS0.service
```

3.3. This will display the RPi Camera as a UVC gadget on the laptop

****N.B:** When set up as a webcam, the RPi won't be available as a headless ssh connection. To restore the headless connection, take out the SD card and insert it into the laptop and change the cmdline.txt back to:

```
modules-load=dwc2,g-ether
```

You'll then be able to open command prompt and login via `ssh@hostname`

- 3.4. Unplug the replug RPi and wait about 10 seconds (until a positive connection sound occurs)
- 3.5. Open the Windows Camera App and click the switch camera icon in the top right corner
- 3.6. A live feed from the RPi Camera Unit should now be showing. Press the record button to trigger the camera. Videos will be saved by default to the pictures directory on the local C: drive

4. Triggering the cameras through ssh, command prompt and Python

4.1. Open command prompt and login via ssh (`ssh pi@antcam`)

4.2. Perform the following updates and installs:

```
pi@antcam:~ $ sudo apt update && sudo apt full-upgrade -y
pi@antcam:~ $ sudo apt install proftpd (access files via WinSCP)
pi@antcam:~ $ sudo apt install -y gpac (converts video formats)
```

4.3. In order to easily transfer video files from the RPi to the computer, a file exchange programme is required such as WinSCP (Figure 8). Download WinSCP via the following link and login to the RPi directory with the hostname, username and password: <https://winscp.net/eng/download.php>

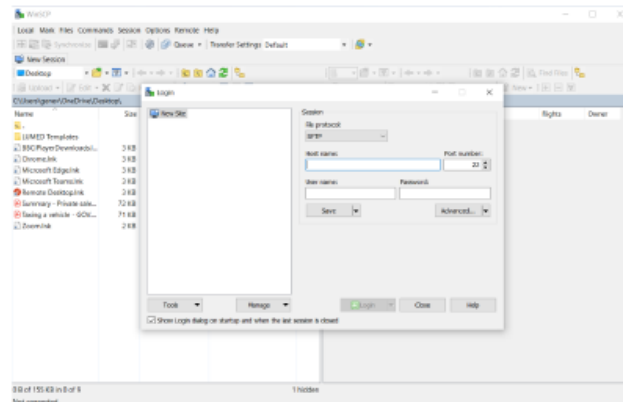


Figure 8. WinSCP file exchange application interface. For transferring video files from the RPi to the laptop

- 4.4. In command prompt type the following to enable the use of RPi cameras in python scripts

```
pi@antcam:~ $ sudo apt install python3-picamera
```

- 4.5. Open a new empty python script called cam.py:

```
pi@antcam:~ $ sudo nano cam.py
```

- 4.6. Write the following python script to record a 6 second mp4 video at 90fps, with a resolution of 1280 x 720 (labelled as 'test'). Click Ctrl+X and Y to save and exit:

N.B You can change these parameters as you so wish (eg: 30fps, 1920 x 1080). See camera parameters documentation:

<https://www.raspberrypi.com/documentation/accessories/camera.html>

```
import picamera
from subprocess import call
from datetime import datetime
file = 'test'

with picamera.PiCamera() as camera:
    camera.resolution = (1280,720)
    camera.framerate = 90
    camera.sensor_mode = 1
    camera.exposure_mode = 'sports'
    camera.shutter_speed = 2000

    #Record a 6 second video
    camera.start_recording('%s.h264' % file, format = 'h264', level='4.2')
    camera.wait_recording(6)
    camera.stop_recording
```

Figure 9. Python script (cam.py) to capture video

- 4.7. Run the script by typing the following (there is a couple of seconds delay before the trigger)

```
pi@antcam:~ $ python cam.py
```

- 4.8. Next type these lines to change the file from .h264 format to .mp4:

```
pi@antcam:~ $ MP4Box -add test.h264 test.mp4
```

- 4.9. Refresh WinSCP and drag and drop the mp4 file over to the desktop (**Figure 10**). Rename the video to something meaningful and then delete the videos off the raspberry pi when moved and backed up to the PC. The video can be viewed via the default windows video application. The output video will play in

slow motion at 25fps at default. The shutter speed is set to 2000 microseconds which equates to 1/250th second. This should reduce motion blur providing there is a lot of light

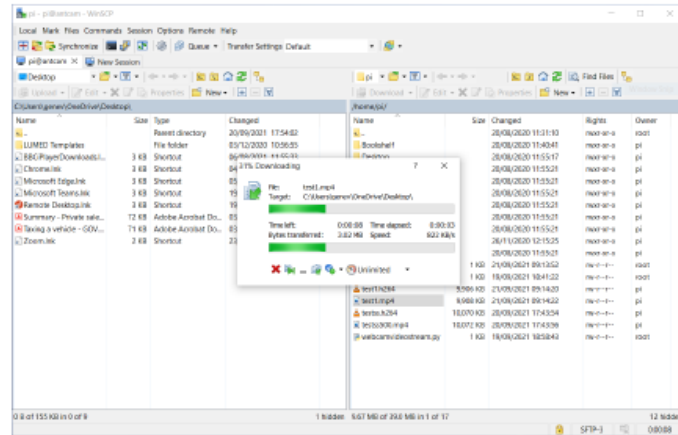


Figure 10. Transferring files from RPi to desktop

4.10. To take a 1 second calibration video on the RPi through python write the following script called cal.py (Figure 11) using the same process in sections 4.5 to 4.7. Note that the resolution of the images taken for calibration purposes should be the same as the videos taken through cam.py (1280 x 720)

```
import picamera
from subprocess import call
from datetime import datetime
file = 'cal'

with picamera.PiCamera() as camera:
    camera.resolution = (1280,720)
    camera.framerate = 90
    camera.sensor_mode = 1
    camera.exposure_mode = 'sports'
    camera.shutter_speed = 2000

#Record a 1 second video
camera.start_recording('%s.h264' % file, format = 'h264', level='4.2')
camera.wait_recording(1)
camera.stop_recording
```

Figure 11. Python script (cal.py) to take a 1 second calibration video at the same resolution

4.11. Then type these lines to change the file from .h263 format to .mp4:

```
pi@antcam:~ $ MP4Box -add cal.h264 cal.mp4
```

4.12. Move cal.mp4 to PC via WinSCP and delete from Raspberry Pi directory (see 4.9)

5. Setting up a web live feed through ssh and python

A live feed is useful to know the position of the frame with respect to what is being captured. The RPi Zero W have an IP address installed which can be used as a tool to view a live feed

5.1. Log in via command prompt and make sure your camera is connected to the same network as your computer (eg: phone hotspot) by opening the configuration tool again:

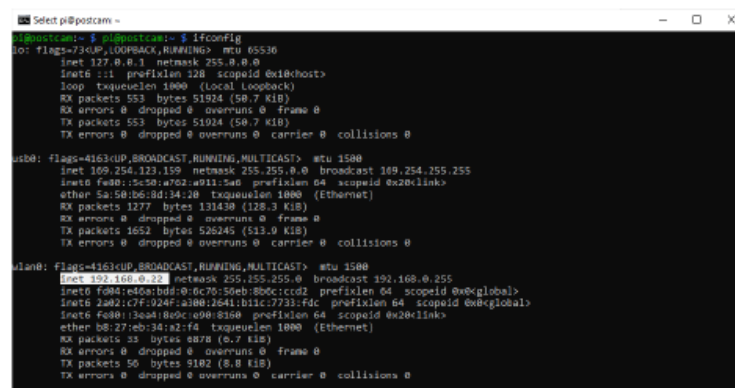
```
pi@postcam:~ $ sudo rasp-config
```

5.2. Select network options > H2 wifi and enter the SSID and password

5.3. Find out the camera's IP address by typing:

```
pi@postcam:~ $ ifconfig
```

The IP address is highlighted in **Figure 12**, for example: 192.168.0.22



```
Select pi@postcam ~
pi@postcam:~$ ifconfig
lo: flags=73<UP,LOOPBACK,RUNNING> mtu 65536
    inet 127.0.0.1 netmask 255.0.0.0
    inet6 ::1 prefixlen 128 scopeid 0x10<host>
    loop txqueuelen 1000 (Local Loopback)
    RX packets 553 bytes 51924 (50.7 KiB)
    RX errors 0 dropped 0 overruns 0 frame 0
    TX packets 553 bytes 51924 (50.7 KiB)
    TX errors 0 dropped 0 overruns 0 carrier 0 collisions 0

usb0: flags=4163<UP,BROADCAST,RUNNING,MULTICAST> mtu 1500
    inet 169.254.123.119 netmask 255.255.0.0 broadcast 169.254.255.255
    inet6 fe80::5c50:e762:a911:5a6 prefixlen 64 scopeid 0x20<link>
    ether 5a:5b:b6:8d:34:28 txqueuelen 1000 (Ethernet)
    RX packets 1277 bytes 131438 (128.3 KiB)
    RX errors 0 dropped 0 overruns 0 frame 0
    TX packets 1652 bytes 526245 (513.0 KiB)
    TX errors 0 dropped 0 overruns 0 carrier 0 collisions 0

wlan0: flags=4163<UP,BROADCAST,RUNNING,MULTICAST> mtu 1500
    inet 192.168.0.22 netmask 255.255.255.0 broadcast 192.168.0.255
    inet6 f084:e46a:bd9:0:6c70:50eb:8b6c:ccd2 prefixlen 64 scopeid 0x0<global>
    inet6 2a02:c7f:024f:a388:2641:b11c:7733:fdc prefixlen 64 scopeid 0x0<global>
    inet6 f080:2e41:1b0c:090:8268 prefixlen 64 scopeid 0x20<link>
    ether b8:27:eb:34:a2:f4 txqueuelen 1000 (Ethernet)
    RX packets 33 bytes 6878 (6.7 KiB)
    RX errors 0 dropped 0 overruns 0 frame 0
    TX packets 56 bytes 5192 (6.0 KiB)
    TX errors 0 dropped 0 overruns 0 carrier 0 collisions 0
```

Figure 12. Finding the IP address for the Raspberry Pi (highlighted)

5.4. Open a new python script called weblivefeed.py using:

```
pi@postcam:~ $ sudo nano weblivefeed.py
```

5.5. Type the following code:

```
# Web streaming example
# Source code from the official PiCamera package
# http://picamera.readthedocs.io/en/latest/recipes2.html#web-streaming

import io
import picamera
import logging
import socketserver
from threading import Condition
from http import server

PAGE="""\
<html>
<head>
<title>Posterior Camera</title>
</head>
<body>
<center><h1>Posterior Camera</h1></center>
<center></center>
</body>
</html>
"""

class StreamingOutput(object):
    def __init__(self):
        self.frame = None
        self.buffer = io.BytesIO()
        self.condition = Condition()

    def write(self, buf):
        if buf.startswith(b'\xff\xd8'):
            # New frame, copy the existing buffer's content and notify all
            # clients it's available
            self.buffer.truncate()
            with self.condition:
                self.frame = self.buffer.getvalue()
                self.condition.notify_all()
            self.buffer.seek(0)
        return self.buffer.write(buf)

class StreamingHandler(server.BaseHTTPRequestHandler):
    def do_GET(self):
        if self.path == '/':
            self.send_response(301)
            self.send_header('Location', '/index.html')
            self.end_headers()
        elif self.path == '/index.html':
            content = PAGE.encode('utf-8')
            self.send_response(200)
            self.send_header('Content-Type', 'text/html')
            self.send_header('Content-Length', len(content))
            self.end_headers()
            self.wfile.write(content)
```



```

elif self.path == '/stream.mjpg':
    self.send_response(200)
    self.send_header('Age', 0)
    self.send_header('Cache-Control', 'no-cache, private')
    self.send_header('Pragma', 'no-cache')
    self.send_header('Content-Type', 'multipart/x-mixed-replace;
boundary=FRAME')
    self.end_headers()
    try:
        while True:
            with output.condition:
                output.condition.wait()
                frame = output.frame
            self.wfile.write(b'--FRAME\r\n')
            self.send_header('Content-Type', 'image/jpeg')
            self.send_header('Content-Length', len(frame))
            self.end_headers()
            self.wfile.write(frame)
            self.wfile.write(b'\r\n')
        except Exception as e:
            logging.warning(
                'Removed streaming client %s: %s',
                self.client_address, str(e))
    else:
        self.send_error(404)
        self.end_headers()

class StreamingServer(socketserver.ThreadingMixIn, server.HTTPServer):
    allow_reuse_address = True
    daemon_threads = True

with picamera.PiCamera(resolution='1280x720', framerate=25) as camera:
    output = StreamingOutput()
    #Uncomment the next line to change your Pi's Camera rotation (in degrees)
    #camera.rotation = 90
    camera.start_recording(output, format='mjpeg')
    try:
        address = ('', 8000)
        server = StreamingServer(address, StreamingHandler)
        server.serve_forever()
    finally:
        camera.stop_recording()

```

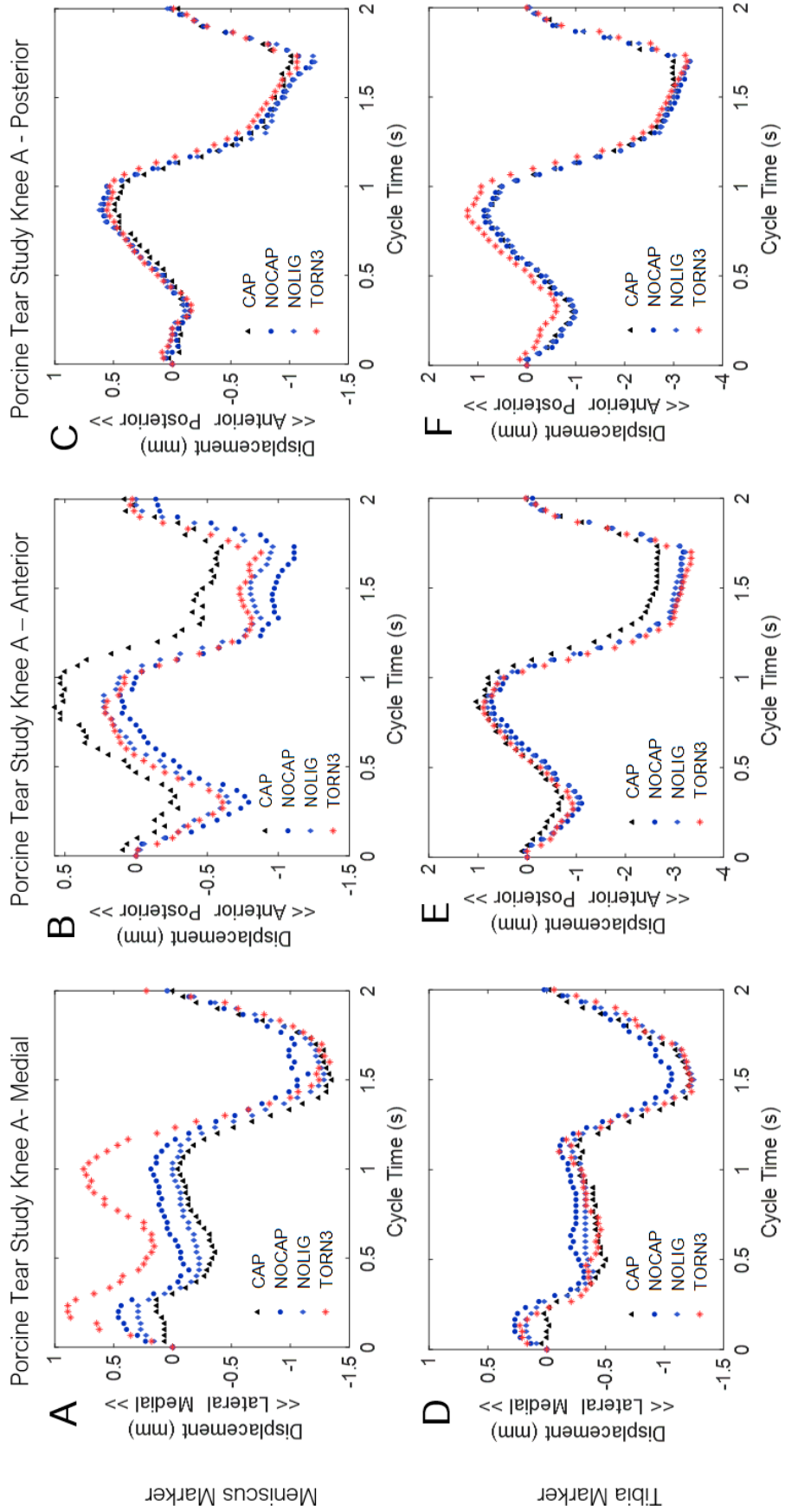
5.6. Click Ctrl+X to exit and Y to save

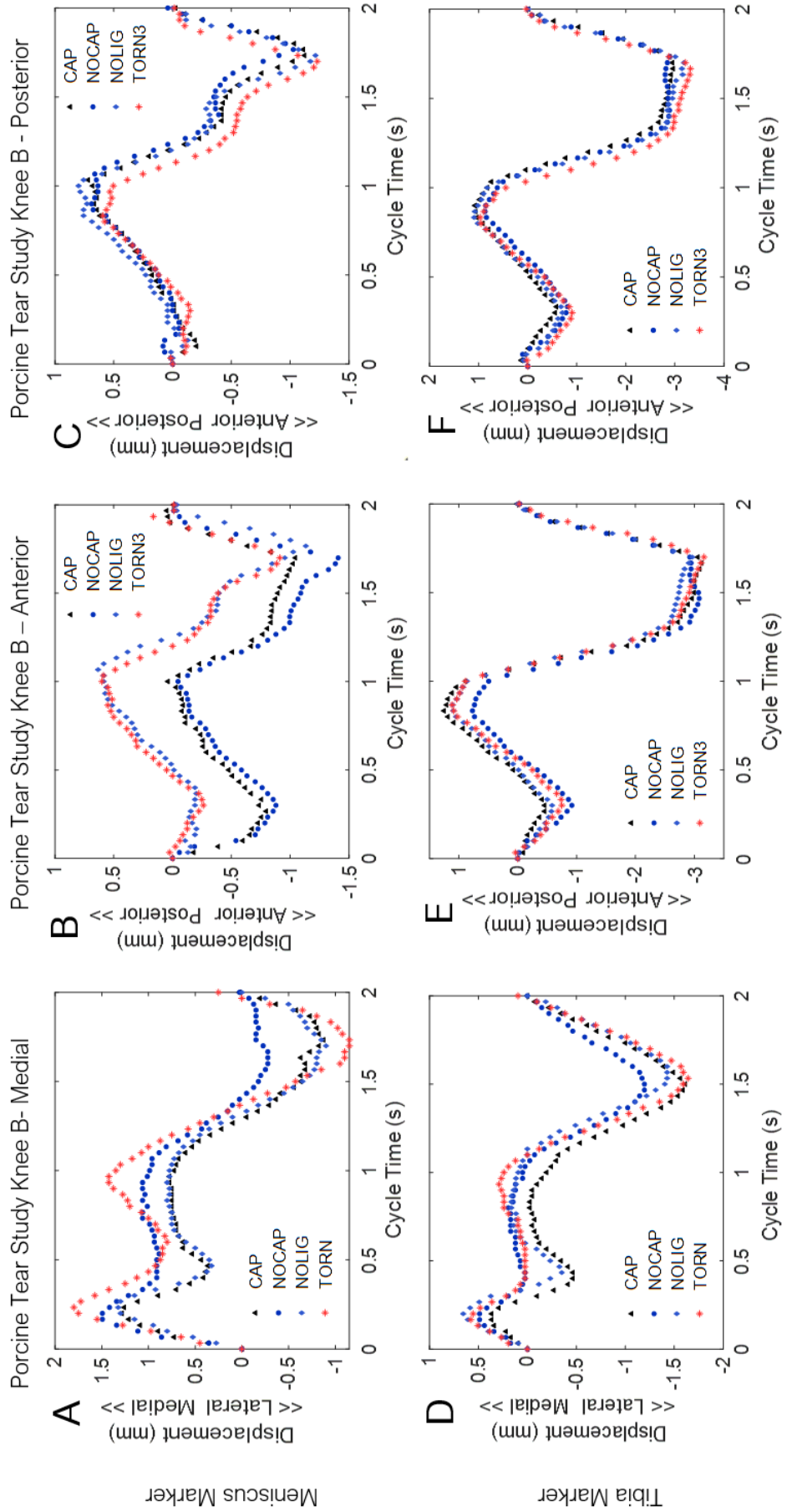
5.7. To activate the script type (remember to use Python 3):

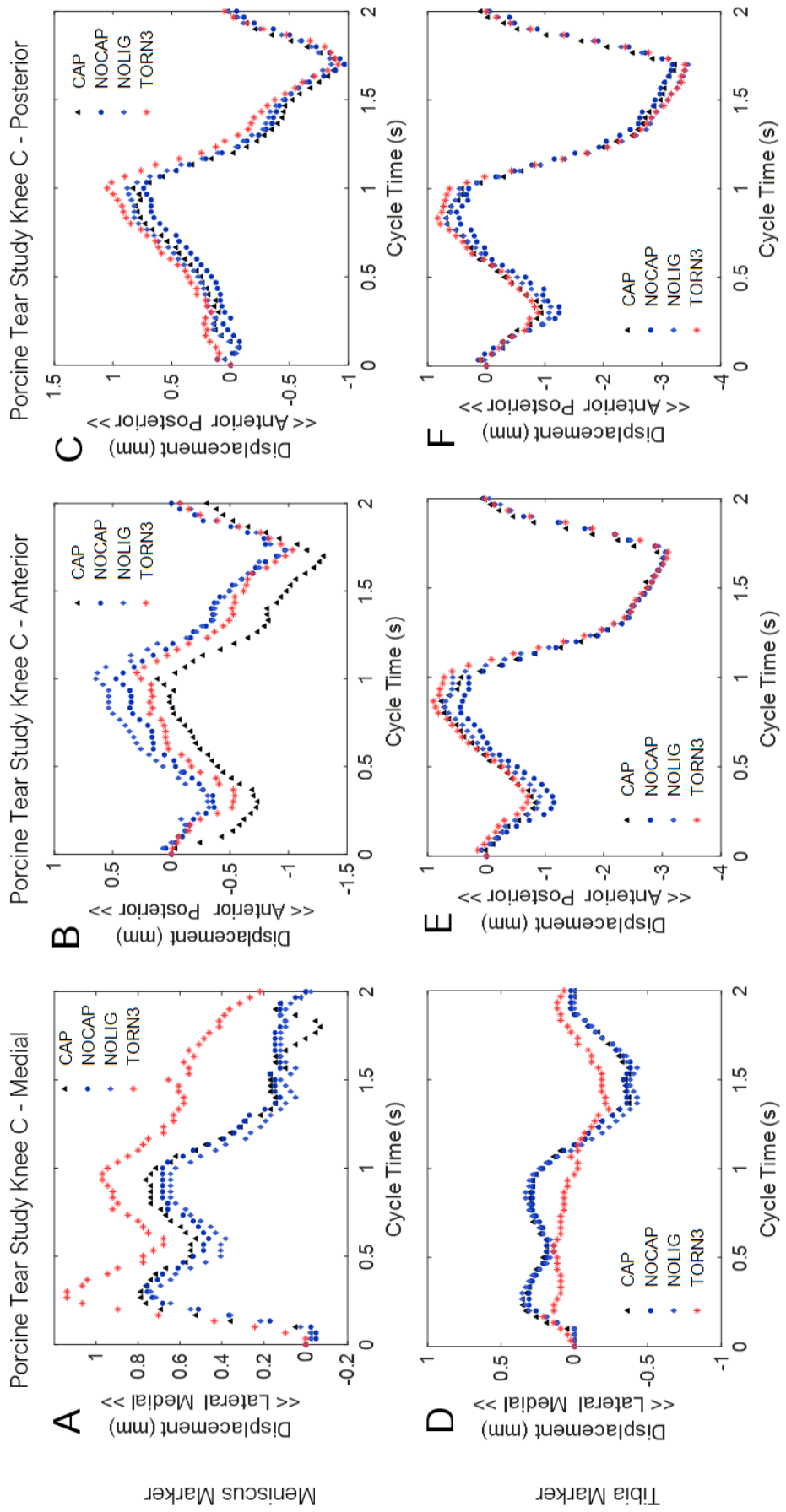
```
pi@postcam:~ $ python3 weblivefeed.py
```

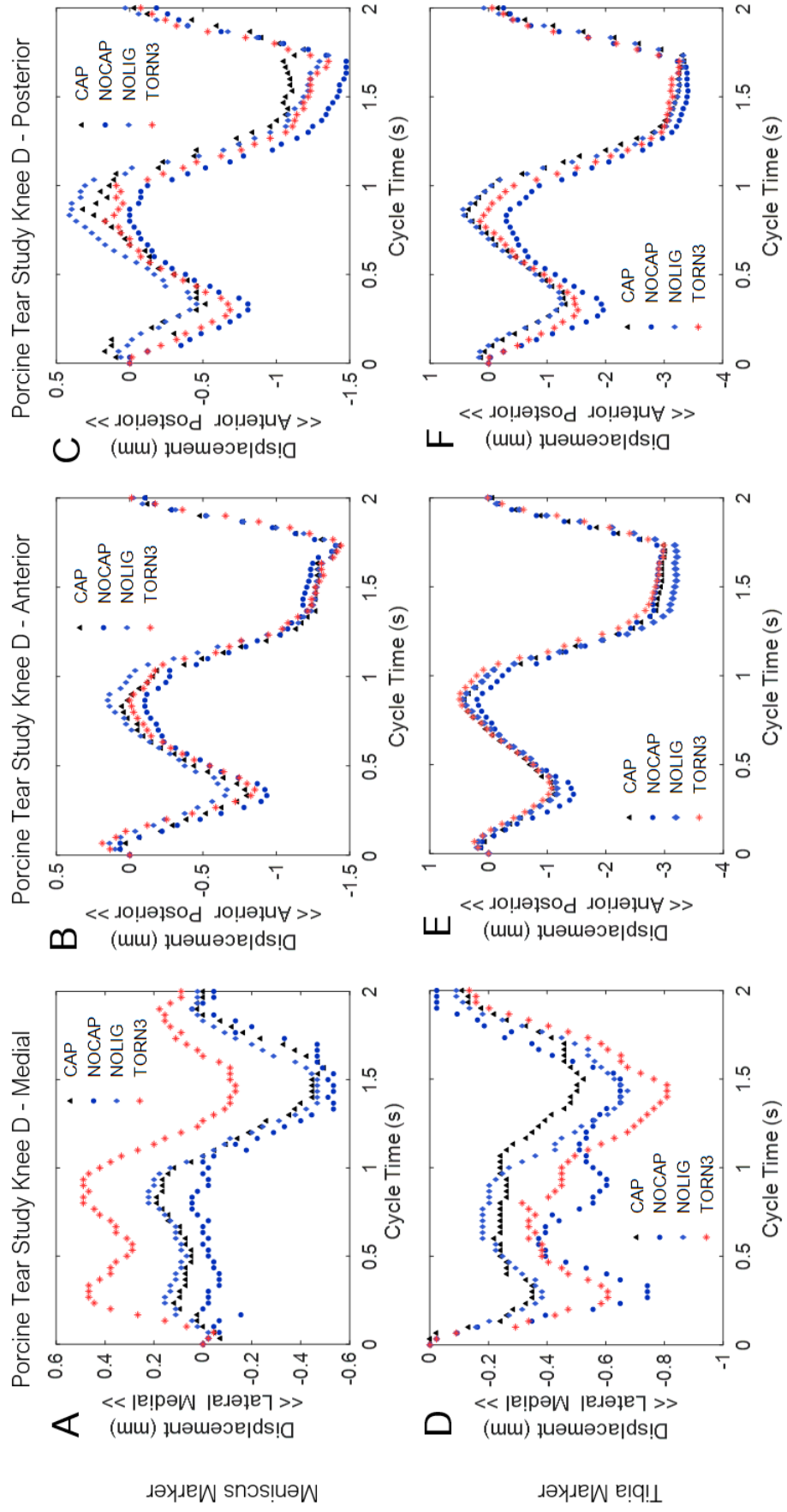
5.8. Once the script is running, open a browser (eg Google Chrome) to access the video streaming web server at: **http://<Your_Pi_IP_Address>:8000**. Replace with the RPi IP address, in this case **http://192.168.0.22:8000**

Appendix E – Porcine Study: Meniscus and Tibial Marker Results

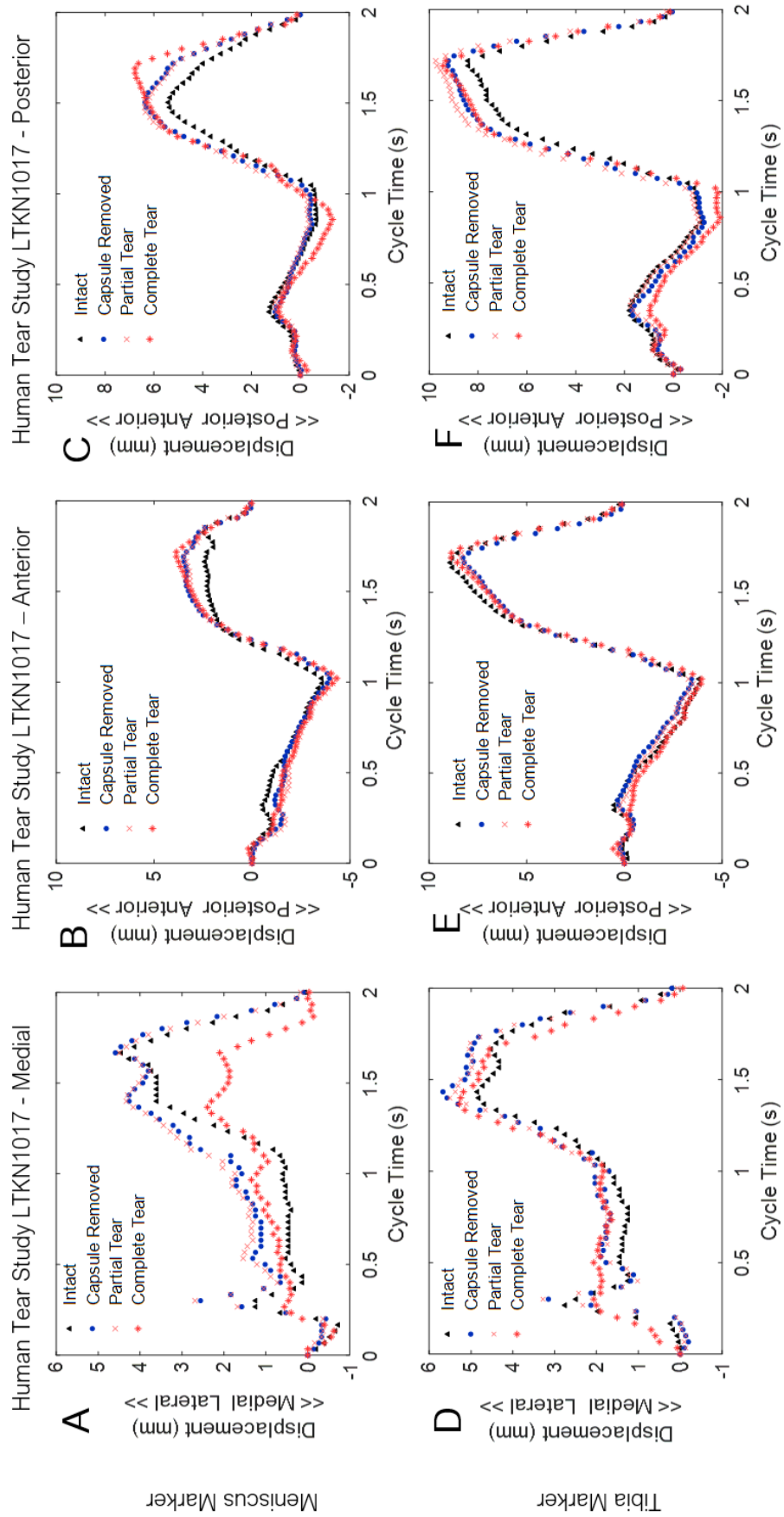


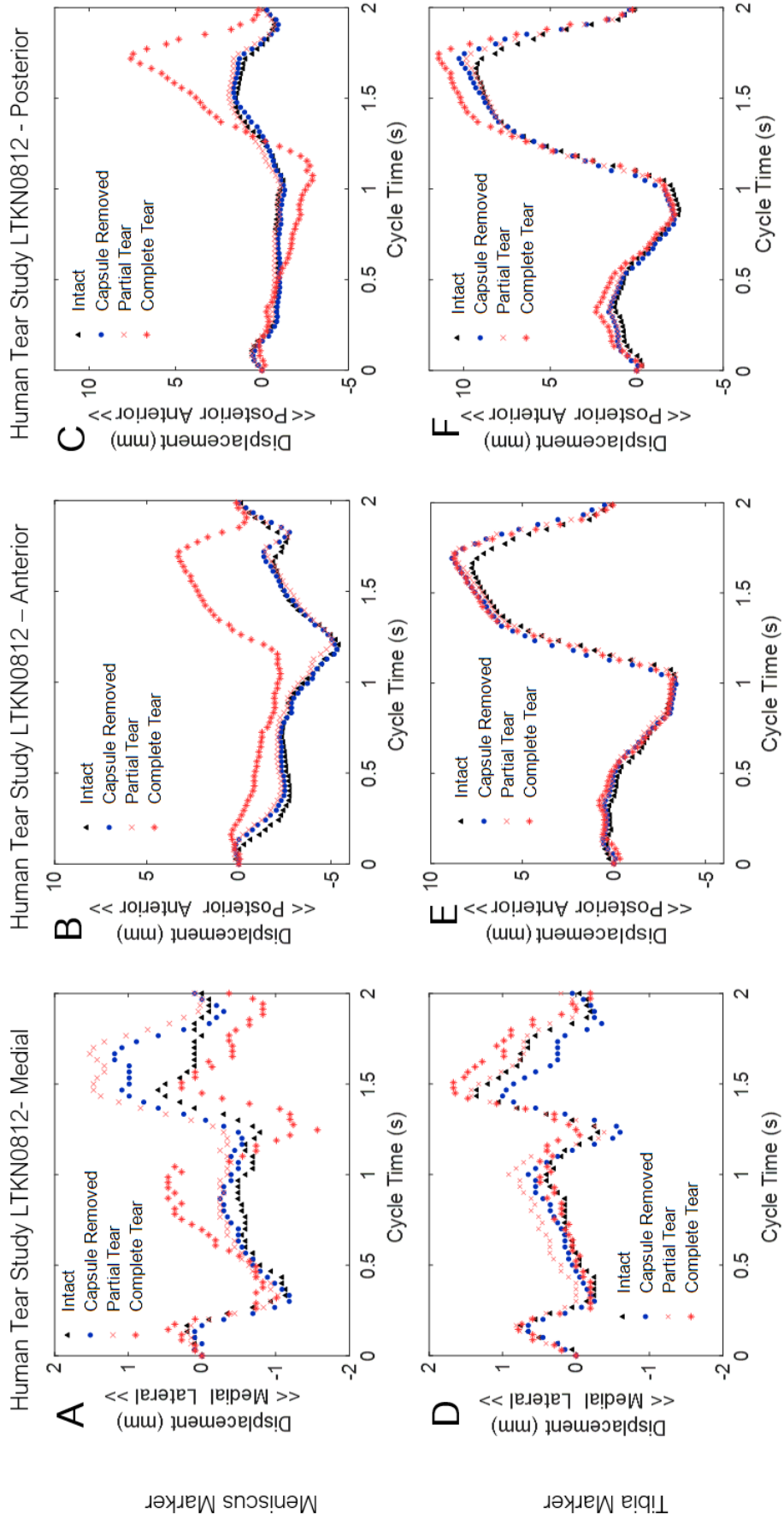






Appendix F – Human Study: Meniscus and Tibial Marker Results





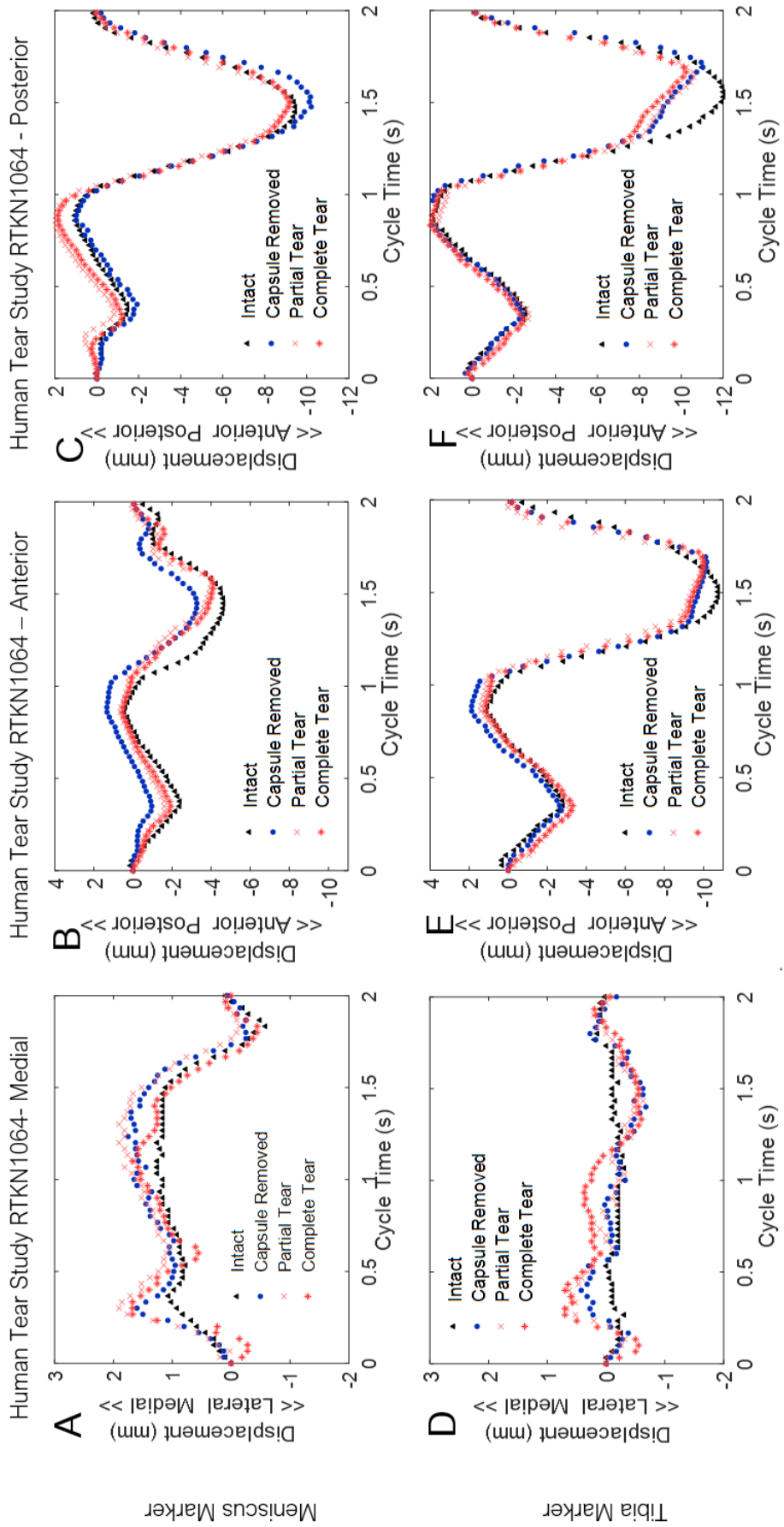
Human Tear Study LTKN0812 - Posterior

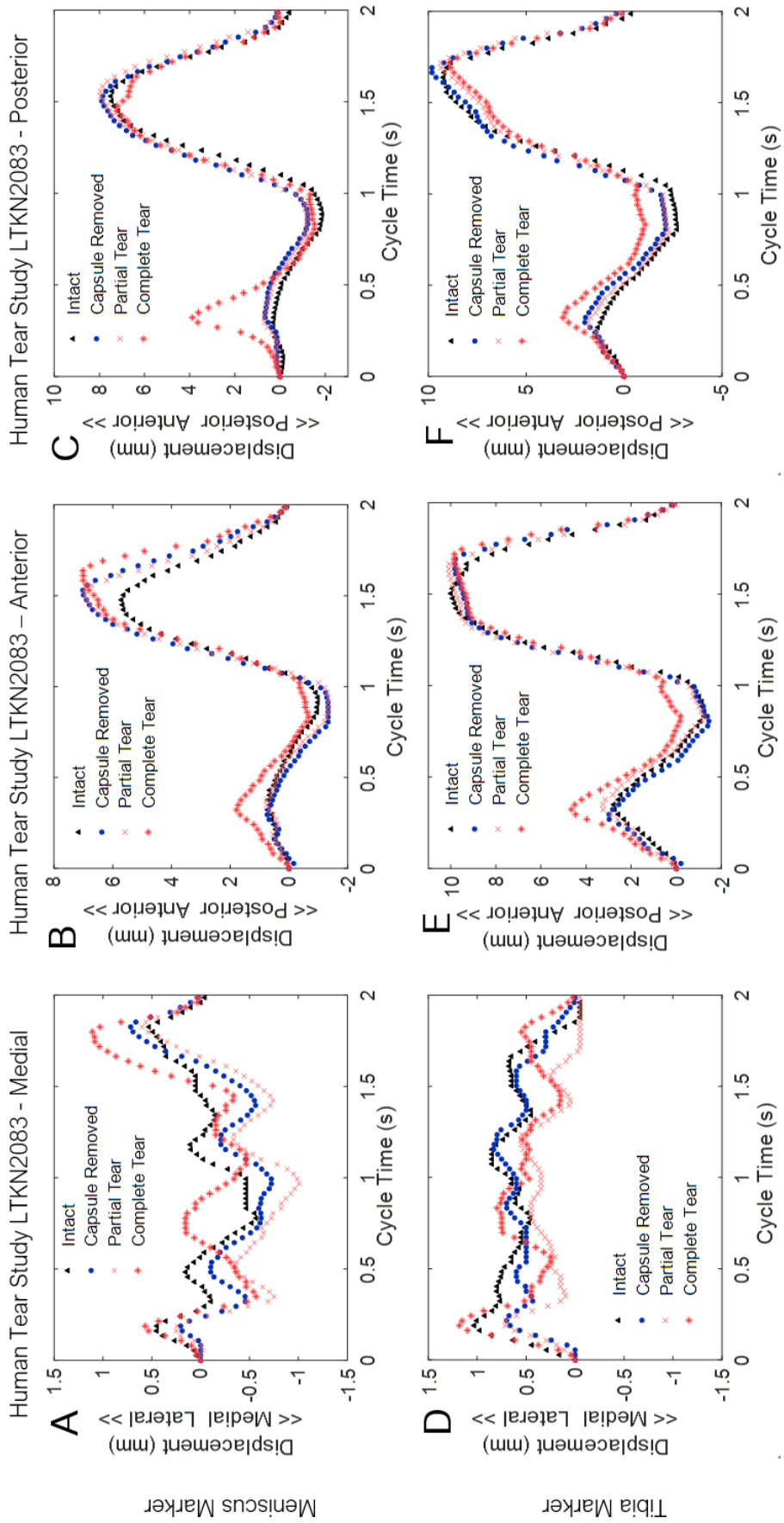
Human Tear Study LTKN0812 - Anterior

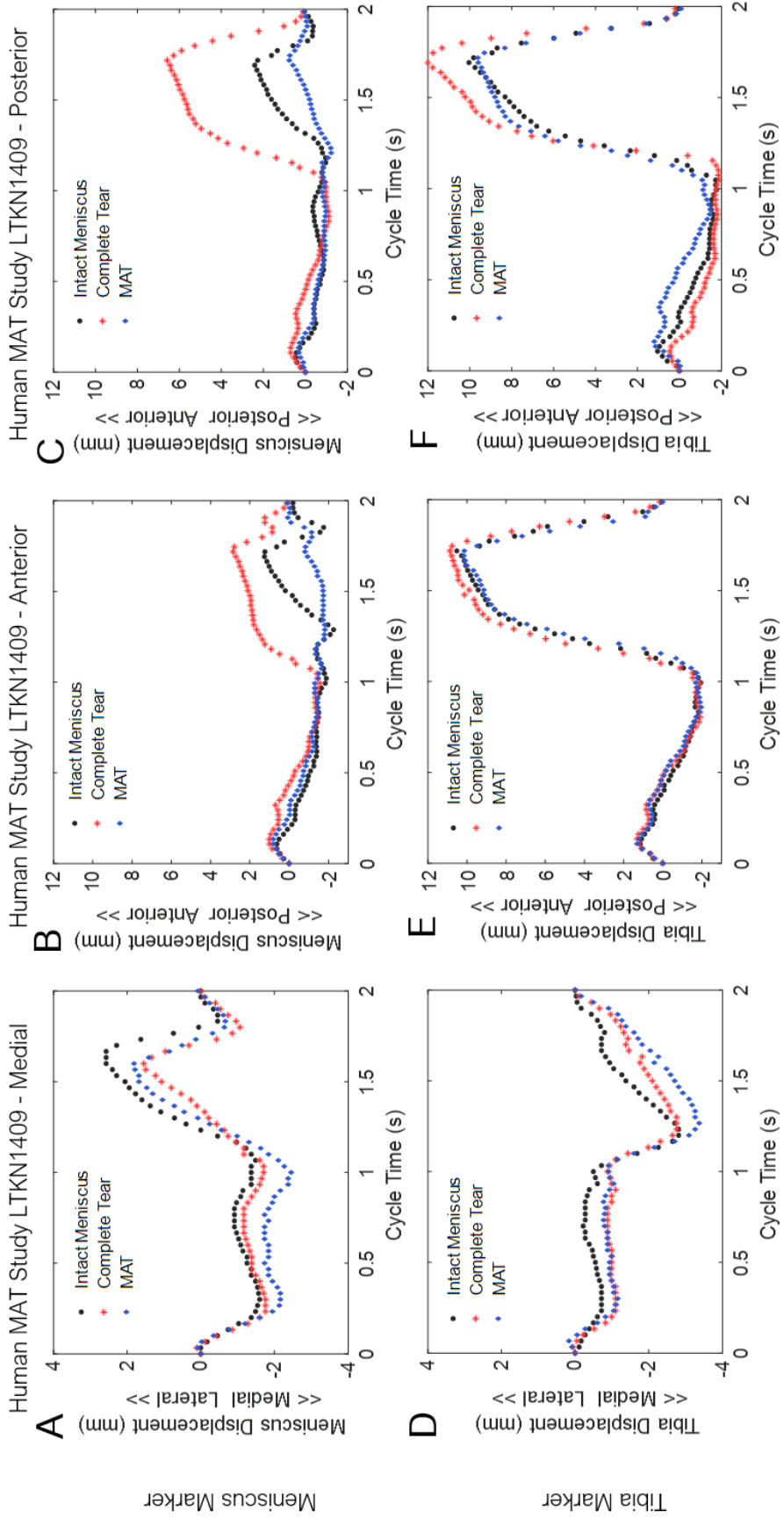
Human Tear Study LTKN0812- Medial

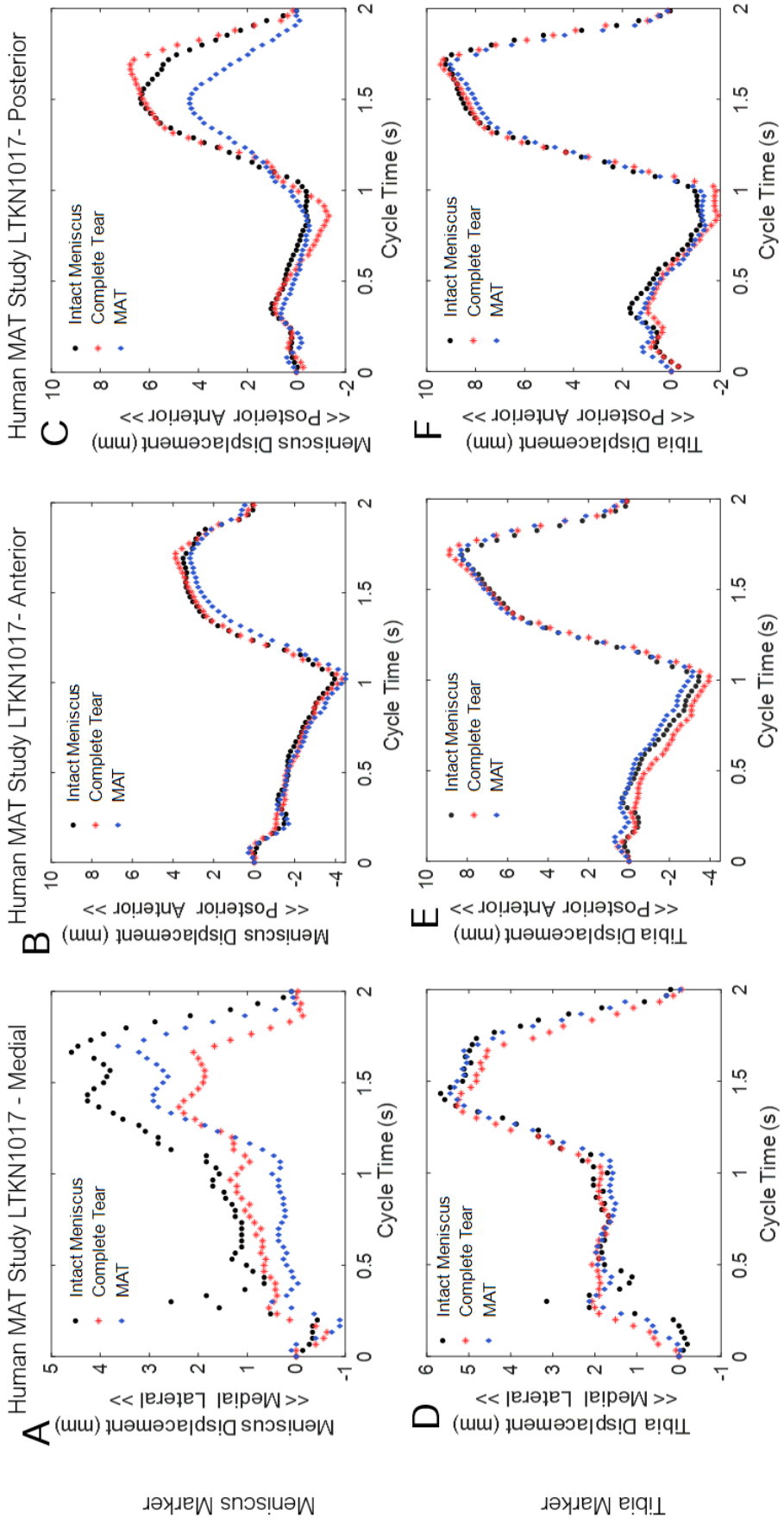
Meniscus Marker

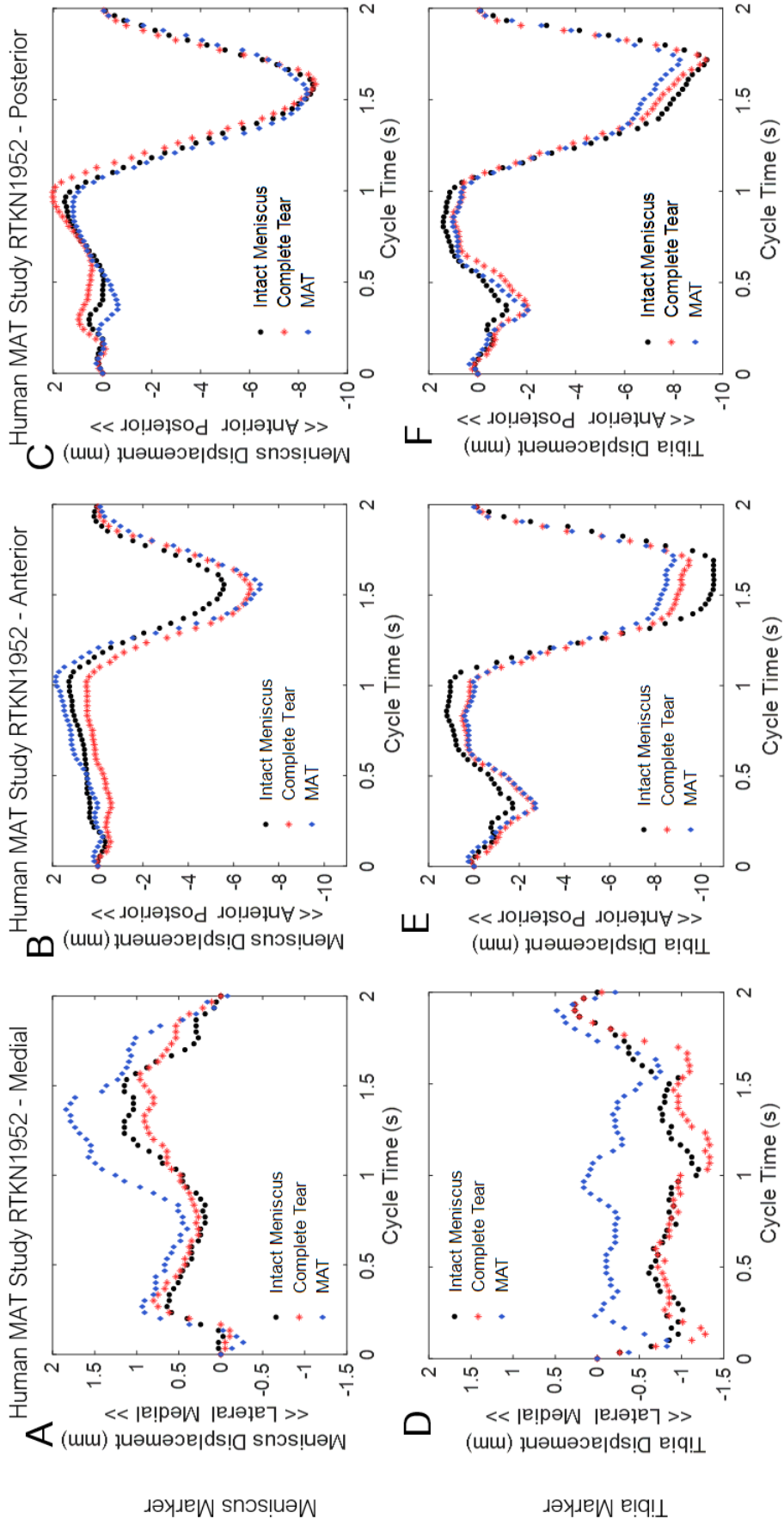
Tibia Marker











Appendix G – Figure Permissions

	Date	Article Title	Publication	Type Of Use	Price	Status	Expiration Date	Order Number
1	31-Mar-2023	Displacement of the medial meniscus within the passive motion characteristics of the human knee joint: an RSA study in human cadaver knees	Knee Surgery, Sports Traumatology, Arthroscopy	Thesis/Dissertation	0.00 £	Completed		5519390670301
2	31-Mar-2023	Effects of medial meniscal posterior horn avulsion and repair on meniscal displacement	The Knee	reuse in a thesis/dissertation	0.00 £	Completed		5519381279788
3	16-Mar-2023	Medial meniscocapsular separation: MR imaging criteria and diagnostic pitfalls	European Journal of Radiology	reuse in a thesis/dissertation	0.00 £	Completed		5510711247189
4	18-Jan-2023	Biomechanical Basis of Human Movement	WK Health Book	Dissertation/Thesis	0.00 £	Completed		5472071190814
5	11-Nov-2022	Meniscus Body Position, Size, and Shape in Persons With and Persons Without Radiographic Knee Osteoarthritis: Quantitative Analyses of Knee Magnetic Resonance Images From the Osteoarthritis Initiative	Arthritis & Rheumatology	Dissertation/Thesis	0.00 £	Completed		5425890619009

1. Tienen et al. (2005) 2. Hein et al. (2011) 3. De Maeseneer et al. (2002) 4. Hamill et al. (2015). 5. Wenger et al. (2013)

Order Number: 1343039
Order Date: 08 Apr 2023

[Print order](#)

Payment Information

Genevieve Pounds
sp13gp@leeds.ac.uk
Payment method: Invoice

Billing Address:
Miss Genevieve Pounds
Miss. Genevieve Pounds
University of Leeds
Leeds, LS29JT
United Kingdom

+44 7969646552
sp13gp@leeds.ac.uk

Customer Location:
Miss Genevieve Pounds
Miss. Genevieve Pounds
University of Leeds
Leeds, LS29JT
United Kingdom

Order Details

1. The Journal of Bone & Joint Surgery (British volume)
Article: Meniscal movement. An in-vivo study using dynamic MRI.

Billing Status:
Open

Order License ID: 1343039-1
Order detail status: Completed
ISSN: 0301-620X

Type of use
Publisher
Portion


[Print License](#)
Republish in a thesis/dissert...
BRITISH EDITORIAL SOCIETY ...
Image/photo/illustration

^ (Vedi et al., 1999)

[Copyright](#) ©2017 Kean et al.

This is an open access article distributed under the terms of the [Creative Commons Attribution License](#), which permits unrestricted use, distribution, reproduction and adaptation in any medium and for any purpose provided that it is properly attributed. For attribution, the original author(s), title, publication source (PeerJ) and either DOI or URL of the article must be cited.

^ (Kean et al., 2017)



[Home](#) [Help](#) [Live Chat](#) [Sign in](#) [Create Account](#)

Current concepts on structure–function relationships in the menisci

Author: Stephen H. J. Andrews, Adetola B. Adesida, et al
Publication: CONNECTIVE TISSUE RESEARCH
Publisher: Taylor & Francis
Date: May 4, 2017
Rights managed by Taylor & Francis

Thesis/Dissertation Reuse Request

Taylor & Francis is pleased to offer reuses of its content for a thesis or dissertation free of charge contingent on resubmission of permission request if work is published.

[BACK](#)
[CLOSE](#)

^ (Andrews et al., 2017)